Vol. 50, No.3 / 2016

e: ISSN 2068 – 2239
p: ISSN 2068 – 4215

INMATEH - AGRICULTURAL ENGINEERING

SEPTEMBER - DECEMBER

Editorial

The National Institute of Research-Development for Machines and Installations designed to Agriculture and Food Industry - INMA Bucharest has the oldest and most prestigious research activity in the field of agricultural machinery and mechanizing technologies in Romania.

Short History

- *In 1927, the first research **Center for Agricultural Machinery** in Agricultural Research Institute of Romania - ICAR (Establishing Law was published in O.D. no. 97/05.05.1927) was established;*
- *In 1930, was founded **The Testing Department of Agricultural Machinery and Tools** by transforming Agricultural Research Centre of ICAR - that founded the science of methodologies and experimental techniäues in the field (Decision no. 2000/1930 of ICAR Manager - GHEORGHE IONESCU ŞIŞEŞTI);*
- *In 1952, was established the Research Institute for Mechanization and Electrification of Agriculture - ICMA Băneasa, by transforming the Department of Agricultural Machines and Tools Testing;*
- *In 1979, the Research Institute of Scientific and Technological Engineering for Agricultural Machinery and Tools – ICSITMUA was founded - subordinated to Ministry of Machine Building Industry - MICM, by unifying ICMA subordinated to MAA with ICPMA subordinated to MICM;*
- *In 1996 the National Institute of Research-Development for Machines and Installations designed to Agriculture and Food Industry – INMA was founded – according to G.D. no.1308/25.11.1996, by reorganizing ICSITMUA, G.D no. 1308/1996 coordinated by the Ministry of Education and Research G.D. no. 823/2004;*
- *In 2008 INMA has been accredited to carry out research and developing activities financed from public funds under G.D. no. 551/2007, Decision of the National Authority for Scientific Research - ANCSno. 9634/2008.*

*As a result of widening the spectrum of communication, dissemination and implementation of scientific research results, in 2000 was founded the institute magazine, issued under the name of SCIENTIFIC PAPERS **(INMATEH)**, ISSN 1583 – 1019.*

*Starting with volume 30, no. 1/2010, the magazine changed its name to **INMATEH - Agricultural Engineering**, appearing both in print format (ISSN 2068 - 4215), and online (ISSN online: 2068 - 2239). The magazine is bilingual, being published in Romanian and English, with a rhythm of three issues / year: January-April, May-August, September-December and is recognized by CNCSIS – with B^+ category. Published articles are from the field of AGRICULTURAL ENGINEERING: technologies and technical equipment for agriculture and food industry, ecological agriculture, renewable energy, machinery testing, environment, transport in agriculture etc. and are evaluated by specialists inside the country and abroad, in mentioned domains.*

*Technical level and performance processes, technology and machinery for agriculture and food industry increasing, according to national reäuirements and European and international regulations , as well as exploitation of renewable resources in terms of efficiency, life, health and environment protection represent referential elements for the magazine „**INMATEH - Agricultural Engineering**".*

We are thankful to all readers, publishers and assessors.

Editor in chief,
Ph.D. Eng. Pirnă Ion

In the present, *INMATEH - Agricultural Engineering* journal is indexed in the next international databases:
ULRICHS Web: Global Serials Directory, CABI, SCIPIO, ELSEVIER /SciVerse SCOPUS, Index COPERNICUS International, EBSCO Publishing, Elektronische Zeitschriftenbibliothek

INMATEH - Agricultural Engineering

vol. 50, no.3/ 2016

NATIONAL INSTITUTE OF RESEARCH-DEVELOPMENT FOR MACHINES AND INSTALLATIONS DESIGNED TO AGRICULTURE AND FOOD INDUSTRY - INMA Bucharest

6 Ion Ionescu de la Brad Blvd., sector 1, Bucharest

Three issues per year,
eISSN: 2068 – 2239
pISSN: 2068 – 4215

Edited by: INMA Bucharest

CONTENT

DESIGN AND STUDY ON THE EDGE CURVE OF BLADE OF A HANDHELD TILLER'S ROTARY BLADE
/
微耕机用旋耕弯刀刃口曲线设计及研究

Ms. Stud. Eng. Li S.T.[1)], As. Eng. Yang L.[1)], Ph.D. Eng. Niu P.[1)], Ms. Stud. Eng. Zhang Y.H.[1)], Prof. Eng. Xie S.Y.[1)], Prof. Eng. Chen X.B.[*2)], Prof. Eng. Yang M.J.[*1)]
[1)] Southwest University, College of Engineering and Technology / P. R. China;
[2)] Agricultural Machinery Quality Control and Inspection Technology Centre,
Nanjing Research Institute for Agricultural Mechanization Ministry of Agriculture / P. R. China
Tel: 8613883002509; E-mail: chxibi@126.com; ymingjin@swu.edu.cn

Keywords: *rotary blade, edge curve, design parameters, mathematical model, CAD system, handheld tiller*

ABSTRACT
The shapes and parameters of the edge curve of a rotary blade have important influence on the slip cutting performance, soil cutting resistance and soil throwing performance of the rotavators of a handheld tiller. In this study, taking the handheld tiller's rotary blade as a case study, the mathematical model of the edge curve of the rotary blade was built, and the CAD system of the rotary blade was obtained by means of the secondary development of AutoCAD based on Visual BASIC. Three rotary blades with different diameters and different edge curves were designed through the CAD system, the relative error of system output and calculated values (Excel) of parameters were studied, and the variation of grass removing angle of edge curve, scoop angle and tilling width were analyzed as well. The results showed that: the relative error of the system output and calculated values are at the level of 0.5%; the grass removing angle and scoop angle of edge curve edge are in the preferred value range; with cornerite increase, the grass removing angle and scoop angle linearly increase at large; on conditions of other parameters being constant, the tilling width decreases with increase of alpha angle.

摘要
旋耕弯刀刃口曲线形状和对微耕机刀辊的滑切性能、切土阻力和抛土性能等具有重要影响。本文以刀盘式湿地弯刀为例，建立了微耕机用旋耕弯刀刃口曲线的数学模型，通过基于 Visual Basic 的 AutoCAD 二次开发，得到了旋耕弯刀的 CAD 系统。通过该 CAD 系统，设计了 3 把具有不同直径和不同形状刃口曲线的旋耕弯刀，研究了其参数输出值和计算值(Excel)的相对误差，分析了刃口曲线滑切角、背角和工作幅宽的变化规律。结果表明：系统输出值和计算值的相对误差均在 0.5%水平，刃口曲线滑切角和刃口背角在较佳取值范围；滑切角和背角随着包角的增大而增大，呈近似线性关系；在其他条件不变的情况下，工作幅宽随着阿尔法角的增大而减小。

INTRODUCTION
The arable land of China that locates in the hills, mountains and plateaus region accounts for 69.3%, and the arable land located in the plains and basins accounts for only 30.7% *(Hao, et al, 2003).* Currently, handheld tillers are mainly used in the arable land in the hilly and mountainous areas. The functions of soil cutting, pulverization, soil turning, soil throwing and soil levelling, etc., and function that pushes the tillers forward by the soil reacting force from the soil-tilling are all achieved by the interaction of rotavator and soil while soil-tilling. The rotavator consists of some rotary blades and a shaft, and the geometric parameters of the blade directly affect the performance of a rotavator and the corresponding handheld tiller *(Niu, et al, 2015)*. The shape of rotary blade edge including lengthwise edge and sidelong edge is decided by curve equation, maximum cornerite of the lengthwise edge curve, sidelong edge apex cornerite, bending angle and bending radius. And it has a significant impact on the grass removing angle and scoop angle, etc., thereby it affects the performance of grass removing of rotary blade, cut soil resistance and throwing soil properties.

At present, many scholars made some extensive investigations on the edge curve of blade of a handheld tiller's rotary blade, but they mainly focused on the performance of a single parameter or parameters of the experimental optimization. Hao et al studied the grass removing angle of lengthwise edge, and found that the optimal values of the angle were in the range of 35-55° *(Hao, et al, 2014)*; Gai et al studied the bending angle of sidelong edge, and found that the best values of the angle should be in the range of 115-125° *(Gai et al, 2011)*; Sakai et al. experimentally studied the effects of scoop angle on soil cutting process, and obtained the reasonable range of scoop angle of the rotary blade under different soil conditions *(Sakai et al, 1984)*; Saimbhi et al analyzed the force between the rotary blade and soil, and optimized the geometric parameters of edge curve of the blade *(Saimbhi et al, 2004)*. However, the systematic research on the edge curve of rotary blade is not enough. For example, the principles to determine each parameter and the relationship between the various parameters are not quite clear. Standard GB / T5669-2008 (China) only provides curve equation and some parameters of common rotary blade, and it is difficult to define the sidelong edge curve as it is a space curve. Furthermore, there is no standard for the edge curve design of a handheld tiller's rotary blade, and reference is only given to the edge curve of blade of common rotary blade.

In this study, taking the handheld tiller's rotary blade as a case study, with reference to the standard GB / T5669-2008 (China) and JIS B 9210-1988 (2008 confirmed) (Japan), the mathematical model of the edge curve of a handheld tiller's rotary blade was established according to the geometric relations between each parameter, and the CAD system of rotary blade was obtained by means of the secondary development of AutoCAD based on Visual BASIC. The variation of grass removing angle, scoop angle and tilling width of rotary blade curve with different diameters and different shapes were studied as well. As a result, the study can provide references to the design, force and vibration reduction, and performance optimization for a handheld tiller's rotary blade.

MATERIAL AND METHOD

Material

The rotary blade, adaptable for wetland sticky paddy field tillage, is shown in fig.1. It was designed according to Chinese National Standard GB/T 5669-2008 "Rotary tiller-rotary blades and blade holders", Chongqing Standard DB50/T 277-2008 "Blades of micro-cultivator", and Japanese National Standard JIS B 9210-1988 (2008 confirmed) "Blades for tillers". The main design contents of a rotary blade include curve equation, maximum cornerite of the lengthwise edge curve, cornerite of sidelong edge apex, bending angle, bending radius, tilling width, grass removing angle and scoop angle etc.

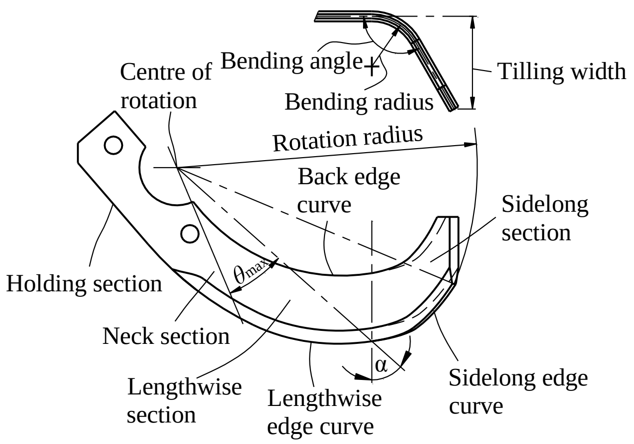

Fig. 1 - Structure and composition of the rotary blade

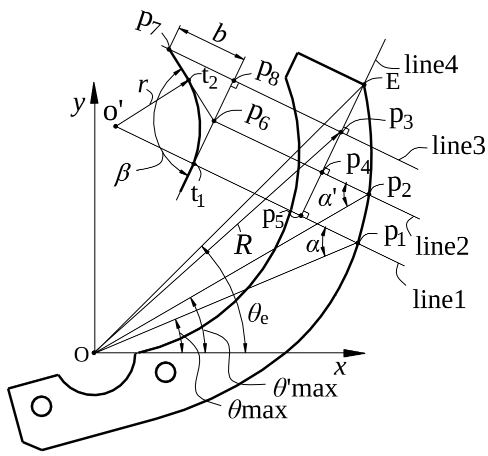

Fig. 2 - Developed view of the rotary blade in plane containing lengthwise edge curve

To simplify the modelling of the blade curve, the sidelong edge of the rotary blade was unfolded along the plane of lengthwise edge, and the coordinate system was defined as well, as shown in fig.2. Where:

θ'_{max} is the cornerite of bending point;

θ_{max} - maximum cornerite of the lengthwise edge curve;

α' - angle between rotary radius of bending point with bending line;

α - angle between rotary radius of end point of the lengthwise edge curve;

E - apex of sidelong edge;

θ_E - cornerite of the apex of sidelong edge;
r - bending radius;
β - bending angle;
b - tilling width;
line 1- line 4 are auxiliary lines;
p_1- p_8 are points of intersection;
t_1 and t_2 are points of tangency.

The edge curve is a spiral of Archimedes when it has been unfolded, and its equation is as follows:

$$R_n = a_0 R + a_1 R\theta \quad , \quad \text{[mm]} \tag{1}$$

where:
R_n is rotation radius at a selected point on the edge curve, [mm];
R – rotation radius of a rotary blade, [mm];
θ – cornerite of the edge curve, [degree];
a_0 and a_1 – constants.

Taking three rotary blades with different diameters and different edge curves as a case study, the construction process of the mathematical models and CAD system of the rotary blade was illustrated, and the parameters of the rotary blades were shown in table 1. The grass removing angle, scoop angle and tilling width, etc., of the blades were analyzed subsequently.

Table 1

Parameters of 3 rotary blades

Rotary blade	R [mm]	a_0	a_1	B [°]	R [mm]	θ'_{ma} [°]	α' [°]	e_0 [mm]	c_0 [mm]	l_0 [mm]
1	180	0.58	0.0128	120	30	27	50	4	2	8
2	200	0.56	0.011	120	30	27	50	4.5	2	8
3	225	0.50	0.008	120	30	27	50	6	2	8

Method

The mathematical models of edge curve

The edge curve of rotary blade includes lengthwise edge and sidelong edge. The sidelong section takes the main responsibility for the soil-cutting *(Yue, 2008)*. The lengthwise section is not only closely related to the performance of slip-cutting of the rotary blade, but also has a significant impact on the grass removing performance.

The design parameters of lengthwise edge curve include maximum cornerite of the lengthwise edge curve θ_{max}, the angle between rotary radius of end point of the lengthwise edge curve with bending line α (namely the alpha angle for simplification), and grass removing angle τ.

Line 1 is the bending line of sidelong edge, line 2 is the bending midline, and line 1 is parallel to line 2. Point p_1 is the end of sidelong edge, and it corresponds to the maximum cornerite of the lengthwise edge curve θ_{max}, as shown in fig. 2. Angles of θ_{max} and α can be calculated as follows:

$$\left(\frac{k_2 x_2 - y_2}{k_2 - \tan\theta_{max}}\right)^2 + \left(\frac{k_2 x_2 - y_2}{k_2 - \tan\theta_{max}}\tan\theta_{max}\right)^2 = \left(a_0 R + a_1 R\theta_{max}\right)^2 \tag{2}$$

$$\alpha = \alpha' - \theta'_{max} + \theta_{max} \quad \text{[degree]} \tag{3}$$

where:
(x_2, y_2) is the coordinate of the bending point p_2,
$x_2 = \left(a_0 R + a_1 R\theta'_{max}\right)\cos\theta'_{max}$, [mm];
$y_2 = \left(a_0 R + a_1 R\theta'_{max}\right)\sin\theta'_{max}$, [mm];
k_2 – the slope of line 2;
$k_2 = \tan\left(180 - \alpha' + \theta'_{max}\right)$.

The grass removing angle of a point is defined as the angle between velocity vector and normal plane, as shown in fig.3. Apply the derivative to equation of lengthwise edge curve, and the grassing moving angle can be expressed as:

$$\tau = \arctan\left(\lim_{\Delta\theta\to 0}\frac{R(\theta+\Delta\theta)\cos(\theta+\Delta\theta)-R(\theta)\cos\theta}{R(\theta+\Delta\theta)\sin(\theta+\Delta\theta)-R(\theta)\sin\theta}\right)-\theta \text{, [degree]} \tag{4}$$

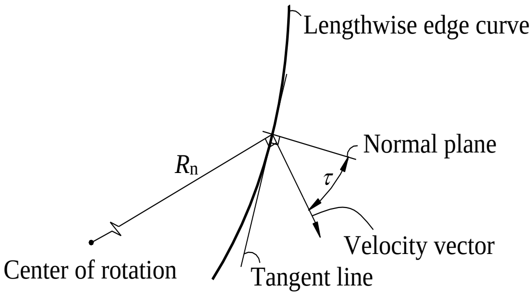

Fig. 3 - Definition of grass removing angle

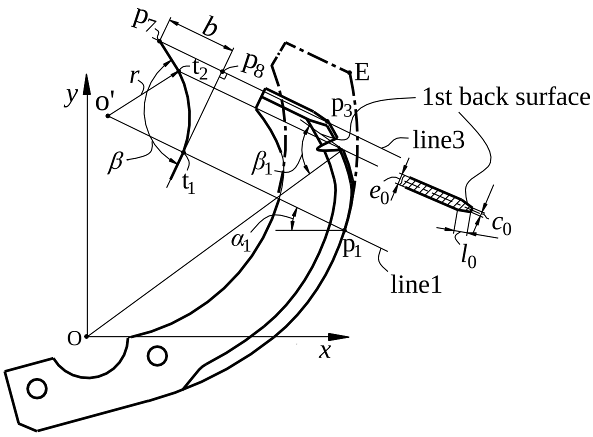

Fig. 4 - The schematic diagram of scoop angle

The design parameters of sidelong edge curve include cornerite of the apex of sidelong edge θ_E, the bending radius r; the bending angle β, scoop angle β_1, and the tilling width b. where, r is generally set as 30 mm, and β is generally set as 120°.

Since the length of the edge curve keeps constant before and after the bending deformation, there is:

$$A-\left(A-t_1t_2\right)\cos\left(180-\beta\right)-r\sin\beta = B \tag{5}$$

where:

A – the distance between E and p_5, and : $A = t_1p_7$, [mm];

B – the distance between E and p_3, [mm].

When the end point of lengthwise edge P_1 is known, dimensions of A and B contain only one unknown parameter θ_E, thus θ_E can obtained by equation (5).

Similarly, the tilling width b can be expressed as:

$$b=\left(A-t_1t_2\right)\sin\beta+\left(r-r\cos\left(180-\beta\right)\right),\ \text{[mm]} \tag{6}$$

According to literature *(Zhang Y., Yang L., et al., 2016)*, the scoop angle has the following expression:

$$\beta_1 = \arctan\left(\frac{(e_0 - c_0)\cos\varepsilon}{2\cos\left(\beta-\frac{\pi}{2}\right)\sqrt{l_0^2-\frac{(e_0-c_0)^2}{4}}}\right)+\arctan\frac{y}{x}+\alpha_1,\ \text{[degree]} \tag{7}$$

where:

e_0 is the blade thickness, [mm];

c_0 – edge width, [mm];

l_0 – edge surface width, [mm];

ε – the angle of plane conversion, [degree], and it is generally set as 60°;

(x, y) – the coordinate of a point after the sidelong edge is bended, [mm];

α_1 – the angle between bending line and x-axis, [degree], as shown in fig.4.

The CAD system of edge curve

The relevant design parameters of the rotary blade curve can be calculated in accordance with mathematical models. However, since some design parameters are interrelated and the mathematical models of some parameters are complex, lots of iterations are required to define the parameters. The CAD system of the edge curve is an important part of CAD system of the rotary blade. By developing the CAD system of edge curve, the design calculations can be greatly simplified, and the design efficiency can be greatly improved. The CAD system of the edge curve consists of subsystems of computing and graphics, and the program flow of the CAD system is shown in fig.5. The computing subsystem performs the calculation function of design parameters and the graphics subsystem performs the drawing function of blade curve designed.

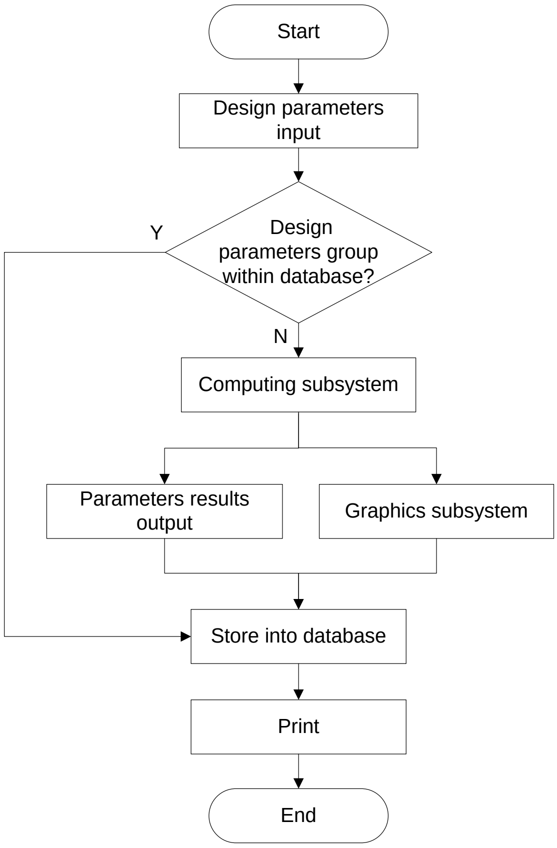

Fig. 5 - The program flow of CAD system

RESULTS

Interface of the CAD system

The main interface of the CAD system of edge curve of the rotary blade is shown in fig.6. Click the Parameters input button, and this will open a panel for parameters input; Close the Parameters input panel by clicking the Close button after parameters input; then click the Compute button in the main interface, and the design parameters of the edge curve that meet the design requirements will be obtained; then click the Print Button, and this will open a panel for displaying outline of the edge curve of a rotary blade, as shown in fig.7.

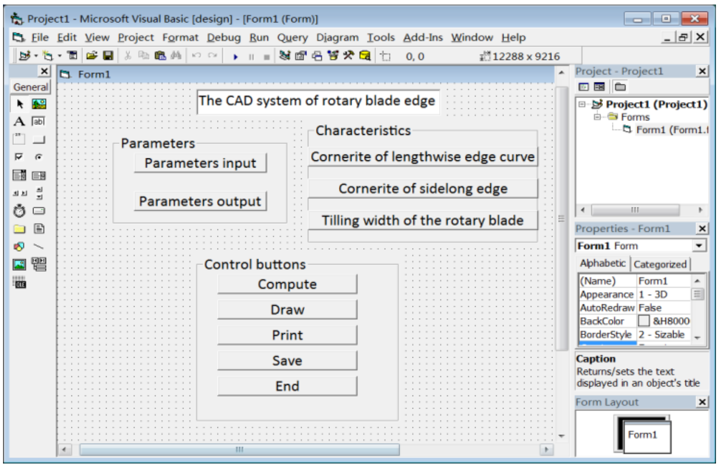

Fig. 6 – Main interface of the CAD system

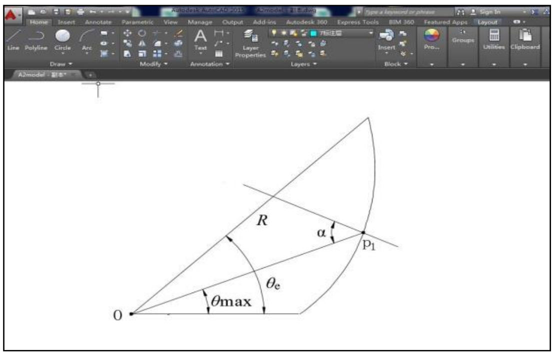

Fig. 7 – Interface of edge curve print

Accuracy verification of the CAD system

There are 2 ways in which we can obtain the final design parameters, namely by means of Excel calculation and CAD system. The former is obtained through direct calculation based equations of mathematical models of edge curve, and it needs much calculation and time for the calculation; the latter being obtained through iterations, accompanying by such errors as iterative error and approximation error, thus parameter values of CAD system output deviate from those calculated values. Take 3 main parameters of edge curve of the rotary blades, namely alpha angle α, the cornerite of the apex of sidelong edge θ_E and the tilling width b, for the accuracy verification, and the results of error analysis are shown in table 2.

Table 2

Error analysis

Rotary blade	Parameters	Results		
		Calculated (Excel)	Output (CAD system)	Relative error [%]
1	α [degree]	45.396	45.250	0.32
	θ_E [degree]	45.858	45.620	0.51
	b [mm]	61.524	61.457	0.32
2	α [degree]	46.426	46.20	0.44
	θ_E [degree]	47.020	46.836	0.39
	b [mm]	58.640	58.374	0.45
3	α [degree]	46.824	46.647	0.37
	θ_E [degree]	47.256	47.018	0.50
	b [mm]	56.284	50.062	0.39

As can be seen from table 2, the relative error of the system output and calculated values is at the level of 0.5%, which confirms that the accuracy of CAD system is good and it meets the design requirements of a handheld tiller's rotary blade.

Effects of parameters of edge curve on the performance of a rotary blade

By the CAD system of edge curve of the rotary blade, values of grass moving angle with different cornerite of lengthwise edge were obtained for the rotary blades with other parameters listed in table 1, as shown in fig.8. As can be seen from fig.8, for a preselected point on the edge curve with certain cornerite, the grassing moving angle of rotary blade 3 has the maximum value and those angles of rotary blade 2 and rotary blade 1 decrease sequentially. With the increase of cornerite of the lengthwise edge, the grass moving angle approximately increases linearly. The grass moving angle of the lengthwise edge for the rotary blades with parameters in table 1 ranges from 38.3 to 53.1°, and it is in the recommended range of 35- 55°, according to literature *(Hao X., Li Z., et al., 2014)*. The grassing moving angle contributes much to the performance of slip cutting and grass removing performance, and the bigger of grassing moving angle, the better of the performance of slip cutting and grass removing.

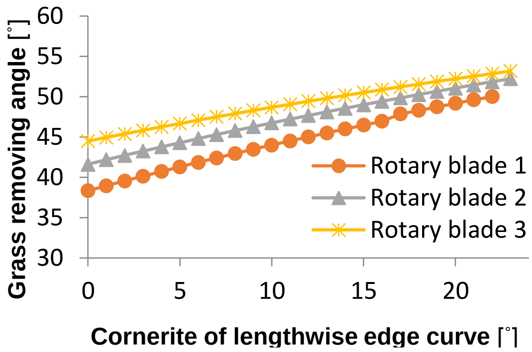

Fig. 8 - Grass removing angle of lengthwise edge curve

Similarly, values of scoop angle with different cornerite of sidelong edge were obtained by the CAD system for the rotary blades with other parameters listed in table 1, as shown in fig. 9. As can be seen from fig.9, for a preselected point on the edge curve with certain cornerite, the scoop angle of rotary blade 3 has the maximum value and those angles of rotary blade 2 and rotary blade 1 decrease sequentially. With the increase of cornerite of the sidelong edge, the scoop angle approximately increases linearly. The scoop angle of the sidelong edge for the rotary blades with parameters in table 1 ranges from 57.8 to 69.2° and it is in the recommended range of 55-75°, according to literature *(Sakai J. et al., 1984)*. The rotary blade is suitable for tilling in loam and clay loam, and it is consistent with the application situation of soil type of wet and sticky soil for the rotary blades studied.

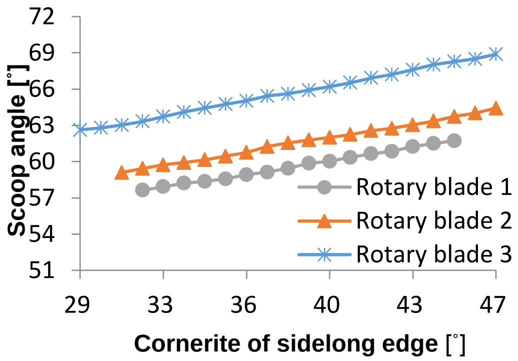

Fig. 9 - Scoop angle of sidelong edge curve

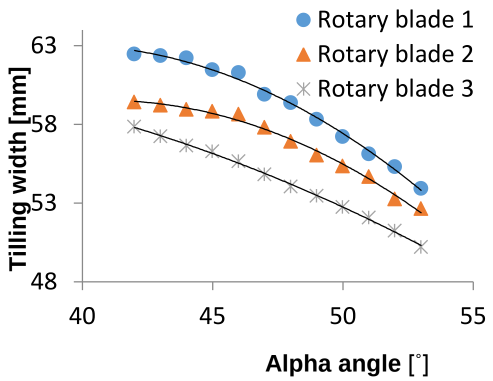

Fig. 10 - Tilling width of the rotary blade

Changing the alpha angle leads to the change of tilling width of a rotary blade, and this can be employed to obtain the required tilling width of the rotary blade. While keeping parameters of rotation radius of rotary blade, bending angle and bending radius, etc. constant, the values of tilling width of the rotary blades (listed in table 1) of different alpha angle were obtained by the CAD system, as shown in fig. 10. As can be seen from fig.10, with the increase of alpha angle, the tilling width decreases. According to the literature *(Chinese Academy of Agricultural Mechanization Sciences, 2007)*, the number of rotary blade of rotavator and production costs can be reduced by increasing tilling width. Nevertheless, tilling width that exceeds the suitable values will seriously affect the stiffness of rotary blade and pulverization, therefore the actual application requirements need to be considered while determining the tilling width.

CONCLUSIONS

(1) Based on mathematical model of edge curve, a CAD system of edge curve of the rotary blade was developed in this study. The relative error of the system output and calculated values is at the level of 0.5%, and it can meet the design requirements of a handheld tiller’s rotary blade.

(2) With increase of cornerite of the lengthwise edge, the grass moving angle approximately increases linearly. And the grass moving angle of lengthwise edge for the rotary blades with parameters in table 1 ranges from 38.3 to 53.1°, which indicates good performance of slip cutting and grass removing of the rotary blade.

(3) With increase of cornerite of the sidelong edge, the scoop angle approximately increases linearly. The scoop angle of sidelong edge for the rotary blades with parameters in table 1 ranges from 57.8 to 69.2°, which is consistent with the application situation of soil type of wet and sticky soil for the rotary blades studied.

(4) With increase of alpha angle, the tilling width of the rotary blades decreases. While keeping parameters of rotation radius of rotary blade, bending angle and bending radius, etc. constant, the required tilling width could be obtained by adjusting the alpha angle.

ACKNOWLEDGEMENT

The study was funded by Chongqing Science & Technology Commission (cstc2016shmszx80037), Ph.D. Research Project of Southwest University (SWU115011), and Fund from Key Laboratory of Modern Agricultural Equipment, Ministry of Agriculture, Republic of China (201601001).

REFERENCES

[1] Ding W., Peng S., et al., (1995), Study on the grassing moving of rotary blade and equation (旋耕刀滑切角及滑切角方程的研究), *Transactions of the Chinese Society of Agricultural Engineering*, issue 4, pp.67-72;

[2] Gai C., Dong Y., et al., (2011), Optimization of bending angle of rotary machine rotary tilling blade based on COSMOS (基于 COSMOS 的还田机械旋耕刀弯折角优化), *Journal of Agricultural Mechanization Research*, issue 3, pp.30-33;

[3] Hao F., Chang Y., et al., (2003), Farmland resource faced with challenge and its countermeasures for sustainable utilization in China (中国土地资源面临的挑战与可持续对策), *Nature Ecological conservation*, issue 4, pp.30-33;

[4] Hao X., Li Z., et al., (2014), Optimum design and experiment about parameters of rotary blade and rotavator (微耕机旋耕刀片及其刀辊的参数的优化设计与实验), *Farm Machinery*, issue 5, pp.155-158;

[5] Jun S., Hai L., Koichi L., et al. (1984), Tillage resistance characteristics of Japanese rotary blades– distribution of tilling resistance to the tipless (straight) blade and bending tip portion of a rotary blade, *Journal of the Japanese Society of Agricultural Machinery*, vol.46, issue 1, pp.593-598;

[6] Niu P., Yang L., Zhang Y., Gao B., Li Y., Yang M., (2015), Finite element analysis of the rotary blade of a mini-tiller based on ANSYS Workbench (基于 ANSYS Workbench 的微耕机用旋耕弯刀有限元分析), *Journal of Southwest University (Natural Science Edition)*, vol.37, Issue 12, pp.162-147;

[7] Peng B., Yang L., Yang M., Guo M., Ye J. Chen J., (2014), On connotation analysis and development countermeasures of the mini-tiller stand system (微耕机标准体系内涵分析及其发展对策), *Journal of Southwest Normal University (Natural Science Edition)*, vol.39, issue 4, pp.141-146;

[8] Saimbhi V., Wadhwa D., Grewal P.,(2004) , Development of a rotary tiller blade using three. -dimensional computer graphics, *Biosystems Engineering*, vol.89, issue 1, pp.47-58;

[9] Sakai J., Lam Van H., Iwasaki K., Shibata Y., (1984), Tillage resistance characteristics of Japanese rotary blades– distribution of tilling resistance to the tipless (straight) blade and bending tip portion of a rotary blade (ロータリ耕なたづめの耕うん抵抗特性-直刃部とわん曲部へのトルク分配), *Journal of the Japanese Society of Agricultural Machinery,* vol. 46, issue 1, pp. 593-598;

[10] Yue G., (2008), An elementary analysis to blade of a handheld tiller's rotary blade (微耕机配套用旋耕刀浅析), *Farm Machinery*, vol.1, issue 7, pp.50-51;

[11] Zhang Y., Yang L., et al., (2016), Study on the sloop angle characteristics of a handheld tiller's rotary blade (微耕机用旋耕弯刀正切刃背角特性研究), *INMATEH Agricultural Engineering Journal*, vol.49, issue 2, pp.5-12;

[12] ***Ministry of Industry and Information Technology of the P. R. China, (2013), Handheld tillers JB/ T 10266-2013 (微型耕耘机 JB/ T 10266-2013), China Machine Press, P. R. China;

[13] ***Chinese Standard Committee, (2008), Rotary tiller - rotary blades and blade holders, GB/T 5669-2008 (旋耕机械刀和刀座, GB/T 5669-2008), Chinese Standard Press, P. R. China;

[14] ***Chinese Academy of Agricultural Mechanization Sciences, (2007), *Agricultural Machinery Design Manua, (农业机械设计手册)*, China Agricultural Science and Technology Press, P.R. China;

[15] ***Chongqing Bureau of Quality and Technology Supervision, (2008), Blades of micro-cultivator, DB50/T 277-2008 (微耕机配套用旋耕刀, DB50/T 277-2008), Chongqing, P. R. China;

[16] ***Japanese Industrial Standards Committee, (2008), Blades for tillers, JIS B 9210-1988(2008 confirmed)(耕うんづめ, JIS B 9210-1988 (2008 確認)), Japanese Standards Association, Japan.

IMPROVEMENT OF EQUIPMENT FOR BASIC TILLAGE AND SOWING AS INITIAL STAGE OF HARVEST FORECASTING
/
ВДОСКОНАЛЕННЯ ТЕХНІКИ ДЛЯ ОСНОВНОГО ОБРОБІТКУ ҐРУНТУ ТА ПОСІВУ – ПОЧАТКОВИЙ ЕТАП ПРОГРАМУВАННЯ ВРОЖАЮ

Asst.Ph.D. Stud. Eng. Vasylkovska K.V., Lect.Ph.D.Eng. Leshchenko S.M.,
Lect.Ph.D.Eng. Vasylkovskyi O.M., Lect. Ph.D. Eng. Petrenko D.I.
Kirovohrad National Technical University / Ukraine;
Tel: +380667103625; E-mail: vasilkovskakv@ukr.net

Keywords: *harvest forecasting, chisel tillage, soil deformers, precision seeding, pneumatic and mechanical seeding*

ABSTRACT
The article presents the key tendencies of improving machines for subsoil basic tillage and sowing machines in order to implement resource-saving cultivation technologies and the basics of harvest forecasting. The suggested design of the combined chisel deep tiller with additional deformers and twin toothed rollers enable achieving better quality indicators of tillage while cultivating heavy soil. The new pneumatic and mechanical sowing device with peripheral layout of cells on the seeding disk and passive device for taking out excess seeds by centering method was developed. The new sowing device assures even distribution of seeds on the feeding area. The article presents key results of the research and recommendations for application of the suggested machines.

РЕЗЮМЕ
В статті наведені основні тенденції вдосконалення машин для безполицевого основного обробітку ґрунту та посівних машин з метою запровадження технологій ресурсозберігаючого землеробства і реалізації основ програмування врожаю. Запропонована конструкція комбінованого чизельного глибокорозпушувача із додатковими деформаторами та спареними зубчастими котками, використання якого дозволяє досягти покращених показників якості обробки під час роботи на важких ґрунтах. Для інтенсифікації посівних операцій розроблено новий пневмомеханічний висівний апарат з периферійним розташуванням комірок на висівному диску та пасивним пристроєм для видалення зайвого насіння відцентровим способом, що дозволяє забезпечити рівномірний розподіл насіння за площею живлення. В роботі представлені основні результати досліджень та рекомендації що до використання запропонованих машин.

INTRODUCTION
The basis of effective achievement of technologies of agricultural production is the forecasting of harvest which is based on the system of reclamation of productivity and soil protective technologies. Another important factor is the quality of seeds preparation, resource saving mechanization and production automation including effective plant protection from diseases, pests and weeds.

It is well-known that fertility is the ability of soil to feed plants with necessary quantity of nutrients, water, warmth and air (*Horunzhenko V.E., 1996*).Today we face constant lack of fertility which is the result of intensive cultivation, growing monocultures that exhaust soil and pollute the environment in Ukraine. Another important aspect is the decrease of organic stuff in the cultivated layer and systematic application of erosion-dangerous agricultural machines (*Horunzhenko V.E., 1996*). Therefore, the search for new technologies and ways of mechanization to preserve the fertility and decrease resource losses, preservation of the environment and growing ecologically safe products are the guarantee of rich harvests and welfare of the country.

Harvest forecasting is one of the important and prospective trends in production technologies particularly tilled crops that make possible to use material, labour and energy resources rationally to get maximum production with high quality (*Moroz N.V., 2011*). Today there are separate trends of harvest forecasting that help analyzing and assessing the quality of growing of tilled crops but the trends can only partially assist in the provision of quality and fertility of crop production (*Osadchij S.I., 2014*). Complete implementation of harvest forecasting technology into the real economic conditions is constrained by a range of problems which have to be solved complexly. One of the key problems is the choice of the tools for soil cultivation that provide the realization of the technologies of soil protection and resource saving agriculture including precision seeding as even distribution of seeds on the feeding area guarantees good harvest in future.

In order to implement the basics of harvest forecasting it is important to go through certain stages. The first step towards harvest forecasting is to choose moistness conservative, soil protective and energy saving cultivation. The second step is to prepare seeds for sowing and the third step is to assure equal distribution of seeds on the feeding area while sowing (*Vasylkovska K., 2013*; *Vasylkovska K.V., 2013; Vasylkovska K.V., 2014*).

To improve seed germination the qualitative cultivation should be done which helps to keep moistness due to destruction of soil and stimulating effective development of the plant root system because of the qualitative soil loosening of the cultivated layer.

Saving and restoring soil fertility is necessarily accompanied by a deep loosening of soil which minimizes the number of further tillage operations and provides conditions for humus accumulation (*Leshchenko S., 2014*). It should be noted that the application of traditional tools for basic tillage does not allow intensifying all factors that ensure effective increase and reproduction of fertility. Certain types of mechanical cultivation such as traditional mouldboard and disk ploughing, cultivation and rototilling can lead to intense biological destruction and compaction of soil, and it loses its structure. Taking into account the necessity of basic tillage in the conditions of high moistness as well as in dry conditions especially in the areas with possible erosions, the traditional methods of basic tillage cannot be used and the effective alternative method is subsoil tillage in the form of deep loosening (*Vetokhin V.I., 2008*; *Leshchenko S.M., 2013; Salo V.M., 2014*).

It is known that sowing should be done in certain agricultural periods. They influence the conditions of plant sprouting (even sprouting) and its further development. It is also connected with moistness and temperature of the upper soil layer. If the agricultural period of sowing is assured then there will be better sprouting.

Even sowing and even distribution of seeds assure not only good germination but also good harvest in future. Moreover, while increasing the evenness of seeds distribution on the feeding area we decrease the amount of weeds in the field.

Therefore, the issue of improvement of technical appliances for basic tillage and sowing can become the initial stage in harvest forecasting and practical solving of this task will enable increasing the competitiveness of crop products and implement the basics for soil protective and energy saving cultivation.

MATERIAL AND METHOD

The basis of minimal soil cultivation is a subsurface deep loosening which can be done with the help of chisel deep tiller *(Leshchenko S., 2014; Vetokhin V.I., 2008; Leshchenko S.M., 2013)*. Chiseling allows increasing the tilling width of the machine compared to ploughing and to decrease fuel losses for basic tillage (40-50%), destruct compacted subsoil layer. But there are some disadvantages in this operation including incomplete cutting of weeds, impossibility to achieve solid furrow sole after tillage, low level of incorporation of residues into the soil, weed seeds and fertilizers, creation of big clods on the surface of the field.

Chisel deep tillers produced in Ukraine and in the former Soviet countries are not much different from their foreign analogues but the quality of working elements and the material used for their production shorten the terms of exploitation. Taking into consideration scientific research in the sphere of technologies of subsoil tillage the Department of Kirovohrad National Technical University under the supervision of Professor Vasyl Salo designed the construction of the universal combined chisel adapted to the real soil and climatic conditions of Ukraine (Fig.1a).

The main working elements of the designed machine are chisel plough which consists of stem 7, spike 8, tooth for breaking clods 9 and the wings 10 (Fig. 1b). The additional working element is a twin toothed roller 4 (Fig.1a) which has the mode of tillage depth regulation as well as it breaks big clods, incorporates and mixes plant residues into lower layers at the depth of 15-20 cm. Depending on working conditions of the twin toothed roller, it is possible to adjust the chisel tilling depth and the intensity of mixing and crushing of residues after tillage.

While loosening of soil with chisel plough the spike 8 cuts solid soil, tooth 9 crushes clods intensively and takes them away from stem 7 and the wings 10 cut weeds and additionally crush the soil and depending on their adjustment can even the furrow bottom.

In its turn, the precision seeding is provided with dispensing element of the seed drills. Since the beginning of the twentieth century there have been made searches for constructions implying single-grain sowing. One of the first pneumatic and mechanical sowing machines was a seed drill with drum-digital dispenser designed in the USA in 1904 *(Patent US of America №773205, 1904)*. By their design, the pneumatic and mechanical appliances may be of disk or drum type, and by the way of their application they are divided into vacuum and extreme pressure devices.

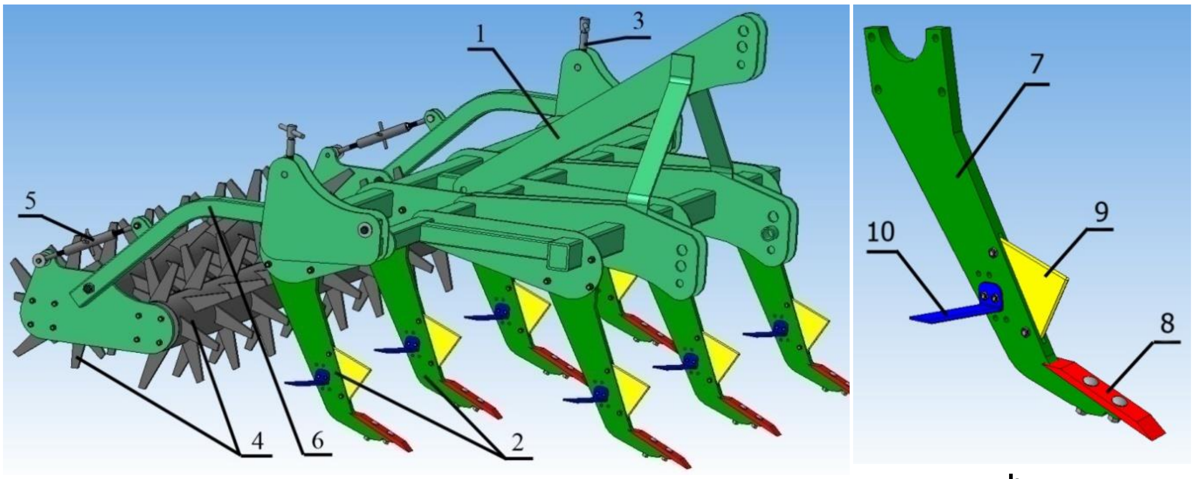

a b

Fig. 1 – Combined chisel deep tiller

a – general view of deep tiller ; b – 3D model of chisel plough
1 – frame; 2 – chisel plough; 3 – screw mechanism of adjustment of tillage depth; 4 – toothed rollers;
5 – screw mechanism of roller adjustment; 6 – roller frame; 7 – stem; 8 – spike; 9 – tooth; 10 – wing

Sowing machines that are used in mass production have insufficient dispensing capacity caused by limited seed disk rotary velocity and random uncontrolled redistribution of spacing between seeds in the furrow because of the high relative velocity of the seeds *(Horunzhenko V.E., 1996; Sysolin P.V., 2001; Vasylkovska K,. 2013)*. To increase the efficiency of seeding precision of cultivated crops the Department of Agricultural Engineering of Kirovohrad National Technical University designed and manufactured a prototype of the new pneumatic and mechanical disk for sowing device *(Vasylkovska K., 2013; Vasylkovska K.V., 2013; Vasylkovska K.V., 2014)* (Fig. 2).

The main feature of the new sowing device is the application of sowing disk 1 with peripheral layout of cells 2. Behind the cells there are blades 3 on the inner surface of the disk for enforced seizure of seeds by the disk 9 in the chamber and their further transportation to the release spot.

To remove excess seeds from the cells of seeding disk 1 at the top of the cylindrical surface of the body there is a passive cavity-shaped device 7, that gets excess seeds and separate them from the disk transporting the seeds back to the filling zone. In the lower part of the housing surface there is seeding hole 6 which provides free release of the seeds to the furrow.

The design of the pneumatic and mechanical disk sowing device due to the enforced seizure of seeds by blades 3 ensures the reliability of the process of filling the cells of the sowing disk and increases the efficiency of removal of excess of seeds with the help of passive device 7. It makes reliable the process of releasing seeds from the cells in the sowing area. This ensures an even distribution of seeds in the furrow through the stabilization of the dispensing process and releasing seeds from the sowing disk.

In order to confirm the hypothesis about the necessity of harvest forecasting we conducted testing of implementation of new highly efficient working elements for tilling and sowing machines in the system of resource-saving technologies of cultivation of agricultural crops.

Tests of combined chisel -deep tillers were conducted during 2013-2015 in the fields of Kirovohrad region. The conditions of testing corresponded to the average conditions in the region: mechanical soil texture was heavy and with medium loam; soil hardness was 20...35 kg/cm^2 at the depth of 0-10 cm, 35...65 kg/cm^2 at the depth of 10-20 cm, and 60...100 kg/cm^2 at 20-30 cm. Permissible humidity was limited to soil sticking to the chassis system of the tractor and working elements of the chisel. Technical characteristics of combined chisel deep tillers (Table 1) makes possible to assess their competitiveness in comparison with the best foreign analogues.

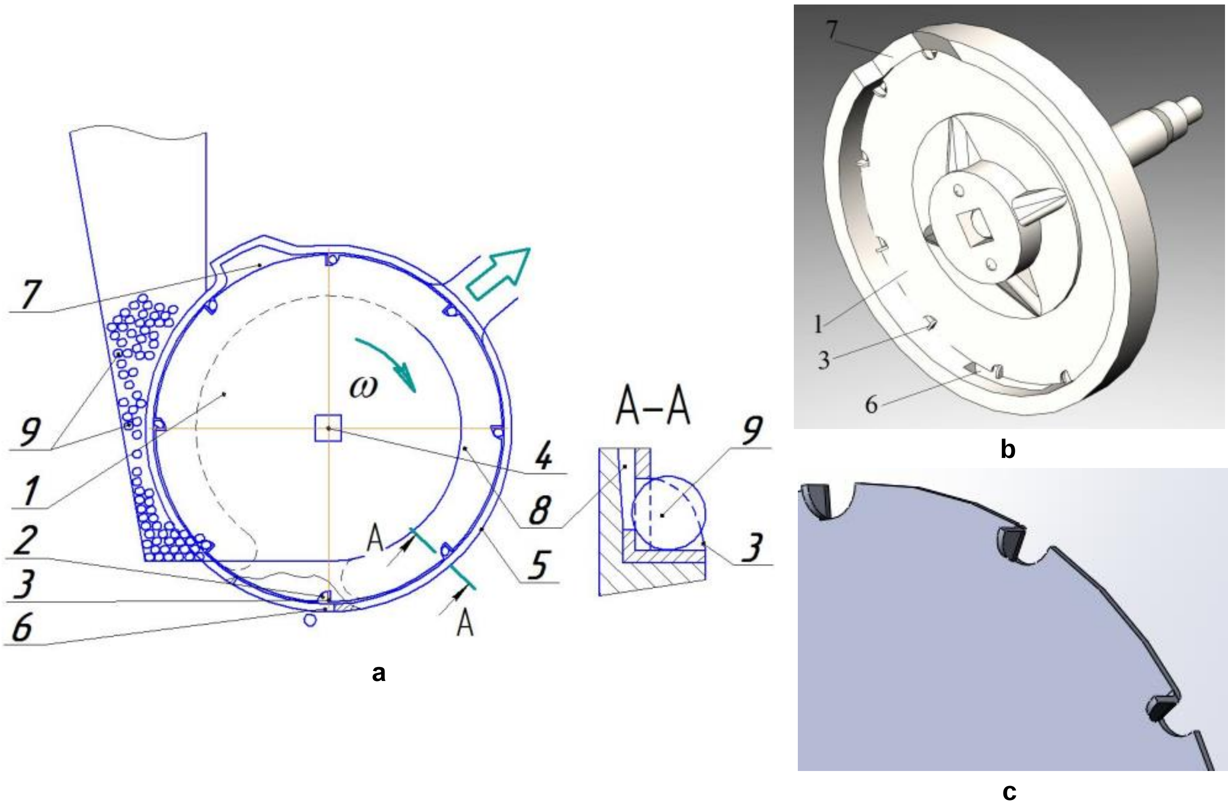

Fig. 2 – Pneumatic and mechanical sowing device
a – scheme; b – 3D model of the sowing device; c – 3D model of the fragment of sowing disk

1 – sowing disk; 2 – cell; 3 – blade; 4 – drive shaft; 5 – housing; 6 – seeding hole;
7 – passive device (container) for removing excess seeds; 8 – vacuum chamber; 9 – seeds

Table 1

Characteristics of combined chisel deep tillers

Machine-Type	CN-1,5	CN-2,5	CN-3,5	CN-4,5
Productivity, ha/hour	1.2	2.0	2.8	3.6
Working width, m	1.5	2.5	3.5	4.5
Tillage depth, cm	50	50	50	50
Number of working elements, pieces	3	5	7	9
Depth of roller tilling, cm	15	15	15	15
Necessary tractor power, HP	80 - 120	120-180	160-220	250-340
Weight, kg	750	1200	1700	2300

After deep loosening we made performance assessment by the coefficient of soil crushing and evenness of depth tilling. We considered structural elements of soil to be appropriate if they did not exceed the size of 50 mm. Also we conducted the assessment of the impact of speed rate on quality performance. The experiments were repeated five times and the results have average values.

The results of experimental studies to determine the quality indicator of loosening were evaluated at the depth of tilling h=32-40 cm. The height of the ridge that is formed between adjacent passages of chisel ploughs on the bottom of the furrow was $h1$=18-20 cm. The maximum speed of the machine was limited by critically possible speed at maximum transmission in specific soil and climatic conditions based on providing the necessary traction which is developed by tractor suspension system without tractor drive wheels slip. The analysis of the results (Fig. 3) shows that the lowest quality of soil crushing is achieved by chisel working without rollers and this figure ranges from 49% to 60%, and the increase of working speed improves quality indicator. Similar result is observed when chisel is used with one roller (operation with one roller is achieved by changing position of the adjusting screw 5 (Fig. 1)), but the quality indicators of the unit are much higher *k*=55-69%.

Field tests of experimental prototype of pneumatic and mechanical sowing device mounted on the serial seed drill section УПС-12 connected to the tractor MTZ-82 were conducted in fields of agro-industrial Group "Favorit" Ltd (Pidhaitsi of Kirovohrad district, Kirovohrad region) (*Vasylkovska K., 2015; Vasylkovska K., 2015*).

Sowing seeds of sugar beet variety «Yaltushkivskyy ЧС-72» was held on 2 ploughing beds with the area of 0.86 hectares each after ploughing and pre-seeding tillage. The speed of the tractor was 4.26 km/h on the first ploughing bed, and 7.24 km/h on the second bed. Sowing rate of seeds was 10.65 pc./line m. Checking the quality of sugar beet seeding was held on 10 scoring areas with the total length of 40 m.

Sowing seeds of maize variety «Orzhytsa 237 MB» was held on the ploughing bed with area of 0.43 hectares. Sowing rate of seeds was 7 pcs/line m. Sowing seeds of soybean variety «Jubilee» was held on the ploughing area of 0.43 hectares. Sowing rate of seeds was 10 pcs/line m.

Quality control of corn and soybeans sowing was held on 5 scoring areas with the total length of 20 m.

Quality of seeding was estimated by the coefficient of variation υ of distribution of seeds along the length of the row which shows standard deviation to the arithmetic mean of the plurality and variability is considered to be small if the coefficient of variation is not higher than 10%, the average variability is more than 10% but less than 20%, and significant variability is with the coefficient of variation of 20% (*Voytyuk P., 2005*).

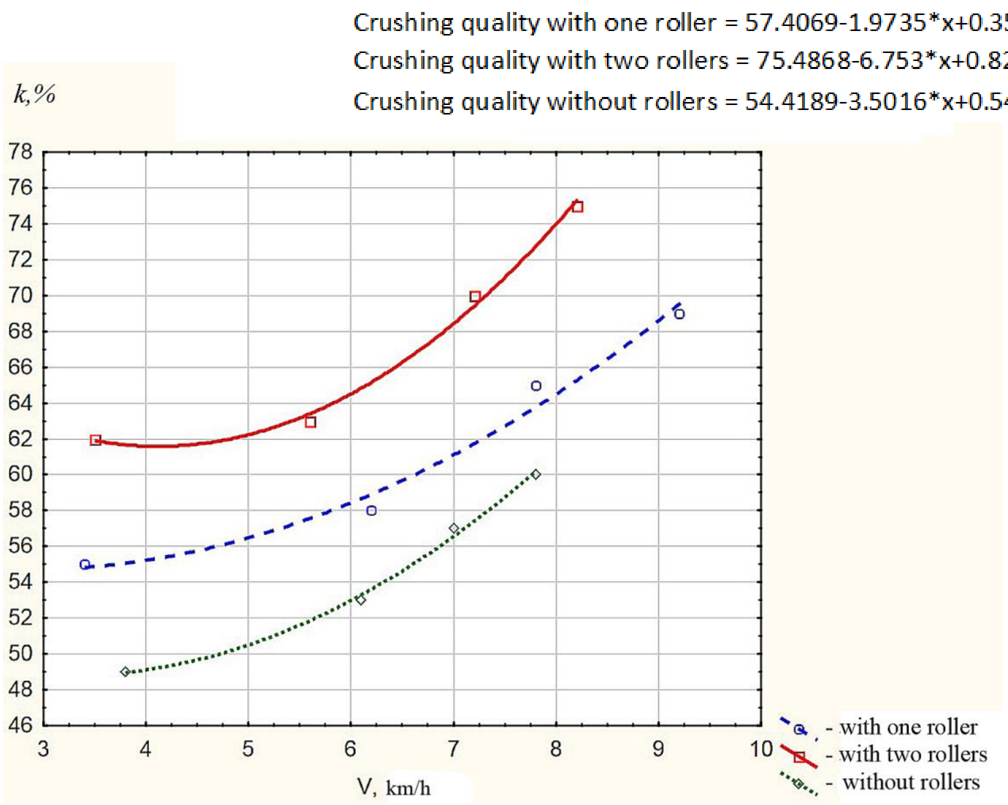

Fig. 3 – Correlation of the quality of soil crushing *k* on the chisel working speed *V* in different modes of operation of the twin toothed roller

RESULTS

After analyzing the results of experimental studies of combined chisel unit which operates in the conditions of heavy and medium loam it is possible to state that the most efficient soil tillage is achieved during chiselling with two rollers at the speed of 7-8 km/h. Quality indicator of crushing soil in these conditions is 70-75% which is higher than the corresponding figures of some foreign machines (for example, under heavy black soil conditions for Artiglio S 250-500 «Gaspardo» *k*=55-60%, Cenius 400/18 «AMAZONE» *k*=58-65% (*Leschenko S., 2014; Leshchenko S., 2015*).

Quality assessment of sowing sugar beets showed the following results (Fig. 4):

- the first ploughing bed showed that coefficient of variation of distribution of sugar beet seeds along the length of the row was 10.3% for the prototype and 14.6% for the serial;

- the second ploughing bed showed that coefficient of variation of distribution of sugar beet seeds along the length of the row was 9.8% for the prototype and 18.4% for the serial.

Quality assessment of sowing maize and soy seeds showed the following results (Fig. 4):

- coefficient of variation of distribution of maize seeds along the length of the row was 11.2% for the prototype and 14.4% for the serial;

- coefficient of variation of distribution of soy seeds along the length of the row was 9.8% for the prototype and 15.9% for the serial.

The results of testing of sowing device of the suggested design showed that the coefficient of variation of distribution of seeds in the furrow in all cases has little variation (compared with serial type). This fact confirms the hypothesis of stabilization of seeding parameters.

CONCLUSIONS

In summary, we can state that deep loosening by chisel deep tiller is an alternative to the traditional tillage which improves water and air condition of soil, reduces biological destruction of useful soil components, ensures the destruction of compacted subsoil and reduces energy costs for conducting basic cultivation. The design of the universal combined chisel significantly expands the possibilities of its use in various operations of deep loosening with additional possibility to crush clods and incorporate crop residues to a certain depth by the twin roller as well as the traditional chiselling and soil slotting. It was established that the combined chisel of the proposed construction with two toothed rollers has quality index of crushing soil *k*=68-75% at the speed of the machine *V*=7-8 km/h.

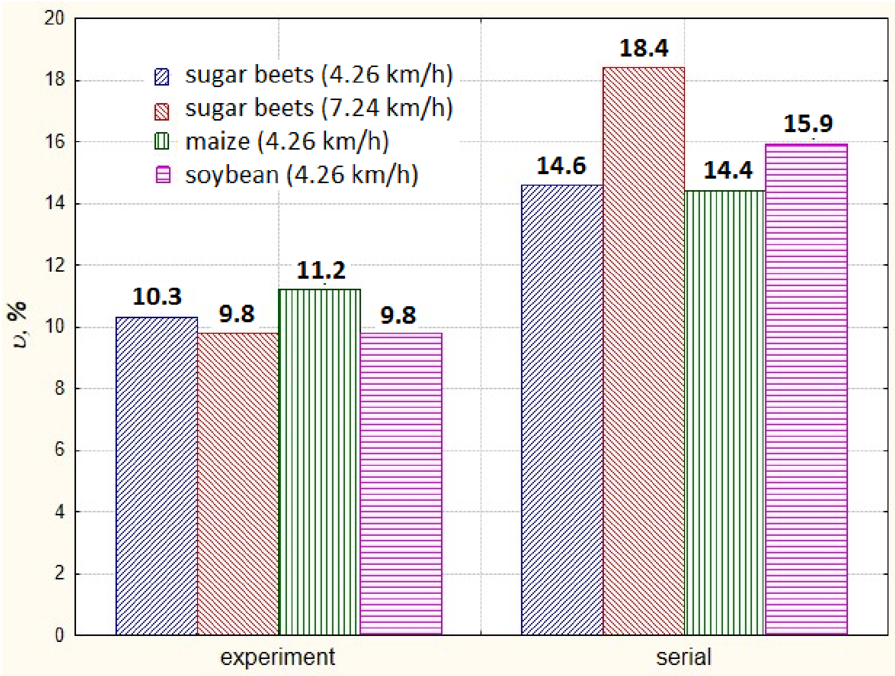

Fig. 4 – Variation of distribution of seeds of the studied cultivated crops in the row for the prototype and serial sowing units

The experimental studies of the pneumatic and mechanical seed drill for precision seeding with new pneumatic seeding device with peripheral layout of cells on the seeding disk and passive device for removing excess seeds by centrifugal method proved a more even distribution of seeds in a row. The application of new pneumatic and mechanical sowing machine allows reducing seed costs while maintaining high quality seed distribution in the line, thus even seed distribution on the feeding area. The coefficient of variation of distribution of sugar beet seeds in the furrow υ=9.8...11.2 at minor variation is possible with the following parameters: dilution in the vacuum chamber ΔP - from 0.2 to 0.3 kPa (*Vasylkovska K.V., 2016*), the rotary velocity of cells of the seeding disk $V_к$ from 2.0 to 2.5 m/s, and the speed of the sowing unit V_c 1.0 to 2.0 m/s.

Therefore, consistent implementation of the designed devices in the processes of growing crops will practically enable achieving certain basic techniques of harvest forecasting in the system of soil protective and resource saving agriculture.

REFERENCES

[1] Horunzhenko V.E., (1996), Concept of development of sowing technologies and new generation of machines for the industrial and farming establishments, *Theory and methods of creating soil-cultivating machines: Collection of scientific works NPO "Lan",* pp. 6-19, Edited by Academician of the Academy of Engineering Sciences of Ukraine V.E., Horunzhenko, Kirovohrad/Ukraine;

[2] Leschenko S., Salo V., Petrenko D., (2014), Experimental estimate of the efficiency of basic tilling by chisel equipment in the conditions of soil, *Design, production and operation of agricultural machines. A national interdepartmental scientific and technical collection of works,* Vol.44, pp.237-243, Kirovohrad/Ukraine;

[3] Leshchenko S., Salo V., Petrenko D., (2015), Assessment of quality of the operation of the combined chisel with additional horizontal and vertical deformers, *Journal of Kharkov National Technical University named after P. Vasylenko*, Vol.156*,* pp. 25-34, Kharkiv/Ukraine;

[4] Leshchenko S., Salo V., Vasylkovskyi A., (2014), Present situation and the prospects of intensification of operation of chisel tools in order to keep natural fertility, *MOTROL. Commission of motorization and energetics in agriculture. An international journal on operation of farm and agri-food industry machinery*, Vol.16, No 2, pp. 195-201, Lublin-Rzeszów / Poland;

[5] Leshchenko S.M., Salo V.M., (2013), Technical approach in preservation of soil fertility in the system of resource saving technologies, *Design, production and operation of agricultural machinery*, *A national interdepartmental scientific and technical collection of works,* Vol.43, Part 1, pp. 96-102, Kirovohrad/Ukraine;

[6] Moroz N.V., (2011), Harvest forecasting and quality of grain cultures, *Bulletin of the National University "Lviv Polytechnic", "Computer systems and networks",* №717*,* Lviv/Ukraine, pp. 105-107;

[7] Osadchij S.I., Macuj A.M., Zubenko V.O., (2014), Modernized Multidimensional Wiener Filtering of Navigational Information with Correction of Noise, *IEEE 3 rd International Conference «Methods and Systems of Navigation and Motion Control»,* pp.50-53, Kyiv/Ukraine;

[8] Patent US of America №773205, dated October 25, 1904, *Seed-planting machine*, George William Green, New York/USA;

[9] Salo V.M., Bohatyrev D.V., Leshchenko S.M., Savytskyi, (2014), National technical support of modern processes in plant growing, *Engineering and Technology of APK*. *Scientific and production journal,* №10 (61), pp. 16-19, Kyiv / Ukraine;

[10] Sysolin P.V., Salo V.M, Kropivnyy V.M., (2001), Agricultural machines: theoretical bases, design, engineering, Book 1. *Arable farming machines*, Edited by Chernovol M.I., p.384, Kyiv/Ukraine;

[11] Vasylkovska K., Petrenko N., Goncharova S., (2013), Rationalization of the design scheme of pneumatic and technical device for precision seeding of the seeds of cultivated cultures, MOTROL. Commission of motorization and energetics in agriculture. *An international journal on operation of farm and agri-food industry machinery,* Vol.15, No.2, pp.99-105, Lublin Rzeszów/Poland,;

[12] Vasylkovska K., Vasylkovskyy O., Anisimov O., Trykina N., (2015), Research of pneumatic sowing machine with peripheral cells location and inertial superfluous seeds extraction, *Econtechmod. An international quarterly journal*, Vol.4, No.4*,* pp. 85-89, Lublin-Rzeszów/Poland;

[13] Vasylkovska K.V., Petrenko M.M., Goncharova S.Y., (2013), Analysis of operation of pneumatic and mechanical sowing device with peripheral layout of cells *Design, production and operation of agricultural machines. A national interdepartmental scientific and technical collection of works,* Vol.43, Part 1, pp. 18-22, Kirovohrad/Ukraine;

[14] Vasylkovska K.V., Vasylkovskyi O.M., Moroz S.M., (2015), Field testing of pneumatic and mechanical seed drill with the suggested seeding device, *Collection of scientific works of Lutsk National Technical University: Agricultural machinery*, Vol.30*,* pp.32-36, Lutsk/Ukraine;

[15] Vasylkovska K.V., Vasylkovskyi O.M., Petrenko M.M, (2016), Assessment of quality of sowing by pneumatic and mechanical seeding device with a peripheral layout of cells and inertial remove of excess seeds, *Mechanization and electrification of agriculture*, Vol.3 (102), pp.147-157, Glevakha/Ukraine;

[16] Vasylkovska K.V., Vasylkovskyy O.M., (2014), Influence of the shape and type of seed cells drive on the quality of dispensing seeds, *Eastern European Journal of latest technology*, Vol.6, No.7 *(72),* pp.33-36, Kharkov/Ukraine;
[17] Vetokhin V.I., (2008), Systematization of working elements for soil loosening based on physics process, *Techniques APK*, No.9-10, pp.21-25, Kiev/Ukraine;
[18] Voytyuk P., (2005), Preconditions of the future harvest of sugar beets: seeds quality, performance pre-sowing tillage and seeding. *Propozytsia,* № 4*,* pp.17-19, Kyiv/Ukraine.

EXPERIMENTAL STUDY ON CUTTING CHARACTERISTICS OF CORN SEEDLING SEPARATOR WITH PAPER POT

/

玉米纸钵盘分苗机构切割特性试验研究

Ph.D. Hu Jun [1)], B.S. Song Yujie [1)], Ph.D. Li Hailiang [1)], B.S. Fu Qiang [1)], Ph.D. Khokan Kumer Sarker [2)]

[1)]College of Engineering, Heilongjiang BA YI Agricultural University, Daqing / China;

[2)]Bangladesh Agricultural Research Institute, Dhaka / Bangladesh

Tel: +86-187-45957355; E-mail: 18745957355@163.com

Keywords: *corn, paper potted seedlings, seedling separator, cutting force*

ABSTRACT

Seedling picking is important in corn transplantation and can directly influence the efficiency of transplanters. To avoid high injury rate caused by the seedling picking system to separate seedlings and the pot, a pot separator that can cooperate with tube transplanters was designed. First, design requirements of the pot separator were proposed according to corn transplantation demands and the characteristics of the paper pot. Second, based on the transplantation technology of paper potted cultivation, 35-day potted corn seedlings were chosen as test materials. Finally, the cutting characteristics of the paper pot were experimentally studied using a home-made cutting device and a microcomputer control electronic universal testing machine. Results showed that soil with 60%–67% soil moisture content is more suitable for potted corn seedlings. Single paper pot cutting in the shearing mode had the highest integrity and the damage rate was lower than 5%. The conditions to obtain the minimum cutting force of the paper pot were: 63%–67% soil moisture content, 500 mm/min cutting speed, and 30° cutting angle. The cutting force decreased with the increase of soil moisture content, and the maximum cutting force decreased with the increase of cutting speed. Research results provide reference for future optimization of the pot separator and are significant for promoting the development of fully automated corn transplanters.

摘要

取苗是玉米移栽过程中的重要工序，直接影响移栽机的工作效率。为了避免取苗机构将秧苗和钵盘分离导致伤苗率高等问题，设计了一款可与导管式移栽机配合使用的分钵机构。首先，根据玉米移栽农业要求和纸钵盘特点，提出分钵机构的设计要求。其次，基于纸质钵育移栽技术，培育苗龄 35 天左右的玉米钵苗为试验材料。最后，利用自制的切割装置和微机控制电子万能试验机等设备对纸钵盘切断特性进行了试验研究。结果表明：含水率在 60%-67%之间的育秧土更适宜培育玉米移栽钵苗；剪切方式切割玉米纸钵盘后的单钵完整度高，破损率低于 5%；玉米纸钵苗切断力最小的条件：含水率为 63%—67%，切割速度为 500mm/min，切割角度为 30°；切割力随着含水率的升高而减小，切割力最大值随着切割速度的增大而减小。研究结果为以后分钵机构的优化提供了参考，对推进全自动玉米移栽机的发展具有重要意义。

INTRODUCTION

Corn is not only considered a main grain crop but also an important raw material for chemistry, fuel, and other industries. Compared with direct sowing, transplantation increases accumulated temperature that can accelerate the sowing time, prolong the growth period of crops, and increase corn yield and quality (*Xiang W, et al., 2015; Lu Y T, et al., 2011*). Most corn transplanters are semiautomatic (*Cui W, et al., 2015; Yu X X, et al., 2014; Xu B X, et al., 2015*) and require manual cultivation of seedlings, which is labor intensive and has low efficiency. The existing fully automated transplanters (*Shi T, 2015*) have complicated structures and are expensive, which prevents the large-scaled promotion and application of mechanized transplantation.

Seedling picking mechanism is an important component of fully automated transplanters and distinguishes the fully automated transplanters from the semi-automatic ones. Fully automated transplanters mainly have the pick-up and push-out types. In foreign countries, Kumar designed a double row vegetable transplanter for paper pots, which was highly customizable and had an 81% working efficiency (*Kumar G, et al., 2011*). Tian S B designed a fully automated transplanter for vegetables and flowers based on the PLC system (*Tian S B, et al., 2010*). Some studies have studied the law of motion of planetary gear trains in the seedling separator and navigation control algorithm of the transplanting robot.

They found that the structure was relatively complicated (*JOVAN D, et al., 2011; Tong-jie Li, et al., 2012; Zhou Z Y, et al., 2014; Li S, et al., 2014; Zheng F Y, et al., 2016*). Mao Hanping et al. designed a seedling picking mechanism, but the mechanism failed to integrate the mechanical structures of the pot (*Mao H P, et al., 2011*). In China, Yu Gaohong (*YU G H, et al., 2011*) designed an incomplete intermittent driving planetary gear system with a non-circular gear, which realized the non-uniform velocity rotation of the planet gear relative to the planet carrier. Li Hua (*Zhang L, et al., 2014*) developed an automatic control system for a clamp plug-seedling picking mechanism by a single chip. Zhang Min (*Zhang M, et al., 2014*) simplified the overall structure, and designed a crank sliding push-out device with a connecting rod without a seedling delivery system. Liu Weixiang (*Liu W X, et al., 2016*) et al. designed a push-out and pick-up automatic seedling picking system, which resulted in a seedling picking rate of 98.44% and a matrix loss ratio of 36.67 %. Yan Xiaoyue et al. developed a row seedling picking transplanter based on cucumber seedlings (*Yan X Y, et al., 2013*), which increased the automation and efficiency of the transplanter. Liao Qingxi et al. designed a potted seedling separator with a conveyer belt for grape seed oil (*Liao Q X, et al., 2015*) and conducted a pot integrity test under different extrusion modes; seedling separation efficiency was at 90%. Yu Lei et al. designed a double row fully automated corn transplanter with a paper pot (*YU L, et al., 2015*), which had a planting missing rate of less than 3%. However, this transplanter had high standardization requirements on the seedling container. All of these machines have to pick up seedlings from the pot and the seedling separator has to contact with the matrix, which can damage the matrix and the seedling root system to different extents.

To avoid damages to pot and seedlings caused by the machine, a pot separator that directly cuts pots was designed. The cutting characteristics of the paper pot separator were studied using the mechanical engineering research method. Research results provided references for the succeeding optimization design of the seedling separator.

MATERIAL AND METHOD

Overall design of the seedling separator

The seedling separator could transplant potted corn seedlings without separating the pot and seedling, which increases efficiency and ensures the high survival rate of seedlings. According to the service conditions and agricultural requirements, the following technological requirements were proposed to the seedling separator:

(1) Replace manual seedling separation to reduce labour intensity and increase production efficiency.

(2) Meet the requirements of corn transplantation by cutting a single row of paper potted seedlings into single potted seedlings and orderly delivering it to the seedling guide tube.

(3) Avoid the seedling pot separator and protect the corn root system to increase the survival rate of transplanted corn seedlings.

To accomplish pot separation and deliver single pots to the seedling guide tube orderly, the overall design of the seedling separator was proposed according to these technological requirements. The seedling separator consists of a cutter, a transporter, and a rack (Figure 1). The cutter is the main part of the seedling separator and the object of this study.

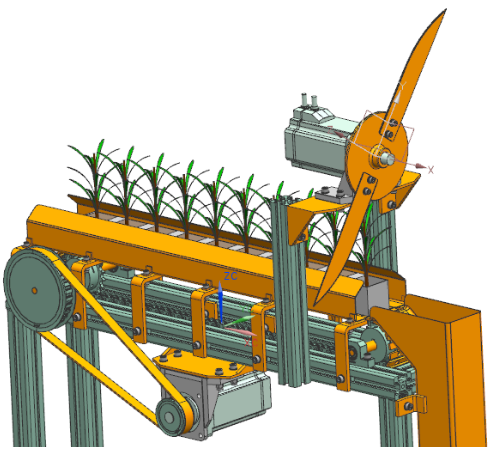

Fig. 1 - Three-dimensional assembly map of the seedling separator

The disc cutter cuts the paper pots at a uniform rotation speed. The conveying chain makes intermittent movements. It stops moving when cutting paper pots and delivers cut paper pots to the seedling guide tube. The disc cutter is above the transporter end and consists of a disc cutterhead and two symmetric cutting edges. The cutting edges are connected to the cutterhead by bolts. During the cutting rotation, each cutting edge passes through the space between the conveyer belt end and the inclined gusset plate.

Finite element analysis on the cutting edge

The finite element analysis on the cutting edge was performed by UG. The cutting edge was made of 65 MN steel, and the applied force was 100 N. Deformation and deformation displacement of the cutting edge are shown in Figure 2. The deformation was recorded at <0.099 mm, which is small and negligible. This datum provides the reference for the next experimental verification.

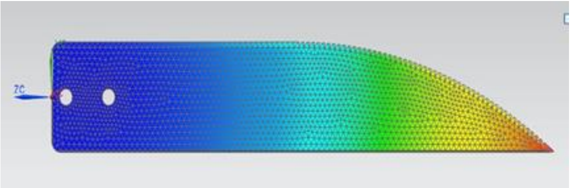

Fig. 2 - Finite element analysis of the cutting edge

Test materials

The square paper pots used in the experiment were designed by the Heilongjiang Bayi Agricultural University. They are made by the compaction of paper and thin film with 10 connected pots in one row (Figure 3). Paper pots ensure material biodegradability, low injury rate to seedlings, and high survival rate of transplanted seedlings. Compared with plant pots, paper pots are easier to cut and consume less dynamics. Square pots have smaller intervals than columnar ones, which is beneficial for the root growth of seedlings because of the uniformity in water distribution and their larger matrix capacity.

Fig. 3 - Paper pot

Fig. 4 - Paper potted seedlings

Paper pots are degradable and have excellent strength. Pot sizes are listed in Table 1. In this experiment, about 35-day paper potted seedlings were chosen as test materials (Figure 4).

Table 1

Size parameters of corn paper pots

Name	Numerical value
Overall size (Length*Width*Height) [mm]	500*38*38
Single pot Size(Length*Width*Height) [mm]	45*38*38
Holes	10
Rows	1
Cutting wall thickness [mm]	5

Experimental equipment

Soil moisture content was tested by a drying oven and a balance. The paper pot cutting test was done using the universal testing machine and the home-made cutting device. Consistent initial cutting position was maintained under the assistance of scale calibration. Experimental equipment used are as follows:

(1) Pot cutter device. Figure 5 is the bending cutter device that cuts pots by applying stress on the upper pot surface through the press cake. Figure 6 is the shearing cutter device that cuts pots using the cutting edge.

(2) WDW-200E microcomputer control electronic universal testing machine. The maximum test force was 200 KN.

(3) JD series multifunctional electronic balance with an accuracy of 0.001 g.

(4) Scale with an accuracy of 1 mm.

(5) DGG-9070B electric heating constant temperature air dry oven.

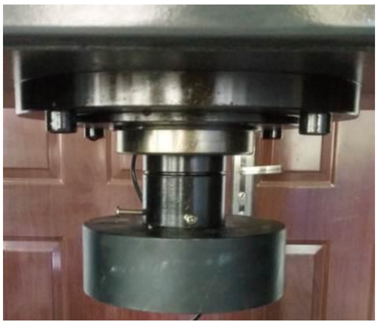

Fig. 5 - Bending cutter device

Fig. 6 - Shearing cutter device

Test method

Soil moisture content measurement by drying method

Soil samples were dried in the 105°C dry oven with constant weight. Carbonization of the organic matter in soil is easily obtained over high temperature. Soil samples were then placed into a dry glass container and covered to cool to room temperature. Soil moisture content was calculated. Soil moisture content was obtained from a single-factor experiment as presented in this calculation formula:

$$P(\%) = \frac{B-C}{C-A} \times 100 \quad (1)$$

where P is soil moisture content, A is the weight of aluminum specimen box (g), B is the weight of wet aluminum specimen box (g) and C is the weight of dry aluminum specimen box (g).

Bending cutting of corn paper pots

Pots are placed on the platform during bend cutting, while the waiting pot for cutting is suspended out of the platform. This process provides a uniform load from the universal testing machine until the pot is damaged completely (Figure 7). The initial descending position was kept constant by using a straight ruler.

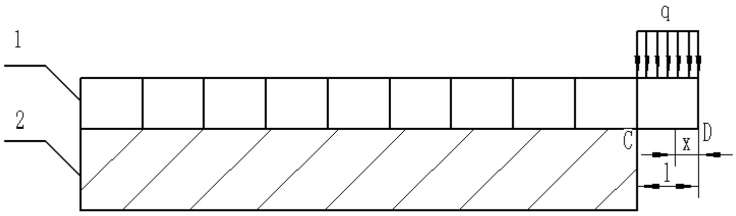

1. Paper pots 2. Platform

Fig. 7 - Bending cutting of corn paper pots

In the bending failure experiment, pots on the platform bear no stress, and the suspending pot is equal to the cantilever with a uniform load. According to the bending stress analysis of the cantilever, shearing force and bending moment on any section of the suspending pot can be presented as:

$$\mathrm{F}(x) = qx (0 \le x < l) \text{ [N]} \quad (2)$$

Where q is uniformly distributed load, [N/m]; x - extended length, [m]

$$\mathrm{M(x)} = -\frac{qx^2}{2} (0 \le x < l) \text{ [Nm]} \quad (3)$$

where point C has the largest shearing force, $F=ql$, and the largest bending moment, $M_{max} = ql^2/2$.

Thus, point C is considered a dangerous section and the suspending pot can break at point C.

The positive bending stress on any section of a single suspending pot is:

$$\sigma = \frac{M_x}{W_z} \quad (4)$$

σ is bending normal stress, [N/m^2];

M_x — bending moment of the section whether point *X* is in [Nm];

W_z — coefficient of the bending section [m^3]

Pots are uniform and W_z is a fixed value. Pots are cut when point C reaches the critical positive bending stress.

Shear cutting of corn paper pots

In the shear cutting experiment, pots are placed on the testing platform and the pot lined up for cutting is suspended out of the platform (Figure 8). Applied loads are concentrated at the pot located on the platform edge, that is, the section where point *C* is in, thus stress at point *C* quickly increases to the critical positive stress. The pot breaks at point *C*, thus completing the cutting process.

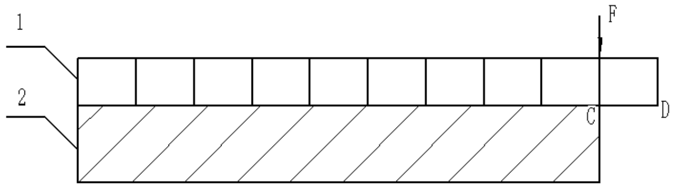

1. Paper pots 2. Platform

Fig. 8 - Shear cutting of paper pots

Orthogonal test

According to the orthogonal test, soil moisture content, cutting speed, and cutting angle (the angle between the interface of two paper pots and the plane of cutting edge) were considered the influencing factors. Corn paper pots were numbered in sequence. Soil moisture content, cutting speed, and cutting angle of each paper potted seedling are shown in Table 2.

Table 2

Levels of test factors

Factors	**Levels**		
	1	**2**	**3**
Soil moisture content A [%]	60–63	63–67	67–70
Cutting speed B [mm/min]	200	350	500
Cutting angle C [°]	10	20	30

RESULTS

Effect of cutting mode on pot integrity

Figure 9 shows the bending failed pot. The pot has serious deformation failures and random breakage position, which is inappropriate for transplanting. The shear failed pot is shown in Figure 10. The potted seedling retains high integrity, regular cutting section, and an injury rate that is lower than 5%. Therefore, shear cutting shall be adopted.

Fig. 9 - Potted seedling after bending failure

Fig. 10 - Potted seedling after shear failure

Effect of soil moisture content on cutting force

Based on agricultural requirements, soil moisture content for corn transplantation should be kept at 60–70%. Potted seedlings were cultivated under three different soil moisture contents. Each of moisture content was tested three times, and the mean was obtained. The variation curve of the cutting force with time is shown in Figure 11. According to the test data, the pots with 67–70%, 63–67%, and 60–63% soil moisture content require a cutting form of 48 N, 53 N, and 58 N, respectively, which indicates that cutting force is negatively correlated with soil moisture content. This decrease in cutting force is due to the reduction of soil cohesion as the thickness of the water film surrounding soil particles increases when soil moisture content increases.

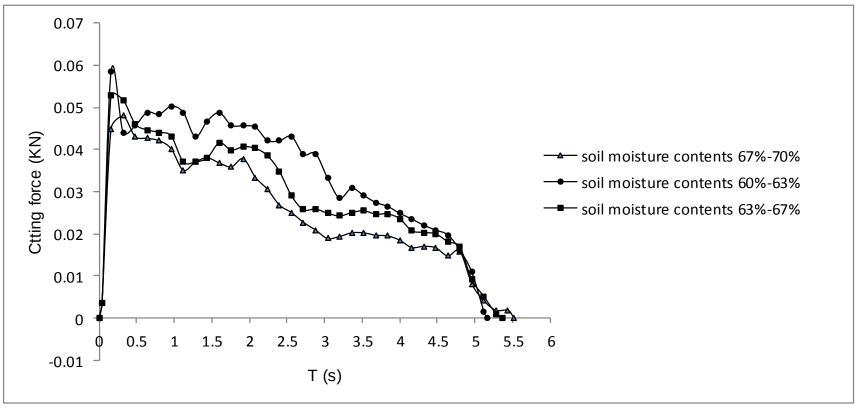

Fig. 11 - Variation of cutting force with time under different soil moisture contents

After cutting, potted seedlings with 60–67% soil moisture content showed the lowest injury rate, and cut pots maintained high pot integrity. The potted seedlings with 67–70% soil moisture content reached an injury rate of 10% because of the high soil moisture content and high porosity, which prevents high pot integrity after cutting. Based on the results, corn pots with 60–67% soil moisture content are appropriate for cultivation of corn seedlings.

In general, cutting force increased first and then decreased as the cutting depth of the pot increased. The maximum cutting force was between 50–70 N, while the maximum cutting force loaded by the cutter in the finite element analysis was smaller than 100 N. This result confirmed that the cutter design was reasonable. The cutting force reached the extreme value at 0.5 s of contact between the cutter and the pot. The desired cutting force gradually declined until the failure process ended.

Effect of cutting speed on maximum cutting force

The variation of the maximum cutting force with the cutting speed is shown in Figure 12. Maximum cutting force decreased to some extent with the increase of cutting speed. With the increase of cutting speed, the time for contact deformation of the pot shortened and the cutting force decreased, which also decreased the maximum cutting force.

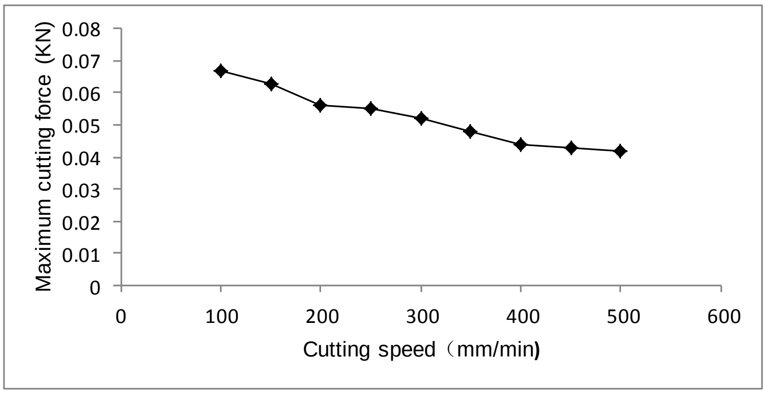

Fig. 12 - Variation of maximum cutting force with cutting speed

Orthogonal test results

According to the factors and levels selected, a three-factor, three-level orthogonal test was carried out. The test plan and results are shown in Table 3.

Table 3

Test plan and results of the three factors and three levels

Test No.	Factors			Integrity η (%)	Cutting force F (N)
	A (%)	B (mm/min)	C (°)		
1	1 (60-63)	1 (200)	1 (10)	96	62
2	1 (60-63)	1 (200)	1 (10)	95	62
3	1 (60-63)	2 (350)	2 (20)	97	57
4	1 (60-63)	2 (350)	2 (20)	96	59
5	1 (60-63)	3 (500)	3 (30)	96	52
6	2 (63-67)	3 (500)	1 (10)	97	52
7	2 (63-67)	1 (200)	1 (10)	96	60
8	2 (63-67)	2 (350)	2 (20)	96	57
9	2 (63-67)	3 (500)	2 (20)	97	50
10	2 (63-67)	3 (500)	3 (30)	96	46
11	3 (67-70)	1 (200)	1 (10)	90	48
12	3 (67-70)	1 (200)	1 (10)	91	50
13	3 (67-70)	2 (350)	2 (20)	90	47
14	3 (67-70)	2 (350)	2 (20)	89	49
15	3 (67-70)	3 (500)	3 (30)	90	46

As shown in Table 3, cutting speed is the most important influencing factor of cutting force. Conditions to achieve the minimum cutting force of corn paper pot are A2B3C3: 63–67% soil moisture content, 500 mm/min cutting speed and 30° cutting angle. This data coincides with the single-factor test results and confirms the reasonability of the design angle (30°) of cutting edges in the seedling separator.

CONCLUSIONS

Cutting characteristics of paper pots are experimentally studied to address high seedling injury rate and low efficiency of existing seedling separators. Based on the results, a seedling separator that can directly cut paper pots is designed. We can conclude that soil moisture content for potted corn seedling should be controlled between 60–67% to meet the agricultural requirements and maintain the integrity of a single potted seedling after the cutting process. Shear cutting is superior to bend cutting for corn paper pots, and the injury rate of seedlings is lower than 5%. The maximum cutting force decreases with the increase of cutting speed. The minimum cutting force of the corn paper pot is achieved under 63–67% soil moisture content, 500 mm/min cutting speed, and 30° cutting angle. A cut single pot is delivered to the seedling guide tube. This seedling separator can lessen labor intensity and increase transplantation efficiency. In this design, two cutting edges are installed on the cutter head. In future research, installing four cutting edges on the cutter head can be done to further study seedling separation efficiency.

ACKNOWLEDGEMENT

The work was supported by Construction planned project for innovation team of Heilongjiang Universities: mechanical cultivation technological innovation team of plant potted seedlings (2014TD010) and by the Postgraduate innovation program of Heilongjiang Bayi Agricultural University: research on corn seedling separator based on paper potted transplantation technology (YJSCX2016-Y36) and by Scientific and Technological Project: in Heilongjiang Province (2014BAD06B00).

REFERENCES

[1] Cui W, Yan H, Gao X W, Chen K., (2015), Development Status and Trend of Dryland Transplanting Machine. *Agricultural Engineering*, Issue 2, Academy of agricultural mechanization/Peking, pp.15-18;

[2] Ding W Q, Mao H P, et al., (2011), Structure design and simulation analysis on the plug seedling automatic transplanter. *IFIP Advance in Information and Communication Technology, Computer and Computing Technologies in Agriculture IV*, Issue 10, Journal of Agricultural Mechanization Research/Harbin, pp.75-77+137;

[3] Jovan D, Ivan K, Marko D, (2011), One approach for modelling intermittent motion mechanism with noncircular gears. *Machine Design*, Vol.2,Issue 3, Machine Design/Netherlands, pp.121-126;

[4] Kumar G. V. Prasanna, Raheman H, (2011), Development of a walk-behind type hand tractor powered vegetable transplanter for paper pot seedlings. *Biosystems engineering*, Vol.110, Issue 2, Elsevier Science BV/Netherlands, pp.189-197;

[5] Lu Y T, Li Y X, et al., (2011), Situation analysis of transplanting machine and transplanting technology at home and abroad. *Xinjiang Agricultural Mechanization*, Issue 3, Xinjiang Agricultural Mechanization /Xinjiang, pp.29-32;

[6] Liu W X, Jin X, et al., (2016), Kinematic analysis of out - clip type automatic seedling mechanism. *Jiangsu Agricultural Sciences*, Issue 7, Jiangsu Agricultural Sciences /Jiangsu, pp.385-389;

[7] Li T J, Zhu R P, et al., (2012), Stability of motion state and bifurcation properties of planetary gear train. *Journal of Central South University*, Vol.19, Issue 6, Central South University / Changsha, pp.1543-1547;

[8] Liao Q X, Hu X P, et al., (2015), Analysis on detaching process of detaching device and seedling pot integrity about rape transplanter. *Transactions of the Chinese Society of Agricultural Engineering*, Vol.31,Issue 16, Chinese Society of Agricultural Engineering / Peking, pp.22-29;

[9] Li S, Wu Q M, et al., (2014), Bifurcation and chaos analysis of multistage planetary gear train. *Nonlinear Dynamics*, Nonlinear Dynamics / Changsha, pp.751-752;

[10] Shi T. (2015), Development and test of automatic corn seedling transplanter. *Transactions of the Chinese Society of Agricultural Engineering*, Vol.31, Issue 3, Chinese Society of Agricultural Engineering / Peking, pp.23-30;

[11] Tian S B, Qiu L C, et al., (2010), Development of Automatic Transplanter for Plug Seedling. *IFAC Proceedings Volumes*, Vol.43, Issue 26, IFAC Proceedings Volumes/Netherlands, pp.79-82;

[12] Xu B X, Cao S M, et al., (2015), Design of 2ZS-2 semi-automatic block seedling transplanting machine. *Journal of Chinese Agricultural Mechanization*, Vol.36, Issue 1, Chinese Agricultural Mechanization / Nanjing, pp.1-3;

[13] Xiang W, Wu M L, Xu YJ. (2015), Present Status and Prospects of Seedling Transplanting Machinery. *Journal of Agricultural Mechanization Research*. Issue 8, Agricultural Mechanization Research / Harbin, pp.6-9;

[14] Yu G.H., Yu T.F., et al., (2013), Research on a New Planetary Gear Train Mechanism. *Journal of Mechanical Engineering*, Vol.49, Issue 15, Mechanical Engineering / Peking, pp.55-61;

[15] Yu X Zhao Y, et al., (2014), Current Situation and Prospect of Transplanter, *Transaction of the Chinese Society for Agricultural Machinery*, Vol.45, Issue 8, Chinese Society for Agricultural Machinery / Peking, pp.44-53;

[16] Yan X.Y., Hu J.P., et al., (2013), Design and Experiment of Full-row-pick-up and Single-dropping Seedling Transplanter. *Transaction of the Chinese Society for Agricultural Machinery*, Vol.44, Issue 1, Chinese Society for Agricultural Machinery / Peking, pp.7-13;

[17] Yu L, Shi T, et al. (2015), Research on 2ZYZ-2 Two-line Automatic Corn Seedling Transplanter. *Agricultural Science Technology and Equipment*, Issue 8, Agricultural mechanization research institute of Liaoning province/Liaoning, pp.13-15+17;

[18] Zhou Z, Zhang Z, Luo X, (2014), A Fuzzy Path Preview Algorithm for the Rice Transplanting Robot Navigation System. *Journal of Software*, Vol.9, Issue 4, Pergamon - Elsevier Science LTD / Netherlands, pp.94;

[19] Zheng F.Y, Lin H, Han X.H, (2014), Synthesis of indexing mechanisms with non-circular gears. *Mechanism and Machine Theory,* Vol.75, Issue 1, Nonlinear Dynamics/Qingdao*,* pp. 217-233;

[20] Zhang M, Feng J. et al., (2014), Analysis on Ejector Seedlings Mechanism of Automatic Dry Farmland Transplanting Machine, *Journal of Agricultural Mechanization Research*, Issue 3, Agricultural Mechanization Research / Harbin, pp.85-89;

[21] Zhang L, Zhang G.L., et al., (2014), Design of New Roller-type Plastic Film Collector for Cotton Fields. *Journal of Agricultural Mechanization Research*, Issue 7, Agricultural Mechanization Research / Harbin, pp.107-109.

KINEMATICS AND STATICS ANALYSIS OF A NOVLE 4-DOF PARALLEL MECHANISM FOR LASER WEEDING ROBOT

/

基于激光除草机器人的一种新型 4 自由度并联机构运动学和静力学分析

Ph.D. Wang Xuelei, Ph.D. Huang Jie, Ph.D. Zhao Dongjie, Ph.D. Guo Honghong, Ph.D. Li Chuanjun, Prof. Zhang Bin*)

College of Engineering, China Agricultural University, Beijing / China

Tel: +8615650715561; E-mail: zhangbin64@cau.edu.cn

Keywords: *parallel mechanism, kinematics, statics, inverse/forward velocities*

ABSTRACT

To eliminate the serious threat of weeds to farmland crops, this study proposes a laser weeding robot based on a novel 3UPS-RPU parallel mechanism (PM). The robot uses laser thermal effects to eliminate weeds in crop rows. The novel 3UPS-RPU PM is composed of three UPS-type active legs and one RPU-type active leg. Approaches for solving the inverse kinematics, inverse/forward velocities, inverse/forward accelerations, active forces, and constrained forces of this PM are derived and unified for other PMs with linear active legs. The kinematic curves demonstrate that the input of active legs 1 and 3 are consistent, while the moving platform moves according to a line-type translational movement which is the unique characteristic of the proposed PM. The active legs move according to a non-linear motion law, while the moving platform of the PM moves according to a line-type patterns, which is a common characteristic. The kinematic curves show that this PM has steady movement with no sudden changes or breakpoints which satisfies the stability requirements for the laser in the robot. Theoretical formulas and results provide a basis for the optimization of the structure design, control, dynamic performance analysis, manufacturing, and applications of the 3UPS-RPU PM.

摘要

为消除杂草对农作物的严重影响，论文提出了基于一种新型 4 自由度并联机构的激光除草机器人，该机器人利用激光的热效应来消除农作物中的杂草。新型并联机构包括 3 个 UPS 主动件和 1 个 RPU 主动件。论文推导了该并联机构的运动学反解，速度，加速度，主动力和约束力公式，本推导方法同样适用于其他由直线主动件控制的并联机构。当 3UPS-RPU 并联机构动平台只有平移运动时，主动件 1 和 3 的运动实时同步，这是本机构特有的性质。当动平台按照线性方式运动时，四个主动件为非线性运动，这也是并联机构共有的特性。从运动学曲线可以看出该机构运动平稳，运动过程中没有突变和断点，满足该激光除草机器人对激光束稳定性的要求。理论方程和结果为机构的优化设计、控制、动力学性能分析、制作和应用提供了基础。

INTRODUCTION

Farmland weeds grow and spread easily thus compete for different resources, such as moisture, nutrients, sunlight and space, that crops need to grow. Weeds also become sources of infection through pathogenic bacteria, which seriously affect the normal growth of crops, resulting in the decrease in yield and quality.

Chemical weed control has always been used in traditional agricultural production and has been proven to have harmful side-effects *(Martins et al., 2016; Nath et al., 2016; Datsch Silveira et al., 2016)*. *(Datsch Silveira et al., 2016)* evaluated the mutagenic effects of two herbicides, namely, Clorimurom Nortox® and Imazaquim Ultra Nortox®, which are widely used on soybean crops in Brazil. Allium cepa assay was used as the test system. The two herbicides caused mutagenic damages in the Allium cepa cells, which implied the need for careful handling of these products to minimize the risk of human and environmental contamination. Ecotoxic effects of commonly used herbicides i.e. glyphosate, atrazine, metribuzin and alachlor were evaluated on the biological and demographic parameters of Zygogramma bicolorata Pallister on parthenium in laboratory by Hasan *(Hasan et al., 2016)* Based on the present study, none of the tested herbicide can be classified as safe to Zygogramma bicolorata, while glyphosate was found to be least toxic. Therefore, this weeding process not only affects the growth of crops but also pollutes the soil, resulting in herbicide wastes—a serious threat to the health of farmland workers. Furthermore, the safety of agricultural products is also affect by the drug residue.

Mechanical weed control was developed to replace its chemical counterpart, which utilizes standard tools, such as field hoes to weed. *(Cordill et al., 2011)* proposed a mechanical weed control machine containing a sensing arrangement, control algorithm and dual mechanical end effectors was successfully developed and tested. The overall functionality of the machine was proven, but the percentage of fatally damaged plants was 8.8% in the absence of weeds and reaching 23.7% in heavy weed infested areas with hundreds of weeds per m^2. *(Pérez-Ruiz et al., 2012)* described a fully automatic intra-row mechanical weed knife path control system for transplanted row crops. A real-time kinematics global positioning system (GPS) was used to automatically detect crop planting positions and to control the path of a pair of intra-row weed knives travelling between crop plants along row centerline. *(Pérez-Ruiz et al., 2014)* also described the development and in-field assessment of an automatic intra-row, hoe-based weeding co-robot system with real-time pneumatic hoe actuation based on an accurate odometry sensing technique. In this work, mechanical weed control was achieved by a co-robot actuator that automatically positioned a pair of miniature hoes into the intra-row zone between crop plants.

However, mechanical damage to crop seedlings can be easily inflicted because of the restriction of the movement precision of mechanical weeding devices. The soils turned over by mechanical weeding device tend to bury the seedlings. Moreover, weed seeds may be spared from mechanical weeding, which may lead to their re-germination.

Currently, concerning about the impact of eco-agriculture from western countries, a growing number of consumers demand natural food with little to no chemicals because of the eco-agricultural effect from Western countries. Automated, non-chemical, intra-row weed control techniques for crop production systems have become a necessary challenge for industrialized countries. To satisfy the needs of the market, new methodologies need to be developed to produce satisfactory outcomes without damaging the environment. Therefore, this research presents a laser weeding robot that does not rely on chemical resources.

In recent years, PMs have been extensively studied and applied because of their high durability, lower manufacturing cost, simple structure, large bearing capacity and easy to control, etc *(Ganesh et al., 2015; Li et al., 2016; Yang et al., 2016)*. Various PMs have been used in fields such as walking legs, parallel machine tools, rehabilitation robots, industrial robots, heavy-duty forging manipulators, etc *(Jiang et al., 2016; Lin et al., 2016; Song et al., 2016)* . Generally, PMs with four degree of freedom (4-DoF) have attracted significant attentions because they are simpler in structure, easier manufacture, cheaper, and more sustainable than PMs with 6-DoF *(Dong et al., 2016; He et al., 2015)* . To create some novel 4-DoF PMs and investigate their kinematic characteristics have great significances in current industrial manufacturing and other fields.

However, up to now, no study have been found existed on 3UPS-RPU PM with two rotations and two translations and this is the first time that PMs will be used in laser weeding robot. This research focuses on the kinematics and statics analysis of the proposed PM and proposes a unified method for solving the kinematics and statics of PMs with linear active legs because a 3-UPS-RPU PM is the basis for the laser weeding robot. In addition, this paper provides a theoretical basis for its optimum structural design, control, manufacturing, and different applications.

MATERIAL AND METHODS

Description of the Laser Weeding Robot

The laser weeding robot uses laser thermal effects to eliminate weeds in crop rows. The main robot components are the frame, a 3UPS-RPU 4-DoF PM, a laser, a control system, batteries, and two vision systems, as illustrated in Figure 1.

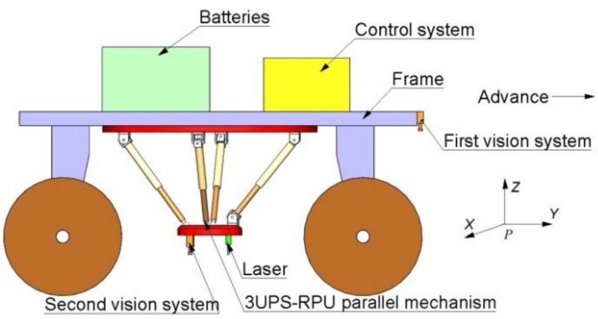

Fig. 1 - Scheme of the laser weeding robot

The 3UPS-RPU PM is held over the frame and trailed by a conventional tractor. The first vision system is placed in the front of the tractor to detect weeds in real time and send their coordinates to the control system while the robot is in motion. A secondary vision camera is used to improve robot precision and it is placed close to the laser. Its mission is to correct inertial perturbations by relocating every individual weeds detected by the first vision system.

The 3UPS-RPU PM is composed of a moving platform, a fixed base, three UPS-type (U represents universal joint, P represents prismatic joint, S represents spherical joint) active legs and one RPU-type (R represents revolute joint) active leg with the linear actuators, see Figure 2. Since each of the active legs with the linear actuator only bears the axial force that along its own axis, it has a larger capacity of load bearing and is simple in structure.

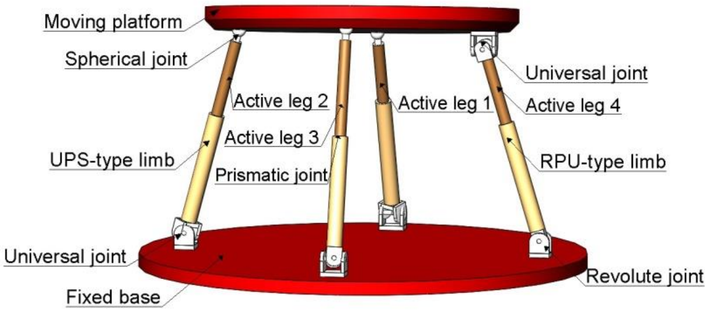

Fig. 2 - The 3UPS-RPU parallel mechanism

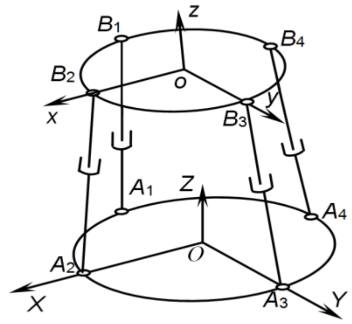

Fig. 3 - Schematic model of 3UPS-RPU PM

In the 3UPS-RPU PM, the number of independent common constraints is λ= 0; the order of mechanism is d = 6 - λ = 6; the number of links is n =10 including one moving platform, four cylinders, four piston-rods and one fixed base; the number of joints is g = 12, including three universal joints, four prismatic joints, four spherical joints and one revolute joint; the DoFs of the joints are f_P = f_R = 1 for prismatic or revolute joint, f_U= 2 for universal joint, f_S = 3 for spherical joint; the number of redundant constraints is v = 0; the redundancy DoFs is ζ = 0. Based on the revised Kutzbach-Grübler equation *(Huang et al., 1997)*, the DoF of the 3UPS-RPU PM is calculated as

$$M = d\left(n-g-1\right)+\sum_{i=1}^{g} f_i + v - \zeta = 6\times\left(10-12-1\right)+\left(2\times3+4\times1+3\times3+2\times1+1\times1\right)=4 \qquad (1)$$

Thus, the 3UPS-RPU PM has four DoFs with two translational DoFs and two rotational DoFs.

In the laser weeding robot illustrated in Figure1, the Y axis of the coordinate system P-XYZ is along the advance direction of the robot, Z axis is perpendicular to the frame, while X axis is confirmed by the right-hand rule. The 3UPS-RPU 4-DoF PM can achieve movements along the Y and Z axes directions and rotations around the X and Y axes. Among them, the movement along the Y axis is used to compensate for the positional change of the weeds so that the laser beams of the robot will remain stationary to the weeds. The movement along the Z axis allows the robot to work in the field with different crop heights, greatly improving the working space. With its simple structure, the laser weeding robot can be used in different height or line spacing crops without the risk of burying seedlings and damaging crops.

Analysis of 3UPS-RPU PM

The coordinate system O-XYZ is fixed at the centre of the fixed base at O, and o-xyz is fixed at the centre of the moving platform at o, as illustrated in Figure 3. A_i (i=1, 2...4) are equally distributed around a circle with a radius of r_a on the fixed base. B_i (i=1, 2…4) are uniformly distributed around a circle with a radius of r_b on the moving platform. At the initial time, the coordinate systems O-XYZ and o-xyz are parallel, and Z-axis is coincident with z-axis.

Before analyzing the inverse kinematics of the 3UPS-RPU PM, the position of A_i (i =1, 2…4) in O-XYZ, B_i (i =1, 2…4) in o-xyz, and B_i (i=1, 2…4) in O-XYZ must be determined, and they can be expressed as:

$$A_i = \begin{bmatrix} A_{iX} \\ A_{iY} \\ A_{iZ} \end{bmatrix}, \quad B_i = \begin{bmatrix} B_{ix} \\ B_{iy} \\ B_{iz} \end{bmatrix}, \quad B_i^O = \begin{bmatrix} B_{iX} \\ B_{iY} \\ B_{iZ} \end{bmatrix}, \quad R_o^O = \begin{bmatrix} l_x & m_x & n_x \\ l_y & m_y & n_y \\ l_z & m_z & n_z \end{bmatrix},$$

$$o=\begin{bmatrix}X_o\\Y_o\\Z_o\end{bmatrix},\quad B_i^O=R_o^O B_i+o \quad (i=1,2\ldots4) \tag{2}$$

Where $o=[X_o\ Y_o\ Z_o]^T$ is the position vector of *o-xyz* in *O-XYZ*, matrix R_o^O is a rotation transformation matrix from *o-xyz* to *O-XYZ* and it's formed by two Euler rotations of (x y_1), namely, a rotation of α about x-axis, followed by a rotation of β about y_1-axis, where y_1 is formed by y rotating about x by α. Let λ be one of (α, β) and set $c\lambda=\cos\lambda$, $s\lambda=\sin\lambda$, thus, R_o^O is derived as follows:

$$R_o^O=\begin{bmatrix}c\beta & 0 & s\beta\\ s\alpha s\beta & c\alpha & -s\alpha c\beta\\ -c\alpha s\beta & s\alpha & c\alpha c\beta\end{bmatrix}$$

Each active leg, $\boldsymbol{l_i}$ (i = 1, 2…4) can be expressed as:

$$l_i=B_i^O-A_i \tag{3}$$

Thus, the formula for solving $\boldsymbol{l_i}$ (i = 1, 2…4) are derived as:

$$l_i^2=\left|B_i^O-A_i\right|^2\Rightarrow\begin{cases}l_1^2=\left|B_1^O-A_1\right|^2\\ \quad =X_o^2+(-r_b c\alpha+r_a+Y_o)^2+(-r_b s\alpha+Z_o)^2\\ l_2^2=\left|B_2^O-A_2\right|^2\\ \quad =(r_b c\beta+X_o-r_a)^2+(r_b s\alpha s\beta+Y_o)^2+(-r_b c\alpha s\beta+Z_o)^2\\ l_3^2=\left|B_3^O-A_3\right|^2\\ \quad =X_o^2+(r_b c\alpha+Y_o-r_a)^2+(r_b s\alpha+Z_o)^2\\ l_4^2=\left|B_4^O-A_4\right|^2\\ \quad =(-r_b c\beta+X_o+r_a)^2+(-r_b s\alpha s\beta+Y_o)^2+(r_b c\alpha s\beta+Z_o)^2\end{cases} \tag{4}$$

The unit vector n_i of l_i (i = 1, 2…4) can be derived as:

$$n_i=\frac{l_i}{l_l}=\frac{1}{l_i}\begin{bmatrix}B_{iX}-A_{iX}\\B_{iY}-A_{iY}\\B_{iZ}-A_{iZ}\end{bmatrix} \tag{5}$$

Let V and v_i be the velocities of the moving platform at o and B_i, respectively, written as:

$$V=\begin{bmatrix}v\\\omega\end{bmatrix}_{6\times1},\ v=\begin{bmatrix}v_x\\v_y\\v_z\end{bmatrix},\ \omega=\begin{bmatrix}\omega_x\\\omega_y\\\omega_z\end{bmatrix},\ v_i=v+\omega\times r_i \quad (i=1,2\ldots4) \tag{6}$$

Where v and ω are the velocity and angular velocity of *o-xyz* at o, r_i (i=1, 2…4) are the vectors from point o to B_i. Through Equation (6), the velocities along the active legs l_i (i = 1, 2…4) are derived as follows:

$$v_{li}=v_i\cdot n_i=(v+\omega\times r_i)\cdot n_i=n_i\cdot v+(r_i\times n_i)\cdot\omega \qquad (i=1,2\ldots4) \tag{7}$$

$$\Rightarrow\begin{bmatrix}v_{l_1}\\v_{l_2}\\v_{l_3}\\v_{l_4}\end{bmatrix}=\begin{bmatrix}n_1^T & (r_1\times n_1)^T\\ n_2^T & (r_2\times n_2)^T\\ n_3^T & (r_3\times n_3)^T\\ n_4^T & (r_4\times n_4)^T\end{bmatrix}_{4\times6}\cdot\begin{bmatrix}v\\\omega\end{bmatrix}_{6\times1} \tag{8}$$

The force situation of the 3UPS+RPU PM is shown in Figure 4. Constrained force F_U, which is applied on the moving platform, is in parallel to the revolute joint R of the RPU limb.

The restriction moment M_U, applied on the moving platform, is parallel to the z-axis. Let n_5 be the unit vector of revolute joint R, and n_6 be the unit vector of z-axis.

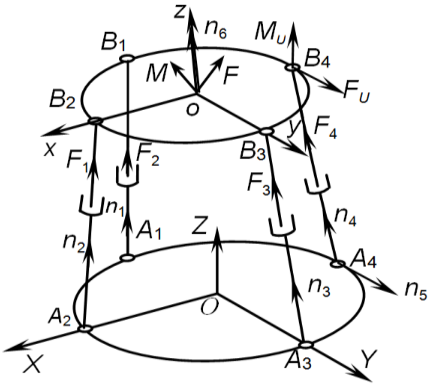

Fig. 4 - The force situation of the 3UPS + RPU PM

Since constrained force F_U and restriction moment M_U don't do any work during the movement of moving platform, there must be:

$$F_U n_5 \cdot v + (r_4 \times F_U n_5)\cdot\omega = 0\,, \quad (M_U n_6)\cdot\omega = 0 \quad \Rightarrow \begin{bmatrix} n_5^T & (r_4\times n_5)^T \\ 0_{1\times3} & n_6^T \end{bmatrix}_{2\times6} \cdot V = \begin{bmatrix} 0 \\ 0 \end{bmatrix} \tag{9}$$

By combining Equations (8) and (9), the formula for solving the inverse/forward velocities and the Jacobian matrix G are derived as follows:

$$\Rightarrow \begin{bmatrix} v_{l_1} \\ v_{l_2} \\ v_{l_3} \\ v_{l_4} \\ 0 \\ 0 \end{bmatrix} = G\cdot V\,, \quad V = G^{-1}\cdot \begin{bmatrix} v_{l_1} \\ v_{l_2} \\ v_{l_3} \\ v_{l_4} \\ 0 \\ 0 \end{bmatrix}$$

$$\Rightarrow G = \begin{bmatrix} n_1^T & (r_1\times n_1)^T \\ n_2^T & (r_2\times n_2)^T \\ n_3^T & (r_3\times n_3)^T \\ n_4^T & (r_4\times n_4)^T \\ n_5^T & (r_4\times n_5)^T \\ 0_{1\times3} & n_6^T \end{bmatrix}_{6\times6} \tag{10}$$

Let A be the acceleration of the moving platform at o. Let a and ε be a linear acceleration and an angular acceleration of moving platform at o, respectively.

They can be expressed as follows:

$$A = \begin{bmatrix} a \\ \varepsilon \end{bmatrix}_{6\times1} \qquad a = \begin{bmatrix} a_x \\ a_y \\ a_z \end{bmatrix}, \quad \varepsilon = \begin{bmatrix} \varepsilon_x \\ \varepsilon_y \\ \varepsilon_z \end{bmatrix} \tag{11}$$

Suppose there are two vectors η, ζ and a skew-symmetric matrix $\hat{\eta}$ .There must be the following relevant Equations *(Huang et al., 1997)*:

$$\eta = \begin{bmatrix} \eta_x \\ \eta_y \\ \eta_z \end{bmatrix}, \quad \zeta = \begin{bmatrix} \zeta_x \\ \zeta_y \\ \zeta_z \end{bmatrix}, \quad \hat{\eta} = \begin{bmatrix} 0 & -\eta_z & \eta_y \\ \eta_z & 0 & -\eta_x \\ -\eta_y & \eta_x & 0 \end{bmatrix}, \quad \eta\times\zeta = \hat{\eta}\zeta\,, \quad \hat{\eta}^T = -\hat{\eta} \tag{12}$$

By differentiating the first four rows of Equation (10) with respect to time, four accelerations $\boldsymbol{a}_{l_i}$ along the i th active leg are expressed as follows:

$$a_{l_i} = \left[n_i^T \;\; (r_i \times n_i)^T \right] A + V^T H_i V \quad (i=1, 2\ldots4) \tag{13}$$

Where
$$H_i = \frac{1}{l_i}\begin{bmatrix} E_{3\times3} & -\hat{r}_i \\ \hat{r}_i & -\hat{r}_i^2 \end{bmatrix}_{6\times6} - \frac{1}{l_i}\begin{bmatrix} n_i \\ r_i \times n_i \end{bmatrix}\left[n_i^T \;\; (r_i \times n_i)^T \right] + \begin{bmatrix} 0_{3\times3} & 0_{3\times3} \\ 0_{3\times3} & \hat{r}_i\,\hat{n}_i \end{bmatrix}_{6\times6}.$$

By differentiating the fifth row of Equation (10) with respect to time, we obtain:

$$0_{1\times6} = \left[n_5^T \;\; (r_4 \times n_5)^T \right] A + V^T H_5 V \tag{14}$$

Where $H_5 = \begin{bmatrix} 0_{3\times3} & 0_{3\times3} \\ 0_{3\times3} & -\hat{r}_4\,\hat{n}_5 \end{bmatrix}_{6\times6}$.

By differentiating the sixth row of Equation (10) with respect to time, we obtain:

$$0_{1\times6} = \left[0_{1\times3} \;\; n_6^T \right] A + V^T H_6 V \tag{15}$$

Where, $H_6 = \begin{bmatrix} 0_{3\times3} & 0_{3\times3} \\ 0_{3\times3} & J_\alpha \end{bmatrix}_{6\times6}$, $J_\alpha = \left[\begin{bmatrix} c\beta & 0 & 0 \\ s\alpha s\beta & c\alpha & 0 \\ -c\alpha s\beta & s\alpha & 1 \end{bmatrix}^{-1}\right]^T \cdot \begin{bmatrix} 0 & -c\alpha c\beta & -s\alpha c\beta \\ c\beta & s\alpha s\beta & -c\alpha s\beta \\ 0 & 0 & 0 \end{bmatrix}$

Combining Equations (13) with (14) and (15), an inverse acceleration a_{in}, a forward acceleration A, and a Hessian matrix H are derived as follows:

$$a_{in} = GA + V^T HV, \quad A = G^{-1}\left(a_{in} - V^T HV\right) \tag{16}$$

Where $a_{in} = \left[a_{l_1}\; a_{l_2}\; a_{l_3}\; a_{l_4}\; 0\; 0 \right]^T$ and $H = \left[H_1\; H_2\; H_3\; H_4\; H_5\; H_6 \right]^T$.

Active/Constraint Forces and Torque

The 3UPS-RPU PM is an ideal constrained system when the gravity and friction of all the links are ignored, and its workload can be simplified as a wrench (F, M) applied on the moving platform at o, where F is the central force and M is the central torque. (F_X, F_Y, F_Z, M_X, M_Y, M_Z) are the components of (F, M) and they are balanced by four active forces F_i (i=1, 2…4), one constrained force F_U, and one restriction moment M_U, each of F_i is applied on and along the active legs l_i (i=1,2…4).

Based on the principle of virtual work, and Equation (10), the formula for solving the active/constrained force and torque are derived as follows:

$$\begin{bmatrix} F_1 \\ F_2 \\ F_3 \\ F_4 \\ F_U \\ M_U \end{bmatrix}^T \cdot \begin{bmatrix} v_{r_1} \\ v_{r_2} \\ v_{r_3} \\ v_{r_4} \\ 0 \\ 0 \end{bmatrix} + \begin{bmatrix} F \\ T \end{bmatrix}^T \cdot V = 0, \quad \begin{bmatrix} F_1 \\ F_2 \\ F_3 \\ F_4 \\ F_U \\ M_U \end{bmatrix}^T \cdot G + \begin{bmatrix} F \\ T \end{bmatrix}^T = 0$$

$$\Rightarrow \begin{bmatrix} F_1 \\ F_2 \\ F_3 \\ F_4 \\ F_U \\ M_U \end{bmatrix} = -\left(G^{-1}\right)^T \begin{bmatrix} F \\ T \end{bmatrix} = -\left(G^T\right)^{-1} \begin{bmatrix} F \\ T \end{bmatrix} \tag{17}$$

Where, $-\left(G^T\right)^{-1}$ is defined as a force Jacobian matrix.

RESULTS

Results Analysis and Discussion

In the 3UPS-RPU PM, when given pose parameters of moving platform with respect to time, the length, velocity, acceleration of four active legs can be calculated. Set r_a = 400 mm, r_b = 300 mm, and the original distance between two platforms is H = 600 mm. Two cases are employed in analysis of the PM.

In case one, the moving platform is presumed to move according to a line-type translational movement, that is,

$$\begin{cases} \alpha = 0 \\ \beta = 0 \\ X_0 = 5 * t \\ Z_0 = 5 * t \end{cases} \tag{18}$$

Based on the relevant analytics of Equations (4), (10) and (16), the lengths, velocities and accelerations of the four active legs that over time are obtained through the Matlab software, and are presented in Figures 5(a), 5(b), and 5(c), respectively.

According to the results and data shown in Figure 5(a), the lengths of the four active legs are initially the same. As time goes by, the lengths of active leg 4 becomes the longest while active leg 2 becomes the shortest. According to the results and data shown in Figure 5(b), the velocity of active leg 4 is at a maximum while active leg 2 is constant at a minimum. According to the results and data shown in Figure 5(c), the acceleration of active leg 2 is at the maximum while active leg 4 is constantly at the minimum, but the values are greater than zero. The lengths, velocities, and accelerations of active legs 1 and 3 are always consistent with each other, and their values are between that of active legs 2 and 4, that is, the input of active legs 1 and 3 are always consistent. The results and data shown in Figure 5(a), 5(b), and 5(c) are consistent with the actual movement and in accordance with the geometric characteristics of PMs. The velocity and acceleration of the four active legs are changing all the time. Therefore, the movements of the PM are non-linear.

Case two is the presumption that the moving platform of the mechanism moves according to a line-type rotational movement, that is,

$$\begin{cases} \alpha = (\pi/90) * t \\ \beta = (\pi/90) * t \\ X_0 = 0 \\ Z_0 = 0 \end{cases} \tag{19}$$

Based on the relevant analytics of Equations (4), (10) and (16), the lengths, velocities and accelerations of the four active legs over time are obtained through the Matlab software, which are presented in Figures 5(d), 5(e), 5(f).

According to the results and data shown in Figure 5(d), the lengths of the four active legs are initially the same. As time goes by, the lengths of active legs 1 and 2 become shorter while those of active legs 3 and 4 become longer. According to the results and data shown in Figure 5(e), the velocities of active legs 1 and 2 gradually increase while those of active legs 3 and 4 continually decrease. According to the results and data shown in Figure 5(f), the accelerations of active legs 1 and 2 are always greater than zero, while those of active legs 3 and 4 are always less than zero. Moreover, the slopes of active legs 2 and 4 are larger than those of active legs 1 and 3. The results and data shown in Figures 5(d), 5(e), and 5(f) are consistent with the actual movement and in accordance with geometric characteristics of PMs. The velocities and accelerations of the four active legs shift at all times. Therefore, their movements are also non-linear two.

As a result, the moving platform of the PM moves according to line-type patterns, but all active legs move according to the non-linear motion law and all the PMs have the same Characteristics.

The kinematic diagrams show that the PM movement is steady and its displacement, velocity, and acceleration curves exhibit no sudden changes or breakpoints, illustrating the correctness of this PM, and satisfying the stability requirements for the laser in the robot.

Theoretical formulas and results provide a basis for the optimization of the structure design, control, dynamic performance analysis, manufacturing, and applications of the 3UPS-RPU PM.

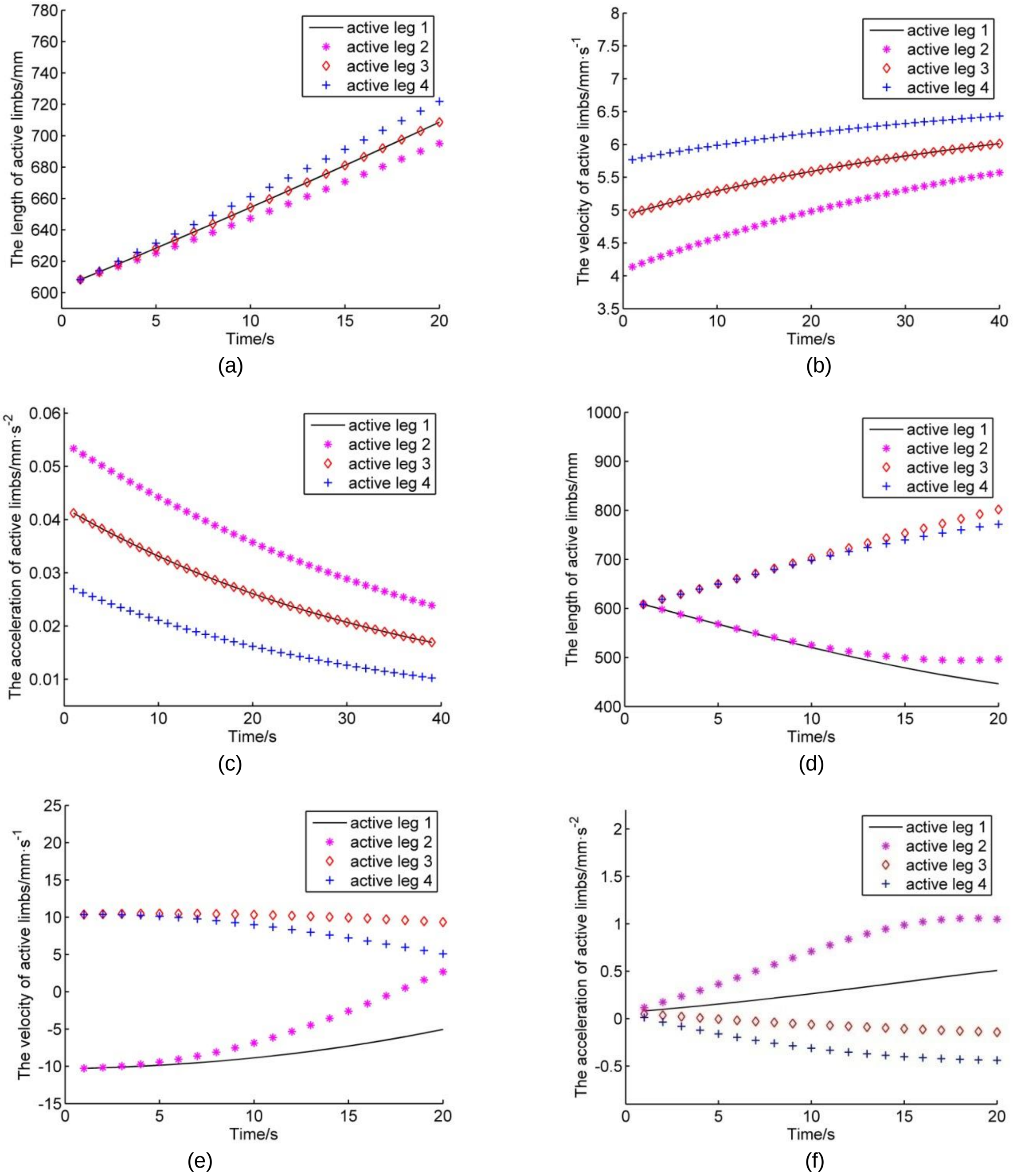

Fig. 5 - Kinematic analysis of active legs

CONCLUSIONS

With the increase in the demand for green vegetables and make up the inadequacies of Chemical and mechanical weeding, a more efficient method of weeding has become a necessity. This research demonstrated a laser weeding robot based on a novel 3UPS-RPU PM, which utilizes laser thermal effects to eliminate weeds in crop rows. This research focus on kinematics and statics analysis of the 3UPS-RPU PM as it is basis of the weeding robot. The conclusions are shown as follows:

(1) The approaches for solving the inverse/forward velocities and accelerations of the 3UPS-RPU PM were derived and unified for other PMs with linear active legs. The velocity Jacobian matrix and Hessian matrix derived can be used to analyze the kinematic singularity of PMs.

(2) The curves of the lengths, velocities, and accelerations of the four active legs showed that the movement of active legs 1 and 3 were consistent with each other, while the moving platform moved according to a line-type translational movement, which is a unique characteristic of the proposed PM. All active legs moved according to the non-linear motion law, while the moving platform of the PM moved according to a line-type pattern, which is a common characteristic of PMs. These results are used for the control system of the robot. The stability of the kinematic curves show that the PM satisfies the stability requirements for the laser in the robot. Thus, the weeding quality can be improved greatly.

(3) A simple approach for solving the active constrained forces of the 3UPS-RPU PM was derived based on the principle of virtual work, and this approach can be used on other PMs.

In addition, this paper provides a theoretical basis for the optimum structural design, control, manufacturing, and different applications of the robot. Future work should combine theoretical analysis with field experiments.

ACKNOWLEDGEMENT

This work is supported by the Doctoral Fund from the National Education Ministry of China no. 20120008110046. The authors would like to thank the reviewers for their critical reviews and suggestions to improve the clarity of this article. They would also like to thank the managing editor for the works on the manuscript.

REFERENCES

[1] Cordill C., Grift T. E., (2011), Design and testing of an intra-row mechanical weeding machine for corn, *Biosystems Engineering*, Vol.110, Issue 3, pp.247-252, *Academic Press Inc Elsevier Science*, San Diego/USA;

[2] Datsch Silveira M.A., Ribeiro D. L., Dos Datsch Santos T. A., et al., (2016), Mutagenicity of two herbicides widely used on soybean crops by the Allium cepa test, *Cytotechnolygy*, Vol.68, Issue 4, pp.1215-1222, Springer Netherlands, Dordrecht/Netherlands;

[3] Dong G., Sun T., Song Y. M., (2016), Mobility analysis and kinematic synthesis of a novel 4-dof parallel manipulator, *Robotica*, Vol.34, Issue 5, pp.1010-1025, Cambridge University Press, New York/USA;

[4] Ganesh S. S., Rao A. B. K., (2015), Inverse dynamics of a 3-DOF translational parallel kinematic machine, *Journal of Mechanical Science and Technology,* Vol.29, Issue 11, pp.4583-4591, Korean Society of Mechanical Engineers, Seoul/Korean;

[5] Hasan F., Shafiq Ansari M., (2016), Ecotoxicological hazards of herbicides on biological attributes of Zygogramma bicolorata Pallister (Coleoptera: Chrysomelidae), *Chemosphere*, Vol.154, pp.398-407, Pergamon, Elsevier Science Ltd, Oxford/England;

[6] Huang Z., Kong L. F., Fang Y. F., (1997), *Theory on Parallel Robotics and Control*, Machinery Industry Press, Beijing/China;

[7] He J., Gao F., Meng X. D., et al., (2015), Type synthesis for 4-dof parallel press mechanism using gf set theory*, Chinese Journal of Mechanical Engineering*, Vol.28, Issue 4, pp.851-859, Editorial Office of Chinese Journal of Mechanical Engineering, Beijing/China;

[8] Jiang X. L., Gosselin C., (2016), Trajectory generation for three-degree-of-freedom cable-suspended parallel robots based on analytical integration of the dynamic equations, *Journal of Mechanisms and Robotics-Transactions of the ASME*, Vol. 8, Issue 4, pp.1110-1117, American Society of Mechanical Engineers, New York/USA;

[9] Lin H. T., Chiang M. H., (2016), The integration of the image sensor with a 3-dof pneumatic parallel manipulator, *Sensors*, Vol.16, Issue 7, pp.1–17, Molecular Diversity Preservation International, Basel/Switzerland;

[10] Li B., Li Y. M., Zhao X. H., (2016), Kinematics analysis of a novel over-constrained three degree-of-freedom spatial parallel manipulator, *Mechanism and Machine Theory*, Vol.104, pp.222-233, Pergamon-Elsevier Science Ltd, Oxford/England;

[11] Martins D., Goncalves C. G., da S. J., et al., (2016), Winter mulches and chemical control on weeds in maize, *Revista Ciencia Agronomica*, Vol.47, Issue 4, pp.649-657, Universidade Federal do Ceará, Fortaleza/Brazil;

[12] Nath C. P., Das T. K., Rana K. S., (2016), Effects of herbicides and tillage practices on weeds and summer mungbean (Vigna radiata) in wheat (Triticum aestivum)-mungbean cropping sequence, *Indian Journal of Agricultural Sciences*, Vol.86, Issue 7, pp.860-864, Indian Council of Agricultural Research, New Delhi/ Indian;

[13] Pérez-Ruiz M., Slaughter D. C., Gliever C. J., et al., (2012), Automatic GPS-based intra-row weed knife control system for transplanted row crops, *Computers and Electronics in Agriculture*, Vol. 80, pp.41-49, Elsevier Science Ltd, Oxford/England;

[14] Pérez-Ruiz M., Slaughter D. C., Fathallah F. A., et al., (2014), Co-robotic intra-row weed control system, *Biosystems Engineering*, Vol.126, pp.45-55, Academic Press Inc Elsevier Science, San Diego/USA;
[15] Song Y. M., Zhang J. T., Lian B. B., et al., (2016), Kinematic calibration of a 5-dof parallel kinematic machine, *Precision Engineering*, Vol.45, pp.242–261, Elsevier Science Inc, New York/USA;
[16] Yang S. F., Sun T., Huang T., (2016), A finite screw approach to type synthesis of three-DOF translational parallel mechanisms, *Mechanism and Machine Theory*, Vol.104, pp.405-419, Pergamon-Elsevier Science Ltd, Oxford/England.

THE SERVICE LIFE EVALUATION OF FERTILIZER SPREADERS UNDERCARRIAGES /
ОЦІНКА ДОВГОВІЧНОСТІ НЕСУЧИХ СИСТЕМ РОЗКИДАЧІВ ДОБРИВ

Prof.Dr.Sc.Eng. Popovych P.V.[1], Prof. Dr.Sc. Eng. Lyashuk O.L. [1], Lect. Ph.D. Eng. Murovanyi I.S. [2], Lect. Ph.D. Eng. Dzyura V.O.[*2], Lect. Ph.D. Eng. Shevchuk O.S. [2], Lect. Ph.D. Eng. Myndyuk V.D.[3]
[1]Ternopil Ivan Pul'uj National Technical University, Ternopil / Ukraine
[2]Lutsk National Technical University, Lutsk / Ukraine
[3]Ivano-Frankivsk National Technical University of Oil and Gas, Ivano-Frankivsk / Ukraine
E-mail: volodymyrdzyura@gmail.com

Keywords : *spreader, mineral fertilizers, organic fertilizers, aggressive environment, crack, stress*

ABSTRACT
The analytical models to determine the residual service life of metal undercarriages of open profile fertilizer spreaders at exposure in organic and mineral fertilizers environments are developed. The service life of rail elements is considered as the sum of periods of formation and subcritical growth of fatigue cracks. The formulae for determining stress intensity factors near existing cracks are developed, as well as the formulae for determining the service life of "Z" cross section and "Ω" cross section. The kinetic equations for determining the formation and distribution periods are deduced. When examining the calculations, it was found that mineral fertilizers in comparison with organic ones greatly reduce the service life of elements under study.

РЕЗЮМЕ
Побудовано аналітичні моделі для визначення залишкової довговічності несучих металоконструкцій розкидачів добрив відкритого профілю з урахуванням впливів середовищ органічних і мінеральних добрив. Довговічність балкових елементів записана як сума періодів зародження і докритичного росту втомних тріщин. Записано формули для визначення коефіцієнтів інтенсивності напружень в околі наявних тріщин, кінетичні рівняння для визначення періодів зародження і поширення, а також формули для визначення ресурсу для Z-подібного і Ω-подібного перетину. На основі розрахунків встановлено, що мінеральні добрива зменшують ресурс розглядуваних елементів в більшій мірі ніж органічні.

INTRODUCTION
Some aggressive agricultural environments, in particular fertilizers, acting as an additional fatigue factor, significantly reducing the resistance to cracks formation (*Gaydar S.M., 2011*; *Severnev M.M. et al, 2011*). Some of the well-known theoretical approaches to reducing the phase of cracks formation are substantiated by electrochemical heterogeneity of the material in active slip planes. This fact causes the formation of pittings, which can be considered as the initial defects and additional stress concentrators (Fig.1).

Fig. 1 – Corrosion-fatigue damages of fertilizer spreaders metal structures after two seasons of operation

Other approaches associate the acceleration of cracks formation with the weakening of protective films on the metal surface (*Yarema S.Y., 1973; Panasiuk V.V. et al, 1988; Romaniv O.N. et al, 1990; Troshchenko V.T., 1981; Cherepanov G.P., 1974; Schijve J., 2003; Andreykiv A.E., Darchuk A.I., 1992*). It is well known that these films are formed due to exposure of a specimen in aggressive corrosive environment and are destroyed by slip lines. During this process, in the destruction area of a film, a galvanic couple originates with a small anode zone and with a large cathode zone, which is a solid oxide layer on a specimen surface. Thus, the process of local metal solution accelerates in slip bands, and the cracks formation period N_3 is significantly shortened. This type of destruction is characteristic for metal structures elements of fertilizer spreaders because of joint influence of dynamic load and aqueous solutions of mineral or organic fertilizers. In most cases, the main carriage components of agricultural machinery metal structures under study are thin rod components.

MATERIAL AND METHOD

The known deformation-minimizing method of rod systems was applied to define the stress-strained state of a trailing fertilizer RTD-9. The energy of bending deformation and torsion that greatly influences the undercarriage was considered. All stated above is proved by correlation with experimental data. To perform the calculations, the values of internal power factors were developed. Based on these factors, the stress-strained state in the most loaded sections of metal structures was defined (Table 1).

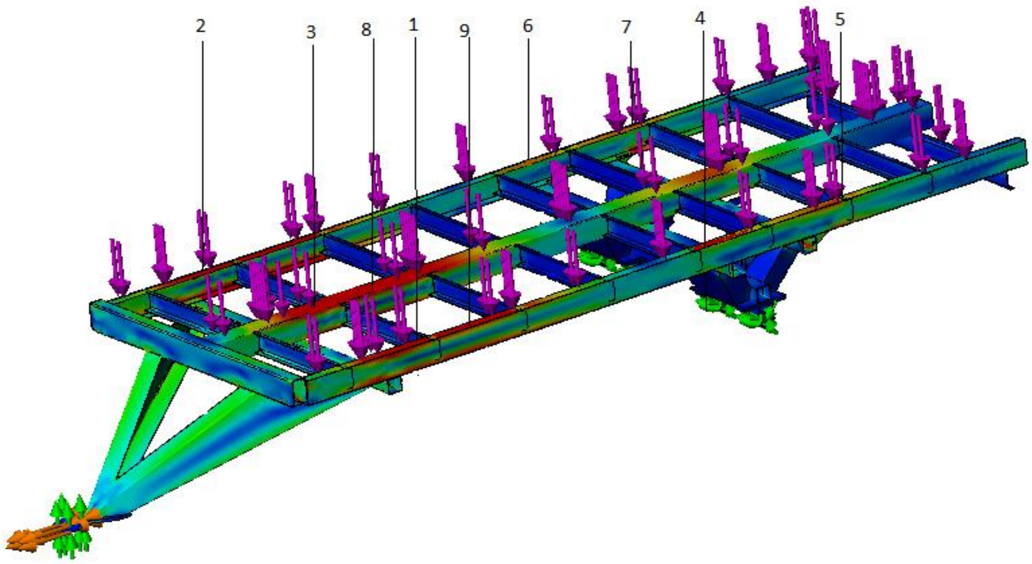

Fig. 2 – Sections of the undercarriage of organic fertilizer spreader RTD - 9 with maximum stresses

Table 1

Stresses in the most dangerous sections of the undercarriage of solid organic fertilizer spreaders RTD -9

№ section	The values of normal stresses, MPa
1.	160 MPa (“Z” cold-bent section 200×60×5, GOST 13229-78).
2.	152 MPa (“Z” cold-bent section 200×60×5, GOST 13229-78).
3.	188 MPa (two “Z” cold-bent welded sections 200×60×5)
4.	66 (“Z” cold-bent section 200×60×5, GOST 13229-78).
5.	126 (“Z” cold-bent section 200×60×5, GOST 13229-78).
6.	68 (“Z” cold-bent section 200×60×5, GOST 13229-78).
7.	105 (“Z” cold-bent section 200×60×5, GOST 13229-78).
8.	99 (two “Z” cold-bent welded sections 200×60×5)
9.	152 (“Z” cold-bent section 200×60×5, GOST 13229-78).

In all calculations, the solution of mixed organic fertilizer acts as the corrosive working environment. It is a solution of mixed cattle manure and pig manure (1/2+1/2) and a saturated solution of nitro-phosphate.

Further calculations should be performed for the most loaded elements of section №1 (longeron – “Z” cold-bent section 200×60×5, normal stresses in cross-section 160 MPa); section №3 (“Ω” section - two “Z” cold-bent welded sections 200×60×5, the normal stress in intersection 188 MPa, geometric characteristics of profiles) *(Pisarenko G.S., Yakovlev A.P., Matveev V.V., 1988)*.

Residual service life of a metal structure is defined by the durability of its most loaded elements. According to the modern theory of delayed fracture mechanics of structural elements, the service life of a structural element N_p with variable loads (*Yarema S.Y., 1973; Andreikiv O.E., Kit M.B., Khyl' S.V. 2013; Romaniv O.N. et al., 1990; Troshchenko V.T., 1981; Cherepanov G.P., 1974; Schijve J., 2003; Andreykiv A.E., Darchuk A.I., 1992*). is defined:

$$N_p = N_З + N_Д \tag{1}$$

where $N_З$ - period of formation of fatigue cracks; $N_Д$ - period of subcritical growth of fatigue cracks.

The period of formation of a fatigue crack $N_З$, in the element of structure with the external loading of amplitude σ_0 in variable in time stresses (*Romaniv O.N. et al, 1990*) is presented as follows:

$$N_З = N_0 10^{-\sigma/\sigma_0} \tag{2}$$

Thus, to determine $N = N_З$ of corrosion macro-crack formation in the element under study, it is necessary to specify experimentally the characteristics of an area of fatigue curve finite life σ_0, N_0 (*Romaniv O.N. et al., 1990*). Methods of testing results under the influence of aggressive environments are presented in. Specified characteristics of metal structure materials of fertilizer spreaders are analyzed in the same work.

Based on the results, the definition $N = N_Д$ of subcritical growth of a corrosion - fatigue crack is depicted by the following mathematical problem:

$$V = V_c, \quad K_{scc} < K_{I\max} \le K_{Ii}; \tag{3}$$

$$\frac{dl}{dN} = \beta_1 (1-R)^4 (K_{I\max}^4 - K_{th\max}^4)(K_{fC}^2 - K_{I\max}^2)^{-1}, \quad K_{Ii} < K_{I\max} < K_{fC},$$

with the given initial and final conditions

$$N = 0,\ l(0) = l_0;\ N = N_Д,\ l(N_Д) = l_*,\ K_I(l_*) = K_{fC} \tag{4}$$

where:

$K_{I\max}$ - maximum stress intensity factor (SIF) for the cycle;

$K_{fC}, K_{th\max}$ - correspondingly, the upper and lower SIF threshold values in the kinetic diagrams of propagating fatigue and corrosion mechanical cracks, $MPa \cdot m^{1/2}$;

$R = K_{I\min} / K_{I\max}$ - loading cycle asymmetry;

V_c - constant speed value of near-threshold corrosion-fatigue crack propagation to the intersection with a diagram of fatigue crack propagation with a stress intensity factor $K_{I\max} = K_{Ii}$;

β_1 - corrosion fatigue characteristic features of the material that are defined experimentally.

Based on experimentally developed V_c, β_1, $K_{fC}, K_{th\max}$, K_{Ii}, the period $N = N_Д$ of subcritical growth of a corrosion-fatigue crack in the element under study is defined by means of calculation (3) and (4).

In metal structures of agricultural machinery frames, thin rod elements are commonly used. For these elements, the stress due to bending deformation is defined according to *(Pisarenko G.S. et al., 1988).*

$$\sigma = M W_x^{-1} \tag{5}$$

where M - value of the bending moment, W_x - section modulus.

In undercarriages of fertilizer spreaders, the rail elements of open and closed profiles are commonly used: channels, "Z" profiles and "Ω" profiles. Service life of maximum loaded elements determines the service life of a metal structure in general. Thus, the service life of the given elements is determined by the formula (1), where the period of corrosion-fatigue crack formation is determined according to Weller curve (2). Determination of subcritical growth period $N_Д$ associates with some mathematical difficulties. For this reason, in this paper, the research is devoted to the determination of periods of subcritical growth of corrosion-fatigue cracks in rails of the given profiles due to bending loads.

The open profile rail elements weakened by a straight surface crack of a length l_0 under the action of cyclic bending load are analysed. It is necessary to determine the period of subcritical crack growth (remaining life) $N = N_Д$. Definition of the period of subcritical growth of a fatigue crack is the number of cycles of loading the structure element. Finally, the crack growths a size $l = l_*$. Thus, the further operation of a construction is possible only after the debugging. The problem is solved by relations (3) and (4). The most complex task is to determine the SIF of a kinetic equation (3). When determining the stress intensity factor, K_I, a thin-walled metal element of a metal structure with a surface crack of a length l is assumed to be loaded in such a way that its stress-strain state is relatively symmetrical to the line of crack placement. Therefore, when determining the value K_I, a half-plane with a surface crack *(Andreikiv O.E., Dolins'ka I.Y., Kukhar V.Z., 2013)* is considered as one of the limiting states.

$$K_I = 1.12\sigma_{ном}\sqrt{\pi \cdot l} \tag{6}$$

$\sigma_{ном}$ - nominal normal stress, MPa;

Based on the above, SIF of a crack is defined by the formula

$$K_I = \sigma\sqrt{\pi \cdot l}\left(1.12 + F(\varepsilon)\right) \tag{7}$$

where $\varepsilon = l / D$; D - the maximum size of a cross section of the structure element under study behind the line of crack placement; σ – nominal tension at the crack top; $F(\varepsilon)$ – dimensionless function, if $\varepsilon \to 0$ $F(\varepsilon) \to 0$. In each given case, the function $F(\varepsilon)$ is defined according to the specific features of the structural cracked element.

The rail of "Z" cross section is loaded with the bending moment *M* (Fig.3).

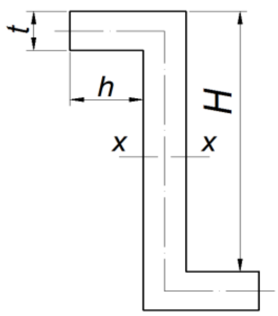

Fig.3 – "Z" profile cracked rail

To implement the mathematical models (3) and (4), it is necessary to account analytically the SIF as a stress function and section modulus W_x. The section modulus is determined *(Pisarenko G.S. et al., 1988)*

$$W_x = (6H)^{-1}[hH^3 - (h-t)(H-2t)^3] \tag{8}$$

RESULTS

To account the SIF, two cases were investigated. The first case: a crack length *l* is short as compared to the outline cross-sectional dimensions. Thus, the state of stress near the crack top is equivalent to stresses σ_{max} that occur during the tensile of a half-infinite plate with an edge crack *(Panasyuk V.V., 1988)* (6). The second case: the contour of the crack is in a zone close to the neutral axis of a cross section. To determine the SIF, the problem solution of the bending moment *M* of a band with an edge crack is applied *(Panasyuk V.V., 1988)*. The unknown function was assumed as $F_1(\varepsilon_1)$ in the form of polynomial coefficients that maximum approximate the correlations for the SIF. Thus, in these two limiting cases, the dependence for SIF K_I is developed:

$$K_I = \sigma\sqrt{2h+H}\sqrt{\pi\varepsilon_1}[1.12 + F_1(\varepsilon_1)] \tag{9}$$

$$F_1(\varepsilon_1) = 0.52\sqrt{\varepsilon_1}(1 + 6.42\varepsilon_1^2 - 6.53\varepsilon_1^3 + 5.86\varepsilon_1^4), \quad \varepsilon_1 = l(2h + H)^{-1}$$

After substitution (9) into (3) and integration within the initial and final conditions (4), in order to determine the period of subcritical crack growth $N = N_{Д}^{(1)}$ the following formulae are deduced:

$$N_{Д}^{(1)} = \frac{l_i - l_0}{V_c} + \frac{K_{fC}^2 (H + 2h)}{\beta_1 K_{th}^4 (1 - R)^4} \int_{\varepsilon_i}^{\varepsilon_*} \frac{1 - f_1(\varepsilon)}{f_2(\varepsilon) - 1} d\varepsilon, \quad \varepsilon_* = \frac{l_*}{2h + H}, \varepsilon_i = \frac{l_i}{2h + H} \tag{10}$$

$$f_1(\varepsilon) = \frac{\pi\sigma^2 \varepsilon (2h + H)}{K_{fC}^2} [1.12 + F_1(\varepsilon)]^2, \quad f_2(\varepsilon) = \frac{\pi^2 \sigma^4 \varepsilon^2 (2h + H)^2}{K_{th}^4} [1.12 + F_1(\varepsilon)]^4$$

The resulting formula (1), (2), (10) enable to account the service life of the rail N_P

$$N_P = N_0 10^{-\sigma/\sigma_0} + \frac{l_i - l_0}{V_c} + \frac{K_{fC}^2 (H + 2h)}{\beta_1 K_{th}^4 (1 - R)^4} \int_{\varepsilon_s}^{\varepsilon_*} \frac{1 - f_1(\varepsilon)}{f_2(\varepsilon) - 1} d\varepsilon \tag{11}$$

Characteristic features of the material $N_0, \sigma_0, V_c, K_{th}, K_{fC}, K_{Ii}, \beta_1$ are under experimental study. In eq. (11), a component l_0 is the value of a small order depending on a size of the material structural parameter *(Savruk M.P., 1988)*.

To consider an incipient crack as a macroscopic one and to apply rightfully the formula (11), it is more efficient to assume the value l_0 of at least two millimeters. In this case, the calculated value N_P will be reduced and the error will increase the service life.

The study (service life calculation $N = N_P$) of the structure element of undercarriage ("Z" cross-section $200 \times 60 \times 5$, is St 37-3) is carried out according to the formula (11). The element is cyclically loaded by the moment M (Fig.3) in the previously mentioned working environments. Based on the analysis of kinetic diagrams of fatigue *(Schijve J., 2003),* mechanical and fatigue properties of St 37-3 should be described as follows (Fig. 4-6):

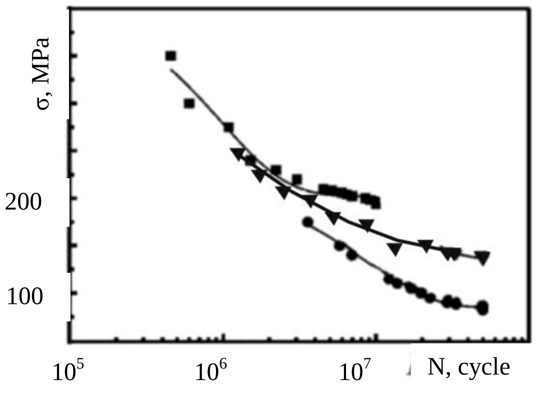

Fig. 4 – Weller curves for St 37-3 are squares; in a fertilizer solution of nitro-phosphate – circles; in mixed organic fertilizer - triangles

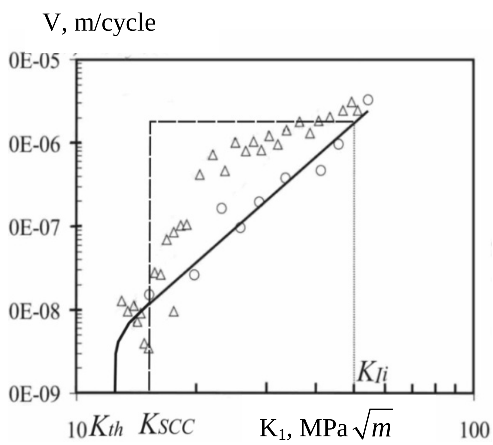

Fig. 5 – Kinetic diagrams of fatigue cracks propagation in St 37-3 in air–circles, at exposure in a mineral fertilizer solution of nitro-phosphate - triangles

- testing in air

$$N_0 = 1.51 \cdot 10^8 \text{cycle}, \quad \beta_1 = 4.51 \cdot 10^{-9} (\text{cycle})^{-1} (MPa)^{-2}, \quad K_{fC} = 102 \quad MPa\sqrt{m},$$
$$\sigma_0 = 120{,}18 MPa, \quad K_{th} = 12{,}81 MPa\sqrt{m}, \quad R = 0{,}1; \tag{12}$$

- testing in a fertilizer solution of nitrophosphate

$$\sigma_0 = 95.63 \quad MPa, \quad N_0 = 2.34 \quad \cdot 10^8 \text{cycle}, \quad K_{Ii} = 50 MPa\sqrt{m},$$
$$V_C = 2,32 \cdot 10^{-6} \quad m/cycle; \qquad (13)$$

- testing in mixed manure

$$\sigma_0 = 121.56 MPa, \quad N_0 = 1.44 \cdot 10^8 \text{cycle} \quad \beta_1 = 4.81 \cdot 10^{-9} (\text{cycle})^{-1} (MPa)^{-2}, \quad l_i = l_0,$$
$$V_C \approx 0, \quad K_{th} = 11.21 MPa\sqrt{m}, \quad R = 0.1, K_{fC} = 101 \quad MPa\sqrt{m} \qquad (14)$$

Based on (12) - (14), the formula (11) is deduced for all cases of loading in environments.

$$N_p^{(\Pi)} = 1.51 \cdot 10^{8-\sigma/120.18} + 4.18 \cdot 10^7 \int_{0.00625}^{\varepsilon_*} \frac{1 - f_1(\varepsilon)}{f_2(\varepsilon) - 1} d\varepsilon \qquad (15)$$

- nitro-phosphate solution

$$N_p^{(K)} = 2.34 \cdot 10^{8-\sigma/95.63} + 4.31 \cdot 10^5 (558.43\sigma^{-2} - 0.002) + 4.18 \cdot 10^7 \int_{\varepsilon_i}^{\varepsilon_*} \frac{1 - f_1(\varepsilon)}{f_2(\varepsilon) - 1} d\varepsilon, \qquad (16)$$

$$\varepsilon_i = 1745.09\sigma^{-2}, \quad \varepsilon_* = 5513.66\sigma^{-2}.$$

- mixed organic fertilizer

$$N_p^{(\Gamma)} = 1.44 \cdot 10^{8-\sigma/121.56} + 6.5 \cdot 10^7 \int_{0.00625}^{\varepsilon_*} \frac{1 - f_3(\varepsilon)}{f_4(\varepsilon) - 1} d\varepsilon, \qquad (17)$$

$$f_1(\varepsilon) = 9.66 \cdot 10^{-5} \sigma^2 \varepsilon [1.12 + F_1(\varepsilon)]^2, \quad f_2(\varepsilon) = 3.75 \cdot 10^{-5} \sigma^4 \varepsilon^2 [1.12 + F_1(\varepsilon)]^4,$$

$$f_3(\varepsilon) = 9.86 \cdot 10^{-5} \sigma^2 \varepsilon [1.12 + F_1(\varepsilon)]^2, \quad f_4(\varepsilon) = 6.40 \cdot 10^{-5} \sigma^4 \varepsilon^2 [1.12 + F_1(\varepsilon)]^4$$

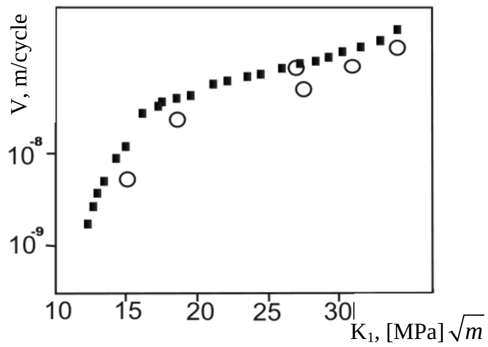

Fig. 6 – Kinetic diagrams of fatigue cracks propagation In St 37-3 in air – circles, at exposure in a solution of mixed organic fertilizers–squares

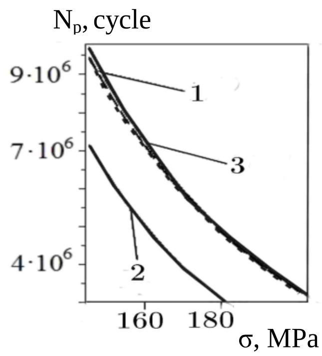

Fig. 7. – Graphic dependence of service life $N = N_P$ of "Z" profile rail on stresses σ curve :

1 - air; 2–nitro-phosphate solution; 3 (dashes)– mixed manure

The value l_i in formulae (11), (16) is deduced from $K_I(\varepsilon_i) = K_{Ii}$, $l_i = (H + 2h)\varepsilon_i$ and determined, approximately, for the given case, $l_i \approx 558.43\sigma^{-2}$.

Based on (15), (16) and (17), the graphical dependences of service life $N = N_P$ of "Z" profile rail as a stress function σ are developed (Fig.5). Corrosive environment significantly reduces the metal structure service life.

The study of a metal undercarriage element of "Ω" cross section (Fig.8). The given rails are commonly used in frame constructions of tractor-trailers and fertilizer spreaders.

The case of loading by a cyclical bending moment *M* is considered in the mentioned corrosive environments. The challenge is to determine the service life N_P, that is, to determine the necessary number of loading cycles that cause the formation and symmetrical intersection of two corrosive fatigue cracks on the bottom part of the element. The component $N_З$ is defined according to (2), $N_Д$ - during the solving of mathematical problems (3), (4).

To implement the mathematical model (3), (4), the stress intensity factor as a stress function and W_x should be analytically accounted. The section modulus due to bending W_x *(Pisarenko G.S., et al, 1988)*

$$W_x = 2(6H)^{-1}[hH^3 - (h-t)(H-2t)^3] \tag{18}$$

The stress intensity factor is determined by means of σ and based on (9), where the value σ is defined by means of correlations (5) and (18). It stands to reason that, the service life N_P of the given rail element is determined according to (11) and with consideration of data (12)-(14). Based on the above mentioned, the equations (15)-(16) should be developed. Their solution is shown in Fig.7. As Fig.5 shows, the service life N_P of rail elements at the given loads is significant. Nevertheless, their residual service life $N_Д$, if the crack of initial length l_0 is available, could be relatively shorten. Thus, the service life of a spreader framework largely depends on the value l_0. Therefore, the determination of residual service life of cracked rail elements is of great importance. The residual service life of the 'Ω'cross section element with two symmetrical cracks on the parts (Fig.6) is $N_Д$. The cross section $200\times60\times5$, St 37-3 under bending by the moment *M* (Fig.6) and maximum stresses of amplitude $\sigma = 188 \ MPa$ are analyzed when loaded in air, in a solution of nitro-phosphate, and at exposure in mixed organic manure.

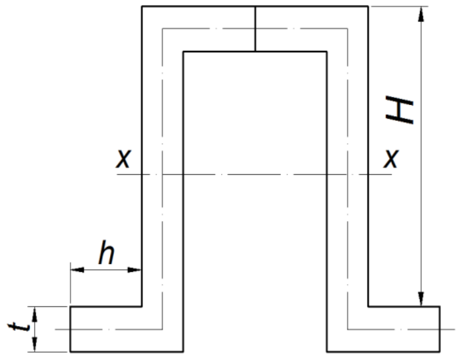

Fig 8 – "Ω" cross section cracked rail

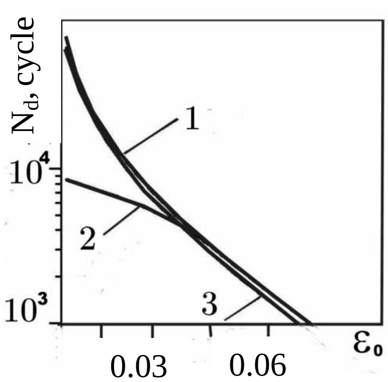

Fig 9 – Service life of "Ω" cross section rail

1 - air; 2–nitro-phosphate solution; 3 – mixed organic manure

Solution is based on the implementation of the mathematical model (3), (4) taking into account the relations (12) - (14). As a result, to determine the residual life $N_Д$, the following formulae are deduced

- air

$$N_Д^{(П)} = 4.18\cdot10^7 \int_{\varepsilon_0}^{0.156} \frac{1-f_1(\varepsilon)}{f_2(\varepsilon)-1} d\varepsilon, \tag{19}$$

- nitro-phosphate solution

$$N_Д^{(H)} = 1.37\cdot10^5(0.049-\varepsilon_0) + 4.18\cdot10^7 \int_{0.049}^{0.156} \frac{1-f_1(\varepsilon)}{f_2(\varepsilon)-1} d\varepsilon \qquad N_Д^{(H)} = 4.18\cdot10^7 \int_{\varepsilon_0}^{0.156} \frac{1-f_1(\varepsilon)}{f_2(\varepsilon)-1} d\varepsilon,$$

$$0.00625 \langle \varepsilon_0 \langle 0.056$$

$$0.049 \langle \varepsilon_0 \langle 0.23 \tag{20}$$

- mixed organic manure

$$N_Д^{(Г)} = 6.5\cdot10^7 \int_{\varepsilon_0}^{0.141} \frac{1-f_3(\varepsilon)}{f_4(\varepsilon)-1} d\varepsilon \tag{21}$$

$$f_1(\varepsilon) = 3.41\varepsilon[1.12 + F_1(\varepsilon)]^2, \quad f_2(\varepsilon) = 4.68\cdot10^4 \varepsilon^2[1.12 + F_1(\varepsilon)]^4$$

$$f_3(\varepsilon) = 3.48\varepsilon[1.12 + F_1(\varepsilon)]^2, \quad f_4(\varepsilon) = 7.99\cdot10^4 \varepsilon^2[1.12 + F_1(\varepsilon)]^4$$

Based on (19) - (21), in Fig. 9 the graphical dependences of residual service life of "Ω" cross section on the initial length of a crack ε_0 are developed. The nitro-phosphate solution could significantly shorten the residual service life.

CONCLUSIONS

The analytical models to determine the service life of rail elements of fertilizer spreaders undercarriages with cyclic bending deformation, taking into account the mode of operation, are developed.

Based on (15), (16) and (17), the graphical dependences of service life $N = N_P$ of "Z" profile rail as a stress function σ are developed (Fig.5). Corrosive environment significantly reduces the metal structure service life.

Based on (19) - (21), in Fig. 9 the graphical dependences of residual service life of "Ω" cross section on the initial length of a crack ε_0 are developed. The nitro-phosphate solution could significantly shorten the residual service life.

REFERENCES

[1] Andreikiv O.E., Dolins'ka I.Y., Kukhar V.Z., (2013), A mathematical model for determining the lifetime of plates with systems of cracks under long-term static breaking loads and high temperatures, *Journal of Mathematical Sciences*, pp.1-10; U.S.A.;

[2] Andreikiv O.E., Kit M.B., Khyl' S.V., (2013), Mathematical modeling of fatigue fracture of plates with cracks under block loading, *Journal of Mathematical Sciences,* vol.190, no.6, pp.752-763, ISSN 10723374, U.S.A.;

[3] Andreykiv A.E., Darchuk A.I., (1992), Fatigue failure and durability of structures (Усталостное разрушение и долговечность конструкций), *Naukova dumka*, p.184, Kyiv/Ukraine;

[4] Cherepanov G.P., (1974), *The mechanics of brittle fracture (Механика хрупкого разрушения*), Nauka, p.640, Moscow/Rusia;

[5] Gaydar S. M., (2011), *Protection of agricultural equipment against corrosion and wear with the use of nanotechnology (Защита сельскохозяйственной техники от коррозии и износа с применением нанотехнологий: дис. на соиск научн. степ докт. техн. наук)*, p.442, Moscow/Rusia;

[6] Panasiuk V.V., Andreykiv O.Y., Parton V.Z., (1988), Fundamentals of fracture mechanics (Основы механики разрушения), *Naukova dumka*, p.488, Kyiv/Ukraine;

[7] Pisarenko G.S., Yakovlev A.P., Matveev V.V., (1988), Handbook on resistance of materials (Справочник по сопротивлению материалов), *Naukova dumka*, p.734, Kyiv;

[8] Romaniv O.N., Yarema S.Y., Nikiforchin G.N., Makhutov N.A., Stadnyk M.M., (1990), Fatigue and cyclic crack resistance of structural materials (Усталость и циклическая трещиностойкость конструкционных материалов), *Naukova dumka*, p.680, Kyiv/Ukraine;

[9] Severnev M. M., Podlekarev N. N., Sokhadze V. Sh., Kitikov V.O., (2011), *Wear and corrosion of agricultural machinery (Износ и коррозия сельскохозяйственных машин)*, Belarus, Navuka, p.333, Minsk;

[10] Schijve J., (2003), Fatigue of materials and structures in the 20th century: state-of-the-art, *Materials Science*, Vol. 39, no.3, pp.7-27;

[11] Troshchenko V.T., (1981), Deformation and fracture of metals at low-cycle loading (Деформирование и разрушение металлов при малоцикловом нагружении), *Naukova dumka*, p.343, Kyiv/Ukraine;

[12] Yarema S.Y., (1973), Stages of fatigue failure and its consequences (Стадийность усталостного разрушения и ее следствия), *Physical and chemical mechanics of materials*, №6. pp.66–72.

CFD SIMULATION OF DIFFERENT WATER TANK SHAPES ON TEMPERATURE DISTRIBUTION UNIFORMITY

/

شبیه‌سازی CFD مخزن آب با شکل‌های متفاوت در یکنواختی توزیع دما

Ph.D. Stud. Eng. Farhadi R.[1)], Lect. Ph.D. Eng. Farrokhi Teimourlou R.*[1)], Lect. Ph.D. Eng. Abbasalizadeh M.[2)]
[1)] Urmia University, Department of Mechanical Engineering of Biosystems / Iran;
[2)] Urmia University, Department of Mechanical Engineering / Iran
E-mail: r.farrokhi@urmia.ac.ir

Keywords: *Disinfection, hydroponic, solar heat pipe, tank shape, uniform temperature distribution*

ABSTRACT

Reusing water drainage can effectively reduce water consumption in greenhouses. However, disinfection is unavoidable. A proper solar disinfection system needs uniform temperature distribution. Four different adiabatic tanks (prism, changed prism, cube and half-cylinder) were compared to achieve temperature distribution using a 3D computational fluid dynamics simulation. The tanks were equipped with solar heat pipes and their heat flux was assumed constant. A 30 minutes transient simulation was performed. The results showed that the cube tank had the most temperature uniformity, then the prism but with lower mean temperature. The changed prism and half-cylinder had almost similar effects and lower uniformity.

چکیده

استفاده دوباره از زه‌آب می‌تواند به طور موثر مصرف آب در گلخانه‌ها را کاهش دهد. اما ضدعفونی گریزناپذیر است. یک سامانه ضدعفونی خورشیدی مناسب، نیاز به توزیع یکنواخت دما دارد. چهار مخزن بی درو مختلف (منشور، منشور تغییر شکل یافته، مکعب و نیمه استوانه با حجم یکسان) مقایسه شدند تا توزیع دما با استفاده از شبیه سازی سه بعدی دینامیک سیالات محاسباتی بدست آید. مخزن به لوله های حرارتی خورشیدی مجهز و شار حرارتی ثابت فرض گردید. سی دقیقه شبیه سازی گذرا انجام شد. نتایج نشان دادند که مخزن مکعبی و بعد از آن منشور ولی با دمای پایین تر، بیشترین یکنواختی را داشتند. منشور تغییر شکل یافته و نیمه استوانه تاثیر های مشابه و یکنواختی کمتری داشتند.

INTRODUCTION

Clean and safe water is one of the most basic human needs. WHO-UNICEF (2015) reported that 663 million people still lack improved drinking water sources. “Although three-quarters of the earth’s surface is water, only 1% is available for direct use, and this often requires treatment before it can be used safely. Water contains many kinds of microbes and organisms, which can cause disease. It is estimated that 80% of all sickness and disease in developing countries is caused by unsafe water and inadequate sanitation” (*Aniruddha Bhalchandra and Jyoti Kishen, 2013*).

“Over the last 25 years, droughts covered more than 37% of EU territory and affected more than 100 million people. The total cost of droughts over the past 30 years amounts to more than 100 billion Euros” *(Andreu et al., 2014)*. Iran with dry and semi-dry region has water scarcity and approximately 92% of total water consumption pertains to agriculture (the ministry of energy, 2016). Wastewater treatment for agriculture has positive benefits and it is necessary due to water scarcity (EPA, 2012). Hydroponic system is one of the proper methods in dry regions. Reusing hydroponics water drainage can save 20 to 30 per cent in water consumption *(Tripanagnostopoulos and Rocamora, 2007)*. However, all of these need water disinfection.

One method that can actually kill pathogens instead of simply removing them is heat *(Burch and Thomas, 1998)*. Thermal energy can be supplied for disinfection by two nonrenewable and renewable resources. Nonrenewable resources of energy will finally finish and their prices have vicissitudes. In addition, global warming and climate changes are other disadvantages. Solar energy is a renewable, clean, free and sustainable resource. One of the existing methods to use solar energy is collectors. Solar heat pipe is an advanced collector and has some privileges: lower losses, higher efficiency, protected from freezing and overheating and absorbing beam and diffuse radiation *(Kalogirou, 2014)*. Thus it was selected in this study.

Various applications demand different temperature distribution in a storage tank. In some applications, such as for domestic hot water systems, stratification is attractive because, hot and cold water are separated inside a well stratified tank and this can improve hot water supply *(Alizadeh, 1999)*. However, for disinfection purposes a uniform temperature distribution is desirable, because pathogens must stand in a certain temperature for a while in order to be killed *(Feachem et al., 1983)*.

Temperature adjustment method has always a main contribution in the final decision related to the solar disinfection system. Some researchers have been applied solar collectors for disinfection purposes by various temperature controlling systems. *Bansal et al. (1988)* designed a solar collector where only near boiling water could exit from system. *Duff and Hodgson (2005)* made a solar water pasteurization system without valves. Water flow was adjusted based on density difference. Thermostatic valves have been used in some solar collectors to control output water temperature for disinfection *(Hameed and Ahmad, 1997; Bigoni et al., 2014)*.

Ali (2012) studied gained energy of two flat plate solar collectors (cylindrical and cubic shape) and recommended the cylindrical collector for continuous loading (tank has valves to supply required flow rate).

Yang et al. (2016) compared different tank shapes in cooling process to find which tank has more energy storage capacity and thermal stratification. They recommend sphere and barrel water tank for thermal energy storage and shapes with sharp corners for thermal stratification.

Heat source inside a storage tank tends to create two parts of cold and hot region, and nature of heat transfer tends to create uniformity. However, tank geometry can effect temperature distribution. Previous researches *(Joudi et al., 2004; Jordan and Furbo, 2005; Garnier et al., 2009; Oshchepkov and Frid 2015)* focused on stratification in a solar water heating systems. A solar collector designed for disinfection, especially with a non-continuous form, should provide a uniform temperature distribution. This paper attempts to show which tank shape has a more uniform temperature distribution.

MATERIAL AND METHOD

In this research, four tanks with different shapes (fig.1) and same volume (0.02940 m^3) were selected. The lengths of changed prism, cube and half-cylinder were 0.9424, 1, 0.96105 and 0.95634 m, respectively. Tank walls were supposed to be in adiabatic state.

The condenser part of solar heat pipe is 60 mm long and its diameter is 14 mm. This part should be completely inside water as shown in the changed prism and cube tanks in fig. 1, but due to limitations caused by geometry and the angle of condensers, the whole part of condenser could not enter the prism and half-cylinder tanks (fig.1). There were five condensers in each tank and their distance was the constant value of 0.174 m. All five condensers in all tanks had the constant angle of 35 degrees with the horizon (all tanks were full of water).

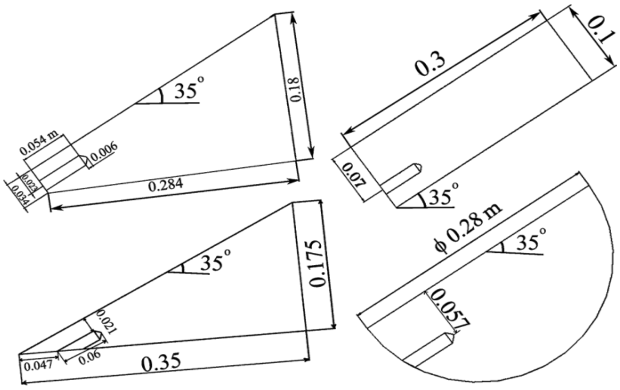

Fig. 1 - Tank with different sections of changed triangle, rectangle, triangle and semi-circle (units: meter)

To measure heat flux of condensers, one solar heat pipe (length=1800 mm, Ø=58 mm, Deno solar equipment Co.) was exposed to the sun with the angle of 35° on 9 March 2016 (location: 37°39'36.4"N 44°58'59.0"E) from 9:00 to 15:00, as is shown in fig.2, and the amount of energy (*q*) was calculate by equation (1). A small tank was placed on the condenser part and a small pump used to circulate the water. Two waterproof temperature sensors (DS18B20) were placed in inlet and outlet path and connected to by an electronic board to measure the temperature. The average of one-day data resulted in the flux of 20186 W/m^2 and it was applied as a constant flux for simulations.

$$\dot{q} = \dot{m}c\Delta T = \dot{m}c(T_{out} - T_{in}) \tag{1}$$

Where: $\dot{q}$ - gained energy (J/s); *c* - water specific heat (J/kg K);
T - temperature (K); $\dot{m}$ - mass flow rate (kg/s).

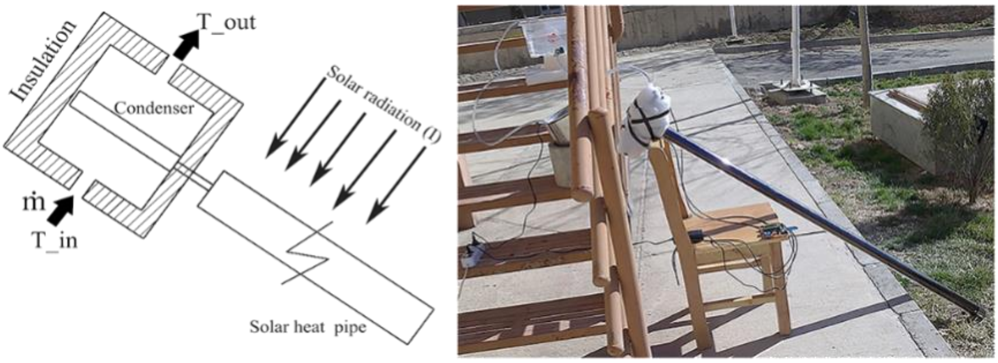

Fig. 2 - Measuring condenser heat flux

A 3D computational fluid dynamics simulation was used by ANSYS-CFX software. A 30 minutes transient analysis with the k-epsilon turbulence was chosen. "One of the most prominent turbulence models, the k-ε (k-epsilon) model, has been implemented in most general purpose CFD codes and is considered the industry standard model. It has proven to be stable and numerically robust and has a well established regime of predictive capability. For general purpose simulations, the k-ε model offers a good compromise in terms of accuracy and robustness" *(ANSYS, 2013)*. For as much as there is free convection, buoyancy model was activated. Initial water temperature inside the tank was set to 15°C. During simulation, tanks had constant water without any inlet or outlet flow. As geometry and boundary conditions were symmetric, the half part of tanks was considered in simulations and also in figures.

Results should not vary with different mesh numbers and time steps. Thus, the independency of mesh and time step were done as described by *Angermann (2010)*.

Two-sample Kolmogorov–Smirnov statistical test (*Dytham, 2011)* was used for comparing temperature distribution in different tanks using IBM SPSS statistics.

The results were evaluated by considering equation (1). Tanks had the constant mass of water (29.4 kg), heat flux was (20186 W/m^2), simulation total time was 30 minutes and initial water temperature was 15°C as mentioned above. Therefore, final uniform water temperature was calculated. The calculated temperature (expected uniform temperature in table 1 and table 2) was compared with the average temperature of all nodes estimated by the simulation.

RESULTS

Table 1 and table 2 present the results of mesh and time step independency. Meshes, which had lower difference with expected uniform temperature in table 1, were selected and used with different time steps. Expected uniform temperature in the prism and half-cylinder (table 1) was different from other tanks because, as described previously, the length of condenser in these tanks was different.

As can be seen in table 2, the results do not vary considerably by the time steps. In addition, standard deviation, coefficient of variation (CV) and standard error of mean in the table 1 and table 2 have low values representing results uniformity. Thus, for final simulation, the time step of one second was applied to discriminate more accurately the temperature distribution.

Table 1

The results of simulation for different mesh numbers and tank shapes

Tank section	Element number	Mean temperature [K]	Standard deviation	coefficient of variation (CV) [%]	Standard error of mean	Expected uniform temperature [K]	Difference [%]
Changed prism	67493	291.4202	0.5277	0.1811	0.0048	294.95	1.20
	156837	291.6140	0.6949	0.2383	0.0040		1.13
	419100*	292.0197	1.1444	0.3919	0.0042		0.99
Prism	58300	290.8417	0.6672	0.2294	0.0065	293.93	1.05
	91860*	290.9510	0.5898	0.2027	0.0044		1.01
	597751	290.8510	0.5471	0.1881	0.0017		1.05
Cube	80500	291.3151	0.5216	0.1790	0.0061	294.95	1.23
	167416*	291.7085	0.8387	0.2875	0.0067		1.10
	578612	291.2710	0.3898	0.1338	0.0017		1.25
Half-cylinder	202446*	292.1846	0.9145	0.3130	0.0048	294.76	0.87
	393865	291.9053	0.7298	0.2500	0.0027		0.97
	718581	291.9717	0.8149	0.2791	0.0023		0.95

* selected mesh numbers

Table 2

The results of simulation with the selected mesh numbers for different time steps

Tank section	Selected element number	time step (s)	Mean temperature (K)	Standard deviation	CV (%)	Standard error of mean	Expected uniform temperature (K)	Difference (%)
Changed prism	419100	5	292.2311	1.0795	0.3694	0.0039	294.95	0.92
		10	292.0197	1.1444	0.3919	0.0042		0.99
		20	292.3350	1.1333	0.3877	0.0041		0.89
Prism	91860	5	290.9298	0.5980	0.2055	0.0045	293.93	1.02
		10	290.9510	0.5898	0.2027	0.0044		1.01
		20	290.7972	0.6105	0.2099	0.0046		1.05
Cube	167416	5	291.7649	0.8413	0.2883	0.0068	294.95	1.08
		10	291.7085	0.8387	0.2875	0.0067		1.10
		20	291.6504	0.8287	0.2841	0.0067		1.12
Half-cylinder	202446	5	292.2788	0.9029	0.3089	0.0047	294.76	0.84
		10	292.1846	0.9145	0.3130	0.0048		0.87
		20	292.1173	0.8988	0.3077	0.0047		0.90

Table 3 and table 4 show results with the time step of one second. All data have low standard deviation, CV and standard error of mean. It confirms uniformity of the results. However, velocity values have higher CV because in some parts of tanks water velocity is zero.

The cube and then the prism had the minimum value of variation in temperature and velocity. The changed prism and half-cylinder had similar conditions. The prism and half-cylinder had lower mean temperature as described for expected uniform temperature.

The temperature and velocity distribution are illustrated in fig. 3 and fig. 4 based on nodes data. The Kolmogorov-Smirnov test certified that all tanks had significantly different temperature and velocity distribution (table 5).

Table 3

The results of final simulation (temperature data)

Tank section	Mean temperature [K]	Standard deviation	CV [%]	Standard error of mean	Expected uniform temperature [K]	Difference [%]
Changed prism	291.9727	0.9367	0.3208	0.0057	294.95	1.01
Prism	290.5577	0.4849	0.1669	0.0033	293.93	1.15
Cube	291.2542	0.3142	0.1079	0.0022	294.95	1.25
Half-cylinder	291.7044	0.8880	0.3044	0.0059	294.76	1.04

Table 4

The results of final simulation (velocity data)

Tank section	Mean velocity [m/s]	Standard deviation	CV [%]	Standard error of mean
Changed prism	0.003893	0.002336	60	0.000014
Prism	0.003213	0.001847	57.50	0.000013
Cube	0.004207	0.002003	47.61	0.000014
Half-cylinder	0.003627	0.002184	60.20	0.000014

According to fig. 3, the best temperature uniformity belongs to the cube tank followed by the prism, changed prism and half-cylinder tanks. The prism tank had lower mean temperature because a little part of condenser was outside of the tank. Although velocity distribution in all tanks was statistically different, the cube and prism tanks had approximately similar distribution. The distribution was also the same in the half-cylinder and changed prism (fig. 4). It is expected that high velocity value assist to better temperature distribution *(Cengel and Ghajar, 2015)* as happened in the cube case (table 4). The higher velocity and flow in fluid will cause an increase in the mixture level and, consequently, result in higher uniformity.

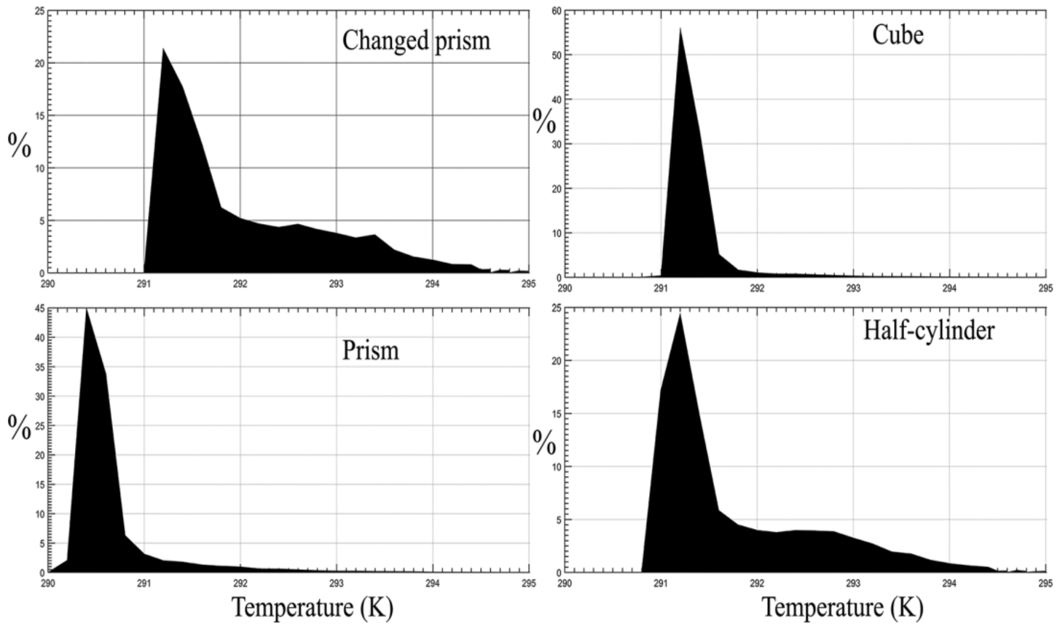

Fig. 3 – The histogram of nodes with different temperatures

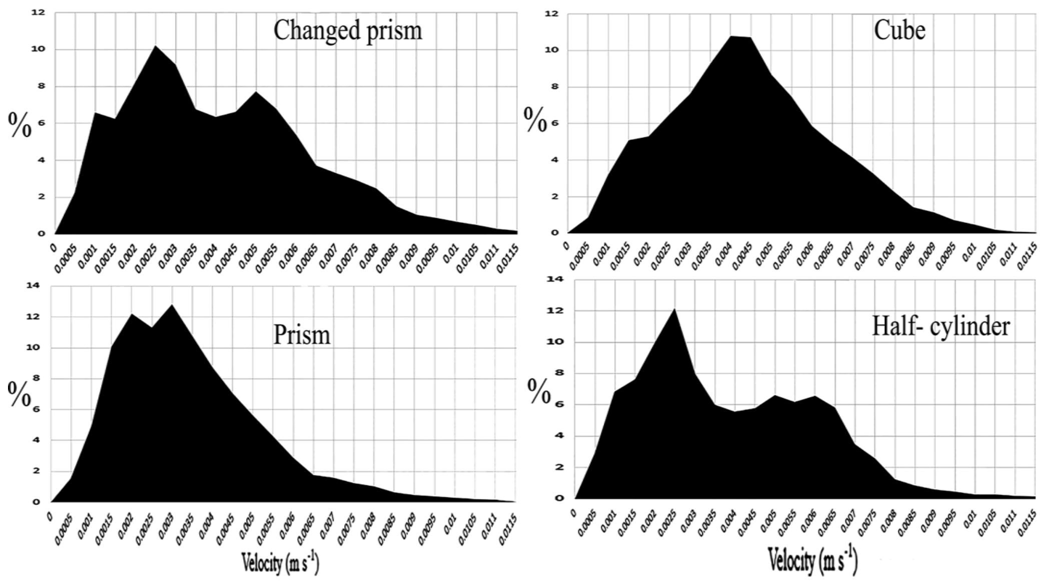

Fig. 4 - The histogram of nodes with different velocities

Table 5

Two-sample Kolmogorov-Smirnov test for comparing temperature and velocity distribution

Comparison item	Kolmogorov-Smirnov Z		*p*-valve	
	Temperature	Velocity	Temperature	Velocity
Changed prism, prism	98.370	18.824	0.000**	
Changed prism, cube	54.196	15.503		
Changed prism, half-cylinder	30.529	6.734		
Half-cylinder, cube	34.581	20.301		
Prism, cube	92.089	26.756		
Prism, half-cylinder	91.839	15.509		

** $p<0.01$

It should be noted that the prism tank with lower mean velocity had proper uniformity because its mean temperature was lower than other tanks. For considering more details, nodes having top percentage in the fig. 3 are presented in fig. 5 (figures are the half of tanks due to symmetry). The picture confirms the similarity of changed prism and half-cylinder tanks, but cube tanks in right side perform differently. A vortex formed inside the tank disturbs uniformity (fig. 6). Although the cube tank had the best uniformity, reducing marginal space or optimizing condensers distance can boost uniform distribution. In addition, *Ali (2012)* recommended a cube tank in non-continuous flow for gaining more energy.

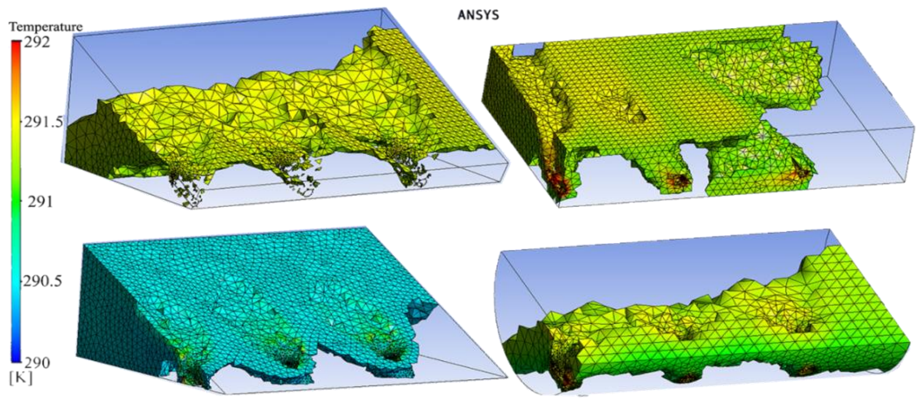

Fig. 5 - The location of most frequent temperature in each tank

(changed triangle and rectangle: 291.19-291.41 K, triangle: 290.39-290.61 K and semi-circle: 290.99-291.21 K)

As it can be seen from fig 5, the prism tank has apparently better conditions than the cube tank; although distribution data do not prove it. However, approximately 44.8 % nodes had lower temperature than the average in the prism tank while about 55% nodes in the cube tank were close to the average. Fig. 7 shows nodes with the mean temperature of tanks. In these nodes, the volume of water in the cube was 13.1% higher than the prism tank (0.001244 m^3 in front of 0.0011 m^3). In addition, the nodes with mean temperature in the prism only occupied top parts of tank, while in the cube case, they were distributed in different parts. Therefore, all cases certify that the cube tank presents more uniformity. Furthermore, considering velocity in the prism tank reveals that most nodes of fig. 5 (prism) have low velocity.

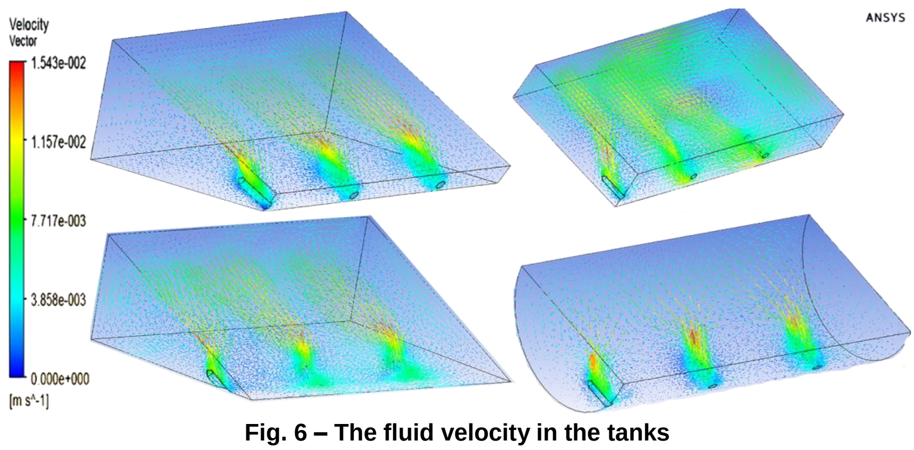

Fig. 6 – The fluid velocity in the tanks

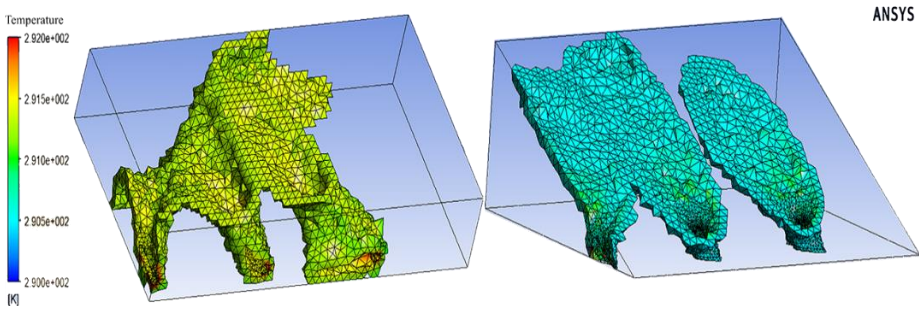

Fig. 7 – Nodes with mean temperature (rectangle: 291.25, triangle: 290.56 K)

In the symmetry and mid plane of the tanks, temperature contour plots (fig. 8 and fig. 9) show that the cube tank is different from others. It has the less stratified model while similar stratification exists in the changed prism and half-cylinder tanks, approximately. The prism tank has intermediate status among the tanks. *Yang et al. (2016)* reported similar status for tanks being in cooling process. It was proved that shapes with horizontal plane surface had lowest stratification.

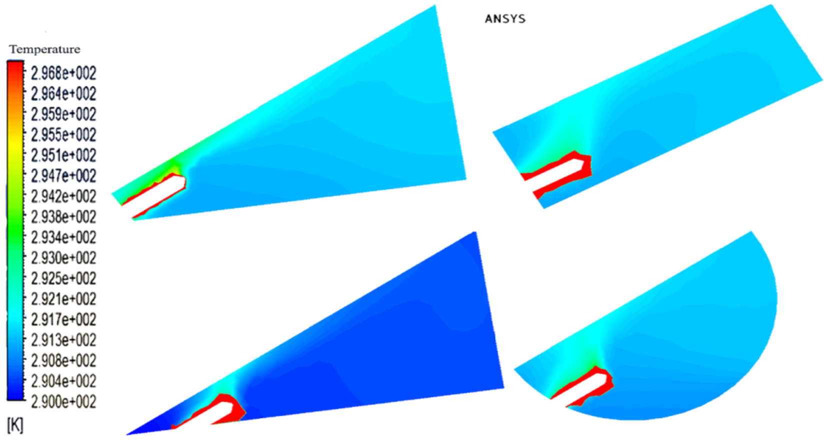

Fig. 8 - Temperature contours on the symmetry plane

There is not adiabatic wall in nature; therefore, collected hot water at the top of condenser in changed prism (fig. 8) will be unsuitable for real applications due to heat losses.

All tanks had three regions with higher temperature placed above the condensers except for the cube tank having four parts (fig. 9). It increases temperature uniformity in the cube tank.

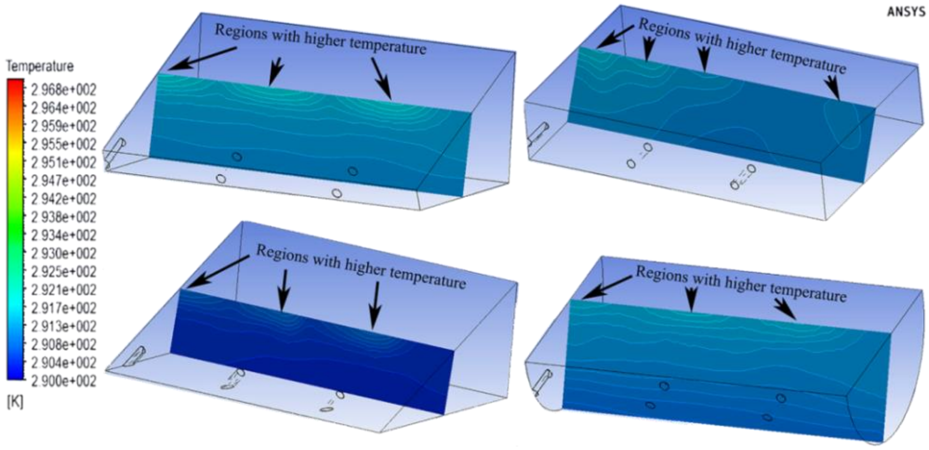

Fig. 9 - Temperature contours on the mid plane perpendicular to the symmetry plane

CONCLUSIONS

A 3D transient computational fluid dynamics simulation on a solar heat pipe collector with four tank shapes (prism, changed prism, cube and half-cylinder) was done. The collector had non-continuous flow, constant heat flux, adiabatic walls and natural heat convection. Comparing different tanks it has revealed that the cube tank had the best uniform temperature while the half-cylinder was unfit in temperature uniformity. Temperature distribution in the changed prism was similar to the half-cylinder and the prism had intermediate status. Since the tanks had maximum temperature variation in the start of simulation, first 30 minutes duration was selected in this study. The two-sample Kolmogorov-Smirnov test certified that distributions had statistically significant differences. Transient CFD simulation is time consuming and requires much time for reaching higher temperatures. Therefore, further experimental research should be conducted in order to analyze the operation of the proposed tanks for real disinfection temperatures (60-100°C).

ACKNOWLEDGEMENT

We would like to thank Dr. Youbert Ghosta, (Department of plant protection, Urmia University) for his help and guidance during this experiment and research.

REFERENCES

[1] Ali O.M., (2012), Effect of Storage Heater Shape on Performance of Built-In-Storage Solar Collector Suitable for IRAQ Environment, *Al-Rafadain Engineering Journal,* Vol. 20, Issue 2, pp. 1-8;

[2] Alizadeh S., (1999), An experimental and numerical study of thermal stratification in a horizontal cylindrical solar storage tank, *Solar Energy,* Vol. 66, pp. 409-421;

[3] Andreu J., Solera A., Paredes-Arquiola J., Haro-Monteagudo D., Van Lanen H., (2015), *Drought: research and science-policy interfacing,* pp: xiii, CRC Press/London, UK;

[4] Angermann L., (2010), *Numerical Simulations - Examples and Applications in Computational Fluid Dynamics,* pp: 27, InTech/Rijeka, Croatia;

[5] Aniruddha Bhalchandra P., Jyoti Kishen K., (2013), *Drinking Water Disinfection Techniques*, p:1, CRC Press/Boca Raton, U.S.A;

[6] ANSYS, Inc., (2013), *ANSYS CFX-solver modeling guide, release 15.0*, p:141, SAS IP, Inc./Canonsburg, Pennsylvania, U.S.A.;

[7] Bansal N., Sawhney R., Misra A., Boettcher A., (1988), Solar sterilization of water, *Solar energy*, Vol.40, Issue 1, pp. 35-39;

[8] Bigoni R., Kötzsch S., Sorlini S., Egli T., (2014), Solar water disinfection by a Parabolic Trough Concentrator (PTC): flow-cytometric analysis of bacterial inactivation, *Journal of Cleaner Production,* Vol. 67, pp. 62-71;

[9] Burch J.D., Thomas K.E., (1998), *An Overview of Water Disinfection in Developing Countries and the Potential for Solar Thermal Water Pasteurization,* p:19, National Renewable Energy Laboratory/Golden, U.S.A;

[10] Cengel Y., Ghajar A., (2015), *Heat and Mass Transfer: Fundamentals and Applications,* p:533, McGraw-Hill Education/New York, U.S.A;

[11] Duff W.S., Hodgson D. A., (2005), A simple high efficiency solar water purification system, *Solar Energy,* Vol. 79, Issue 1, pp. 25-32;

[12] Dytham C., (2011), *Choosing and using statistics: a biologist's guide,* p:86, John Wiley & Sons/Pondicherry, India;

[13] EPA, 2012, *Guidelines for water reuse,* pp: 1-5, U.S. Environmental Protection Agency/Washington DC, U.S.A;

[14] Feachem R., Mara D.D., Bradley D.J., (1983), *Sanitation and Disease,* p: 79, John Wiley & Sons/New York, U.S.A;

[15] Garnier C., Currie J., Muneer T., (2009), Integrated collector storage solar water heater: temperature stratification, *Applied Energy,* Vol. 86, Issue 9, pp. 1465-1469;

[16] Hameed S.K., Ahmad I., (1997), Solar sterilization of water, *Renewable Energy,* Vol. 12, Issue 3, pp. 321-324;

[17] Jordan U., Furbo S., (2005), Thermal stratification in small solar domestic storage tanks caused by draw-offs, *Solar energy,* Vol. 78, Issue 2, pp. 291-300;

[18] Joudi K., Hussein I., Farhan A., (2004), Computational model for a prism shaped storage solar collector with a right triangular cross section, *Energy Conversion and Management,* Vol. 45, Issue 3, pp.391-409;

[19] Kalogirou S.A., (2014), *Solar Energy Engineering: processes and systems,* p:134, Academic Press/California, U.S.A;

[20] Oshchepkov M.Y., Frid S., (2015), Thermal stratification in storage tanks of integrated collector storage solar water heaters, *Applied Solar Energy,* Vol. 51, Issue 1, pp. 74-82;

[21] The Ministry of Energy, (2016), Information and statistic network, http://isn.moe.gov.ir (Accessed May 18 2016);

[22] Tripanagnostopoulos Y., Rocamora M.C, (2008), Use of solar thermal collectors for disinfection of greenhouse hydroponic water, *International symposium on high technology for greenhouse system management: Greensys 2007 801,* ISHS, Naples/Italy, pp: 749-756;

[23] WHO-UNICEF, (2015), *Progress on Sanitation and Drinking Water: 2015 Update and MDG Assessment,* pp: 4, World Health Organization/Geneva, Switzerland;

[24] Yang Z., Chen H., Wang L., Sheng Y., Wang Y., (2016), Comparative study of the influences of different water tank shapes on thermal energy storage capacity and thermal stratification, *Renewable Energy,* Vol. 85, pp. 31-44.

PREDICTION OF BEEF FRESHNESS USING A HYPERSPECTRAL SCATTERING IMAGING TECHNIQUE
/
利用高光谱散射图像技术预测牛肉新鲜度

Lect.Ph.D. Ma Shibang *[1], Lect.Ph.D. Xue Dangqin[2], Ph.D. Stud.Wang Xu [3], Prof. Xu Yang [3]

[1] College of Mechatronic Engineering, Nanyang Normal University, Henan / China; [2] College of Mechanical & Automotive Engineering , Nanyang Institute of Technology, Henan / China; [3]College of Engineering, China Agricultural University, Beijing / China

Tel: +8613503774059; E-mail: mshibang@126.com

Keywords: *beef freshness; hyperspectral scattering imaging; Lorentzian distribution function; genetic algorithm*

ABSTRACT

A rapid and non-destructive method based on hyperspectral scattering technique for determination of beef freshness (i.e.,TVB-N) was studied in this study. Hyperspectral images of 60 beef samples stored at 4°C for 1-18 days were acquired using a VIS/NIR hyperspectral imaging system in the wavelength range of 400-1100 nm, and the scattering profiles of every wavelength were fitted to a Lorentzian distribution function to give three parameters a (asymptotic value), b (peak value) and c (full width at b/2). The single parameters (a, b or c) or their combined parameters (a+b/c or (b-a)/c) were used to develop least square-support vector machine (LS-SVM) models for prediction of beef freshness. The performance of a LS-SVM model developed using (b-a)/c was the best among all the tested models, showing R_c=0.91, R_p=0.86, SEC=5.83 mg/100 g and SEP=5.21 mg/100 g. A genetic algorithm was used to optimize the parameter (b-a)/c for developing a GA-LS-SVM model, which performed best showing R_c=0.97, R_p=0.96, SEC=3.38 mg/100 g and SEP=3.85 mg/100 g. This study provided a new non-destructive method based on a hyperspectral imaging technique combined with a genetic algorithm for rapid prediction of beef freshness.

摘要

利用高光谱散射技术预测牛肉挥发性盐基氮（TVB-N），实现了牛肉新鲜度的无损快速检测。用可见近红外高光谱成像系统，获取储藏在4°C下1~18天60个牛肉样品的400~1100nm波长范围的高光谱图像，利用洛伦兹分布函数拟合各个波长处的散射曲线，获取不同波长处散射曲线的洛伦兹参数。利用洛伦兹单参数a、b、c及组合参数a+b/c、(b-a)/c建立TVB-N的最小二乘支持向量机（LS-SVM）预测模型，结果显示组合参数(b-a)/c所建模型的预测精度最佳，校正集和预测集的预测相关系数和标准差分别为0.91、0.86和5.83mg/100g、5.21mg/100g。用遗传算法(GA)对组合参数(b-a)/c进行优选后重新建GA-LS-SVM预测模型，校正集和预测集的预测相关系数分别提高到0.97、0.96，标准差分别降低为3.38mg/100g、3.85mg/100g。研究结果表明，用高光谱散射特征结合遗传算法能够很好地预测牛肉的TVB-N，为实现牛肉新鲜度的无损快速检测提供了一种新方法。

INTRODUCTION

Beef is a kind of high-value nutritional meat. Because it is important in human diet and highly valued by consumers, beef consumption shows a trend of increase in meat product market *(Ortega et al., 2016)*. Freshness is one important quality of beef, which influences beef consumers' purchase choice and the diet's safety. With the improvement in living standards and life quality, beef consumers show more concerns about the evaluation and grading of beef freshness *(Owusu-Sekyere et al., 2014).* During the course of processing, circulation and marketing of fresh beef, many factors such as environment temperature and microbial breeding can influence beef freshness, making beef physico-chemical characters change with time. Under influences from bacteria and enzymes, beef proteins may be decomposed into basic nitrogen substances such as amines. Those basic nitrogen substances, when subjected to organic acids generated in beef decomposition processes, may form salt-ground nitrogen substances that gather in the meat. Those kinds of substances are volatile and referred to as total volatile base nitrogen (TVB-N). With the increase of storage time and corruption degrees of meat, meat TVB-N content increases gradually. Meat TVB-N content can reflect the freshness of meat. TVB-N content in fresh meat and in metamorphic meat differs significantly, and the content difference is in agreement with consumers' sensory evaluation. Therefore, TVB-N content is an objective criterion for the evaluation of meat freshness. China's current food hygiene evaluation criterion considers TVB-N content as the only indicator for the determination of meat freshness. Therefore, TVB-N content is an important indicator for the determination of beef freshness, and now in China beef freshness is graded according to TVB-N content as required by China's national standard GB2707-2005. However, the detection of beef TVB-N is currently conducted with traditional physico-chemical testing methods showing some limitations such as time-consuming processes and sample-destructive processes as well as influences from artificial factors. The traditional testing methods fail to meet the requirements for rapid, non-destructive and automated detection of beef TVB-N.

Spectrum-based detection methods are convenient, rapid and non-destructive with good measurement reproducibility, and have been widely used in the detection of fresh meat quality and safety *(Peng and Zhang, 2013; Wang et al., 2013; Liu et al., 2016; Lohumi et al., 2015)*. Some studies reported the detection of meat freshness based on near-infrared (NIR) spectrum *(Hou et al., 2006; Xu et al., 2009)*, where the investigators carried out preliminary studies on the detection of meat freshness by using NIR. *Cai et al. (2009; 2011)* predicted pork TVB-N content by using NIR spectrum in two studies, where the prediction correlation coefficients (R_p) were 0.823 and 0.808, respectively. *Ma et al. (2012)* developed a prediction model based on partial least squares-support vector machine (LS-SVM) and predicted beef pH with non-destructive visible and near-infrared spectrum, achieving a good prediction result with a R_p of 0.935 and a *SEP* (standard error of prediction) of 0.111. *Morsy et al. (2013)* developed robust linear and non-linear models of NIR spectroscopy for detection and quantification of adulterants in fresh and frozen-thawed minced beef, which were mixed with pork, beef offal and beef fat trimming，but there are some limitations in the NIR application. Hyperspectral imaging is a new detection technology that can provide many spatially resolved spectral data in a sample, and can comprehensively reflect the surface and internal characteristics of the sample. The hyperspectral imaging technology has been used with high precision and accuracy for the determination of chemical constituents or quality attributes in food and agricultural products *(Gowen et al., 2007; Wu and Sun, 2013; Xie et al., 2015; Kamruzzaman et al., 2016)* and has been used to detect meat quality attributes in recent studies *(Wu et al., 2009; El Masry et al., 2012; Li et al., 2015; Yang et al., 2017). Zhang et al. (2012)* predicted pork TVB-N with a correlation coefficient (R_v) of 0.90 and a *SEP* of 7.80 by using reflectance spectra of hyperspectral images. Spatially resolved hyperspectral scattering profiles were used to predict pork tenderness, *Escherichia coli* contamination in pork and microbial spoilage of beef *(Tao et al., 2012; Peng et al., 2011)*. The hyperspectral scattering technique were used to predict fresh beef tenderness (expressed in terms of the values of Warner-Bratzler Shear Force or WBSF) and color parameters (L*, a*, b*), showing R_{cv} of 0.91 for beef WBSF, and R_{cv} of 0.96, 0.96 and 0.97, respectively, for colour parameters (*Wu et al., 2012*). The aforementioned research examples show that hyperspectral scattering techniques can predict meat quality attributes. However, studies about prediction of beef freshness based on hyperspectral scattering imaging have not yet been reported. This study aimed to build a hyperspectral detection system for beef freshness measurement. In this system, hyperspectral images of fresh beef would be collected and analyzed for extraction of hyperspectral images scattering characteristics that would be used to establish a prediction model for determination of fresh beef TVB-N and beef freshness.

MATERIAL AND METHOD

Hyperspectral imaging system

A hyperspectral imaging system in the wavelength range of 400-1000 nm was established and used to acquire the images of beef meat samples in this study, and is sketched in Fig. 1. The hyperspectral imaging system mainly consisted of a high-performance back-illuminated 12-bit charge-coupled device (CCD) camera, an imaging spectrograph, a light source unit equipped with optical fibers, a computer installed with a data acquisition and control software, a motor, a screw, a sample holder and a shield case. The imaging system was enclosed in the shield case in order to minimize effect of ambient light. The optical fiber functioned as a 150-W point light source in the imaging system, and the diameter of the point light beam was 5 mm. The system worked in a line scanning mode, and all scans were achieved by scanning sample positions at a 4 mm distance from the incident light centre to avoid signal saturation on the CCD detector. The spectral resolution of the imaging system was 2.8 nm. Any image obtained with this system comprised 1376×1040 (spatial×spectral) pixels.

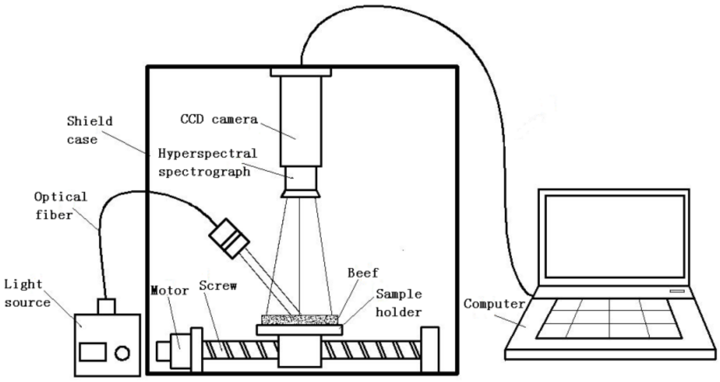

Fig. 1 - The sketch of the hyperspectral imaging system

Fig. 2 - The view of the test system

Experimental procedures

Sample preparation

A fresh beef meat product was purchased from a local supermarket on the day of the experiment and immediately transported to a lab under refrigeration. Sixty beef samples were aseptically prepared by trimming the meat into 60 pieces each in a uniform size of 8 cm×5 cm×2.5 cm (length×width×thickness). The 60 samples were packed separately in commercial food-grade polyethylene bags and placed orderly in a refrigerator at 4^{o}C for 1-18 days. According to characteristics of beef corruption, the time period of experiment was set to be 18 days. During the early 6 days, one sample was randomly withdrawn for the hyperspectral imaging and reference TVB-N analysis with 12-h time intervals. During the late 12 days, two samples were randomly withdrawn for the hyperspectral imaging and reference TVB-N analysis with 12-h time intervals.

Acquisition of hyperspectral images

Before acquiring the hyperspectral imaging and reference TVB-N analysis in each experiment, the beef samples were removed from the polyethylene bags and placed in the air for 20 minutes, which could allow the beef surface's moisture to volatilize minimizing moisture effect on the measurements. In order to eliminate dark current effect of the imaging system, dark images were first collected by covering the camera lens before the imaging of each beef sample. Before imaging, the object distance was measured by a vernier caliper and maintained at a preset value by fine tuning of the vertical stage. For any sample, six positions were selected for imaging, and the mean of the six images was used to denote the hyperspectral image for that sample. In order to improve the signal-to-noise ratios, 2×2 binning was performed on the original images for each sample. Therefore, the resulting image size of each sample was 688×520 (spatial×spectral) pixels. All the acquired sample images were saved in TIFF format for further analysis.

Total volatile base nitrogen (TVB-N) test

Fig. 2 provides a view of the test system. The TVB-N content in the beef samples was measured according to the semi-micro Kjeldahl method as required by China's national standard GB/T 5009.44 for hygienic assessment of fresh and frozen meat of livestock (*Hygiene and Committee, 2003, 2005; Huang et al., 2014*). All beef samples for testing were individually ground using a meat grinder (JYL-C022, Joyong Company Ltd., China). Each ground beef meat sample (10±0.1 g) was placed in a beaker and impregnated with 100 mL of distilled water for 30 min under sporadic beaker shaking every 2 min. The mixture was filtered through a filter paper. Five millilitres of the filtrate was made alkaline by adding 5 mL of 10 g L^{-1} Magnesia (MgO). Steam distillation was conducted for 5 min using a Kjeldahl distillation apparatus (KDY-9820, Jinan Hanon Instrument Co. Ltd., China). The distillate was absorbed by 10 mL of 20 g L^{-1} boric acid and then titrated in triplicate with 0.01 mol L^{-1} HCL. Before the titration of the beef samples' distillate, a blank samples' distillate was titrated in triplicate and the data was subtracted from the above data of the beef samples. The amount of TVB-N in each beef sample was calculated according to eqn. 1.

$$TVB-N(mg/100g)=\frac{(V_1-V_2)\times c\times 14}{m\times 5/100}\times 100 \tag{1}$$

where V_1 is the mean titration volume (in mL) for the test sample measured in triplicate, V_2 is the mean titration volume (in mL) of the blank sample measured in triplicate, c is the concentration (in mol L^{-1}) of HCL, and m is the weight (in g) of the ground beef sample.

Data analysis

Lorentzian function fitting to scattering profiles

When acquiring the hyperspectral images of the beef samples, we illuminated the samples with a small continuous-wave light beam. The hyperspectral scattering image of any beef sample is a diffusely reflected image generated at the sample's surface around the incident light point, and the image was a result of light propagation and light backscattering inside the sample *(Mendoza et al., 2011*). When applying the hyperspectral scattering imaging to the determination of the TVB concentrations, we need to use appropriate mathematical equations to describe the spectral scattering profiles and to reflect the information in the profiles. A Lorentzian function was proposed to fit hyperspectral scattering images and a good fitting result was obtained (*Lu and Peng, 2006*). Following *Lu and Peng* (2006), this study proposed a three-parameter Lorentzian function as shown in eqn. 2 to fit the scattering profiles of the beef samples.

$$I_{wi} = a_{wi} + \frac{b_{wi}}{1+(x/c_{wi})^2} \tag{2}$$

In eqn. 2, I is the light intensity in the CCD count; x (in mm) is the scattering distance measured from the beam incident centre; a is the asymptotic value of light intensity; b is the peak value of the scattering profile at the light incident centre; c is the full scattering width of the scattering profile at one half of the peak value; the subscript w_i represents the i^{th} specific wavelength in the wavelength range of 400-1100 nm where i=1,2,3,…,n and n represents the total number of wavelengths.

Development of Prediction models

In this study, except using individual Lorentzian parameters to develop prediction models for beef TVB-N, we used a combination of the parameters to fully utilize the information associated with the three individual parameters. An LS-SVM model was taken as the prediction model in this study; this kind of model has been widely used as a prediction model and has shown good prediction results in many studies. The details of the LS-SVM model principle can be referred to the study *by Xu et al. (2015)*. Spectra with optimal parameters were defined as best-parameter spectra for developing prediction models. A genetic algorithm method was employed to optimize the spectra variables. In order to reduce effect of noise and light scattering, the best-parameter spectra were subjected to pre-treatment methods such as Multiplication Scatter Correction (MSC) and Savitzky-Golay smoothing (SG). All the data analysis was performed in a Matlab 7.11 software package (Mathworks, Ltd., USA).

Genetic Algorithm

The method of genetic algorithm (GA) is a kind of numerical optimization method based on random search and is particularly suitable for dealing with complex non-linear optimization problems and combination optimization problems. GA begins with a population initialized randomly over the search space of the optimization problem. By simulating the Darwinian evolution principle of "survival of the fittest", GA generates improved approximate solutions or optimal solutions through an iterative procedure. A detailed description of the algorithm can be referred to the literature *(Leardi and Gonzalez, 1998, 2000)*. GA has been successfully used as a feature selection technique, improving predictive ability of prediction models and making it very easy to perform model predictions. In this study, GA-selected feature variables of the best-parameter spectra were taken as input variables for developing prediction models.

Evaluation of model performance

The stability, reliability and dynamic adaptability of prediction models were taken as the evaluation criteria of model performance. As shown in eqns. 3-6, four statistical indices, namely the correlation coefficient of calibration set (R_c), the standard error of calibration (*SEC*), the correlation coefficient of prediction set (R_p) and the standard error of validation were calculated to evaluate the performance of the established models.

$$Rc = \sqrt{\sum_{i=1}^{n_c}(\hat{y}_i - y_i)^2} \Bigg/ \sqrt{\sum_{i=1}^{n_c}(\hat{y}_i - y_m)^2} \tag{3}$$

$$Rp = \sqrt{\sum_{i=1}^{n_p}(\hat{y}_i - y_i)^2} \Big/ \sqrt{\sum_{i=1}^{n_p}(\hat{y}_i - y_m)^2} \quad (4)$$

$$SEC = \sqrt{\frac{1}{n_c - 1}\sum_{i=1}^{n_c}(\hat{y}_i - y_m)^2} \quad (5)$$

$$SEP = \sqrt{\frac{1}{n_p - 1}\sum_{i=1}^{n_p}(\hat{y}_i - y_m)^2} \quad (6)$$

Here, $\hat{y}_i$ is the i^{th} predicted value; y_i is the i^{th} measured value; y_m is the mean of the calibration or prediction set; n_c is the number of samples in the calibration set; n_p is the number of samples in the prediction set. Generally, models with higher R_c and R_p or with lower *SEC* and *SEP* are more satisfactory than models with lower R_c and R_p or with higher *SEC* and *SEP.*

RESULTS

Results of the TVB-N analyses

Sixty beef samples were measured during an 18-day period of storage. Fig. 3 depicts the reference TVB-Ns of all the beef samples tested on each day of the experiment, and shows the change trends of TVB-Ns with time. In Fig. 3, the horizontal axis represents the storage time (day) and the ordinate axis represents the TVB-N content (mg/100 g). The TVB-N trend curve showed the daily mean (with error bars) of TVB-N content tested on each day of the experiment. As shown in Fig. 3, the TVB-Ns content of the reference beef sample stored at 4^{o}C increased with the storage time during 1-18 days of storage, thereby indicating a decrease of the beef freshness with the storage time. After the 7th day, the TVB-N content exceeded 15 mg/100 g, a threshold value for edible beef as mandated in the aforementioned China's national standard, and therefore the beef after the 7th day was no longer edible.

The statistics of the 60 sample reference TVB-N contents are given in Table 1. As shown in Table 1, the maximum TVB-N content was 62.40 mg/100 g and the minimum TVB-N content was 8.64 mg/100 g. The mean value and the standard deviation (SD) were 28.96 and 13.41 mg/100 g, respectively. These data showed a wide range of data coverage for beef meat TVB-N contents, implying that the TVB-N contents measured in this study may represent a complete data set during the course of freshness change in stored beef. Therefore, the freshness prediction model established based on this study's data was likely to be representative.

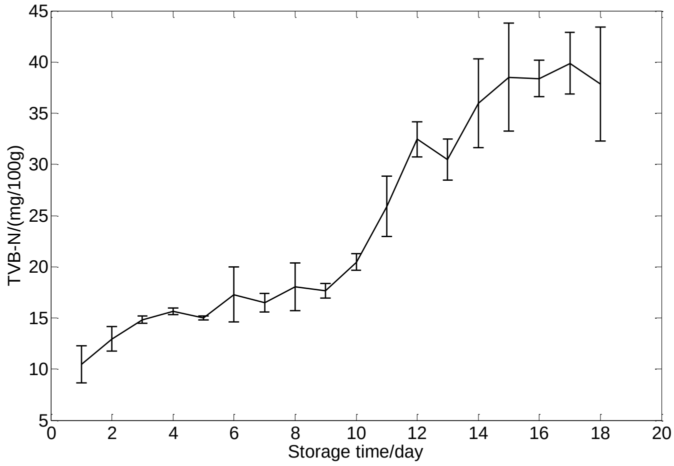

Fig. 3 - Reference beef TVB-N tested on each day of the experiment

Table 1

A summary of measured beef TVB-N contents (in mg/100g)

Number of samples	Max	Min	Mean	Standard deviation
60	62.40	8.64	28.96	13.41

Hyperspectral scattering images

A typical averaged hyperspectral scattering image is shown in Fig.4a.The horizontal axis is a spatial axis and the vertical axis is a wavelength axis. Different colours in the figure represented different reflectance intensities. A vertical line taken from the image represented a spectral profile collected from a particular point of the scanning line at the surface of beef. In essence, each scattering image was composed of hundreds of spectra and each spectrum came from a different point at the beef surface. Therefore, each scattering image reflected the character of beef quality. Fig.4b shows three spectral scattering profiles at 588, 699 and 777 nm wavelength for a beef sample. All the spectral scattering profiles were symmetric about the center point of scanning line, but showed large wavelength-dependence of the scattering intensities. Fig.4c depicts the spatial scattering profiles of different beef samples with different TVB-N contents (14.46, 22.70 and 32.74 mg / 100 g) at the wavelength of 777 nm. The peak intensities of the scattering profiles decreased with the increase of TVB-N, but the half wave bandwidths changed in the opposite direction. To describe the scattering characteristics reflecting the freshness of beef samples, a Lorentz function was used to fit each of the scattering profiles, thereby generating a series of parameters (*a, b* and *c*) that were all wavelength-dependent. The parameters were plotted versus wavelengths to give the best-parameter spectra that were subjected to further analysis, as elaborated below.

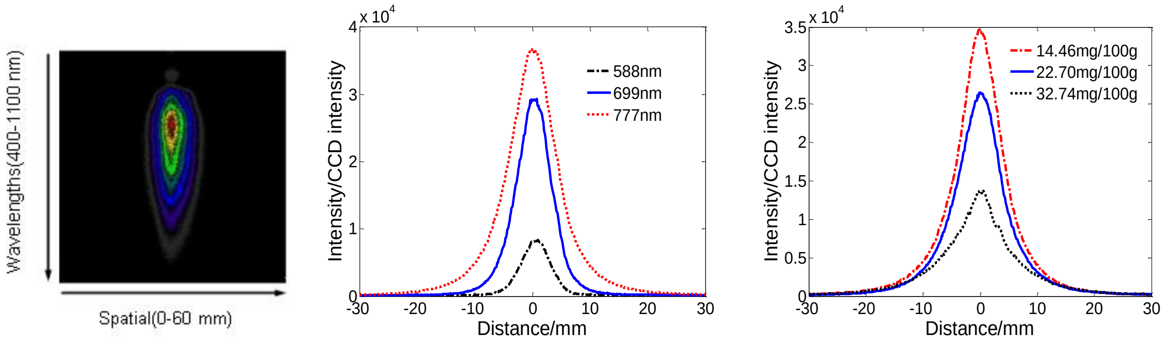

a) An averaged scattering image **b) Spectral scattering profiles at 588, 699 and 777nm** **c) Scattering profiles of different samples at 777 nm**

Fig. 4 - Hyperspectral scattering images of beef

Curve fitting of scattering profiles

The scattering profiles of all the 60 beef samples in the wavelength range of 400-1100 nm were fitted to a Lorentzian function (eqn. 2). Fig. 5 represents the correlation coefficients of the fitting at different wavelengths. As shown in Fig. 5, most of the correlation coefficients for the samples within the wavelength range of 500-1000 nm were greater than 0.95, while the correlation coefficients were lower at wavelengths outside that wavelength range. Therefore, only the data between 500 and 1000 nm were used in the development of beef freshness prediction models.

Fig. 6 showed the extracted Lorentzian function parameters of all the beef samples; different beef samples showed similar patterns of the parameter spectra for the same Lorentzian parameter (*a, b* or *c*) despite the spectra intensity differences among different samples. The three types of parameters spectra contained all scattering profile information in the hyperspectral images of all the beef samples. As shown in Fig. 6, the parameter spectra contained much noise and drifted at the both ends of the wavelength range of 400-1100 nm, thereby indicating that the spectra should be subjected to pre-treatment to improve the data quality prior to the development of prediction models.

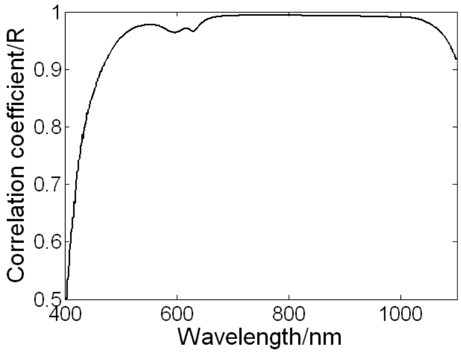

Fig. 5 - Correlation coefficients of fitting at different wavelengths

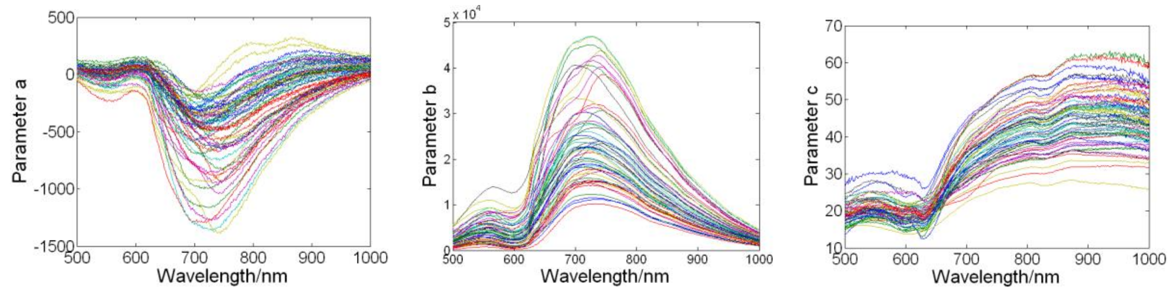

a) Asymptotic parameter *a* **b) Peak-value parameter *b*** **c) Full-width parameter *c* at *b/2***

Fig. 6 - Lorentzian-fitting parameters for 60 beef samples

Modeling results with full-spectra data

The 60 samples were randomly divided into a calibration set of 45 samples and a prediction set of 15 samples. The 45 calibration samples were used to establish the prediction model, and the 15 prediction samples were used to verify the accuracy and reliability of the prediction model. As mentioned earlier in this study, LS-SVM was used to establish two separate quantitative prediction models, one based on the individual parameters of *a, b, c* and the other based on parameter combinations, namely *a+b/c* and *(b-a)/c*. The prediction results were compared among models established by LS-SVM after three different types of data pre-treatment, namely , the MSC pre-treatment, the SG pre-treatment and the MSC+SG pre-treatment , and it was found that the MSC+SG pre-treatment generated the best results. Therefore, the parameter spectra were all subjected to the MSC+SG pre-treatment prior to the development of the aforementioned two quantitative prediction models. Table 2 shows all the TVB-N prediction results of the LS-SVM models that were established either with the individual parameters or with the parameter combinations. As shown in Table 2, the modeling results obtained with the individual parameter *a* and with the parameter combination *a+b/c* were very close. The models using the individual parameter *b* or *c* over-fitted the data. The modeling result obtained with the parameter combination *(b-a)/c* was the best, reporting R_c=0.91, *SEC*=5.83 mg/100 g, R_p=0.86 and *SEP*=5.21 mg/100 g. This showed that the parameter combination *(b-a)/c* contained more information of the scattering profiles of the samples. Therefore, the parameter combination *(b-a)/c* was taken as the best input variable for establishing the prediction model of beef TVB-N.

Table 2

TVB-N prediction results of LS-SVM models using Lorentzian-fitting parameters

Parameter	R_c	SEC	R_p	SEP
a	0.87	7.13	0.88	5.01
b	0.94	4.83	0.75	6.97
c	0.93	5.24	0.83	6.10
a+b/c	0.86	7.36	0.86	5.21
(*b-a*)/*c*	0.91	5.83	0.86	5.21
(*b-a*)/*c(GA)*	0.97	3.38	0.96	3.85

Modeling results with optimized-spectra data by GA

In order to improve the prediction precision, the GA method was used to optimize the parameter combination and select the effective variables for developing the LS-SVM model. In the GA method, the population size of chromosome was set to be 30, the probability of mutation and the probability of cross-over were set as 1% and 50%, respectively, and the number of run times was set to be 100. Because the initial population of GA was generated randomly every time, the GA was randomly run 5 times to select effective variables. Fig. 7 illustrates one among five variable-selection processes, where the selected parameter-combination spectra variables were above the dotted line. On the whole, the GA-selected variables were similar in each of the five selection processes, and were mainly centered at the wavelengths of approximately 630, 710, 930 and 980 nm, greatly reducing the number of variables required for developing the prediction model as well as reducing information redundancy. The optimized variables used to develop the prediction model of TBN-N (referred to as GA-LS-SVM) and the modeling results are shown in Table 2. The prediction results of GA-LS-SVM were relatively satisfactory, as indicated by R_c=0.97, *SEC*=3.38 mg/100 g (Fig.8a) and R_p=0.96, *SEP*=3.85 mg/100 g (Fig.8b). These results also showed that GA was able to extract effective wavelength variables, thereby greatly improving the model's prediction accuracy.

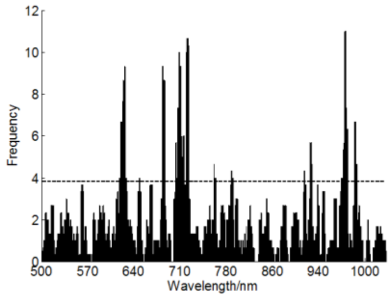

Fig.7 - Occurrence frequency of GA-selected variables

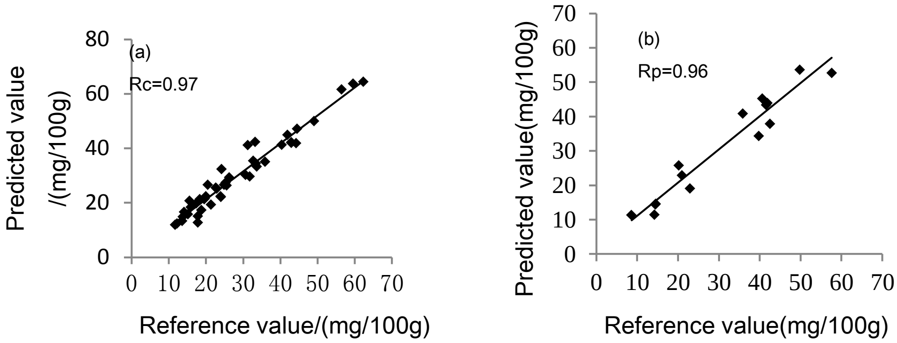

a) calibration set **b) prediction set**

Fig. 8 - Predicted vs. reference values of a GA-LS-SVM model using the optimized *(b-a)/c* parameter

CONCLUSIONS

The study demonstrated that a hyperspectral imaging technique combined with a Lorentzian distribution function could be a rapid and non-destructive tool for prediction of beef meat freshness. A hyperspectral imaging system was used to capture hyperspectral scattering images of fresh beef samples that were stored at 4°C for 1-18 days. Spatial scattering curves were extracted from the hyperspectral images and fitted to a three-parameter Lorentzian distribution function. The fitting-parameters of the Lorentzian distribution function were presented as parameter spectra and used to develop a LS-SVM model for predicting beef TVB-N, an indicator of beef freshness. The primary findings are as follows.

(1) In the wavelengths range of 500-1000 nm, the Lorentzian distribution function could give a better fitting to the scattering curves of the beef hyperspectral images. The beef parameter spectra were obtained and used as input variables for developing prediction models of beef TVB-N.

(2) The MSC+SG pre-treatment method was found to be the best one among the three pre-treatment methods (MSC, SG, and MSC+SG) for developing prediction models. A LS-SVM prediction model of beef freshness was developed. Among the prediction models established with the individual parameters (*a*, *b* or *c*) or with the parameter combinations (*a+b/c* or *(b-a)/c*), the prediction model developed with the parameter combination *(b-a)/c* was the best, showing a correlation coefficient of 0.86 and a standard error of prediction of 5.21 mg/100 g. The variable *(b-a)/c* was optimized by GA and used to develop a prediction model GA-LS-SVM, which showed improved prediction accuracy with R_p=0.96 and *SEP*=3.85 mg/100 g.

This study indicated that hyperspectral scattering imaging combined with Lorentzian distribution functions and genetic algorithms may accurately predict beef TVB-N, providing a promising method for rapid and non-destructive determination of beef freshness. This method is very likely to be applied to real-time detection of meat quality and safety attributes in the future.

ACKNOWLEDGEMENT

The authors gratefully acknowledge the Science and Technology Research Project of Henan Province (Project No.152102310351), Key Research Project of Henan Province Department of Education (Project No.14B460029) and Special Foundation Project of Nanyang Normal University (Project No.ZX2014092) for supporting this Research.

REFERENCES

[1] Anguo Xie , Dawen Sun, Zhongyue Xu, Zhiwei Zhu., (2015), Rapid detection of frozen pork quality without thawing by Vis-NIR hyperspectral imaging technique, *Talanta,* Amsterdam/Netherlands, Ed. Elsevier, Vol.39, pp.208-215;

[2] David L. O., Soo J. H., H. Holly W., Laping Wu.,(2016), Emerging markets for imported beef in China: Results from a consumer choice experiment in Beijing, *Meat Science,* Oxford/England Ed. Elsevier, Vol.121, pp.317-323;

[3] Di Wu, Dawen Sun., (2013), Advanced applications of hyperspectral imaging technology for food quality and safety analysis and assessment: A review-Part II: Applications, *Innovative Food Science and Emerging Technologies*, Amsterdam/Netherlands, Ed. Elsevier, Vol.19, pp.15-28;

[4] Fangrong Wang, Lisheng Jin, Tieqiang Zhang, Yuankun Zhang, Jian Ye, Ruwen Kan., (2013), Research on meat species and freshness identification method based on spectral characteristics, *Optik* , Jena/Germany, Ed. Elsevier, Vol.124, pp.5952- 5955;

[5] Feifei Tao, Yankun Peng, Yongyu Lia, Kuanglin Chao, Sagar Dhakal., (2012), Simultaneous determination of tenderness and Escherichia coli contamination of pork using hyperspectral scattering technique, *Meat Science,* Oxford/England, Ed. Elsevier, Vol.90, pp.851-857;

[6] Fernando M., Renfu. Lu., Diwan A., Haiyan C., Benjamin B., (2011), Integrated spectral and image analysis of hyperspectral scattering data for prediction of apple fruit firmness and soluble solids content, *Postharvest Biol.Technol,* Amsterdam/ Netherlands, Ed. Elsevier,Vol.62, pp.149-160;

[7] Gamal El M., Dawen Sun, Paul A., (2012), Near-infrared hyperspectral imaging for predicting colour, pH and tenderness of fresh beef, *Journal of Food Engineering,* Los Angeles/California, Vol.110, pp.127-140;

[8] Gowen A.A., O'Donnell C.P., Cullen P.J., Downey G., Frias J.M., (2007), Hyperspectral imaging-an emerging process analytical tool for food quality and safety control, *Trends in Food Science&Technology*, London/U.K., Ed. Elsevier, Vol.18, Issue.12, pp.590-598;

[9] Huanhuan Li, Quansheng Chen, Jiewen Zhao, Mengzi Wu., (2015), Nondestructive detection of total volatile basic nitrogen (TVB-N) content in pork meat by integrating hyperspectral imaging and colorimetric sensor combined with a nonlinear data fusion, *LWT-Food Science and Technology*, Amsterdam/Netherlands, Ed. Elsevier, Vol.63, pp.268-274;

[10] Jianhu Wu, Yankun Peng, Fachao Jiang, Wei Wang, Yongyu Li, Xiaodong Gao., (2009), Hyperspectral scattering profiles for prediction of beef tenderness, *Transaction of the Chinese Society for Agricultural Machinery*, Beijing/China,Vol.40, Issue.12, pp.135-150;

[11] Jianhu Wu, Yankun Peng , Yongyu Li, Wei Wang, Jingjing Chen, Sagar Dhakal., (2012), Prediction of beef quality attributes using VIS/NIR hyperspectral scattering imaging technique, *Journal of Food Engineering ,* Los Angeles/California, Vol.109, pp.267-273;

[12] Jianrong Cai, Quansheng Chen, Xinmin Wan, Jiewen Zhao.,(2011), Determination of total volatile basic nitrogen (TVB-N) content and Warner-Bratzler shear force (WBSF) in pork using Fourier transform near infrared (FT-NIR) spectroscopy, *Food Chemistry,* London/U.K., Ed. Elsevier,Vol.126, pp. 1354-1360;

[13] Jianrong Cai, Xinmin Wan, Quansheng Chen, (2009), Feasibility study for the use of near-infrared spectroscopy in the quantitative analysis of TVB-N content in pork, *Acta Optica Sinica*, Shanghai/China, Vol. 29, Issue. 10, pp.2808-2812;

[14] Jinxia Liu, Yue Cao, Qiu Wang, Wenjuan Pan, Fei Ma, Changhong Liu, Wei Chen, Jianbo Yang ,Lei Zheng., (2016), Rapid and non-destructive identification of water-injected beef samples using multispectral imaging analysis, *Food Chemistry,* London/U.K., Ed. Elsevier, Vol.190, pp. 938-943;

[15] Juncai Xu, Qingwen Ren, Zhenzhong Shen, (2015), Prediction of the strength of concrete radiation shielding based on LS-SVM, *Annals of Nuclear Energy,* U.K., Vol.85, pp.296-300;

[16] Leilei Zhang, Yongyu Li, Yankun Peng, Wei Wang, Fachao Jiang, Feifei Tao, Jiajia Shan., (2012), Determination of pork freshness attributes by hyperspectral imaging technique, *Transactions of the Chinese Society of Agricultural Engineering,* Beijing/China, Vol.28, Issue.7, pp.254-259;

[17] Lin Huang , Jiewen Zhao, Quansheng Chen, Yanhua Zhang, (2014), Nondestructive measurement of total volatile basic nitrogen (TVB-N) in pork meat by integrating near infrared spectroscopy, computer vision and electronic nose techniques, *Food Chemistry,* London/U.K., Ed. Elsevier, Vol.145, pp.228-236;

[18] Mohammed K., Yoshio M., Seiichi O., (2016), Rapid and non-destructive detection of chicken adulteration in minced beef using visible near-infrared hyperspectral imaging and machine learning, *Journal of Food Engineering*, Amsterdam/Netherlands, Vol.170, pp.8-15;

[19] Noha M., Dawen Sun,(2013), Robust linear and non-linear models of NIR spectroscopy for detection and quantification of adulterants in fresh and frozen-thawed minced beef, *Meat Science,* Oxford/England, Ed. Elsevier, Vol.93, pp.292-302;

[20] Owusu-Sekyere E., Owusu V., Jordaan H., (2014) Consumer preferences and willingness to pay for beef food safety assurance labels in the Kumasi Metropolis and Sunyani Municipality of Ghana, *Food Control,* Oxford/England, Ed. Elsevier, Vol.46, pp.152-159;

[21] Qian Yang, Dawen Sun, Weiwei Cheng.,(2017), Development of simplified models for nondestructive hyperspectral imaging monitoring of TVB-N contents in cured meat during drying process, *Journal of Food Engineering*, Amsterdam /Netherlands, Ed. Elsevier, Vol.192, pp.53-60;

[22] Renfu Lu, Yankun Peng., (2006), Hyperspectral Scattering for assessing Peach Fruit Firmness, *Biosystems Engineering*,Germany, Ed. Springer, Vol.93, Issue.2, pp.161-171;

[23] Riccardo L., (2000), Application of genetic algorithm-PLS for feature selection in spectral data sets, *Journal of Chemometrics,* U.K., Vol.14, pp.643-655;

[24] Riccardo L., Amparo L. G., (1998), Genetic Algorithms applied to feature selection in PLS regression: how and when to use them, *Chemometrics and Intelligent Laboratory Systems,* Amsterdam / Netherlands, Ed. Elsevier, Vol.41, pp.195-207;

[25] Ruifeng Hou, Lan Huang, Zhongyi Wang, Haishu Ding, Zhilong Xu., (2006), The preliminary study for testing freshness of meat by using near-infrared reflectance spectroscopy, *Spectroscopy and Spectral Analysis,* Beijing/China, Vol.26, Issue.12, pp.2193-2196;

[26] Santosh L., Sangdae L., Hoonsoo L., Byoung-Kwan Ch.,(2015), A review of vibrational spectroscopic techniques for the detection of food authenticity and adulteration, *Trends in Food Science & Technology*, London/U.K., Ed. Elsevier, Vol.46, pp.85-98;

[27] Shibang Ma, Xiuying Tang, Yang Xu, Yankun Peng, Xiaoyu Tian, Xing Fu., (2012), Nondestructive determination of p H value in beef using visible/near-infrared spectroscopy and genetic algorithm, *Transactions of the Chinese Society of Agricultural Engineering,* Beijing/China, Vol.28, Issue.18, pp.263-268;

[28] Xia Xu, Fang Cheng, Yibin Ying., (2009), Application and recent development of research on near-infrared spectroscopy for meat quality evaluation, *Spectroscopy and Spectral Analysis,* Beijing/China, Vol.29, Issue.7, pp.1876-1880;

[29] Yankun Peng, Jing Zhang, Wei Wang, Yongyu Li, Jianhu Wu, Hui Huang, Xiaodong Gao, Weikang Jiang., (2011), Potential prediction of the microbial spoilage of beef using spatially resolved hyperspectral scattering profiles, *Journal of Food Engineering*, Los Angeles/California, Vol.102, pp.163-169;

[30] Yankun Peng, Leilei Zhang., (2013), Advancement and trend of hyperspectral imaging technique for nondestructive detection of agro-product quality and safety, *Transaction of the Chinese Society for Agricultural Machinery*, Beijing/China, Vol.44, Issue.4, pp.137-145.

PATTERNS OF CHANGING SETTINGS OF THE TEMPERATURE FIELD AT VAPOUR-CONTACTING HEATING BY STERILIZING PRODUCTS IN CYLINDRICAL CONTAINERS

/

ЗАКОНОМІРНОСТІ ЗМІНИ ПАРАМЕТРІВ ТЕМПЕРАТУРНОГО ПОЛЯ ПРИ ПАРОКОНТАКТНІЙ СТЕРИЛІЗАЦІЇ ПРОДУКЦІЇ У ЦИЛІНДРИЧНІЙ ТАРІ

Ph.D. Polyevoda Y.A.[1)], Postgraduate Hurych A.J.[1)], Assistant Kutsyy V.M.[2)]
[1)]Vinnitsa National Agrarian University/ Ukraine; [2)]Podiliay State Agricultural and Technical University
Tel: +380672151148; E-mail: vinyura29@mail.ru

Keywords: *heat exchanger mode, temperature field, sterilization, vapour-contacting heating*

ABSTRACT

In the article, we sustained the heat exchange process and regime parameters and defined the changing patterns of temperature characteristics of the pressure in the working area in terms of vapour-contacting heating in container.

РЕЗЮМЕ

У статті обґрунтовано теплообмінні режимні параметри процесу та визначені закономірності зміни температурних характеристик тиску в робочій зоні в умовах пароконтактного нагріву в тарі.

INTRODUCTION

The kinetics of biochemical reactions under varying degrees depends on the thermal, chemical and mechanical sensitivity of the processed product, on pressure, temperature and chemical potential. Pressure is distributed in a liquid by Pascal principle in all directions, accompanied by a large adiabatic pressure changes with the speed of sound. For this reason, we can assume that there is pressure almost instantaneously throughout the chamber. From this assumption it follows that the effect of pressure comparing with the thermal process has the advantage that can influence rapidly and in homogenous way to all the processed stuff regardless of shape, size and composition. However, it was left unattended possibility of physical and thermal heterogeneity *(Alekseev E. and Pakhomov E., 1982; Belyaeva M., 2003; Nechepurenko I., 1991; Tugolukov E. 2004; Voronenko B. et al, 2008).*

Creating high-productive heat exchange equipment that meets modern level of industry and technology development requires significant intensification of heat exchange processes that are sufficiently widely implemented in known scientific schools *(Palamarchuk I. et al, 2013; Terzyev S. et al, 2014; Terzyev S. and Kurakov A., 2012; Tsurkan O. et al, 2010; Tsurkan O. et al, 2015).*

Among the intensification means factors were used devices of mechanical and technological vibration action (*Palamarchuk I., Bandura V., Palamarchuk V., 2013; Palamarchuk I., 2008),* the use of infrared radiation *(Terziev S., Malashevych S., Ruzhytska S., 2011; Terziev S., 2016),* baro-thermal effect and others *(Terziev S. ,2016).*

One effective way, both in terms of the intensification of the process of heat and energy savings is the product contact heating with steam use, which makes technology's impact on processed products.

Heat at products vapour-contacting heating is a complex phenomenon associated with the simultaneous transfer of heat and mass substance. The number of transferred mass is determined by the condensed steam and transferred to the heat (if vapour) - heat of vaporization *(Voronenko B. et al, 2008).*

In vapour-contacting heating it is taken into account a significant number of determining factors, the most important are the thermal properties of the heating steam, and the physical and chemical properties of the product. Taking into account all the factors that affect the process of heat transfer at vapour-contacting heating and analysis are very difficult, not only in theory but in the experimental aspects as well.

The main parameter during heat sterilization of food, including using vapour-contacting heating temperature is a product, which is the major factor for the establishment of canned food sterilization regimes. Therefore, one of the main objectives of the study sterilization process at the appointed method of heating is to determine the product temperature field or identify the dynamics of temperature change at different points in the product, depending on the parameters of steam that heats the conditions of supply to the product and the physical properties of the treated material *(TU 10.1-22769675-001, 2013).*

Therefore, for foundation of heat exchange operational parameters it is necessary to determine the patterns of temperature change characteristics of pressure in the working area in terms of vapour-contacting heating in container.

MATERIAL AND METHOD

Instability of temperature field can be explained by the fact that the pressure rises in the phase of volume increase due to changes in the temperature of the treated environment. The adiabatic change of state in a clean, inert and homogeneous medium changes the temperature according to changes in pressure, which is determined by (1):

$$dT = \frac{T \cdot \beta}{\rho \cdot c_p} dp \tag{1}$$

where:

T – the temperature, (K);

β – coefficient of thermal expansion, (K^{-1});

ρ – liquid density, (kg / m^3);

c_p – specific heat, (J / (kg·K));

p – pressure, (Pa).

Depending on the product being processed at the pressure of 1 GPa temperature rises to several tens of Celsius degrees. Filled chamber pressure is a system consisting of product packaging materials, medium transmitting the pressure (intermediate fluid) and the steel wall of the chamber. These materials have different thermal properties. Consequently, despite the initial parameters of homogeneous temperature distribution, while increasing the pressure in the chamber, it can form a homogeneous temperature field *(Nechepurenko I., 1991).*

For the formal definition of the temperature increase caused by increased pressure, we took the first equation of conservation, which brought the equation (2) of total heat capacity H:

$$\frac{d(\rho \cdot H)}{d\tau} + \nabla \cdot (\rho \cdot \vec{v} \cdot H) = \frac{dp}{d\tau} + \nabla \cdot (\lambda \nabla T) + \nabla \cdot (\xi \cdot \vec{v}) + \rho \cdot \vec{q} \cdot \vec{v} \tag{2}$$

where:

$\vec{v}$ – velocity vector fluid;

q – vector of gravity;

τ – time, (sec).;

λ – thermal conductivity of material, (W / (m·K));

ξ – tensor of stresses in the material.

For specific heat capacity h:

$$\rho \frac{dh}{d\tau} - \frac{dp}{d\tau} = \nabla \cdot (\lambda \nabla T) + \eta \cdot \Phi + \rho \cdot \vec{q} \cdot \vec{v} \tag{3}$$

where:

Φ – dissipation function;

r – container radius, (m);

R_1 – autoclave radius, (m);

$\eta = ln\,(r / R_1)$ – independent argument of desired temperature.

Then, using thermodynamic ratio:

$$\frac{dh}{d\tau} = \left.\frac{dh}{dp}\right|_T \frac{dp}{d\tau} + \left.\frac{dh}{dT}\right|_p \frac{dT}{d\tau} = \frac{1}{\rho}(1 - \alpha \cdot T)\frac{dp}{d\tau} + c_p \frac{dT}{d\tau} \tag{4}$$

where:

α – coefficient of heat on the outer surface of the cylinder.

We got the heat equation:

$$\rho \cdot c_p \frac{dT}{d\tau} = \alpha \cdot T \frac{Dp}{D\tau} + \nabla \cdot (\lambda \nabla T) + \eta \cdot \Phi + \rho \cdot \vec{q} \cdot \vec{v} \tag{5}$$

The last equation shows that the material derivative of temperature T as to time τ carries material derivative of pressure on P as to time τ, until dissipation function Φ and the potential energy and flow that carries high temperature, are low. Taking into consideration this fact, we came to approximate heat transfer equation:

$$\frac{dT}{d\tau} \approx \frac{dT}{\rho \cdot c_p} \frac{dp}{d\tau} \tag{6}$$

It is considered that the fluid motion is obvious in the processing of liquid substance pressure. To show this mathematically, we assumed that the density increases with pressure and decreases with increasing temperature grounded for much of the food and similar substances in the environment *(Palamarchuk I., Tsurkan O., Hurych A., 2015).* The appearance of the flow in the liquid, which initially is at rest was shown using mass balance equation:

$$\frac{d\rho}{d\tau} + \nabla \cdot (\rho \cdot \vec{v}) = 0 \tag{7}$$

During the compression phase density increases with pressure. So, the first member of the equation (7) is different from zero. Since the left side must be zero fluid velocity $\vec{V}$ must accept non-zero value. Therefore, increasing the pressure increases the fluid flow. Temperature gradients are important in handling a deviation from hydrostatic flow conditions. We have traced this conclusion using the basic equations of hydrostatics:

$$\frac{dp}{dx} = 0 \tag{8}$$

$$\frac{dp}{dy} = 0 \tag{9}$$

$$\frac{dp}{dz} = -\rho \cdot \vec{q} \tag{10}$$

The equations (8-10) *x, y* and *z* are Cartesian coordinates. Without loosing *z* overview we accepted that the vector of gravity points in the negative *z* direction. Further conversion of (9) and in respect of (10) in relation it gave the following result:

$$\frac{d^2p}{dydz} = \frac{d^2p}{dzdy} = -\frac{d\rho}{dy}\vec{q} \tag{11}$$

Thus, the right side of equation (11) and original density must be constant and equal to zero:

$$\frac{d\rho}{dy} = 0 \tag{12}$$

However, this condition, as the hydrostatics cannot be kept. While density is a function of temperature, and the latter is exposed to a direction different from the direction of gravity vector, equation (12) is broken. As a consequence, there must necessarily appear vapour stream at a rate different from zero, which leads to convective heat transfer and suspended solids.

For the developed scheme of autoclave where heat is carried by vapour placed outside cup, the problem reduces to the calculation of non-stationary temperature field in a container that is heated from the outer surface of the heat source given by the intensity of the light convection in the radial direction.

It is assumed that the thermal resistance of the outer wall is relatively small, and the thermal properties of the material do not depend on temperature. This heat equation considering the convective component has the form *(Tugolukov E., 2004):*

$$\frac{dt}{d\tau} + u\frac{dt}{dr} = \frac{\lambda}{c_p \cdot \rho \cdot r}\frac{d}{dr}(r\frac{dt}{dr}) \tag{13}$$

where:

u – velocity of the fluid m / s.

Terms of uniqueness:

- Initial conditions for $\tau = 0$

$$t(r,0) = t(r) = t_н \tag{14}$$

- Extreme conditions

$$(\frac{dt}{dr})_{r=R_1} = -q / \lambda \tag{15}$$

$$(\frac{dt}{dr})_{r=R_2} = -a \cdot (t - t_в) / \lambda - \frac{q_2}{\lambda} \tag{16}$$

where:

$t_в$ – ambient temperature, (K);

$t_н$ – the initial temperature of the material processed, (K);

q – specific heat flux on the inner surface of the autoclave, (W/m^2);

R_2 – radius packaging, (m).

RESULTS

As we consider the problem of calculating the temperature field depending on the radius of the autoclave, it is assumed that the specific heat flow and the velocity of steam through the surface of the container does not depend on its length and thus is not considered a limiting effect, manifested through the finite size of the packaging.

Accordingly, we define the relationship between speed and specific heat flow. In vapour-contacting heating steam is fed evenly and specific heat flow is equal to:

$$q_1 = G_n \cdot i_x / 2 \cdot \pi \cdot R_1 \cdot l \tag{17}$$

where: G_n – steam consumption, (kg/s);

i_x – enthalpy of steam (J/kg);

l – the length of container, (m).

The actual amount of steam, creating a convective flow can be determined from the heat balance equation:

$$G_n \cdot i_x = G_ж \cdot t_н \cdot c_{р.ж} \tag{18}$$

where:

$G_{ж}$ – number of newly condensate, (kg/s);

$c_{р.ж}$ – specific heat capacity mass of condensate, (J/(kg K)).

The velocity of steam in an autoclave with *r* radius defined by:

$$u = G_ж / 2 \cdot \pi \cdot r \cdot l \cdot \rho_ж \tag{19}$$

where: $\rho_{ж}$ – density of vapor.

Substituting (17) in (18) and (18) to (13), we get:

$$\frac{dt}{d\tau} = (\frac{\lambda}{c_p \cdot \rho} - \frac{G_n}{2 \cdot \pi \cdot l \cdot \rho}) \frac{1}{r} \frac{dt}{dr} + \frac{\lambda}{c_p \cdot \rho} \cdot \frac{d^2 t}{dr^2} \tag{20}$$

$$\left(\frac{dt}{dr}\right)_{r=R_1} = \frac{G_n \cdot c_p \cdot t_н}{2 \cdot \pi \cdot R_1 \cdot \lambda \cdot l} \tag{21}$$

$$\left(\frac{dt}{dr}\right)_{r=R_2} = -\frac{a}{\lambda}(t - t_в) + \frac{G_n \cdot c_p \cdot t}{4 \cdot \pi \cdot R_2 \cdot \lambda \cdot l} \tag{22}$$

$$t(r,0) = t_н \tag{23}$$

Equation (17-22) can be written in parametric form. As characteristic parameters we introduce the following dimensionless quantities:

$\theta = t / t_н$ – the required dimensionless grand;

$\theta_g = t_в / t_н$ – dimensionless magnificent environment;

$F_0 = \tau \cdot \lambda / c_p \cdot \rho \cdot R_1^2$ – the number of Fourier;

$B_i = a \cdot R_1 / \lambda$ – the number of Biot.

$$Q_1 = G_ж \cdot c_p / 2 \cdot \pi \cdot l \cdot \lambda \quad \ln(R_2 / R_1) \tag{24}$$

With regard introduced dimensionless equations (20-23) will be:

$$\frac{d\theta}{dF_0} = exp(-2 \cdot \eta)\left[(1-Q_1)\frac{d\theta}{d\eta} + \frac{d^2\theta}{d\eta^2}\right] \tag{25}$$

$$\left(\frac{d\theta}{d\eta}\right)_{\eta_1=0} = Q_1 \tag{26}$$

$$\left(\frac{d\theta}{d\eta}\right)_{\eta_2=0} = \left[B_i(\theta_g - \theta) - Q_1 \cdot R_1 \cdot \frac{\theta}{R_2}\right]\exp\eta_2 \tag{27}$$

$$t(\eta_1, 0) = 1 \tag{28}$$

The mathematical model, taking into account boundary conditions of a system of differential equations (25)÷(28), which solution has the form *(Alekseev E. and Pakhomov E., 1982)*:

$$\theta = \theta(F_0, B_i, \eta, Q_1, \frac{R_1}{R_2}) \tag{29}$$

Thus, the mathematical model determining the dynamics of the temperature field in the container is found dependence (29), satisfying the conditions of the field $D\{(F_0,\eta); o \le F_0 \le \phi;\ O \le \eta \le \eta_2)\}$of (25) and limit (26, 27) and the initial conditions (28), respectively.

To solve this problem we apply numerical method *(Belyaeva M., 2003)*. That is why we build a uniform space-time increments chart:

$$\Delta\eta = \eta_2 / N \tag{30}$$

where:

N – number of quantization step of given area $\Delta F_0 = \Phi_1 / M$;

M – the number of partitions of a given region, pc.;

Φ_1 – Fourier pre-specified number (time).

Using conventional implicit difference scheme approximation of (25-27) it will be:

$$\theta_{i,j} - \theta_{i,j-1} = \Delta F_0\, exp(-2\eta_i)\left[(1-\theta_1)(\theta_{i+1,j} - \theta_{i-1,j}) / 2\Delta\eta + (\theta_{i+1,j} - 2\theta_{i,j} + \theta_{i-1,j})\right]\Delta\eta^2 \tag{31}$$

where:

$(i = 1, 2, 3 \ldots N-1;\ j = 1, 2, 3 \ldots M)$

$$\theta_{1,j} - \theta_{o,j} = \theta_1 \Delta\eta \tag{32}$$

$$\theta_{N,j} - \theta_{N-1,j} = \Delta\eta \cdot exp\,\eta_2\left[B_i(\theta_g - \theta_{N,j}) - Q_1\theta_{N,j} \cdot R_1 / R_2\right] \tag{33}$$

We rewrite equation (29, 31, 32) in the form:

$$-A_i\theta_{i-1,j} + C_i\theta_{i,j} - B_i\theta_{i+1,j} = f_i\,(i = 0,1,2,3 \ldots N) \tag{34}$$

where:

$C_o, B_o, f_o, A_N, C_N, f_N$ – coefficient describing boundary conditions;

$\theta_{i,j}$ – dependent function;

A_i, B_i, C_i, f_i – energy equation coefficient.

Accordingly, (25-28), the expression for the coefficients of the system (33) takes the form:

$$A_o = 0;\ C_o = 1;\ B = -1;\ f_o = -Q_1\Delta\eta$$

$$A_i = \Delta F_o\, exp(-2 \cdot \eta i)\left[(\Delta\eta^{-2} + 0,5 \cdot Q_1 \cdot \Delta\eta^{-1})\right]$$

$$B_i = \Delta F_o\, exp(-2\cdot\eta i)\left[(\Delta\eta^{-2} + 0,5\cdot Q_1\cdot\Delta\eta^{-1})\right] \tag{35}$$

$$C_i = 1 + 2\Delta F_o \Delta\eta^{-2}\exp(-2\cdot\eta i)$$

$$f_i = \theta_{i,j-1}$$

$$A_N = 1; C_N = 1 + \Delta\eta\, exp\,\eta_2 (B_i + Q_1\cdot\frac{R_1}{R_2})$$

$$B_N = 0;\ f_N = B_i\theta_x\Delta\eta\exp\eta_2$$

Thus, using linear approximation of unknown function boundary problem is reduced to a system of algebraic equations.

To solve this system we apply three-diagonal matrix algorithm. The solution of the boundary problem for the *j* th time layer is defined by:

$$\theta_{1,j} = a_{i+1,j}\theta_{i+1,j} + \beta_{i+1,j} \tag{36}$$

where: $a_{i+1,j}$, $\beta_{i+1,j}$ – selective coefficients are determined by recurrent formulas.

$$a_o = B_o / C_o;\ \beta_o = f_o / C_o; a_{i+1,j} = \frac{B_i}{(C_i - A_i a_i)};\ \beta_{i+1} = \frac{f_i + A_i\beta_i}{(C_i - A_i a_i)} \tag{37}$$

Note that the expression for θ the point (N, j), respectively (34) taking into account (36) takes the form:

$$\theta_{N,j} = \beta_N \tag{38}$$

The results of numerical experiment to calculate the temperature field along the radius of the cylindrical container, depending on the parameters of steam that heats and the product, are shown in Fig.1,2.

Fig.1 shows the curve of temperature field at vapour-contacting heating of product from initial temperature $t_н$ = 50°C to a final temperature $t_{н\,к}$ = 100°C condensing steam with temperature $t_п$ = 100°C at the rate of steam equal to 0.001 kg/s, where *r* – distance distribution of temperature field. Ambient temperature accepted $t_в$ = 20°C and the heat transfer coefficient on the outer surface of the cylinder is *a*=10. As shown in Fig.1 at the initial time (1.5-3 sec), the temperature in the central layer almost instantaneously increases to a temperature steam condensation. In the peripheral layers of the product temperature does not change.

With further heating, mainly due to the resulting radial convective flows and thermal conductivity, heat flow gradually reaches the peripheral layers over time τ = 260 s. As a result, throughout the range is set the uniform temperature field. To determine the influence of parameters of the heating steam at the temperature field distribution of the product, we performed calculations at different temperatures vapour.

Fig.2 shows the curve of the temperature field at the heating vapour $t_п$ = 110°C. Apparently, fever helps intensify the process of heat transfer. However, this leads to pronounced temperature difference between central and peripheral fields.

Comparison of computer results with experimental data leads to the conclusion that the solution of the problem of computer calculation the temperature field of product gives very satisfactory results between the calculated and experimental data.

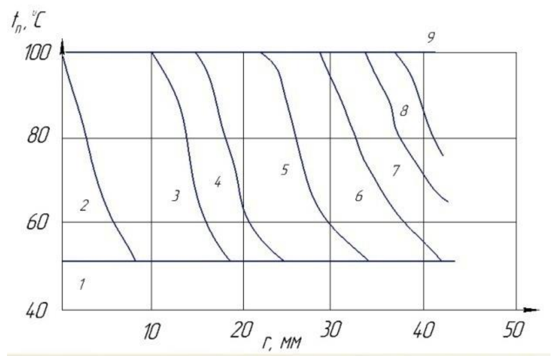

Fig. 1 – Curve of temperature field in the heat vapour-contacting product in a cylindrical container with an external supply of heat at the heating vapor:

$t_п$ = 100°C :1 – t = 0; 2 – t = 1; 3 – t = 20; 4 – t = 40; 5 – t = 80; 6 – t = 120; 7 – t = 160; 8 – t = 180; 9 – t = 200

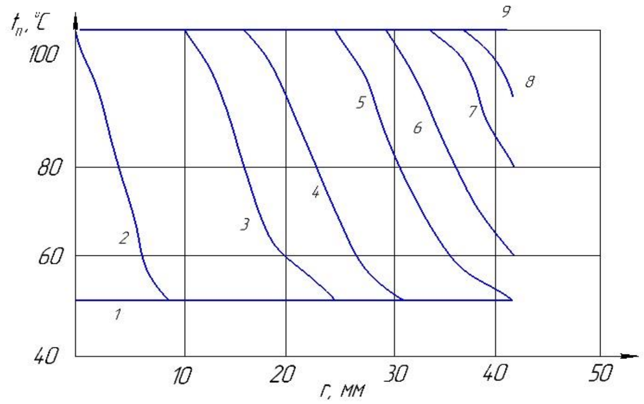

Fig. 2 – Curve of temperature field in the heat vapour-contacting product in a cylindrical container with an external supply of heat at the heating vapor:

$t_п$ = 110°C : 1 – t = 0; 2 – t = 1; 3 – t = 20; 4 – t = 40; 5 – t = 80; 6 – t = 120; 7 – t = 160; 8 – t = 180; 9 – t = 200

CONCLUSIONS

- The presence of thermal heterogeneity in food and its further growth needs forecasting and research measures to counter effectively implemented in the vapor-contacting sterilization.
- In mathematical modeling vapour-contacting heating products during sterilization had composed the heat equation, taking into account factors such as changes in temperature, pressure, fluid flow rate and the basic physical and mechanical properties of interacting environments.
- By using the methods of numerical analysis have been built depending graphic variables of temperature fields that have identified the necessary conditions for intensification of heat exchange in the vapour-contacting sterilization, which allows identifying effective operating modes of treatment.

REFERENCES

[1] Alekseev E., Pakhomov E., (1982), *Simulation and optimization of technological processes in the food industry (Моделирование и оптимизация технологических процессов в пищевой промышленности)*, Moscow/Russia, PA "Agropromizdat", p.272;

[2] Belyaeva M., (2003), *Mathematical modelling of technological processes in food productions (Математическое моделирование технологических процессов пищевых производств),* Tashkent, Publishing Tashkent chemical and technological institute, Tashkent/Uzbekistan, p.168;

[3] Nechepurenko I., (1991), Kinetics of canned sterilization process in continuously sterilizing machine (Кинетика процесса стерилизации консервов в стерилизаторе непрерывного действия). *All-Union scientific technique conference "Cold–People Improvement" (Всесоюзная научно-техническая конференция "Холод – народному хозяйству"),* AL: LTYHP, pp.268-269;

[4] Palamarchuk I., Zozulyak O., Gerasimov A., (2013), Development of management system of bulk materials drying. *MOTROL. Commission of Motorization and Energetics in Agriculture*, Vol.15, №4, pp.212-218;

[5] Palamarchuk I., Bandura V., Palamarchuk V., (2013), Analysis of vibro-conveyor technological system with combined kinematic vibro-stimulator. *MOTROL. Commission of Motorization and Energetics in Agriculture*, Vol.15, № 4, pp.314-323;

[6] Palamarchuk I., (2008), *Scientific and technical bases of development of energy-efficient mechanical vibration action of food and processing industries* (*Науково-технічні основи розроблення енергозберігаючих вібромашин механічної дії харчових і переробних виробництв*), Dis.Dr.Sc. Sciences: 05.18.12, Kyiv/Ukraine, p.461;

[7] Palamarchuk I., Tsurkan O., Hurych A., (2015), Selection electronic devices to operate the autoclave with aerodynamic intensifier (Вибір електронних пристроїв для керування роботою автоклава з аеродинамічним інтенсифікатором), *Innovative aspects of food processing and hospitality industry in terms of modernity: International scientific conference (Міжнародна науково-практична конференція)*, Kharkov/Ukraine, HDUHT, pp.73-74;

[8] Terzyev S., Makyevskaya T., Ruzhytskaya N., (2014), Kinetics of sludge extraction coffee at microwave summing energy, Sciences. pr.ONAFT (*Наукові пр.ОНАХТ*), Odessa/Ukraine, Vol.46, T.2, pp.300-303;

[9] Terzyev S., Kurakov A., (2012), *Electro-diffusion model of heat-and mass transmission in thermo-syphon apparatus (Электродиффузионная модель тепломассопереноса в термосифонных аппаратах)*. Science.pr.ONAFT (Наукові пр. ОНАХТ), Odessa/Ukraine, Vol.41, T.1, pp.219-222;

[10] Terziev S., Malashevych S., Ruzhytska S., (2011), Investigation of sludge drying coffee under infrared (Дослідження процесу сушіння шламу кави під дією інфрачервоного випромінювання), *Scientific Bulletin of Lviv National University of Veterinary Medicine and Biotechnology named. S. Z. Gzhytskoho* (*Науковий вісник Львівського національного університету ветеринарної медицини та біотехнології ім. С. З. Ґжицького*), Lviv/Ukraine, T.13, № 4 (50), C.4, pp.131-134;

[11] Terziev S., (2016), *Innovative heat technologies of food concentrates production based on system modelling and combined heat and mass transfer processes* (*Іноваційні теплотехнології харчоконцентратних виробництв на основі системного моделювання та комбінованих процесів тепломасопереносу*): Author. Dis. on competition sciences. Degree dock. Sc. Science, Odessa/Ukraine, pp.45;

[12] Tsurkan O., Gerasimov O., Hurych A., (2010), Substantiation of equipment for adjusting process parameters autoclave with aerodynamic intensifiers (Обгрунтування комплексу обладнання для регулювання технологічних параметрів автоклава з аеродинамічним інтенсифікатором), *Journal of Kharkov National Technical University of Agriculture Petro Vasilenko* (*Вісник Харківського національного технічного університету сільського господарства імені Петра Василенка*), Kharkov/Ukraine, Vol.166, pp.274-279;

[13] Tsurkan O., Hurych A., Polyevoda Y., (2015), *Substantiation of technological and structural schemes autoclave with aerodynamic intensifier* (*Обгрунтування технологічної та конструктивної схеми автоклава з аеродинамічним інтенсифікатором*). Scientific pr.ONAFT (Наукові пр. ОНАХТ), Odessa/Ukraine, Vol.46, T.2, pp. 312-314;

[14] TU 10.1-22769675-001, (2013), *Paste Canned meat turkeys "Podolsky"* (*Паштет консервований із м'яса індиків "Подільський"*). TC № 132 Derzhspozhyvstandart, Lviv/Ukraine, p.10;

[15] Tugolukov E., (2004), Methods of mathematical modelling of non-stationary temperature subspace device (Методика математического моделирования нестационарных температурных полей емкостного аппарата), *Chemichal industry* (*Химическая промышленность*), Vol.81, № 2, pp.84-92;

[16] Voronenko B., Pelenenko V., Starikov V., (2008), Mathematic description of heat and mass transfer processes in sausage production (Математическое описание процессов тепло- и массопереноса в колбасных изделиях при их тепловой обработке), *Processes and Apparatus of food production* (*Процессы и аппараты пищевых производств*), № 2, pp.27-30.

HEAT AND MASS TRANSFER DURING HOT-AIR DRYING OF RAPESEED: CFD APPROACH AND EVALUATION
/
基于 CFD 的油菜籽热风干燥传热传质研究与验证

Ms. Stud. Gao B.[1)], Ms. Stud. Guo M.B.[2)], As. Ph.D. Yang L.[1)], Asst. Ph.D. Wu D.K.[1)], Prof. Ph.D. Yang M.J.*[1)]
[1)] Southwest University, College of Engineering and Technology / P. R. China; [2)] Dezhou Degong Machinery Co. Ltd / P. R. China
Tel: 8613883002509; E-mail: ymingjin@swu.edu.cn

Keywords: *hot-air drying, drying characteristics, heat and mass transfer, rapeseed, CFD*

ABSTRACT

Moisture content loss of rapeseed (Brassica napus L.) and drying rate change with time during thin layer hot-air drying were obtained through experiments. By means of volume weighed average, the moisture content loss of rapeseed and airflow distribution in the drying box were simulated and analyzed in FLUENT using methodology of CFD. For heat and mass transfer modelling of the rapeseed drying, a code incorporating the effects of heat and moisture transfer was compiled by means of UDFs (User-Defined Functions), and SIMPLE (Semi-Implicit Method for Pressure-Linked Equations) scheme was adopted to solve the constitutive equations governing the rapeseed drying. Numerical findings were compared with the experimental data, and they had good agreement with experiments: mean relative errors of moisture content, air temperature and air velocity of modelling are 7.48%, 1.07% and 7.72 %, respectively.

摘要

通过实验得到了甘蓝型油菜籽在热风干燥条件下的含水率和干燥速率随时间的变化。基于 CFD 和体积加权平均，通过 FLUENT 仿真并分析了油菜籽含水率随时间的变化以及干燥室内的流场分布。为模拟油菜籽干燥的传热传质过程，通过 UDFs 编程并采用压力耦合半隐式 SIMPLE 方法求解决定干燥过程的本构方程。仿真结果和实验数据具有很好的一致性：含水率、热风温度和热风速度的平均误差分别为 7.48%、1.07%和 7.72 %。

INTRODUCTION

Rape (*Brassica campestris* L.) is an annual herbaceous plant. The stem, leaf and tender shoot of rape can be used as vegetables, and they have multiple nutritional ingredients. The blossoms are stable, being a nectar source for honeybees, and nectar of rape blossom accounts for more than 40% of total nectar production in China *(Yang et al., 2014)*.The seed is the most valuable, collected component of the crop, as the world's third leading source of vegetable oil, after soybean and oil palm, and the second leading source of protein after soybean (Yang et al., 2012). The main varieties of rape are *Brassica rapa* L., *Brassica juncea* L. and *Brassica napus* L., and Rape (*Brassica napus* L.*)* are mostly planted in Yangtze valley, China, and the seed production of rape (*Brassica napus* L.) accounts for 90% of the total *(Li et al., 2006)*.

The harvest period of rapeseed often runs into rainy season of high temperature and high humidity. The freshly harvested rapeseed contains high moisture content, then the seed may become deteriorated because of overheat, acidification and mildew, which affect physiological characteristics of the seed for seeding purpose and oil quality of the seed for oil purpose *(Yang et al., 2012)*. Yang et al. (2013) mentioned artificial drying is required to timely decrease moisture content of the rapeseed to safe levels for storage, and hot-air drying is mostly employed among numerous drying methods. For hot-air drying, hot-air functions both as heat supporter and as humidity carrier during the drying process. Uniform airflow distribution inside the drying box is of paramount importance because it determines both the efficiency of drying and the homogeneity of products being dried *(Amanlou et al., 2010)*.

Rapeseed is an unsaturated porous medium with sorptivity, and its kernel owns complex porous medium structure with biomass features. The heat and mass transfer process of rapeseed hot-air drying consists of multi-phase coupling and wet-phase transition *(Jiang et al., 2012)*. Although many experimental works are conducted on drying characteristics of rapeseed and effects of air temperature on physiological quality of the seed, little information is available on heat and mass transfer during hot-air drying of rapeseed, and it is insufficient for dryer design and process control of rapeseed drying. Thakor et al. (1999) studied the size and mass change of individual kernels of rapeseed, both whole kernel (hull attached) and embryo (kernel without hull), during drying using thermo-gravimetric analysis. Corrêa et al. (1999) experimentally studied germination and vigor response of rapeseed to air temperature and relative humidity after hot-air drying. Duc et al. (2011) conducted thin layer drying tests to determine the most appropriate thin layer drying model, effective moisture diffusivity, and activation energy for the moisture diffusion of rapeseed.

Mathematical modelling contributes to better understanding of heat and mass transfer and it is very useful for improvement of dryer design and process control of drying *(Tzempelikos et al., 2015)*. Dong-Hyuk K et al. examined the simultaneous heat and mass transfer between air and rapeseed in a concurrent-flow dryer by combined equations concerning air psychrometrics, physical properties, thermal properties, equilibrium moisture content, thin layer drying of rapeseed, etc. to solve the drying model *(Dong and Woong, 2010*). Yang L. (2004) studied heat and mass transfer process in micro pores during hot-air drying of rapeseed by means of Mixture Model of ANSYS Fluent, and analyzed effects of length to diameter ratio and tortuosity of micro pores of seed kernel on hot-air drying. Amanlou and Zomorodian (2010) applied CFD for designing a fruit cabinet, and experimental and predicted data from CFD analysis revealed good correlation coefficients. An extensive analysis of the different mathematical approaches can be found in the works of Datta, A.K. and Norton, T. et al. *(Datta et al., 2007; Norton et al., 2013)*.

The main objectives of this study are:

(1) To obtain drying characteristics of rapeseed during hot-air drying for thin layer seed experimentally.

(2) To investigate methodology of CFD for analysis of heat and mass transfer during hot-air drying of rapeseed.

(3) To compare numerical findings of the moisture content loss of rapeseed and airflow distribution in the drying box with experimental data.

MATERIAL AND METHOD

Sample preparation

The rapeseed (*Brassica napus* L.), Chuanyou 18, was bought from Chongqing Seed Company. The impurities, cracked, germinated, moldy seed and seed with green color were manually removed so as to obtain uniform test samples. The initial moisture content of rapeseed was determined according to Chinese standard GB/T14489.1-2008: Oil seeds - Determination of moisture and volatile matter content *(China National standardizing committee, 2008)*.

According to the initial moisture content of 8.7% d.b., test samples of the dry rapeseed were rewetted to moisture content of 15% d.b., by adding pre-calculated amount of water, mixed, sealed with plastic bags, and kept in a temperature controlled room at temperature of 2-4°C for no less than 48 h. Before starting experiments, they were taken out from the controlled room and let them attain thermal equilibrium with ambient air.

Experimental setup and procedure

Experiments were conducted in a lab-scale thin layer dryer as shown in fig. 1.

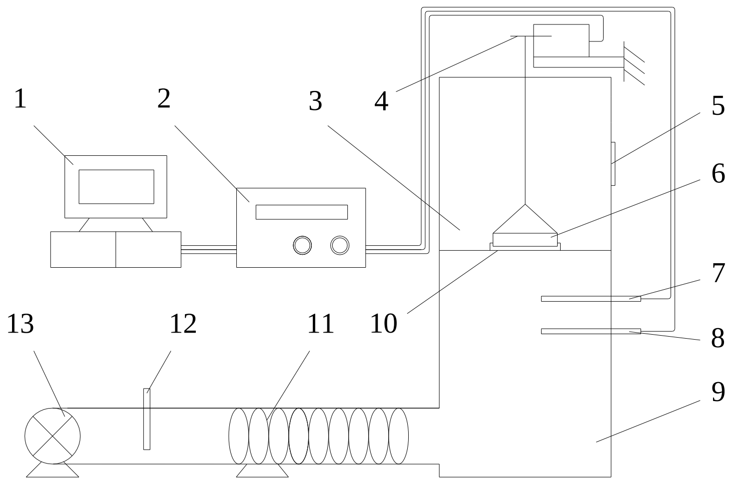

Fig. 1 - Schematic diagram of the thin layer dryer

1 – computer; 2 - data acquisition; 3 - drying box; 4 - load cell; 5 – exit; 6 - sieve tray; 7 - temperature sensor; 8 - humidity sensor; 9 - plenum chamber; 10 – entrance; 11 - heater; 12 - valve; 13 - fan

The experimental setup consists of fan, heater, valve, drying box, load cell, temperature sensor, humidity sensor, data acquisition and computer. Sieve tray with a holding area of 150 mm × 150 mm is included in the drying box. The cube drying box dimensions are of side length 400 mm. Exit of the drying box is of diameter 100 mm. The mass flow rate and heat flow rate of hot-air are regulated by the valve, and the heater, respectively.

The test samples of rapeseed, weighing about 420 g with a seed layer thickness of 20 mm, were placed in the sieve tray. During the drying process, the samples were periodically weighed to determine weight loss at 5 min intervals, from which the drying curves were obtained. The drying rate is determined by *(Zhang et al., 2012)*:

$$DR = -\frac{dW}{dt} = -\frac{W_{i+1} - W_i}{t_{i+1} - t_i}\text{, [d.b./s]} \tag{1}$$

where:

DR is drying rate of rapeseed, [d.b./s];

W – moisture content of seed in dry basis, [d.b.];

t – time, [s];

W_i – moisture contents at t_i, [d.b.];

W_{i+1} – moisture contents at t_{i+1}, [d.b.].

The additional measurements included air temperature and air velocity at 3 different positions, namely top of seed layer, centre and exit of the drying box, and the measurements are for the validation of experimental data and numerical findings of rapeseed hot-air drying. All measurements are of 5 replicas. The measuring instruments are the portable thermometer (DS18B20, Beijing Chuangyiling Control Co. Ltd, China) and the anemometer (SUMMIT-565, Guangzhou Taishi Instrument Co. Ltd, China).

Methodology for modelling and evaluation

In order to model the heat and mass transfer during hot-air drying of rapeseed with simplicity and good validity, the relevant assumptions are described as follows *(Jamaleddine and Ray, 2010)*:

The gas phase is a mixture of air and water vapour. The dispersed phase is a mixture of porous homogeneous structure and liquid water. Both phases are incompressible.

Heat transfer occurs between both phases, and is no heat transfer between phases and walls of the drying box.

There is no shrinkage and deformation of rapeseed kernels, and only water evaporation during drying process.

There are no cohesive moves of rapeseed and effects of cohesive dissipation heat and thermal radiation are not considered.

The hot temperature of air causes heat transfer from carrier, namely hot-air, to rapeseed, while evaporation from water to vapour occurs from the rapeseed to gas phase. Constitutive equations describing the mass and heat transfer are as follows *(Thorpe et al., 2008)*.

The mass transfer equation is:

$$\frac{\partial(\rho_a w)}{\partial t} + \nabla\cdot(\rho_a v w) = \nabla\cdot(\rho_a D_{eff}\nabla w) + S_w \tag{2}$$

where:

ρ_a is density of air, [kg/m^3];

w – moisture content of air, [d.b.];

v – superficial or Darcian velocity of air through seed, [m/s];

D_{eff} – effective diffusion coefficient of moisture through bulk seed, [m^2/s];

S_w – moisture source term, [kg/(s·m^3)];

∇ – the del operator.

The heat transfer equation is:

$$\left(\rho_a \varepsilon c_a + \rho_s(1-\varepsilon)\left(c_s + c_w W + \frac{\partial H_w}{\partial T}\right)\right)\frac{\partial T}{\partial t} + c_a\nabla\cdot(\rho_a u T) = k_{eff}\nabla^2 T + S_h \tag{3}$$

where:

ε is void fraction of seed;

c_a, c_s, c_w – specific heat of air, seed and liquid water, respectively, [J/(kg·K)];
ρ_s – density of seed kernels in dry basis, [kg/m^3];
H_W – integral heat of wetting of water on seed, [J/kg];
T – temperature, [K];
k_{eff} – effective thermal conductivity of seed, [W/(m·K)];
S_h – energy source term, [W/m^3].

The moisture source term S_w in Eq. 2 is expressed as:

$$S_w = -(1-\varepsilon)\rho_s \frac{\partial W}{\partial t}, \text{ [kg/(s·m}^3\text{)]} \quad (4)$$

The energy source term S_h in Eq. 3 takes the form:

$$S_h = -h_s(1-\varepsilon)\rho_s \frac{\partial W}{\partial t}, \text{ [W/m}^3\text{]} \quad (5)$$

where:
h_s is heat of sorption of water on seed, J/kg.

The physical configuration of the drying box for modelling is represented and meshed as shown in fig. 2. The physical configuration has same dimensions as drying box of the thin layer hot-air dryer mentioned above.

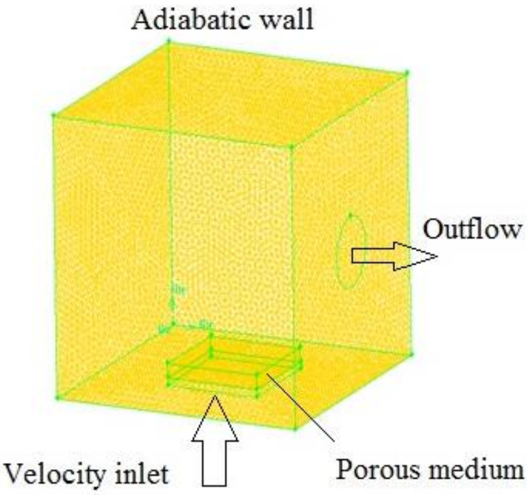

Fig. 2 - Physical configuration, meshing of the drying box

The corresponding boundary and initial conditions are defined as follows: Air in the drying box is defined as fluid, and rapeseed on the sieve tray as porous medium. The initial temperature of rapeseed is 298 K. Entrance of the drying box is defined as velocity inlet, and exit as outflow. The air velocity and temperature of hot-air at entrance of the drying box are 1.0 m/s and 373 K, respectively. Walls of the drying box are defined as adiabatic wall. Interface between fluid and porous medium is defined as interior.

The physical properties of air and rapeseed for the modelling are listed in table 1.

Table 1

Physical properties of air and rapeseed

Properties	Air	Rapeseed
Density, [kg·m^3]	1.225	945.5
Specific heat, [J·kg^{-1}·K^{-1}]	1006.43	1561
Thermal conductivity, [W·m^{-1}·K^{-1}]	0.0242	0.169
Viscosity, [Pa·s]	1.7894×10^{-5}	-
Viscous resistance, [m^{-2}]	-	5.9×10^8
Inertial resistance, [m^{-1}]	-	3.2×10^4
Porosity, [%]	-	36

In order to better demonstrate the coupling of heat and mass transfer during hot-air drying, a code incorporating the effects of heat and mass transfer was compiled by means of UDFs (User-Defined Functions) in a high level language of C. Reference of strategy for the code writing, with small modification, was given to Thorpe's work *(Thorpe G.R., 2008)*. SIMPLE (Semi-Implicit Method for Pressure-Linked Equations) scheme was adopted to solve the constitutive equations governing the rapeseed hot-air drying in FLUENT.

For visual analysis of the CFD data and further explorations of the rapeseed hot-air drying, post-processor of Tecplot 360 was employed to plot the contours of air velocity and air temperature in the drying box.

The relative error of modelling with experiments is evaluated by:

$$E = \frac{\left|D_{M} - D_{E}\right|}{D_{E}} \times 100\% \tag{6}$$

where:

E is relative error, [%];

D_M, D_E – interested parameters from modelling and experiments, respectively.

RESULTS

Experimental results

The drying behavior can be characterized by measuring the moisture content loss as a function of time.

The drying characteristics of rapeseed during thin layer hot-air drying are represented by the moisture content loss curve and the drying rate curve as shown in fig. 3. The conditions for the experiment are as follows: seed layer thickness of 20 mm, air velocity of 1.0 m/s, and air temperature of 373 K.

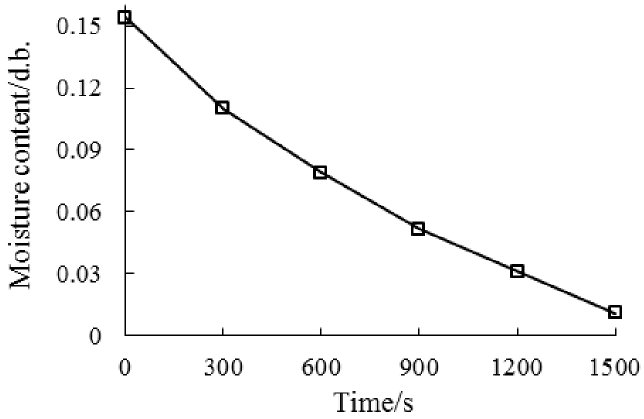

(a) Moisture content loss curve

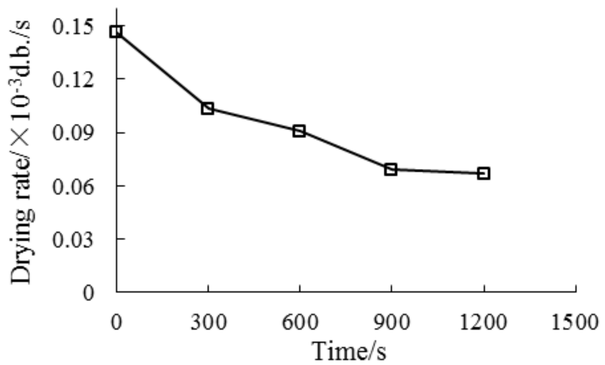

(b) Drying rate curve

Fig. 3 - Drying characteristics of rapeseed by the experiment

Air temperature, air velocity and their distribution are important factors affecting the drying behavior of rapeseed.

The air temperature and air velocity at 3 representative positions of the drying box were measured at 5 min intervals as shown in fig. 4 and fig. 5, respectively.

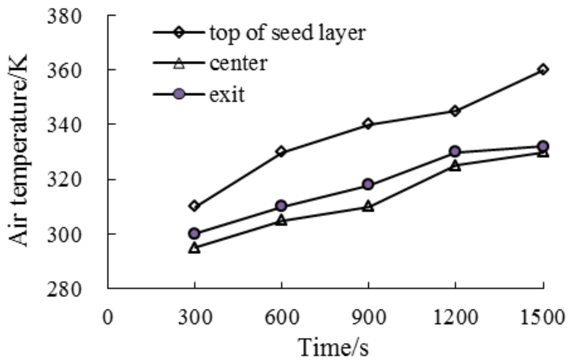

Fig. 4 - Air temperature at different positions of drying box

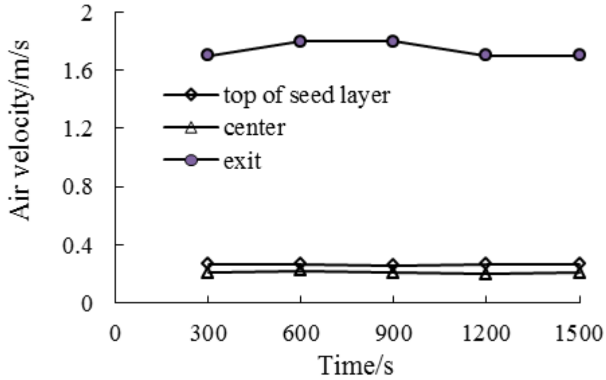

Fig. 5 - Air velocity at different positions of drying box

Modelling results of rapeseed drying

The moisture content loss of rapeseed can be obtained by modelling as shown in fig. 6. It is the volume weighed average of porous medium of the rapeseed in the drying box. The volume weighted average of a quantity is computed by dividing the summation of the product of the selected field variable and cell volume by the total volume of the cell zone in ANSYS Fluent.

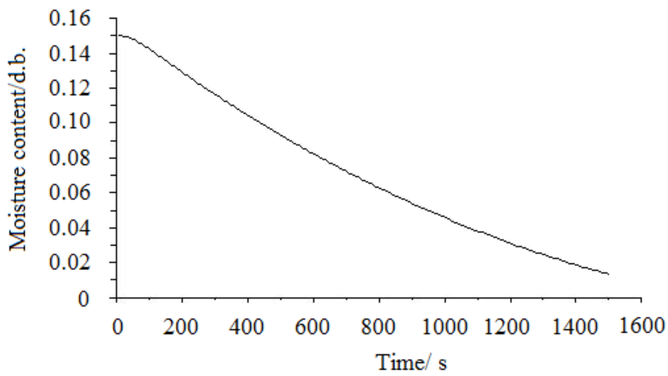

Fig. 6 - Moisture content loss curve by modeling

The flow parameters of the rapeseed during thin layer hot-air drying can be visualized by post processing. As the drying box has symmetrical geometry along vertical plane passing through axis of the exit of drying box, the contours of air temperature and air velocity on this plane are representatively plotted as shown in fig.7 and fig.8, respectively. The time intervals interested for the plotting are 600, 1200, and 1500 s.

For the contours in fig. 7 and fig. 8, the *X* axis is along horizontal direction, and the *Y* axis is along vertical direction, showing the dimensions of the drying box. The colours in the contours depict the difference of parameters interested at different areas in the drying box, and the scales at the side of each contour illustrate the values of parameter at the corresponding area. As a result, changes of air temperature and air velocity in the drying box with the progress of hot-air drying are visually described.

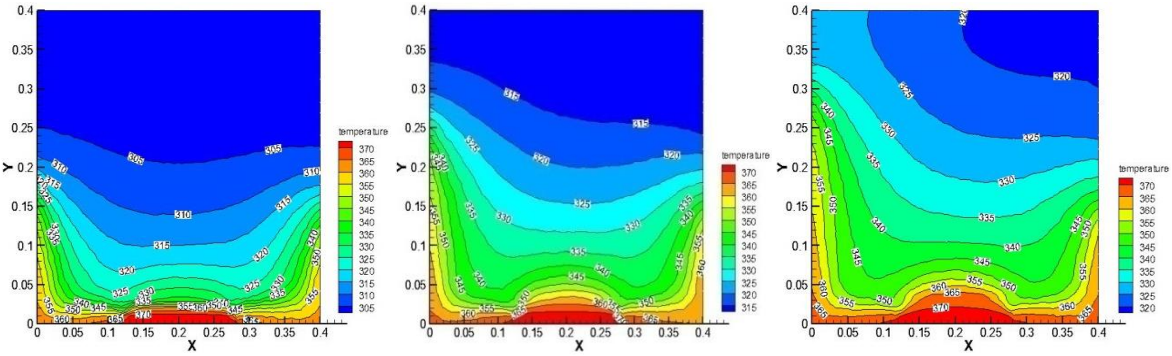

(a) 600 s (b) 1200 s (c) 1500 s

Fig. 7 - Air temperature contour of time intervals

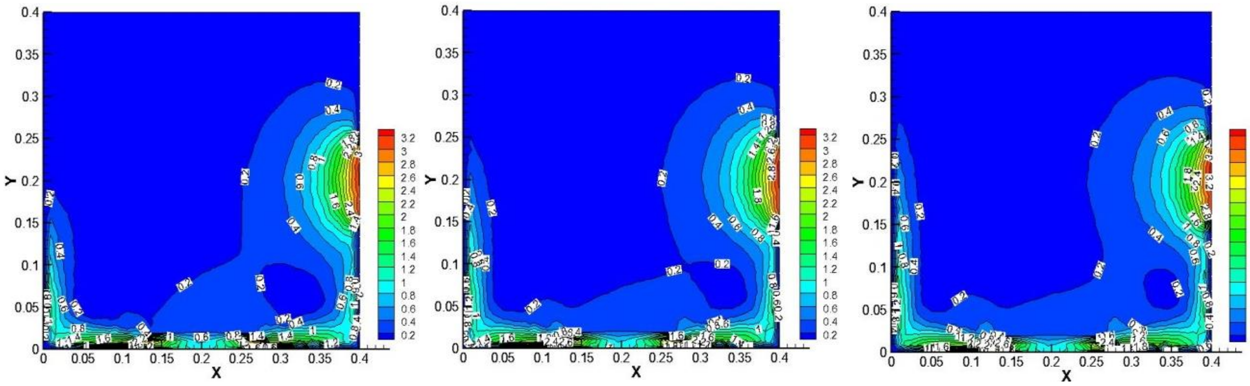

(a) 600 s (b) 1200 s (c) 1500 s

Fig. 8 - Air velocity contour of time intervals

Analysis and discussion

The moisture content loss curves of rapeseed thin layer hot-air drying showed that there is no constant rate drying stage for rapeseed, as shown in Figures 3 and 6. The moisture contents of rapeseed are 11.3%, 7.5%, 5.2%, 3.2% and 1.2% d.b. at 300, 600, 900, 1200 and 1500 s. The drying conditions are air temperature 373 K, air velocity 1.0 m/s, initial moisture content of rapeseed 15% d.b. and layer thickness 20 mm. The moisture transfer of rapeseed is mainly occurred in the former stage, and the drying rate decreases with drying process continued. The moisture content (MC) of rapeseed from modelling and experiments and their relative error are listed in table 2.

Table 2

Relative error of moisture content

Time [s]	MC from modelling [% d.b.]	MC from experiments [% d.b.]	Relative error [%]
300	11.8	11.3	4.4
600	8.1	7.5	6.8
900	5.0	5.2	3.9
1200	2.9	3.2	6.4
1500	1.0	1.2	16.0

The distribution of air temperature in the drying box gradually changes with the drying process continued, and the air temperature at the top of seed layer is much higher than that at centre and exit of the drying box, of which benefits the rapeseed thin layer hot-air drying. The distribution of air velocity reaches a stable status in quite a short period of time, and the air velocities at the top of seed layer and centre of the drying box are nearly same, but with a small loss at centre position, and the air velocity at the exit of the drying box is much higher than those at positions of the former two. The air temperature, air velocity from modelling and experiments, and their relative error, at different positions and process time are listed in tables 3 and 4.

Commercial CFD packages are capable of solving the general constitutive equations that govern conservation of mass, energy and momentum and they must be tailored so that heat, moisture and airflow distributions during drying of porous medium can be obtained. User-Defined Function is a successful approach to model the heat and mass transfer during thin layer hot-air drying of rapeseed for CFD. The moisture content and airflow distributions obtained from modelling showed considerably good agreement with those from experiments: mean relative error of moisture content of modeling with experiments is 7.48%; mean relative errors of air temperature and air velocity are 1.07% and 7.72%, respectively.

By methodology of CFD modelling of the hot-air drying, the following performance parameters or feathers can also be obtained: the time for drying certain amount of rapeseed of pre-measured moisture content to required moisture level; the performance of rapeseed drying with temperature-change technological process, namely different drying stages having different air temperatures; the airflow distribution, including air temperature, air velocity, and pressure, etc., of a drying box with different geometry. Therefore, the technological process and its control strategy of thin-layer hot-air drying of rapeseed, and the structure and parameters of the drying box can be optimized by modelling, which can provide reference and basis for optimization of drying technique and equipment of rapeseed hot-air drying.

Table 3

Relative error of air temperature

Position	Time [s]	Temperature from modelling, [K]	Temperature from experiments, [K]	Relative error, [%]
Top of seed layer	600	325	328	0.9
	1200	345	343	0.5
	1500	355	350	1.4
Centre	600	310	305	1.6
	1200	320	325	1.5
	1500	330	328	0.6
Exit	600	315	310	1.6
	1200	335	330	1.5
	1500	340	340	0

Table 4

Relative error of air velocity

Position	Time, [s]	Velocity from modelling, [$m \cdot s^{-1}$]	Velocity from experiments, [$m \cdot s^{-1}$]	Relative error, [%]
Top of seed layer	600	0.30	0.27	11.0
	1200	0.30	0.27	11.0
	1500	0.29	0.27	11.0
Centre	600	0.20	0.22	9.0
	1200	0.20	0.20	0
	1500	0.20	0.21	4.7
Exit	600	1.60	1.80	11.0
	1200	1.80	1.70	5.9
	1500	1.80	1.70	5.9

CONCLUSIONS

In this study, a numerical investigation of heat and mass transfer during thin layer hot-air drying of rapeseed was carried out, and the experimental measurements were taken for the respective drying conditions. The following conclusions can be drawn from the results of this study:

(1) There is no constant rate drying stage for the thin layer hot-air drying of rapeseed. The moisture transfer of rapeseed is mainly occurred in the former stage, and the drying rate decreases with drying process continued.

(2) User-Defined Function is a successful approach to model the heat and mass transfer during thin layer hot-air drying of rapeseed for CFD, and the moisture content loss of rapeseed and airflow distributions in the drying box can be obtained from the modelling.

(3) Numerical findings had good agreement with experiments: mean relative error of moisture content is 7.48%, and mean relative errors of air temperature and air velocity are 1.07% and 7.72%.

ACKNOWLEDGEMENT

This study was supported by National Natural Science Foundation of China (No. 31301575) and Chongqing Science and Technology Commission (No. cstc2016shmszx80001).

REFERENCES

[1] Amanlou Y., Zomorodian A., (2010), Applying CFD for designing a new fruit cabinet dryer, *Journal of Food Engineering*. vol. 101, issue 1, pp. 8-15;

[2] Corrêa P.C., Martins J.H., Christ D., (1999), Thin layer drying rate and loss of viability modelling for rapeseed (*Canola*), *Journal of Agricultural Engineering Research*. vol. 74, issue 1, pp. 33-39;

[3] Datta A.K., (2007), Porous media approaches to studying simultaneous heat and mass transfer in food processes I: problem formulations, *Journal of Food Engineering*. vol. 80, issue 1, pp. 80-95;

[4] Dong-Hyuk K., Woong K., (2010), Circulating concurrent-flow drying simulation of rapeseed, *Journal of Biosystems Engineering*. vol. 35, issue 6, pp. 401-407;

[5] Duc L.A., Han J.W., Keum D.H., (2011), Thin layer drying characteristic s of rape seed (*Brassica napus* L.), *Journal of Stored Products Research*. vol. 47, issue 1, pp. 32-38;

[6] Jamaleddine T.J., Ray M.B., (2010), Numerical simulation of pneumatic dryers using computational fluid dynamics, *Industry & Engineering Chemistry Research*. vol. 49, issue 12, pp. 5900-5910;

[7] Jiang S., Yang M., Tang T., Li Y., Yang L., (2012), Heat and mass transfer simulation in micro scale pores of a rape seed (油菜籽干燥微尺度孔道传热传质数值模拟), *Journal of Agricultural Mechanization Research*. vol. 34, issue 2, pp. 42-45;

[8] Li P., (2006), *Glucosinolate and their relationship between leaves and Seeds in Brassica napus (甘蓝型油菜叶片与种子硫苷相关性研究)*, PhD dissertation, Huazhong Agricultural University, Wuhan / P. R. China;

[9] Norton T., Tiwari B., Sun D., (2013), Computational fluid dynamics in the design and Analysis of thermal processes: a review of recent advances, *Critical Reviews in Food Science and Nutrition*. vol. 53, issue 3, pp. 251-275;

[10] Thakor N.J., Sokhansanj S., Sosulski F.W., Yannacopoulos S., (1999), Mass and dimensional changes of single canola kernels during drying. *Journal of Food Engineering*. vol. 40, issue 3, pp. 153-160;

[11] Thorpe G.R., (2008), The application of computational fluid dynamics codes to simulate heat and moisture transfer in stored grains, *Journal of Stored Products Research*. vol. 44, issue 1, pp. 21-31;

[12] Tzempelikos, D.A., Mitrakos, D., Vouros, A.P., Bardakasd, A.V., Filiose, A.E., Margarisa, D.P., (2015), Numerical modelling of heat and mass transfer during convective drying of cylindrical quince slices. *Journal of Food Engineering*. vol. 156, pp. 10-21;

[13] Yang G., Ding C., Cai H., Tu C., He S., (2012), Research and development progress on rapeseed drying technology (油菜籽干燥技术研究进展), *Journal of the Chinese Cereal and Oils Association*. Vol. 27, issue 5, pp. 124-128;

[14] Yang G., He S., Ding C., (2013), Study of the rapeseeds' quality storage after hot-air drying (油菜籽热风干燥后储藏品质的研究), *Journal of the Chinese Cereal and Oils Association*. vol. 28, issue 9, pp. 97-102;

[15] Yang L., (2014), *Heat & mass transfer characteristics and model of hot-air drying for seed of rape (Brassica napus L.) (甘蓝型油菜籽热风干燥传热传质特性及模型研究)*, PhD dissertation, Southwest University, Chongqing / P. R. China;

[16] Yang L., Yang M., Chen J., Li Y., Wu D., (2012), Status and development trend of rapeseed drying for seeding purposes (种用油菜籽干燥的现状及发展趋势), *Transactions of the Chinese Society of Agricultural Engineering*. vol. 28, issue S2, pp. 309-315;

[17] Zhang L., Wang X., Yu L., Zhang H., (2012), Drying characteristics and colour changes of infrared drying eggplant (茄子红外辐射干燥特性及色泽变化), *Transactions of the Chinese Society of Agricultural Engineering*. vol. 28, issue S2, pp. 291-296;

[18] *** China National standardizing committee, (2008), Oilseeds - Determination of moisture and volatile matter content, GB/T14489.1-2008 (油料 水分及挥发物含量测定, GB/T14489.1-2008), Chinese Standard Press, P. R. China.

DISCRETE MODELLING OF SURFACES OF EQUAL SLOPES BY MEANS OF NUMERICAL SEQUENCES
/
ДИСКРЕТНЕ МОДЕЛЮВАННЯ ПОВЕРХОНЬ ВІДВАЛІВ ВИЗНАЧЕНОГООБ'ЄМУ ПОДВІЙНИМИ ЧИСЛОВИМИ ПОСЛІДОВНОСТЯМИ

Prof. Ph.D. Eng. Pustiulha S., Khomych A., Ph.D. Eng.Tsiz' I., Ph.D. Eng. Kirchuk R.
Lutsk National Technical University / Ukraine
Tel: +38(0332)74-61-31; Fax: +38(0332)74-61-31; E-mail: lab-amb@ukr.net

Keywords: *numerical sequences, bulk materials, surface, geometric modelling*

ABSTRACT
This paper presents an approach, the mathematical algorithms and software implementation of processes of discrete geometric modelling of open storage of bulk materials, such as surfaces of the equal slope, taking into account the geometrical and technological requirements for newly created objects and the physical and mechanical properties of bulk materials forming them. This approach and developed algorithms will not only make possible to technologically project the construction of open storage of bulk materials in time and provide a variety of geometrical requirements to objects, but also to make recommendations for the selection and organization of transporting machines work which are necessary for.

РЕЗЮМЕ
У роботі запропоновано підхід, математичні алгоритми та програмну реалізацію процесів дискретного геометричного моделювання за допомогою числових послідовностей відкритих складів сипких матеріалів як поверхонь однакового відкосу, з урахуванням геометричних, технологічних вимог до створюваних об'єктів та фізико-механічних властивостей сипких матеріалів, що їх утворюють. Такий підхід та розроблені алгоритми дозволять не тільки технологічно запроектувати зведення відкритих складів сипких матеріалів у часі та забезпечити цілу низку геометричних вимог, що висуваються до об'єктів, а й виробити рекомендації щодо підбору та організації роботи необхідних для цього транспортуючих машин.

INTRODUCTION
When designing the open storage of bulk materials in a defined area that is limited by curved contour of complex geometry, with the defined ceiling height of storage, the building of such structure models is actual as for the organization of lifting machines work so as for the optimization of the storage of given objects. Such models will make possible correctly and technologically design the construction of open storage in time and provide a series of geometric requirements imposed on objects *(Kupriiashkin A., 2015)*.

The main physical and mechanical property of bulk material, e.g. the ability of its elements to roll down the sloping surface is the angle of natural inclination, the angle that is formed between the plane of the base and the cone generatrix by free fall of bulk materials onto the horizontal plane *(Boitsov Y.U. and Kartalis N., 2013; Klein G., 1977; Vaisberh L., Demidov I. and Ivanov K., 2015)*.

This characteristic of the bulk material is basic when creating geometric models of surfaces of the equal slopes as the ratio of the base size, its geometry and height of storage, its volume and mass are directly dependent on this angle (see Fig. 1).

Fig. 1 - Photos of existing dumps of bulk materials

Geometrically, the problem of modelling of open storage of bulk materials as surfaces of equal slopes, based on the curvilinear contour of a defined area, with a certain height of storage leads to the construction: of the lower curvilinear contour, the upper contour that is equidistant *(Hozbenko V. and Lytkina E., 2010)* to the lower one and is the trajectory of motion of the load device.

So the development of new efficient algorithms for constructing models of surfaces of equal slopes considering besides technological requirements (selection, calculation and organization of transport vehicles), geometrical requirements (height, volume, mass etc.) and even the physical and mechanical properties of bulk materials which form them is quite challenging problem.

MATERIAL AND METHOD

Development of methods of discrete modelling by the scientists working, in the field of applied geometry made it possible to simplify the solution of a number of practical problems concerning the designing of complex spatial structures and objects.

One of the methods of discrete geometric modelling of equable structures, that has several advantages over all existing methods, is the formation of images using mathematical tools of numerical sequences *(Pustiulha V., 2006).* In works *(Pustiulha V. et al., 2011; Pustiulha V. et al., 20112014)* efficient algorithms of discrete modelling of storage surfaces of the equal slope using one-dimensional numerical sequences, namely discrete models of closed curves with the defined geometric properties, models which are equidistant to these curves, ensuring the absence of irregular points are proposed. However, the development of algorithms for discrete modelling of curved surfaces of the equal slopes as integral geometric objects that are models of open storage of bulk materials with certain technological initial conditions remains rather challenging problem.

The process of designing an open storage of bulk materials is proposed to carry out by the following steps. First - the formation of a discrete model of the closed curvilinear contour with certain geometric properties, including: smoothness of molded object, passing through a series of basic, points of reference, providing a defined area of the modelled contour. Second - analysis of discrete analogues of curvature at points of discrete model, natural slopes angles of bulk material and consequently, determination of the parameters of equidistant that will serve as the trajectory for lift transporting machines to form uniform surface slopes at a defined closed contour. Third - the formation of a coherent discrete model of the equal surface slopes counting the volume, weight and height of the simulated open storage of bulk material.

Theoretical studies are based on the guidelines of discrete geometry, mathematical tools of numerical sequences, differential geometry and theory of bulk materials. Modelling of surfaces of equal slopes with predetermined requirements was carried out by the software MathCAD.

RESULTS

Into the basis of algorithm for forming a discrete model of closed circuit of surface fundamentals slopes were set by the same system of one-dimensional numerical sequences of such type:

$$\begin{cases} x_n = \left(1-\dfrac{n}{N}\right)x_1 + \dfrac{n}{N}x_N + \dfrac{n}{N}\sum\limits_{v=1}^{N-1}\sum\limits_{s=1}^{v}kP_s^x - \sum\limits_{v=1}^{n-1}\sum\limits_{s=1}^{v}kP_s^x; \\ y_n = \left(1-\dfrac{n}{N}\right)y_1 + \dfrac{n}{N}y_N + \dfrac{n}{N}\sum\limits_{v=1}^{N-1}\sum\limits_{s=1}^{v}kP_s^y - \sum\limits_{v=1}^{n-1}\sum\limits_{s=1}^{v}kP_s^y, \end{cases} \tag{1}$$

where:

x_1, x_N, y_1, y_N are the border restrictions;

N - serial number of the circuit unit;

kP_S^x, kP_S^y - components of functionally distributed load in the units, parameters of which provide the number of restrictions to the geometry of the model, including the defined area of a closed contour, like this:

$$S_k = \frac{1}{2}\cdot\left|\sum_{n=1}^{N-1}\left(x_n\cdot y_{n+1} - x_{n+1}\cdot y_n\right)\right| \tag{2}$$

where:

x_n, y_n are the values of the coordinate points of the components of a discrete model of a closed curve;

n - series number of the unit;

N -number of the end unit, $x_n = x_1, y_n = y_1$;

S_k- surface area.

According to the presentation of discrete model of the lower base of surface of the equal slope, the upper base is formed as the trajectory of movement for the lifting device of bulk materials. Omitting the details which are shown in *(Pustiulha V. et al., 2014)*, the system of formulas of equidistant curve (see Fig. 2), that is a discrete model of the upper base of a searched surface is represented as:

$$\begin{cases} xe_n = x_n \pm \dfrac{le \cdot dy_n}{\sqrt{(dx_n)^2 + (dy_n)^2}}; \\ ye_n = y_n \pm \dfrac{le \cdot dx_n}{\sqrt{(dx_n)^2 + (dy_n)^2}}, \end{cases} \tag{3}$$

where le is parameter of distance between the points of the base (1) and equidistant (3) curves that are determined from geometrical and technological requirements.

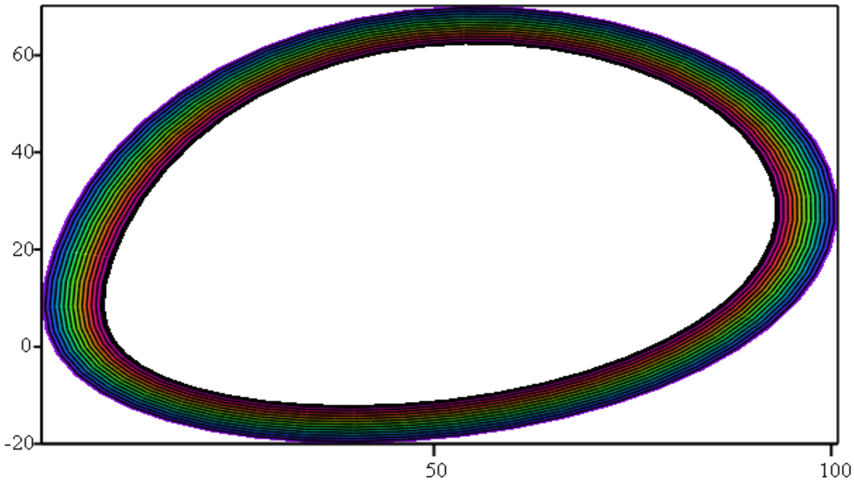

Fig. 2 - Discrete model of set of equidistant curves

At the third stage, namely formation of an integral discrete model of the surface of equal slopes, considering the research results *(Pustiulha V. et al., 2007; Pustiulha V. et al., 2009; Pustiulha V. et al., 2013)*, in parametric form can be represented as follows.

Using supportive contours x_n, xe_n with double numerical sequence $X_{n,k}$ we build the cylindroid like this:

$$X_{n,k} = \left(\left(1-\frac{n}{N}\right)x_1 + \frac{n}{N}x_N + \frac{n}{N}\sum_{v=1}^{N-1}\sum_{s=1}^{v}kP_s^x - \sum_{v=1}^{n-1}\sum_{s=1}^{v}kP_s^x\right)\frac{k}{N} + \left(x_n \pm \frac{le \cdot dy_n}{\sqrt{(dx_n)^2+(dy_n)^2}}\right)\left(1-\frac{k}{N}\right) \tag{4}$$

Discrete model of this cylindroid is shown in Fig. 3.

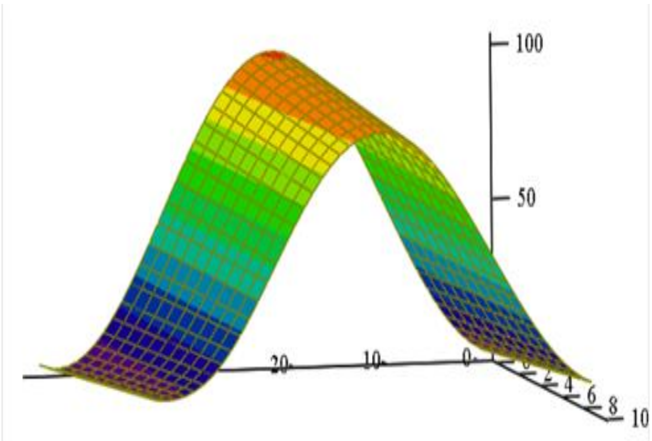

Fig. 3 -Discrete model of surface of equal slope by the component of X

Using supportive contours y_n ye_n for the component of Y we build the second cylindroid $Y_{n,k}$ like this:

$$Y_{n,k} = \left(\left(1-\frac{n}{N}\right)y_1 + \frac{n}{N}y_N + \frac{n}{N}\sum_{v=1}^{N-1}\sum_{s=1}^{v}kP_s^y - \sum_{v=1}^{n-1}\sum_{s=1}^{v}kP_s^y\right)\frac{k}{N} + \left(y_n \pm \frac{le\cdot dx_n}{\sqrt{(dx_n)^2+(dy_n)^2}}\right)\left(1-\frac{k}{N}\right) \quad (5)$$

Discrete model of this cylindroid is shown in Fig. 4.

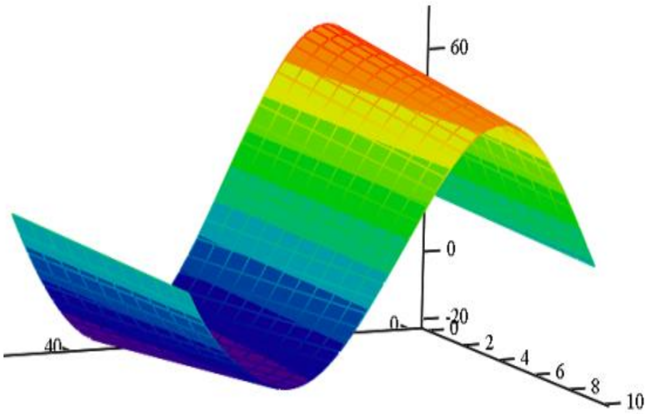

Fig. 4 -Discrete model ofsurfaceofequalslopebythecomponentof Y

The third component Z is given by a double numerical sequence $Z_{n,k}$ in the form:

$$Z_{n,k} = G\cdot\frac{k}{N} + H\cdot\left(1-\frac{k}{N}\right) \quad (6)$$

where G is parameter of the base of a discrete model of the surface and H is model height.

Then the discrete model of the surface of equal slope can be represented by a system of three double numerical sequences (4), (5), (6), a visual representation of which is shown in Fig. 5.

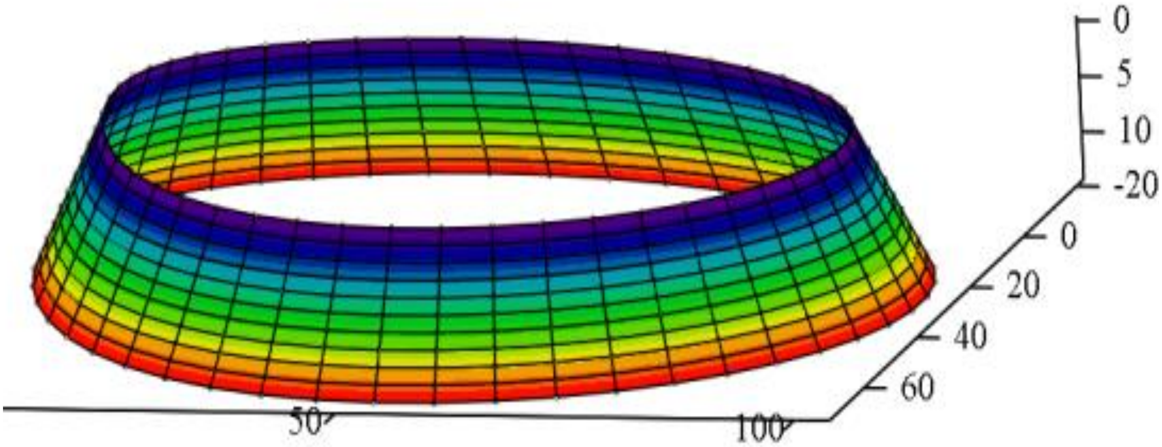

Fig. 5 - Generalized discrete surface model

Each of the generators of the represented discrete model of surface can be interpreted as the contact line of formative cone of natural slope of bulk material at a certain time interval. So, the generalized discrete model of an open storage of bulk material with the defined geometric properties, which are taken into account and technological requirements of its construction is shown in Fig.6.

An important characteristic of a discrete model of open-storage for bulk materials is its volume. It is proposed to make the calculation of storage volume as follows. Suppose V_{zc} is a compartment volume of the outer direct cylinder with the base that is described by the system of numerical sequences x_n, y_n (1).

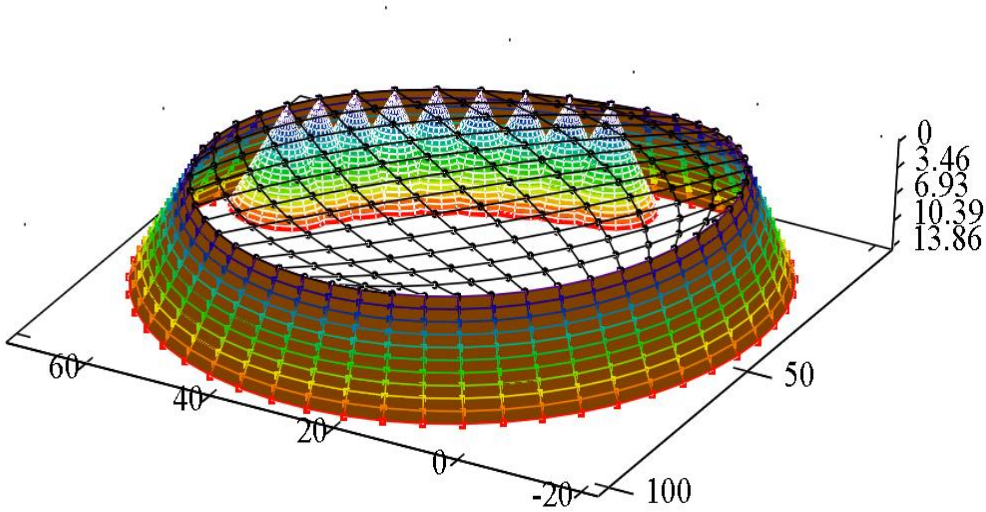

Fig. 6 - Modelling of stepwise process formation of open storage for bulk materials

$$V_{zc} = S_k \cdot H = \frac{1}{2}\left|\sum_{n=1}^{N-1}\left(x_n \cdot y_{n+1} - x_{n+1} \cdot y_n\right)\right| \cdot H \tag{7}$$

where S_k is the area of discrete model of closed curve of the supportive contour and H is height of the cylinder.

Volume of the inner direct cylinder with the base that is described by the system of numerical sequences of xe_n, y_{en} (3) is defined similarly.

$$V_{vc} = S_{ke} \cdot H = \frac{1}{2}\left|\sum_{n=1}^{N-1}\left(xe_n \cdot ye_{n+1} - xe_{n+1} \cdot ye_n\right)\right| \cdot H \tag{8}$$

where S_{ke} is the area of discrete model of equidistant.

So, the full volume of discrete model of open storage for bulk materials can be obtained from:

$$V_s = \frac{V_{zc} + V_{vc}}{2} = \frac{1}{4} \cdot H \cdot \left|\sum_{n=1}^{N-1}\left(xe_n \cdot ye_{n+1} - xe_{n+1} \cdot ye_n\right)\right| + \left|\sum_{n=1}^{N-1}\left(x_n \cdot y_{n+1} - x_{n+1} \cdot y_n\right)\right|. \tag{9}$$

Knowing the bulk density of a certain bulk material γ_0 the total mass of stored bulk material can be determined.

$$m_s = V_s \cdot \gamma_0. \tag{10}$$

Technologically, the reproduction of the model might look like: working part of transporting machine *(Tsyz I. et al., 2015)* should discretely move on the calculated trajectory, the boundary of which is the mode of equidistant (upper base of surface of equal slopes) at a rate that is calculated depending on the given performance (m^3/h). Machines and volumes of basic cones (see Fig. 6) are part of the developed discrete models. In addition, taking into account eq.(9), we can determine the total time required to create an open storage for bulk material.

CONCLUSIONS

This paper reports an approach, mathematical algorithms and software implementation of processes of discrete geometric modelling using double numerical sequences of open storage of bulk materials as surfaces of equal slopes, considering not only technological and geometric requirements for construction of these objects but also physical and mechanical properties of bulk materials which form them.

The process of designing an open storage for bulk materials is proposed to be carried out in three stages. First - the formation of a discrete model of the closed contour with certain geometric properties, second - definition of parameters of equidistant that will serve as the trajectory of loading device for forming uniform surface slopes at a defined closed circuit and create an algorithm for its design, the third - the creation of a uniform discrete surface model with the same slopes calculating volume, mass, height of the modelled open storage of bulk materials and time to create it.

This approach and developed algorithms will not only technologically design the construction of open storage of bulk materials in time and provide a series of geometric requirements that apply to objects, but also make recommendations which concern the selection and organization of work of transporting machines which are necessary for.

REFERENCES

[1] Boitsov Yu., Kartalis, N., (2013), *Definition of internal and external friction of bulk materials (Определение Внутреннего И Внешнего Трения Сыпучих Грузов)*, Ed. NIUIT, p.12, St.Petersburg / Russia;

[2] Hozbenko V., Lytkina E., (2010), *Using of equidistant for solving the applied tasks of technical systems management (Использованиеэквидистант для решенияприкладных задач управлениятехническими системами),* ISBN 978-5-98710-106-03, p.188, Ed. IrGUPC, Irkutsk/Russia;

[3] Klein, G. (1977), *Building mechanics of bulk materials (Строительная Механика Сыпучих Тел),* p.256, Ed.Stroiizdat, Moscow/Russia;

[4] Kupriiashkin A., (2015), *The fundamentals of systems modelling (Основымоделированиясистем),* ISBN 978-5-89009-628, p.9. 135, Ed. CRI, Norilsk/Russia;

[5] Pustiulha S., (2006), *Discrete definition of geometric objects by means of numerical sequences (Дискретне визначення геометричних об'єктів числовими послідовностями),* Ph.D dissertation, Kyiv national university of construction and architecture, Kyiv/Ukraine;

[6] Pustiulha S., Samostian V., Klak Yu., (2007), Discrete forming of frame drabbing on flat scale with the set area of model surface (Дискретне формування двовимірних образів на рівномірній сітці із заданою площею поверхні моделі), *Applied geometry and engineering graphics (Прикладна геометрія та інженерна графіка),* V. 78, ISSN 0131-579X, pp.64-69, Kyiv/Ukraine;

[7] Pustiulha S., Samostian V., (2009), Modeling of equilibrium discretely presented curved surfaces with these boundary conditions of numerical sequences (Моделювання зрівноважених дискретно представлених криволінійних поверхонь із заданими крайовими умовами числовими послідовностями), *Applied geometry and engineering graphics (Прикладна геометрія та інженерна графіка),* V. 82, ISSN 0131-579X, pp. 208-214, Kyiv/Ukraine;

[8] Pustiulha S., Samostian V., Klak Yu., Khomych A., (2011), Discrete modeling of closed trajectories by means of numerical sequences (Дискретне моделювання замкнутих траєкторій числовими послідовностями), *Scientific journal (Наукові нотатки)*, V. 31, ISBN 5-7763-8653-5, pp. 295-298, Lutsk/Ukraine;

[9] Pustiulha S., Samostian V., Khomych A., (2013), Discrete modeling of equilibrium curved scales with uneven step of knots, superposition of double numericals (Дискретне моделювання зрівноважених криволінійних сіток, з нерівномірним кроком вузлів, суперпозицією подвійних числових послідовностей), *Applied geometry and engineering graphics* sequences (*Прикладна геометрія та інженерна графіка)*, Vol. 91, ISSN 0131-579X, pp.219-225, Kyiv/Ukraine;

[10] Pustiulha S., Samostian V., Khomych A., (2014), Discrete forming of equidistant to models of closed curves by the apparatus of numerical sequences (Дискретне формування еквідистант до моделей замкнутих кривих апаратом числових послідовностей), *Scientific journal (Наукові нотатки)*. Vol.44, ISBN 5-7763-8653-5, pp.227-232, Lutsk/Ukraine;

[11] Tsiz'I., Pustiulha S., Tsiz' A., Popko V. *Dosing machine of bulk materials (Дозатор сипких матеріалів)*. Patent № 100854 C2, Ukraine;

[12] Vaisberh L., Demidov I., Ivanov K., (2015), Mechanics of bulk medium by vibration impacts: methods of description and mathematical modeling (Механика Сыпучих Сред При Вибрационных Воздействиях: методы описания математического моделирования), *Ore concentration (Обогащение руд)*, no. 4, pp.21-31, Moscow/Russia.

DEVELOPMENT OF DESIGN AND INVESTIGATION OF OPERATION PROCESSES OF LOADING PIPES OF SCREW CONVEYORS
/
РОЗРОБКА КОНСТРУКЦІЙ ТА ДОСЛІДЖЕННЯ ПРОЦЕСІВ РОБОТИ ЗАВАНТАЖУВАЛЬНИХ ПАТРУБКІВ ГВИНТОВИХ КОНВЕЄРІВ

Prof. Ph.D. Eng Hevko R.B.[1)], Ph.D. Eng. Rozum R.I.[1)], Ph.D. Eng. Klendii O.M.[2)]
[1)]Ternopil National Economic University / Ukraine; [2)]Separated Subdivision of National University of Life and Environmental Sciences of Ukraine Berezhany Agrotechnical Institute / Ukraine
E-mail: alex_ks@mail.ru

Keywords: *flexible screw conveyer, loading pipe, conveying loose materials*

ABSTRACT

Having analyzed the designs and the quality indices of process performance for loading loose materials by screw conveyors, new ways and engineering solutions for loading materials into an input flow pipe-line have been suggested. Load analysis has been conducted and analytic dependences of the operation process of cam and link-leverage slewing mechanisms of loading pipe activator have been deduced. Movement patterns of a flow pipe-line in the process of loading pipe operation have been investigated. Experimental studies have been conducted and rational operational parameters and modes for the designed pipes have been determined.

РЕЗЮМЕ

На основі проведеного аналізу конструкцій та показників якості виконання технологічних процесів завантаження сипких матеріалів гвинтовими конвеєрами, запропоновано нові способи та технічні рішення завантаження матеріалом вхідної технологічної магістралі. Проведений силовий аналіз та виведено аналітичні залежності процесу роботи кулачкового та шарнірно-важільного механізмів повороту активатора завантажувального патрубка. Досліджено закономірності траєкторії переміщення технологічної магістралі під час роботи завантажувального патрубка. Проведені експериментальні дослідження та встановлено раціональні параметри і режими роботи розроблених патрубків.

INTRODUCTION

A review of scientific and patent literature, technical and economic performance of flexible screw conveyors and processes of conveying loose materials in flow pipe-lines *(Boyko A.I. et al., 2011; Vitrovyi A.O., et al., 2012; Klendiy M.B., 2006,2007; Hevko I.B., 2008; Hu G. et al., 2010; Loveikin V. et al., 2012 Pylypets M.I. 2002 and Rohatynskyi P.M., 2014)* shows that they satisfy most of the requirements to a certain extend, but most of these mechanisms require constant operator intervention. That is why, in order to improve the operation of conveyors it is necessary to pay more attention to the development of loading devices of screw conveyors. In addition to that, an important factor is minimization of material capacity of screw conveyors, which, on the one hand, allows reducing their cost and on the other hand, decreasing power inputs in order to convey loose materials. Moreover, it is necessary to provide maximum possible limits for regulating design and kinematic parameters of operating elements as well as to provide fast replacement of technological units for the adjustment of the machines to specific production conditions.

MATERIAL AND METHOD

The aim of this research work was designing, constructing and testing loading pipes of screw conveyors and the determining the effect of the design and kinematic parameters of operating elements on technological process performance.

The effectiveness of the operation of flexible screw conveyors, which depends greatly on the value of the operating efficiency of pipe-lines, is determined by the design concept of a loading pipe. The existing designs of loading pipes require constant conveying of loose materials in a flow pipe-line, which is mostly done by an operator.

The given researches are a continuation of previously conducted ones*(Hevko R.B. et. al., 2014; Hevko R.B., et.al., 2015; Hevko R.B., et.al., 2016; Klendii M.B. and Klendii O.M., 2016).*

In order to solve the given tasks, structural and mechanical diagram of a flexible screw conveyor with a loading pipe has been developed and its experimental sample has been designed, which is shown in Figure 1. It is designed in the form of a base 4, where there is a loading pipe 5 fixed, which provides the transfer of loose materials from a loading flow pipe-line 3 to an unloading one 6 and also the drive of the operating elements located in a cantilever. At the free end of a loading flow pipe-line the developed designs of loading pipes 2 are arranged *(Hevko R.B. and Rozum R.I., 2003; Danylchenko M.H. et. al., 2004)*, which interact directly with the heap of loose materials 1.

Figure 2 presents the design concept of an self-loading pipe with a cam (Fig.2a) and link-leverage (Fig.2b) slewing mechanisms of activators. A pipe includes a helical spiral 2, which is arranged in a cylindrical catcher 3 with separation ports and transfers to an elastic casing 1. An output shaft 4 of a helical spiral is connected to active driving elements 5 through a slewing mechanism 6.

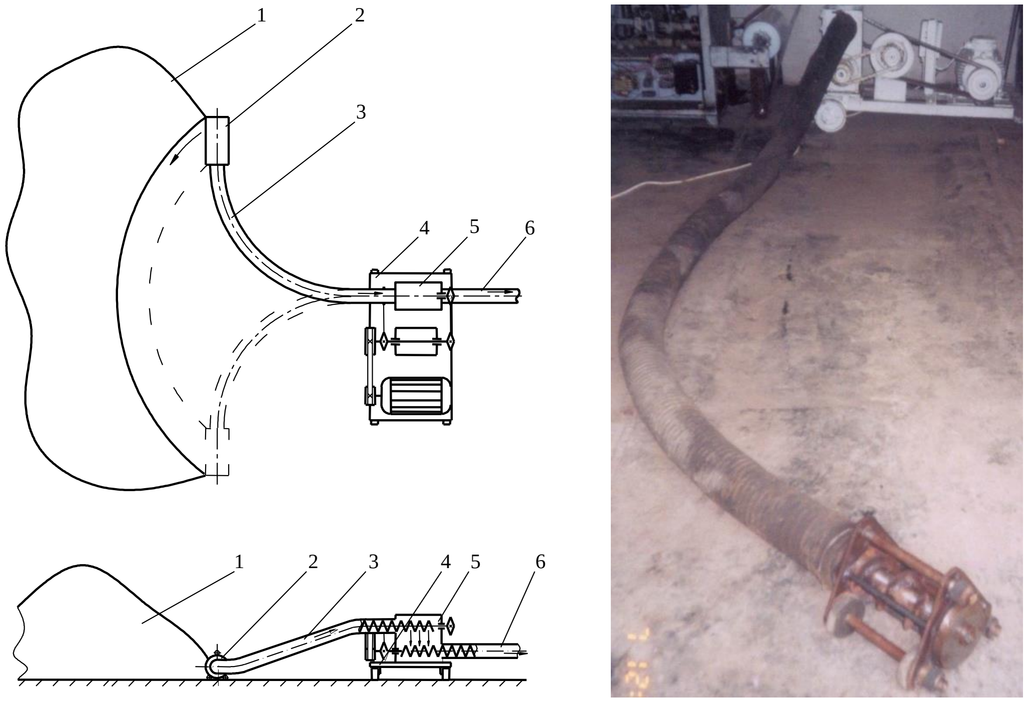

Fig. 1 - Structural and mechanical diagram of a screw conveyor with a loading pipe

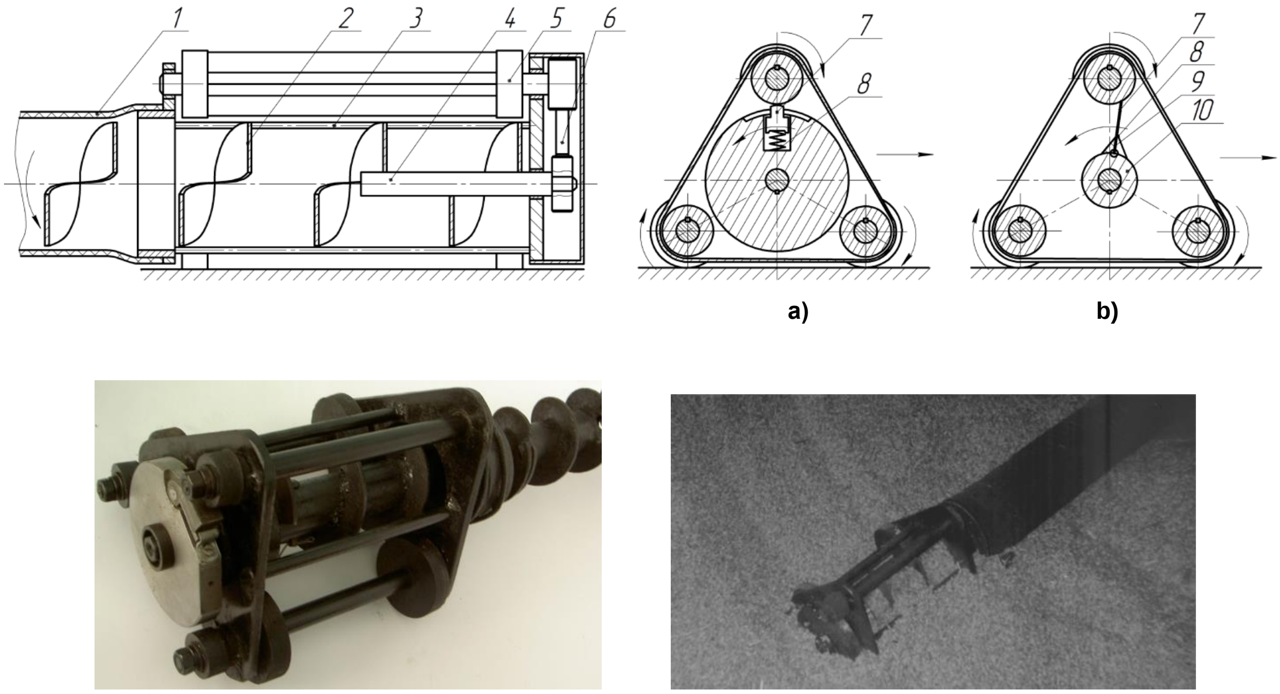

Fig. 2 - Design concept and overview of self-loading pipes

In the first case, a slewing mechanism of activators is made in the form of a radial placed cam *7*, which is spring-loaded *8* toward active driving elements. In the second case, it is made in the form of a disc *10*, which is arranged on an output shaft of a helical spiral, where there is a lever *7* hinged to it, which periodically interacts with activators and is spring-loaded *8* toward a damping catcher *9* of a turning angle of a lever.

In the operation process torque from an output shaft of a helical spiral is imposed through a slewing mechanism on activators, which, when rotating, excite loose materials and, at the same time, transfer self-loading pipe toward the heap of materials as the intake proceeds.

When substantiating rational design and load parameters of a slewing mechanism of activators, two variants of their construction have been considered in order to choose the optimum diagram of a loading pipe, which should be able to provide the intensification of the process of material feed as the intake proceeds.

A design diagram used for the determination of the interrelation between constructive and load parameters of the elements linking a loading pipe and a cam slewing mechanism of activators is shown in Figure 3.

In the diagram *h* denotes the distance between the centre of an activator and a disc centre; r_a denotes the radius of an activator; *r* is written for the radius of a cam; *δ* denotes the clearance between an activator surface and a disc surface; *m* is written for the decentralisation of a cam hemisphere relative to a disc surface; *k* denotes the distance from the centre of a cam hemisphere to the centre of a disc; *l* denotes the arm of action *N*; *z* denotes the arm of action of friction force $F^з_{fr}$; *φ* is written for an angle of disc rotation; F_{sp} denotes spring pressure; F^n_{fr} denotes friction force in the cam – groove pair of a disc; $F^з_{fr}$ denotes friction force in a cam – activator pair; *N* denotes reaction force from the interaction of a cam surface and an activator surface.

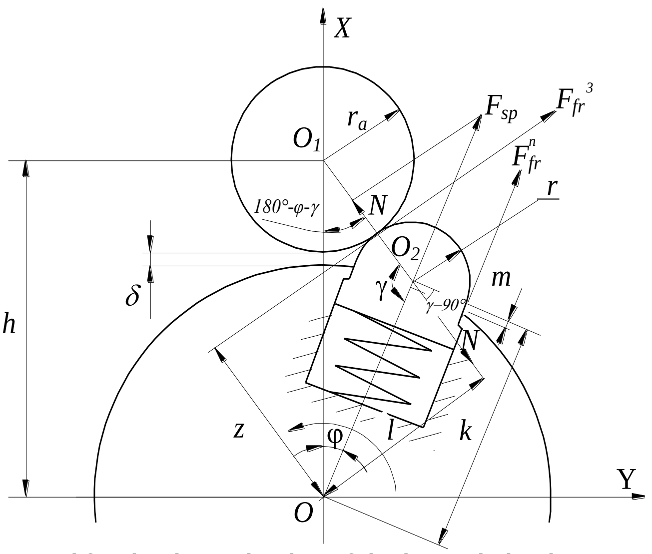

Fig. 3 - A design diagram used for the determination of the interrelation between constructive and load parameters of the elements linking a loading pipe and a cam slewing mechanism of activators

On the basis of the conducted theoretical investigation, equation systems for the determination of torque from the design parameters of the elements of linkage and also a pattern angle *φ* of rotation of a cam relative to an end disc activator have been produced.

Activator torque is determined by the following equation system:

$$\begin{cases} T_a = NfR; \\ N = -C(\Delta_0 + \Delta)\left[1 - 0{,}5 f \sin 2\gamma\right]\cos\gamma; \\ \Delta = h - R - \delta - m - k; \\ k = h\cos\varphi - \sqrt{(R+r)^2 - h^2\sin^2\varphi}; \\ \gamma = \left[180° - \arcsin\left(\dfrac{h\sin\varphi}{R+r}\right)\right]. \end{cases} \tag{1}$$

where C – spring stiffness; Δ_0 – value of spring pretension; Δ – travelling value of spring deflection.

Since peak torques arise at the first stage of the interaction of a cam with an activator, limits of angle φ change is chosen to be from φ_{max} (cam engagement into the contact with an activator) to $\varphi = 0$ (vertical installation of their central axis).

Value φ_{max} is determined by the following dependence:

$$\varphi_{\max} = \arccos\left(\frac{h^2 + k_n^2 - (R+r)^2}{2hk_n}\right) \tag{2}$$

where $k_n = h - R - \delta - m$.

A design diagram used for the determination of the interrelation between constructive and load parameters of the elements linking a loading pipe and a link-leverage slewing mechanism of activators is shown in Figure 4.

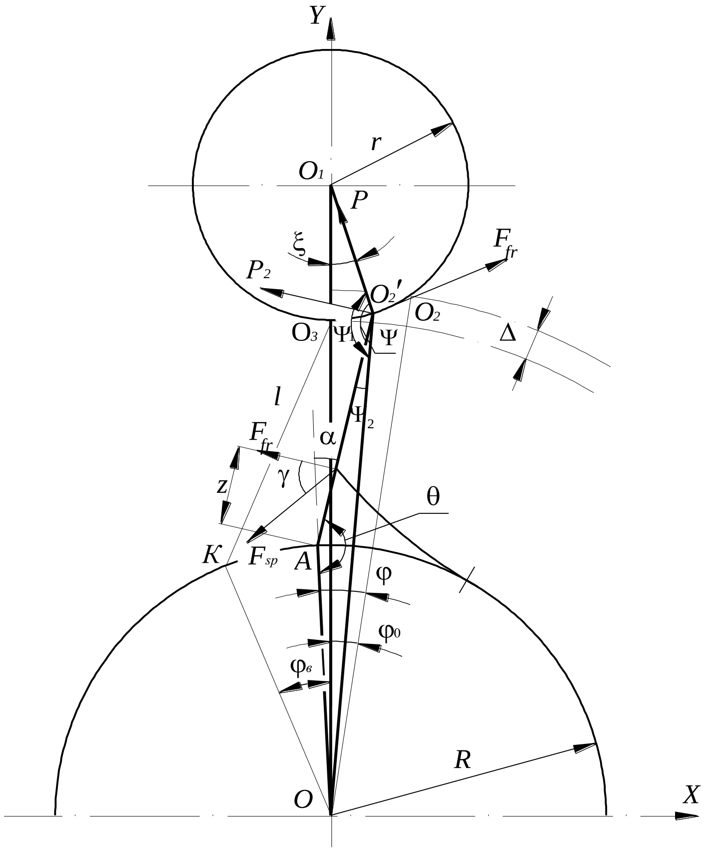

Fig. 4 - Diagram used for determination of constructive and load parameters of a loading pipe with link-leverage slewing mechanism of activators

Activator torque is defined as the function of an angle of cage rotation ($T_a = f(\varphi)$) and takes the following form:

$$\begin{cases} T_a = \dfrac{EIz^2 f\pi}{l \cdot l_{sp}^3 \cdot 60^\circ} l_n(\alpha)\cos\gamma\sin\Psi; \\ \Psi = \arcsin\left(\dfrac{(R+l-\Delta+r)\sin\xi}{\sqrt{R^2+l^2-2Rl\cos\theta}}\right) - \arcsin\left(\dfrac{R\sin\theta}{\sqrt{R^2+l^2-2Rl\cos\theta}}\right); \\ l_n = (R+l-\Delta+r)\sin\xi; \\ \xi = \arccos\left(\dfrac{r^2+(R+l-\Delta+r)^2-R^2-l^2-2Rl\cos\alpha}{2r(R+l-\Delta+r)}\right). \end{cases} \tag{3}$$

Where: I denotes the inertia moment of a flat spring; E denotes the modulus of elasticity of a flat spring; R denotes the radius of a disc; l denotes the length of a hinged lever; l_{sp} denotes the length of a spring beam;

$l_n^з$ denotes the arm of action of friction force; Δ denotes lever and activator overlapping $\Theta = 180^0 - \alpha$.

The deduced equation system gives the opportunity to evaluate the influence of the design elements of a loading pipe on the value of activator torque needed for its self-movement in the process of the material intake with the turning angle of a lever α.

In order to take into consideration load factors, which arise when there is a change in the radius of curvature ρ of an elastic casing with a loading pipe and according to its movement pattern, a diagram of a flow pipe-line load has been considered (Fig.5).

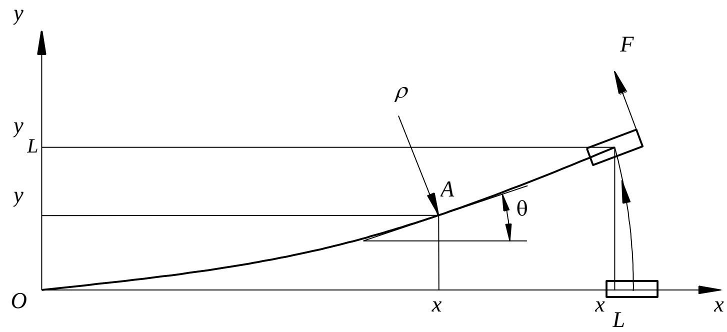

Fig. 5 - A design diagram of a flow pipe-line load

A travelling moment, which causes a change in the curvature of routing by independent variables, namely a bend angle θ and a travelling length *S*, has been determined from the following formula:

$$M(x) = M(\theta) = F\left[\sin\theta_L \int_l^L \sin\theta \cdot dS + \cos\theta_L \int_l^L \cos\theta \cdot dS\right] \tag{4}$$

where *F* denotes equal driving force applied to a pipe, taking into account clamp resistance.

Based on the results of the investigations, the flow routing of a flexible screw conveyor has been simulated using a chain curve, the parametric equation of which, depending on the parameter *S,* takes the following form:

$$x = \frac{C_\varphi}{M} \cdot \ln\left(\frac{S \cdot M}{C_\varphi} + \sqrt{\frac{S^2 \cdot M^2}{C_\varphi^2} + 1}\right) \tag{5}$$

$$y = \sqrt{\frac{C_\varphi^2}{M^2} + S^2} - \frac{C_\varphi}{M} \tag{6}$$

Movement increase of a pipe with coordinates x_L, y_L at variable moment *M*:

$$du_L = u'_y y'_M dM = \frac{C_\varphi}{M^2}\left(L\sqrt{1 + \frac{C_\varphi^2}{M^2 L^2}} - \frac{C_\varphi}{M}\right) dM\ . \tag{7}$$

RESULTS

In order to analyze equation system (1), namely functional relationships, $T_a = f(\varphi)$ the following parameter values were taken: h = 74 mm ; R = 22 mm; δ = 2 mm; m = 2 mm; C = 10 N/m; Δ_0 = 5 mm; f = 0.17. Value φ_{max} = 12.37°.

Using the obtained results it has been determined, that the maximum cam torque corresponds to the moments of its engagement with an end disk and corresponds to the angles of rotation φ = 8°-12°.

When an activator becomes jammed, torque increases by 28% compared to the unrestricted turning of an activator.

Activator torque has reverse absolute value trend and its maximum value is *α=0°*. It can be explained by the fact, that an activator arm is permanent.

Graphical dependencies presented here must be used in order to determine rational design parameters of a loading pipe and also their operating modes.

In order to analyze equation system (3), the following parameter values were taken: h=0.074 m; R=0.025 m; Δ=0.003 m; r_a=0.022 m; l=0.03 m; f=0.17; l_{sp}=0.03 m; γ=60^0; z= 0.02 m, I=5.63$\cdot$10^{-12} m^4.

Using the obtained results it has been determined, that regarding a link-leverage slewing mechanism of activators, the most essential influence on the value of activator torque T_a is exerted by the length of a hinged lever l and the inertia moment of a flat spring I. The limits of rational parameters have been determined: the radius of a disc 0.02...0.03 m, the length of a hinged lever 0.025...0.035 m, the diameter of an activator 0.02...0.024 m, lever and activator overlapping value 0.002...0.004 m.

Using the investigation results of the mechanical trajectory of a loading flow pipe-line (equations 4-7) and the movement of a loading pipe depending on bending moment M, the corresponding motion trajectories have been defined (Fig.6). The following parameter values were taken: unit stiffness C_φ = 500 Nm^2; the length of a flow pipe-line L = 6 m.

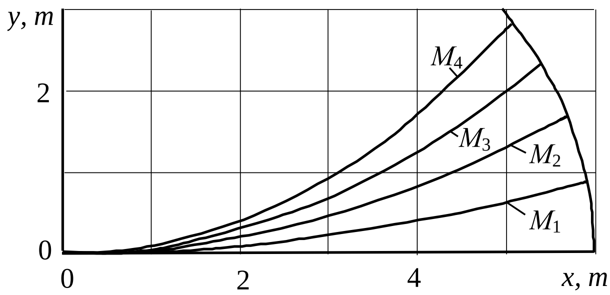

Fig. 6 - Motion trajectories of a loading flow pipe-line and movement of a loading pipe depending on bending moment *M*: M_1 = 25 Nm; M_2 = 50 Nm; M_3 = 75 Nm; M_4 = 100 Nm

In order to examine the developed designs of loading pipes under actual operating conditions, a pilot plant of a flexible screw conveyor has been constructed. It has been made in the form of a base, where there is a loading pipe fixed, which provides the transfer of loose materials from a loading flow pipe-line to an unloading one and also the drive of the operating elements located in cantilever. At the free end of a loading flow pipe-line the developed designs of loading pipes are arranged, which interact directly with loose materials.

A complex experiment using the pilot plant of a flexible screw conveyor has been conducted and, as a result, a regressive dependence, showing its efficiency characteristic $У$ from the rotation frequency of a conveyor helix n, the clearance between an activator surface and a disc surface δ and spring force F_{sp}, has been obtained

$$У = -5.69 + 0.0163n + 430\delta + 0.031F_{sp}. \tag{8}$$

It has been stated that in the operation process of a flexible screw conveyor, equipped with the developed self-loading pipe with a cam slewing mechanism of activators, with the following range of parameter variations: 400 < n < 600 (r/m), 0,002 < δ < 0,004 (m), 10 < F_{sp} < 50 (N), the greatest influence on the process of material intake and the productivity of a conveyor respectively is exerted by the rotation frequency of an operating helix. In addition to that, the increase of values δ and F_{sp} leads to the increase in the process efficiency of loading loose materials into a flexible casing, but their influence in this range of parameter variations is halved.

The determination of a functional dependence between tractive force P on a loading pipe and the value of its cross travel l is needed for defining the value of activator torque, which would provide the movement of a flow pipe-line.

In the process of investigation, force at the beginning of a loading pipe movement together with a flexible casing (that is to say, their transition from a static position into a moving position) have been determined first and, in addition, movement force at the specified values of lateral position (l = 1, 2, 3 m) has been defined as well.

The results of the experimental studies show, that break-down force of a pipe-line from its static position, when a pipe is placed in certain positions, is twice as much as the travel force in these positions. Movement force of a pipe-line without stopping from its initial position to the position, that corresponds to l = 3 m, exceeds movement force of a pipe-line, needed to reach the same position with discrete stops by 13 %.

Taking into consideration the obtained values of tractive force, torque of moving a loading pipe of a flow pipe-line for various standard sizes of supporting rollers with radius r_o has been determined. In case of emergency with a curved four meter pipe-line: $P \approx 100$ N; $r_o = 0.03$m. Then $T_a = Pr_o = 3$ Nm.

Methodology has been developed and experimental studies have been conducted in order to determine the value of the maximum torque for the turning of activators in various loose mediums. Here the width and the height of loose material column were the same.

It has been stated, that for activator turning in loose medium the maximum torque at which the material is shifted by a beater blade, is the following: for bran – 0.31Nm; barley – 0.58Nm; wheat – 0.96Nm.

Having analyzed the results of the experimental studies for certain specified concrete design and process parameters, it can be stated, that torque, which is to provide the appropriate tractive force of a flow pipe-line far exceeds the torque needed for activator turning in loose medium. That is why, design and load parameters of the elements of a loading pipe must be selected based on the tractive force, which is needed for pipe-line movement.

Unit design moment, which provides maximum deflection of a flexible screw, can be determined from the following formula:

$$M_{P\,max} = \frac{mgf}{2} L \tag{9}$$

Accordingly, the length of a flexible screw L, which services operating area with width B, must be chosen using the following statement:

$$L = \sqrt[3]{\frac{B^3}{4} + \frac{2BC_\varphi}{mgf}} \tag{10}$$

where unit stiffness of a conveyor C is specified experimentally in accordance with the following ration:

$$C_\varphi = \frac{F_e L_e^2}{2\theta_e} \tag{11}$$

Where: F_e, L_e and θ_e denote the experimental values of tractive force, the length of a flow pipe-line and the angle of deflection of a loading pipe respectively.

In process testing of a flexible screw conveyor, equipped with the developed self-loading pipe, the transporting grain material has shown the following results: if rotation frequency of a helical spiral is $n = 560$ r/m and the diameter is 96 mm, productivity of a conveyor is about 4600 kg/h.

CONCLUSIONS

Based on the analysis of the state and the development trends of the movement of loose materials in flexible screw conveyors, a new way of loading flow pipe-lines, which envisages the active use of a loading pipe, has been suggested. On the basis of this principle a flexible screw conveyor equipped with a loading pipe has been developed and made; in addition to this, its theoretical and experimental studies have been conducted.

Equation systems in order to determine interrelation between design and load parameters of cam and link-leverage slewing mechanism of activators have been deduced.

The analysis of the movement pattern of a flow pipe-line has given the opportunity to determine, that routing trajectory of a flexible screw can be approximated to the accuracy, sufficient for practical use, by a catenary line, the parameters of which are unit stiffness of a flow pipe-line and a bending moment, which is formed by a pipe drive. It has been determined, that at the stiffness of a flow pipe-line being $C_\varphi = 450...500$ Nm^2 and the length being $l = 4...6$ m the operating area is $B = 3.2...8$ m.

Methodology of conducting experimental studies of the elements and samples of self-loading pipes of flexible screw conveyors has been developed. It allows studying the influence that design and loading parameters of slewing mechanism of activators have on the performance of a loading pipe and the value of a flow pipe-line movement.

The conducted experimental studies of a cam slewing mechanism of activators gave the opportunity to determine the dependence of the maximum torque on the design parameters of the elements of linkage. As for link-leverage slewing mechanism, the change in the value of central plate torque depending on the turning angle of an activator has been determined. The difference between theoretical and experimental studies does not exceed 17%.

Based on the conducted complex experiment, regressive dependencies showing that the efficiency of the performance of a flexible screw conveyor equipped with the developed self-loading pipe is influenced by rotation frequency, the clearance between an activator and a disc and spring pretension, have been obtained.

Based on the investigation results, a design technique of the developed designs of screw self-loading pipes has been developed. The conducted process testing is indicative of the desirability for the application of such types of loading pipes in flexible screw conveyors when operating with loose materials of agricultural production.

REFERENCES

[1] Boyko A.I., Kulikiskiy V.L., (2011), Investigation of contact grain interaction in gap “coil-jacket” of screw feeders grain cleaning machines (Дослідження контактної взаємодії зерна в зазорі “виток-кожук” шнекових живильників зерноочисних машин). *Scientific Bulletin of NUBiP-K.: Red species. Department NUBiP 201*, Vol.166, Engineering and Energy AIC, P.1, pp.267-274;

[2] Danylchenko M.H., Rozum R.I., Hevko R.B., (2004), Pipe of a Screw Conveyor (Патрубок гвинтового конвеєра), Patent. 4003 Ukraine (2004), МРК 7 B65G33/16, 33/24. (Пат. 4003 Україна);

[3] Hevko I.B., (2008), Screw transporting-technological mechanisms. Calculation and designing (Гвинтові транспортно-технологічні механізми. Розрахунок і конструювання), *Bulletin of Ternopil Ivan Puliui State Technical University (Вісник Тернопільського державного технічного університету імені Івана Пулюя)*, p.307, Ternopil;

[4] Hevko R.B., Rozum R.I., (2003), A Loading Pipe of a Screw Conveyor (Завантажувальний патрубок гвинтового конвеєра), Patent. 61435 A Ukraine МРК 7 B65G33/16, B65G33/24;

[6] Hevko R.B., Dzyura V.O., Romanovsky R.M. (2014), Mathematical model of the pneumatic-screw conveyor screw mechanism operation, *INMATEH-Agricultural engineering Journal*, vol.44, no.3, pp.103-110, Bucharest / Romania;

[7] Hevko R.B., Zalutskyi S.Z., Tkachenko I.G., Klendii O.M., (2015), Development and investigation of reciprocating screw with flexible helical surface, *INMATEH-Agricultural engineering Journal*, vol. 46, no.2, pp.133-138, Bucharest / Romania;

[8] Hevko R.B., Klendiy M.B., Klendii O.M., (2016), Investigation of a transfer branch of a flexible screw conveyer, *INMATEH-Agricultural engineering Journal*, vol.48, no.1, pp.29-34, Bucharest / Romania;

[9] Hu G., Chen J., Jian B., Wan H., Liu L., (2010). Modelling and simulation of transportation system of screw conveyors by the discrete element method, *International Conference on Mechanic Automation and Control Engineering*, *MACE2010*, Article number 5536244, pp.927-930;

[10] Klendiy M.B., (2006). Investigation of transfer process of bilk load by screw operating devices (Дослідження процесу перевантаження сипкого вантажу гвинтовими робочими органами), Bulletin *of Ternopil Ivan Puliui State Technical University (Вісник Тернопільського державного технічного університету імені Івана Пулюя*), Vol.3, pp.92-100, Ternopil;

[11] Klendiy M.B., Klendii O.M., (2016), Interrelation between incidence angle and roll angle of concave disks of soil tillage implements, *INMATEH-Agricultural engineering Journal*, vol.49, no.2, pp.13-20, Bucharest / Romania;

[12] Klendiy M.B., (2007), Development and parameters validation of paddle conveyor-mixer design (Розробка конструкції та обґрунтування параметрів лопатевого транспортера-змішувача), *Scientific Bulletin of National Agricultural University*, Vol.92, P.2, pp.533-540;

[13] Loveikin V., Chovniuk Yu., Kulyk V., (2012), Optimizatsii a rezhimov kolebanii zernovykh smesei pri nalichii sukhogo treniia, *Motrol – Motoryzacja I energetyka rolnictva*, Vol.14, v3, pp.140-149, Lublin;

[14] Pylypets M.I., (2002), Scientifical and technological bases of production coiling machine parts billet (Науково-технологічні основи виробництва навивних заготовок деталей машин): PhD.Thesis *Engineering Sciences specials (автореф. дис. на здобуття наук. ступеня доктора техн. наук)*., pp.35, Lviv;

[15] Rohatynskyi R.M. and others, (2014), Scientific and applied backgrounds of creating the screw transport and technological mechanisms (Науково-прикладні основи створення гвинтових транспортно-технологічних механізмів), *Bulletin of Ternopil Ivan Puliui Nationai Technical University (Вісник Тернопільського yfwsjyfktного технічного університету імені Івана Пулюя)*, pp.278, Ternopil;

[16] Vitrovyi A.O., Pik A.I., Hevko R.B., (2012), Advance in technology of flexible screw conveyers: monograph (Підвищення технічного рівня гнучких гвинтових конвеєрів: монографія), Aston, p.204.

REGULATING THE MOISTURE OF OILSEED MATERIAL IN A TOASTER FOR VEGETABLE OILS EXTRACTION
/
РЕГУЛИРАНЕ НА ВЛАЖНОСТТА НА ЗЪРНЕН МАТЕРИАЛ В ПЕКАЧ ЗА ИЗВЛИЧАНЕ НА РАСТИТЕЛНИ МАСЛА

Lecturer Ph.D. Eng. Kadirova S. Y.[1)],
[1)] Rousse University "Angel Kunchev", Faculty of Electrical Engineering, Electronics and Automation / Bulgaria
Tel: 00359 877 089537; E-mail: skadirova@ecs.uni-rue.bg

Keywords: *oilseed moisture, thermal-moisture treatment, electronic system, simulation model*

ABSTRACT
The influence of the moisture in the process of thermal-moisture treatment of oilseed material has been determined. The behaviour of the electronic system for adjustment of oilseed moisture has been investigated. For this purpose, experimental data on the current moisture values have been obtained in treatment period via grain sample method. The obtained experimental data have been statistically compared with the simulation results from a model, which describes the thermal-moisture process.

РЕЗЮМЕ
Определено е влиянието на влажността на зърнения материал в процеса на добиване на растително масло. Изследвано е поведението на електронна система за регулиране влажността на зърнения материал. За целта са получени експериментални данни за моментната стойност на влажността в периода на обработка чрез зърнена проба. Тези данни са статистически съпоставени със симулационни резултати от предварително разработен модел, описващ влаготоплинния процес.

INTRODUCTION
The first operation after harvesting the oilseeds involves grinding, and then heat and moisture treatment. Decortication or shelling separates the oil-bearing portion of the raw material and eliminates the parts that have little or no nutritional value. Small-scale mechanical shellers are available for kernels and nuts although manual cracking is still prevalent. Most oil seeds and nuts are heat-treated by roasting to liquify the oil in the plant cells and facilitate its release during extraction. To increase the surface area and maximize oil yield, the oil-bearing part of groundnuts, sunflower, sesame, coconut, palm kernel and shea nuts is reduced in size. Mechanical disc attrition mills are commonly used in rural operations *(Kabutey et al, 2011; Kadirova S., Manukova A., 2009b; Manukova A., Kadirova S., 2009; Sigalingging R. et al, 2014)*.

Moreover, mechanical pressing is most popular method in the world to separate oil from vegetable seeds crops. Thus, the impact of several variables on oil recovery, oil quality, rupture force of seeds, deformation, and energy cost for pressing is essential for an adequate design of equipment for pressing seeds crops *(Sigalingging R., et al, 2014).* Heat treatment before extrusion is necessary for improvement of the amount of recovered oil. Pre-treatment has a significant impact on the efficiency of pressing *(Sayyar S., et al 2009; Willems P. et al, 2008; Kadirova S., 2008; Kadirova S., Manukova A., 2009a; Kadirova S., Manukova A., 2009b; Sigalingging R et al, 2014; Herák D., et al 2013; Kabutey A., et al, 2012).*

The main point of thermal-moisture processing of meal is accomplished in the simultaneous action of water vapour and heat to the cells of the milled mass. Oleaginous cells consist of two main parts - a hydrophilic, which is associated with the water (carbohydrates, proteins and other nitrogen-containing substances) and hydrophobic, which is not associated with the water (oil and other substances dissolved therein). During the heating of the meal, the water contained in the cells, is associated with the hydrophilic portion that swells and intersects - coagulate. It is thus a sharp demarcation between hydrophilic and hydrophobic phase. To suppress the hydrophilic phase it is necessary a precisely defined amount of water. If naturally the water content of meal is insufficient, then it has to be additionally moistened by water or by wet steam *(Sigalingging R et al, 2014; Herák D., et al, 2013; Kabutey A., et al, 2012)*.

The dynamics of variation of meal moisture and temperature as a function of time depends on many interdependent factors. The main parameters are the temperature values of the heating fluid and the incoming meal, the initial moisture content of meal, the relative weight of dry basis, thermal conductivity, heat exchange etc. The recognition of their influence during the thermal-moisture processing of the meal is possible based on the simulation model *(Kadirova S., 2008; Herák D., et al 2013; Kabutey A., et al, 2012)*.

The moisture content of the meal is necessary to be controlled in each stage of the process. It significantly affects the quality of the treatment, which is necessary for the next operation, for extrusion. This requires control of meal moisture variation in all stages of the process (*Herák D., et al, 2013, Kadirova S., 2008).*

The aim of the publication is to investigate the efficiency of the developed electronic system for control of moisture content in the thermal-moisture treatment of meal the preliminary substantiated control points of the treatment process.

MATERIAL AND METHOD

Object of investigation

The structure of the investigated system is presented in Fig. 1. In the current research the parameters of corn-germ meal are investigated. Starting of the system begins with entering of initial conditions - kind of oilseed material and kind of treatment depending on the next stage of the technological process for oil extraction. The initial moisture and specific density of incoming meal are determined by grain sample method, as there is a possibility for process interruption to enter data and to change the treatment parameters. The opportunity for simulation of the process for two main technological operations is provided in the developed software. They respectively are thermal-moisture treatment of meal for full pressing, and treatment for pre-pressing and next chemical extraction *(Manukova A., Kadirova S., 2009a).*

Because of the continuous character of the process the meal in the toaster passes through the sections for exact duration, which depends on the current values of temperature and moisture content of the treated meal. The heating of the material is done indirectly by energy exchange between the meal and heating fluid through the metal wall of the toaster. The surface of the toaster is heated by the fluid circulating in the heating chamber. The meal is processed as it contacts with the heated surface of the section and receives its heating energy via heat exchange.

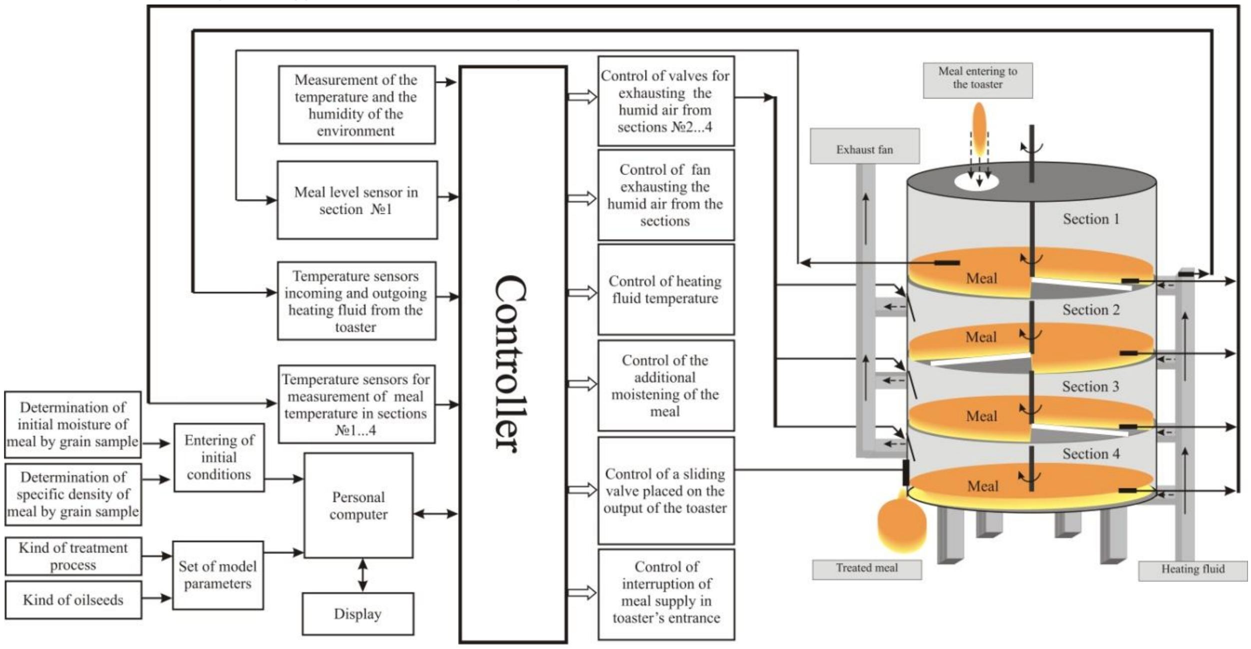

Fig.1 - Structure of the electronic system for control of thermal-moisture processing of oilseeds in a toaster for extraction of vegetable oils

The temperature and humidity of the ambient air are important input data for the environment parameters and they influence the processes' control. The steam saturated air from the section is exhausted by external vent pipe with exhaust fan, as at the output of each section are installed control valves. The initial moisture content of treated oilseeds is determined by grain sample method before it enters into the toaster. The current moisture content of meal is calculated by the proposed model at each stage of the processing. In case of not corresponding to moisture requirements, proposed in the criteria, the electronic system controls the operating mechanisms *(Kadirova S., A. Manukova, 2009a)*.

Toaster's sections are closed vessels containing free airspace intended to absorb the moisture evaporated from meal during heating. This provides a better moisture exchange between the air and the processed material, which helps to intensive the evaporation process of the material and leading away the humid air from the toaster. The movement of meal from one section of the toaster to the other one is realized by cross valves, connected to a mechanical system. It provides constant and uniform passing of meal in the toaster by an exact preliminary defined step in time as well as the quantity of treated meal. In each section are placed temperature sensors for control of the meal temperature in real time.

The amount of the discharging meal is controlled by a sliding valve, placed in section №4. The sliding valve is controlled by the electronic system based on the results obtained from process simulation via the developed model compared with the measured values of parameters at the current time. The position device helps to position the operating mechanism of a sliding valve to a desired position. Thereby, the treated material is being discharged from the toaster at the exact time which leads to a significant increase in system efficiency by reducing the material's duration of stay in the toaster and reduces the energy consumption.

RESULTS

For investigation of the efficiency of the developed electronic control system some experimental studies are implemented. They are based on the variance of the meal moisture. During the experiment the values of the meal moistures at the exit of each section have been measured at each 10 minutes because the process has a significant inertness.

The results are presented in tabular and graphic form. In the control points of the technological scheme, the current values of the meal moisture of the experimentally obtained results are compared with simulation data from developed software. The software is based on literary and experimental data. The root-mean-square deviation, the absolute error and relative error of experimentally obtained moisture data to simulation data, are estimated. The root-mean-square deviation of the current values of meal moisture at the control points is calculated by the following expression:

$$\sigma = \sqrt{\frac{\sum_{i=1}^{n}\left(x_i - \bar{x}\right)^2}{n}}, \text{ [-]} \tag{1}$$

Experimental investigation at various moisture contents has been conducted and the observed data is summarized in Tables 1 to 4. In Figures 2 to 7 are presented graphical parities of change of meal moisture content in time. Studies, based on developed software model in MATLAB environment, have been conducted as the results are summarized in Tables 1 to 4.

Comparison of the experimental data with the simulation results of the meal moisture at the output of section 1 of the toaster.

Table 1 presents the data for current values of the meal moisture at the output of section 1.

Table 1

Values of the meal moisture at the output of section 1

Time	M_{ml}, model	M_{ml}, exp	Root-mean-square deviation	Absolute error	Relative error	Time	M_{ml}, model	M_{ml}, exp	Root-mean-square deviation	Absolute error	Relative error
[min]	[%]	[%]	[-]	[%]	[%]	[min]	[%]	[%]	[-]	[%]	[%]
10	9.5	10.5	0.81	0.9	2.26	110	9.4	10.2	0.64	0.8	2.04
20	9.7	9.9	0.04	0.2	0.51	120	10.3	9.1	1.44	1.2	3.09
30	9.3	10.1	0.64	0.8	2.06	130	9.7	10.1	0.16	0.4	1.01
40	9.9	9.1	0.64	0.8	2.11	140	10.2	8.8	1.96	1.4	3.68
50	10.1	10.2	0.01	0.1	0.25	150	10.4	9.6	0.64	0.8	2.00
60	9.7	10.4	0.49	0.7	1.74	160	9.7	10.2	0.25	0.5	1.26
70	8.8	9.7	0.81	0.9	2.43	170	9.2	10.1	0.81	0.9	2.33
80	9.6	10.1	0.25	0.5	1.27	180	9.9	9.7	0.04	0.2	0.51
90	10.2	8.9	1.69	1.3	3.40	190	9.8	9.9	0.01	0.1	0.25
100	10.1	9.5	0.36	0.6	1.53	200	10.2	9.6	0.36	0.6	1.52

The root-mean-square deviation of meal moisture at the output of section 1 of the toaster is $\sigma = 0.77\%$. At the current moisture values the calculated average value of the absolute error is $\varepsilon_{abs} = 0.69\%$, as the relative is $\varepsilon_{rel} = 1.76\%$.

Fig. 2 illustrates the change of meal moisture at the output of section 1. The moisture range of the meal is within the field of defined criterion diapason. The results presented in Fig. 2 are obtained from the simulation model, and the experimental ones are measured in the real toaster.

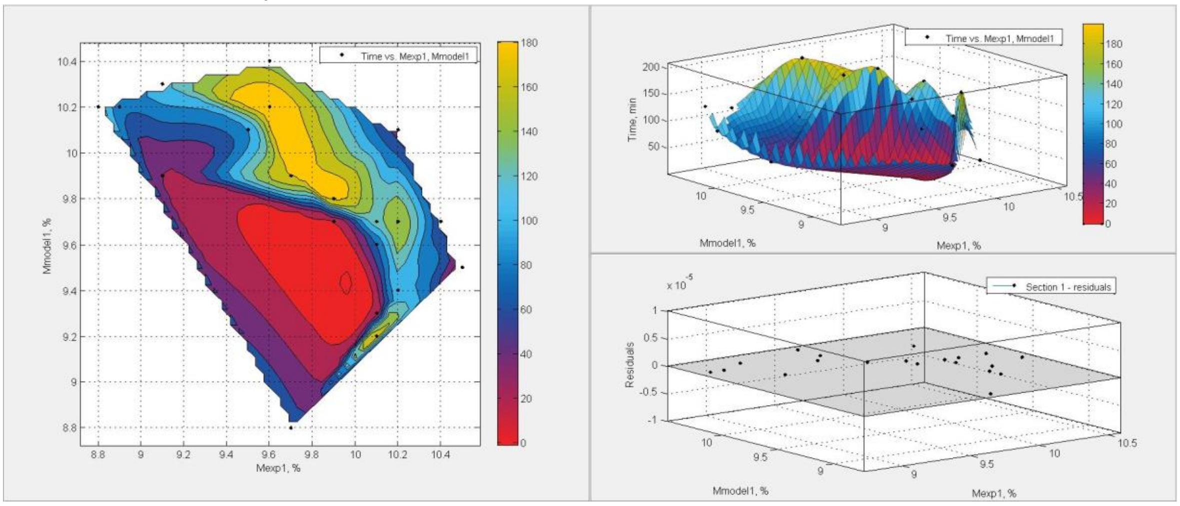

Fig. 2 - Variation of the meal moisture at the output of section 1 in dependence of time

During the model simulation the variation of moisture values is in the range of $M_{meal\_section\_1\_model}$ = (10.4…8.8) %, and the experimentally measured ones in the installation are $M_{meal\_section\_1\_exp}$ = (10.5…8.8) %. For section 1 the diapason of change of the meal moisture is $M_{meal\_section\_1\_criteria}$ = (11…9.5) %. Therefore, the technological requirements for the range of moisture change in section 1 of the toaster are adhered.

Comparison of the experimental data with the simulation results of the meal moisture at the output of section 2 of the toaster.

Table 2 presents the data for current values of the meal moisture at the output of section 2.

Table 2

Values of the meal moisture at the output of section 2

Time	M_{ml}, model	M_{ml}, exp	Root-mean-square deviation	Absolute error	Relative error	Time	M_{ml}, model	M_{ml}, exp	Root-mean-square deviation	Absolute error	Relative error
[min]	[%]	[%]	[-]	[%]	[%]	[min]	[%]	[%]	[-]	[%]	[%]
10	7.7	7.9	0.04	0.2	0.64	110	7.6	7.8	0.04	0.2	0.65
20	7.4	7.6	0.04	0.2	0.67	120	8	7.6	0.16	0.4	1.28
30	7.8	7.4	0.16	0.4	1.32	130	8.2	8	0.04	0.2	0.62
40	7.7	8.2	0.25	0.5	1.57	140	7.5	8.2	0.49	0.7	2.23
50	7.9	7.7	0.04	0.2	0.64	150	7.6	7.5	0.01	0.1	0.33
60	7.8	7.6	0.04	0.2	0.65	160	7.6	7.9	0.09	0.3	0.97
70	8.1	7.9	0.04	0.2	0.62	170	7.9	7.8	0.01	0.1	0.32
80	8	7.6	0.16	0.4	1.28	180	7.6	8.1	0.25	0.5	1.59
90	7.8	8.1	0.09	0.3	0.94	190	8.1	7.6	0.25	0.5	1.59
100	7.5	8.3	0.64	0.8	2.53	200	7.9	7.8	0.01	0.1	0.32

The root-mean-square deviation of meal moisture at the output of section 2 of the toaster is $\sigma = 0.38°C$. At the current moisture values the calculated average value of the absolute error is $\varepsilon_{abs} = 0.33\%$, as the relative is $\varepsilon_{rel} = 1.04\%$.

Fig. 3 illustrates the change of meal moisture at the output of section 2. The moisture range of the meal is within the field of defined criterion diapason. The results presented in Fig. 3 are obtained from the simulation model, and the experimental ones are measured in the real toaster.

During the model simulation, the variation of moisture values is in the range of $M_{meal\_section\_1\_model}$ = (8.2…7.4) %, and the experimentally measured in the installation are $M_{meal\_section\_1\_exp}$ = (8.3…7.4) %. For section 2 the diapason of change of the meal moisture is $M_{meal\_section\_1\_criteria}$ = (9.5…7) %. Therefore, the technological requirements for the range of moisture change in section 2 of the toaster are adhered.

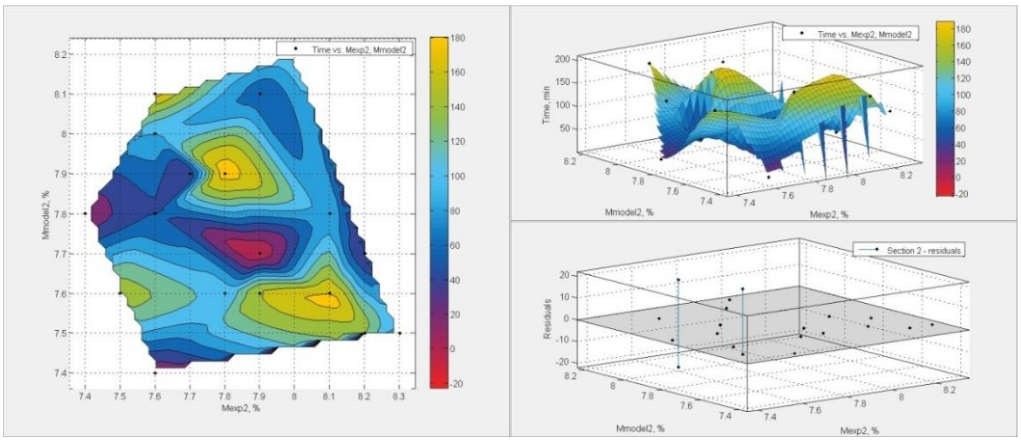

Fig. 3 - Variation of the meal moisture at the output of section 2 in dependence of time

<u>Comparison of the experimental data with the simulation results of the meal moisture at the output of section 3 of the toaster.</u>

Table 3 presents the data for current values of the meal moisture at the output of section 3.

Table 3

Values of the meal moisture at the output of section 3

Time	M_{ml}, model	M_{ml}, exp	Root-mean-square deviation	Absolute error	Relative error	Time	M_{ml}, model	M_{ml}, exp	Root-mean-square deviation	Absolute error	Relative error
[min]	[%]	[%]	[-]	[%]	[%]	[min]	[%]	[%]	[-]	[%]	[%]
10	5	5.5	0.25	0.5	2.38	110	5.3	5.6	0.09	0.3	1.38
20	5.7	5.6	0.01	0.1	0.44	120	5.2	5.9	0.49	0.7	3.15
30	5.8	5.3	0.25	0.5	2.25	130	5.6	5.7	0.01	0.1	0.44
40	5.4	5.4	0	0	0.00	140	5.1	5.2	0.01	0.1	0.49
50	5.3	5.8	0.25	0.5	2.25	150	5.2	5.4	0.04	0.2	0.94
60	5.5	5.6	0.01	0.1	0.45	160	5.3	5.2	0.01	0.1	0.48
70	5.2	5	0.04	0.2	0.98	170	5.7	5.3	0.16	0.4	1.82
80	5.4	5.2	0.04	0.2	0.94	180	5.3	5.8	0.25	0.5	2.25
90	5.3	5.7	0.16	0.4	1.82	190	5.1	5.5	0.16	0.4	1.89
100	5.6	5.8	0.04	0.2	0.88	200	5.2	5.3	0.01	0.1	0.48

The root-mean-square deviation of meal moisture at the output of section 3 of the toaster is $\sigma = 0.34$. At the current moisture values the calculated average value of the absolute error is $\varepsilon_{abs} = 0.28\%$, as the relative is $\varepsilon_{rel} = 1.29\%$.

Figure 4 illustrates the change of meal moisture at the output of section 3. The moisture range of the meal is within the field of defined criterion diapason. The results presented in Fig. 4 are obtained from the simulation model and the experimental ones are measured in the real toaster.

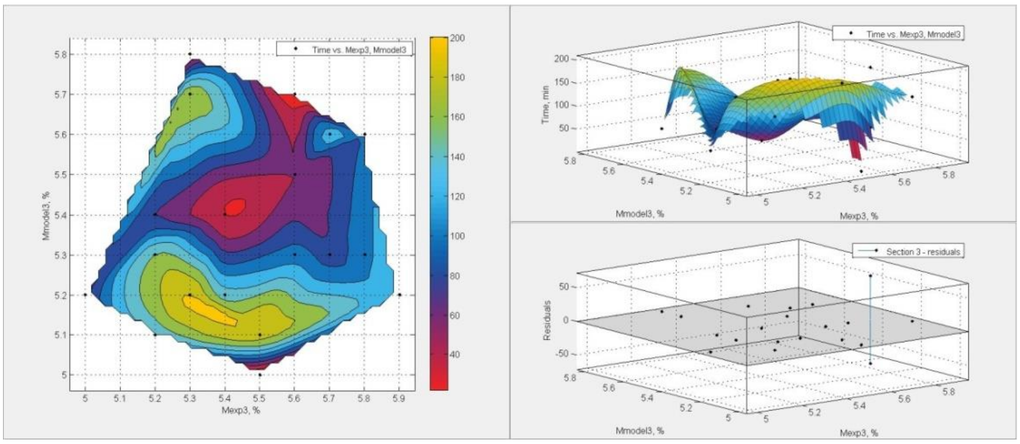

Fig. 4 - Variation of the meal moisture at the output of section 3 in dependence of time

During the model simulation the variation of moisture values is in the range of $M_{meal\_section\_1\_model}$ = (5.8…5.0) %, and the experimentally measured in the installation are $M_{meal\_section\_1\_exp}$ = (5.9…5.0) %. For section 3 the diapason of change of the meal moisture is $M_{meal\_section\_1\_criteria}$ = (7…4.5) %. Therefore, the technological requirements for the range of moisture change in section 3 of the toaster are adhered.

Comparison of the experimental data with the simulation results of the meal moisture at the output of section 4 of the toaster.

Table 4 presents the data for current values of the meal moisture at the output of section 4 (output of the toaster).

Table 4

Values of the meal moisture at the output of the toaster

Time	M_{ml}, model	M_{ml}, exp	Root-mean-square deviation	Absolute error	Relative error	Time	M_{ml}, model	M_{ml}, exp	Root-mean-square deviation	Absolute error	Relative error
[min]	[%]	[%]	[-]	[%]	[%]	[min]	[%]	[%]	[-]	[%]	[%]
10	3.2	2.9	0.09	0.3	2.46	110	2.8	3.1	0.09	0.3	2.54
20	2.5	2.7	0.04	0.2	1.92	120	3.1	2.8	0.09	0.3	2.54
30	2.7	2.6	0.01	0.1	0.94	130	3	2.9	0.01	0.1	0.85
40	2.8	2.9	0.01	0.1	0.88	140	2.5	2.6	0.01	0.1	0.98
50	2.6	3.1	0.25	0.5	4.39	150	2.9	2.6	0.09	0.3	2.73
60	2.9	2.7	0.04	0.2	1.79	160	2.8	2.9	0.01	0.1	0.88
70	3.1	2.5	0.36	0.6	5.36	170	2.9	3.1	0.04	0.2	1.67
80	3.2	2.7	0.25	0.5	4.24	180	2.6	2.9	0.09	0.3	2.73
90	3.2	2.9	0.09	0.3	2.46	190	2.5	2.9	0.16	0.4	3.70
100	2.9	2.8	0.01	0.1	0.88	200	2.6	2.8	0.04	0.2	1.85

The root-mean-square deviation of meal moisture at the output of section 3 of the toaster is $\sigma = 0.3$. At the current moisture values the calculated average value of the absolute error is $\varepsilon_{abs} = 0.26°C$, as the relative is $\varepsilon_{rel} = 2.29\%$.

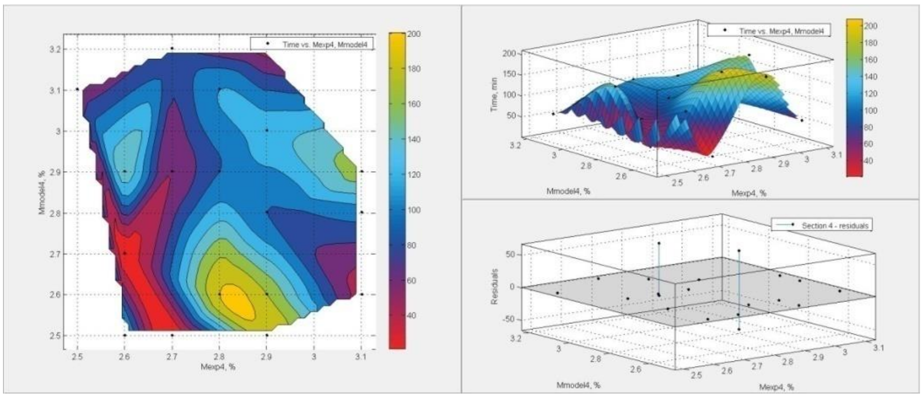

Fig. 5 - Variation of the meal moisture at the output of section 4 in dependence of time

Fig. 5 illustrates the change of meal moisture at the output of section 4. The moisture range of the meal is within the field of defined criterion diapason. The results presented in Fig. 5 are obtained from the simulation model, and the experimental ones are measured in the real toaster.

During the model simulation the variation of moisture values is in the range of $M_{meal\_section\_4\_model}$ = (5.8…5.0) %, and the experimentally measured in the installation are $M_{meal\_section\_4\_exp}$ = (5.9…5.0) %. For section 4 the diapason of change of the meal moisture is $M_{meal\_section\_4\_criteria}$ = (4.5…2.5) %.Therefore, the technological requirements for the range of moisture change in section 4 of the toaster are adhered.

The graphical interpretation of the evaluation of the adequacy of the software model is presented in Fig. 6. The comparative assessment of function $M(_{ml\_model})=f(M_{ml\_exp})$ presents a linear distribution of results which provides a high accuracy of the effectiveness of the model. The deviation of the values of the model to experimental data can be read from Figures 2 to 5, where dependence is presented in time, and the character of the results surface is flat.

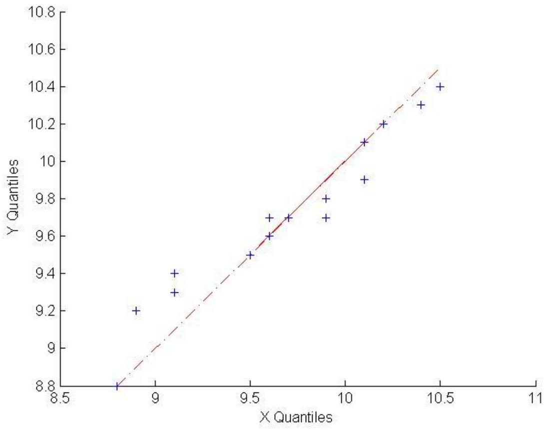

Section 1

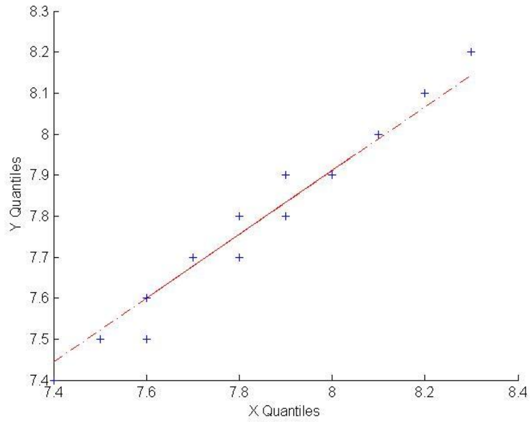

Section 2

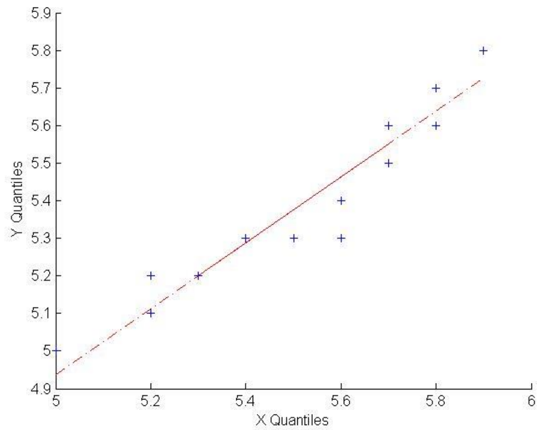

Section 3

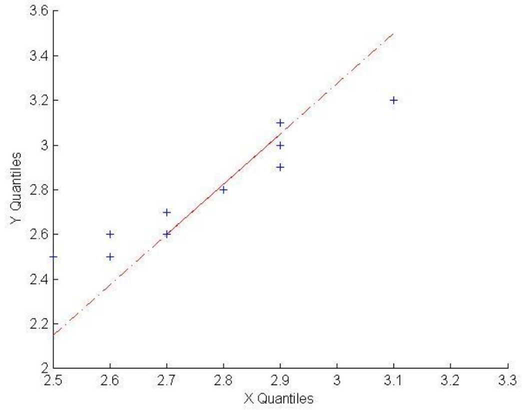

Section 4

Fig. 6 - Variation of the meal moisture at the output of sections – model vs. experiment

The values of relative errors are around the permissible value of 2 %. It is highest at the last section (2.29 %) because the absolute value of the meal moisture is low and closed to 0. Although the variation of the values of the relative errors, the electronic system applies adequate control to the process and the thermal-moisture treated meal is together with parameters substantiated in the criteria.

CONCLUSIONS

The absolute and relative errors for the variation of meal moisture obtained in all control points are lower than the maximum allowable. This is an indicator for the effectiveness of the electronic system for control of meal moisture in the toaster.

The amount of the extracted corn oil increases with a decrease of moisture and increased the processing time. Results of experimental studies present that the electronic system has applied the appropriate variation of control parameters, which affects on the observing of a meal with the exact physicochemical changes and decreasing the effectiveness of the system.

The treated for pressing meal has sufficiently plastic and elastic structure. These properties of the cooked meal are achieved by precise grinding of the oilseeds, and also by applying the most appropriate regime of thermal-moisture treatment that provides the required temperature and moisture properties.

The regulation of the thermal-moisture treatment process via the proposed criteria for assessment of the effectiveness of the developed electronic system based on adequate control, ensuring the reduction of technological processing time of the oilseed material and energy as it guarantees the quality of the final product.

ACKNOWLEDGEMENT

The present document has been produced with the financial support of the project № 2016–FEEA–01 „Modelling of processes for specialized electronic systems", financed by "Scientific Research Fund" at University of Ruse.

REFERENCES

[1] Herák D., Kabutey A., Divisova M., (2013), Analysis of tangential curve equation describing mechanical behaviour of rapeseeds (*Brassica napus L.*) mixture under compression loading, *Research in Agricultural Engineering*, vol.59 (1), pp.9–15;

[2] Kabutey A., Herák, D., Sedláþ ek A., (2011), Behaviour of different moisture contents of Jatropha curcas L. seeds under compression loading, *Research in Agricultural Engineering,* vol.57 (2), pp.72–77;

[3] Kabutey A., Herak D., Choteborsky R., Divisova M., (2012), Model for energy and deformation determination of selected oilseeds under compression loading–Short communication, *Research in Agricultural Engineering*, vol.58, pp.155–158;

[4] Kabutey A., Sedláþ ek, A., Divišová M., Svato Ėová T., (2012), Heat treatment of Jatropha Curcas L. seeds under compression loading, *Scientia Agriculturae Bohemica*, vol.43 (3), pp.116–121;

[5] Kadirova S., (2008), Electronic system for control of oil boiler for meal pretreatment in vegetable oil pressing, *Food science, engineering and technologies*, University of food technologies, Plovdiv, pp.273-278;

[6] Kadirova S., Manukova A., (2009a), Criteria for assessment of the quality of thermal–moisture treatment of meal in oil extraction processes by means of electronic control of a toaster, *Agricultural engineering*, Volume XLVI, 4/2009, Sofia, pp. 8-14;

[7] Kadirova S., Manukova A., (2009b), Computer-based model simulating the thermal-moisture processes in a toaster controlled by an electronic system, *Proceeding of the Union of Scientists-Rousse, the 4th International Conference EE&AE'2009*, Ruse, pp. 457-463;

[8] Manukova A., Kadirova S., (2009), Electronic control for high efficient process in thermal-moisture pretreatment of meal, *Elektronika – konstrukcje, technologie, zastosowania*, No 9, pp.162-168;

[9] Sayyar S., Abidin Z.Z., Yunus R., Muhammad A., (2009), Extraction of Oil from Jatropha Seeds-Optimization and Kinetics, *American Journal of Applied Sciences* 6, pp.1390–1395;

[10] Sigalingging R., Herak D., Kabutey A., Mizera C., Divisova M., (2014), Tangent curve function description of mechanical behaviour of bulk oilseeds: A review, *Scientia Agriculturae Bohemica*, vol.45, pp.259–264;

[11] Willems P., Kuipers N.J.M., De Haan A.B., (2008), Hydraulic pressing of oilseeds: Experimental determination and modelling of yield and pressing rates, *Journal of Food Engineering*, vol.89, pp.8–16.

THE EFFECT OF SPELT ADDITION ON THE PROPERTIES OF EXTRUDED PRODUCTS WITH ENHANCED NUTRITIONAL PROPERTIES
/
WPŁYW DODATKU ORKISZU NA WŁASNOŚCI EKSTRUDOWANYCH WYROBÓW O PODWYŻSZONYCH WŁASNOŚCIACH ŻYWIENIOWYCH

Ph.D.Eng. Żelaziński T.*[1], Ph.D. DSc. Eng. Ekielski A.[1], MSc.Eng Siwek A.[2], Ph.D. Eng. Stachelska M.[2], Ph.D. Stud. Eng. Florczak I.[1]

[1]Department of Production Management and Engineering. Warsaw University of Life Sciences– SGGW / Poland;
[2]Food Technology and Gastronomy Institute, Lomza State University of Applied Sciences / Poland
Tel: +48225934565; E-mail: tomasz_zelazinski@sggw.pl

Keywords: *extrusion, spelt, quality investigation*

ABSTRACT

The aim of the study was to produce extruded material with the highest possible content of spelt and to examine the qualitative properties of the products obtained. Tests were carried out on a synchronous twin-screw extruder with L:D ratio 27, at different temperatures, screw speed, material feeding and raw material moisture. To determine the quality properties there were used parameters such as density, expansion, WSI and WAI, water activity and porosity. The results were promising, all the products were characterized by a high degree of water-holding capacity, and their quality was similar to conventional corn extrudates.

STRESZCZENIE

Celem pracy było wytworzenie surowców ekstrudowanych z możliwie wysokim udziałem orkiszu i zbadanie właściwości jakościowych uzyskanych produktów. Badania przeprowadzono na ekstruderze dwuślimakowym, współbieżnym o stosunku L:D 27, przy różnych ustawieniach temperatury, prędkości obrotowej ślimaków, podawania surowca oraz wilgotności materiału. Do określenia parametrów jakościowych wykorzystano takie parametry jak: gęstość, ekspansję , WSI i WAI, aktywność wody oraz porowatość. Uzyskane wyniki były obiecujące, wszystkie produkty charakteryzowały się wysokim stopniem wodochłonności, a ich jakość była zbliżona do klasycznych ekstrudatów kukurydzianych.

INTRODUCTION

Extrusion is a universal process of raw materials treatment, which enables the production of new and innovative products. It is allowed not only by the specifics of the process itself but also by the possibility of raw materials processing, where traditional processing methods are not cost-effective or economically reasonable *(Żelaziński et al, 2014a)*. Such materials include spelt wheat with numerous positive properties that support its broad application. However, such products range is now very limited.

In Polish and world's literature spelt is described quite widely. The studies include not only the quality characteristics of the finished products but also the physicochemical parameters of grains themselves Sacchetti et al. 2004. Therefore, over the past few years there could be found a number of studies showing different quality characteristics for spelt products or their blends with other cereals. The most popular products include spelt bread and other baked products (e. g. muffins, pastries), widely reported in the research literature *(Abdel et al, 2008; Ruibal-Mendieta et al. 2002; Pierogiovanni et al, 1996; Skrabanja et al, 2001; Escarnot et al, 2010)*. Research areas also include analysis of the spelt baking flour, for example the study conducted by Radomski et al., (2007).

There were also some attempts made to use spelt flour in pasta production *(Marconi et al, 1999, 2002)*. These results suggest that the quality of spaghetti pasta is the highest with the maximum spelt share and relate it with a high content of high-quality protein in the flour. In the literature, there are also other spelt products compared. For example, quality analysis of the bread, pasta and crunchy extruded products manufactured on the basis of spelt flour were conducted by Bonafaccia et al, (2000). In this case, there were found large differences in the degree of starch gelatinization and easily digestible protein content.

The literature however still contains a few studies on the extrusion of spelt or its mixes, and presented research include products based on typical varieties of wheat *(Kim et al, 2006; Yuan et al, 2013)*. It also addresses the topics such as the physical properties of grains, where the aim usually is to improve existing solutions or to find new ways of threshing and hulling spelt *(Borkowska and Robaszewska, 2013; Frączek and Reguła, 2010; Choszcz et al. 2010)*. Difficulties in obtaining clean grains in combination with a smaller wheat yield are also one of the main reasons affecting the small spelt production.

Summing up the above, spelt is certainly a perspective raw material, and researches of its different products carried out in recent years demonstrate the need to search for its new applications, e. g. with the use of extrusion process.

MATERIAL AND METHOD

Material and extrusion process

Input material designed for extrusion was whole-meal spelt flour (total fat 2.7%, total protein approx. 12%) and corn meal (total fat 0.7%, total protein approx. 8.3%, starch approx. 75%). From those materials there were prepared 4 blends in which the share of spelt flour was 70%, 80%, 90% and 100% of total volume. Raw material moisture amounted to approx. 13.6%.

Investigations were conducted in a laboratory twin-screw extruder Clextral Evolum 25 with length to screw diameter ratio L:D of 27. The extruders' cylinder was equipped with six heaters and cooling water system. Such number of sections in conjunction with the two-state automation system allowed very precise adjustment and control of the temperature profile during the extrusion process.

As extruder die was used a circular one with a diameter of 2.5 mm. At the head of the extruder there was placed a cutter, with speed control possibility at the range of 0-1400 obr·min^{-1} (cutter speed was 400 obr·min^{-1}). The extruder was equipped with a calibrated volumetric feeder and a water pump to enable a precise dispensing of liquid directly into the extruder barrel of 0.001 dm^{3}·min^{-1} accuracy.

During the extrusion process, temperature and the screw rotation speed was being changed. Temperature profile set in the individual sections of the extruder barrel was 120°C, 120°C, 110°C, 80°C, 30°C, 30°C and 140°C, 140°C, 110°C, 80°C, 30°C, 30°C. During the extrusion process there was also changed the screw speed in the range 300 or 350 obr·min^{-1}.

The resulting extrudates were prior to being cooled at room temperature for a period of about 3 hours until the moisture stability of approx. 11% was obtained. Below, there is a set points plan for the process of extrusion which was used for all extruded blends.

Table 1

Parameters of extrusion

Extrusion set points	Temperature	Rotation
I	120	300
II	140	300
III	120	350
IV	140	350

Quality properties analysis

Physico-chemical properties of obtained samples were determined by using the basic quality parameters such as density, radial expansion, water absorption (WAI) and water solubility (WSI) indices, water activity and structure measured in the cross-section of the extrudate.

Density was studied with displacement method carried out in accordance with the standard (BN-87/9135-05). Radial expansion (sectional expansion) was determined according to the method (Alvarez-Martinez et al. 1988) as the ratio of the extrudate diameter to the diameter of the nozzle array. Tests of WAI and WSI indices were conducted by the method of Anderson et al. (1969), and shown in detail in the work of Ekielski et al. (2007).

Strength tests of extrudates (texture characteristics) were carried out on the testing machine AXIS 500 (Poland) equipped with a head for measuring the strength (max 25 N). Maximum force needed to cut the extrudate was examined. At the head it was placed a circular mandrel with a diameter of 2 mm (feed rate of 0.02 mm·s^{-1}, displacement of 11 mm). The samples used in the tests had a diameter between 5 and 7 mm and a length between 5.2 and 7.1 mm.

Porosity was studied on a test image analysis stand equipped with a microscope and image analysis software: stereo microscope Opta Tech SL + 3 Mpixel camera. Pictures were recorded in TIF format in the resolution of 2048 x 1536. The porosity was determined according to the method of Gosselin&Rodrigue (2005), using irregular boundaries of the analyzed group of air pores on the evaluated images.

For the porosity analysis it was used package with LabView 2013 and the Vision Assistant 7.1.1 program, where the photos were graphically designed. Then, the obtained images with byte gray scale (256 levels) were converted into divalent bitmaps and were chosen the appropriate thresholds of gray scale range from 1-255 *(Żelaziński et al, 2014b; Ekielski A., 2011)*. In this way, the porosity of the samples was determined on the cross-sectional areas as the number of pores per unit area (cm^2) in accordance with Hayter et al. (1989).

For measuring the water activity of the products obtained there was used AquaLab 4TE measurer (Dekagon, USA). For research results description the Statistical 12 analytical program was used.

RESULTS

On the basis of the analysis of obtained results, it was found that changes in various parameters of the extrusion process had a significant impact on the qualitative changes of the samples obtained. It was found that the density of extrudate (Fig. 1) decreases with the increase of the spelt flour content in the mixture, which could be observed in all samples tested.

At settings of extrusion process I, III, IV charts' courses were similar and the highest density of approx. 0.13 $g \cdot cm^{-3}$ was observed with the spelt participation in a blend of 70%. At settings extrusion process II, all the extrudates have a higher density, the maximum average value being of 0.175 $g \cdot cm^{-3}$ for a mixture of 70% spelt.

The graph course showing the change of radial expansion coefficient looks conversely (Fig. 2). It can be seen that with the increase of the spelt flour content index values clearly increase. In this case, the maximum values of the expansion index were achieved for blends involving 100% of spelt flour. Between the density and the expansion coefficient for process settings I, II, III, IV, it were also found negative correlations at -0.825, -0.648, -0.887, -0.641. Lower density and simultaneously larger degree of the radial expansion suggests that whole-meal spelt flour can be a good structure-forming raw material.

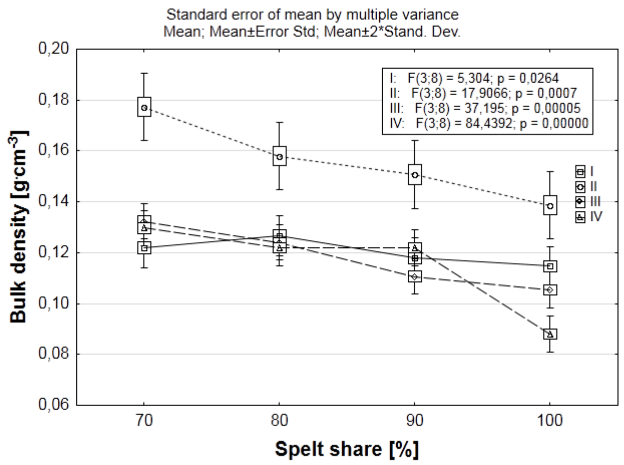

Fig. 1 - Influence of spelt content on density changes of extrudates

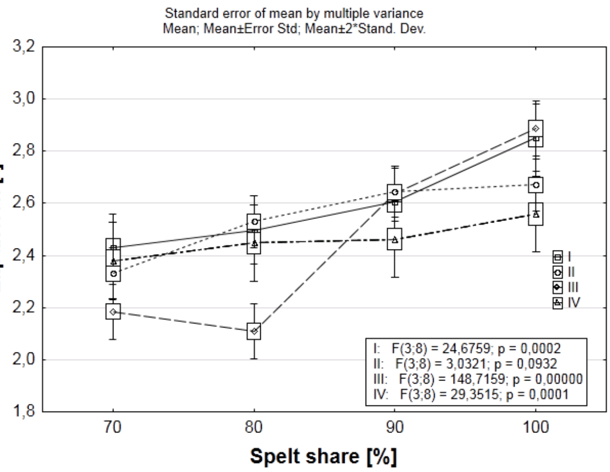

Fig. 2 - Influence of spelt content on expansion changes of extrudates

It was found that with increasing spelt content in the mixture water absorption WAI is also reduced (Fig. 3). In the case of setting I, III and IV, this parameter in the raw material consisting of 100% spelt was 3.45 to 3.5, while for the samples with 70% of spelt was 3.92 to 4.04 on average. The greatest water absorption was characterized by the samples obtained with setting III.

Proportionally and conversely there is presented the course of the WSI index chart (Fig. 4). On the graph it can be thus observed an increase in WSI with the increase of spelt content in the mix, where the maximum water solubility was achieved with 100% spelt participation. In this case, the parameters of the WAI and WSI are also strongly correlated, what is stated in all settings of the process I, II, III, IV (-0.845, -0.774, -0.623, -0.927). Water-holding capacity parameter was also strongly correlated with Aw, what was found with the extruder setting I, II and IV (-0.826, -0.853, -0.954).

Overall, according to the literature (*Ekielski et al, 2007)*, the decrease of water absorption is an indicator of the starch gelatinization degree, so the greater the percentage of consumption-treated starch, thereby digestibility of the product increases. In this case, with the decrease of the WAI increases WSI, which may indicate an increase in the soluble fraction, resulting from the starch and also other components' degradation. This trend can be observed particularly for the specimens produced at 140°C. Charts courses of WAI and WSI may therefore indicate that in the case of spelt extrusion it can be searched temperature range lower than of the conventional extrusion of corn meal.

With the increase in the content of spelt in the mixture it was also observed increase in water activity (Fig. 7), which also can be observed in all settings of the process. The increase of this parameter, however, is disturbing, because it can contribute to the development of microorganisms, which in turn may impede the subsequent storage of these products, particularly after the package is opened.

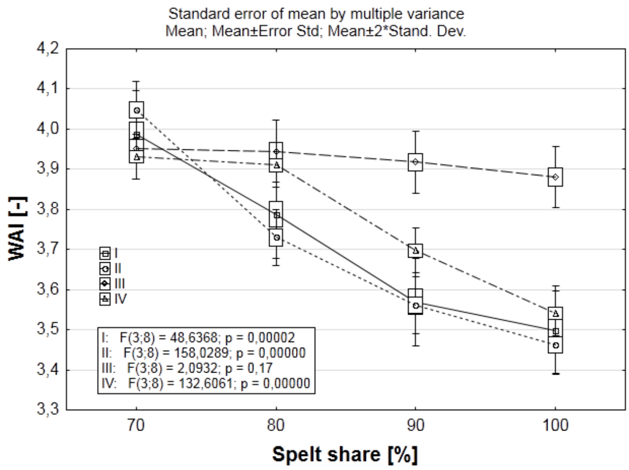

Fig. 3 - Influence of spelt content on WAI changes of extrudates

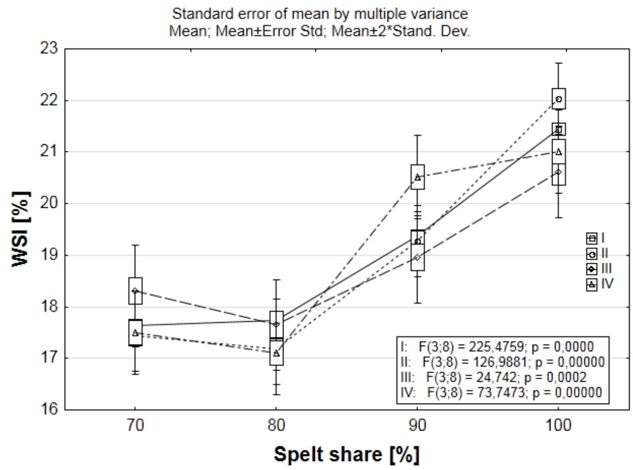

Fig. 4 - Influence of spelt content on WSI changes of extrudates

The increase in the content of spelt in a mixture also caused a reduction in hardness of extrudates (Fig. 5), which clearly could be observed with the use at the process temperature of 140°C. Among the tested samples difference between the hardest sample and the sample with the lowest strength was about 5N. Together with the spelt content in the mix, however, it was observed an increase in the total work "Area" needed to puncture the sample (Fig. 6).

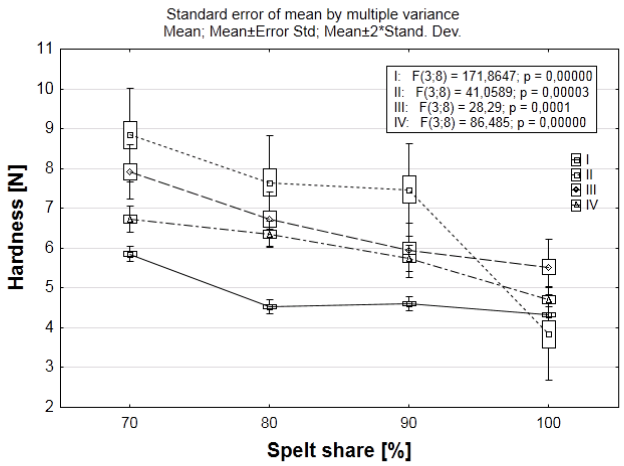

Fig. 5 - Influence of spelt content on hardness changes of extrudates

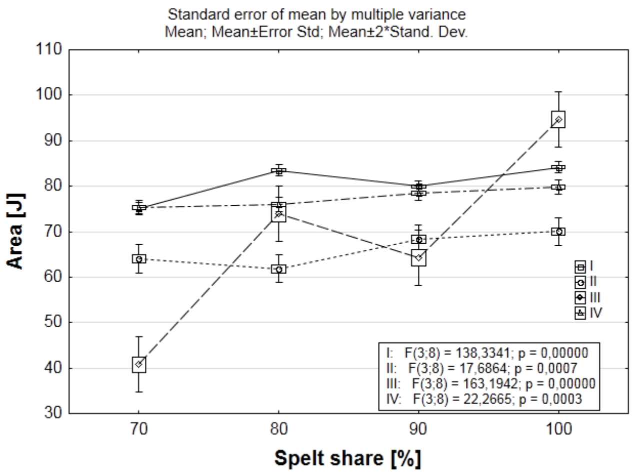

Fig. 6 - Influence of spelt content on "Area-total work" of extrudates

The hardness of the extrudates is in turn highly correlated to the density. It was found at the setting process I, III, IV (0.844, 0.919, and 0.891). Such parameters show that addition of spelt may considerably affect the performance of the textural parameters of extrudates in mixes with e. g. corn.

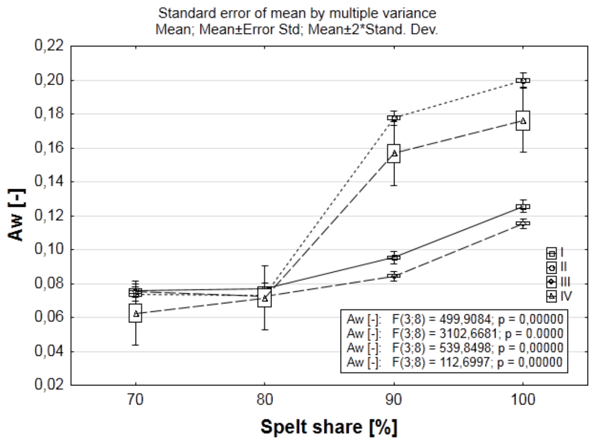

Fig. 7 - Influence of spelt content on water activity Aw of extrudates

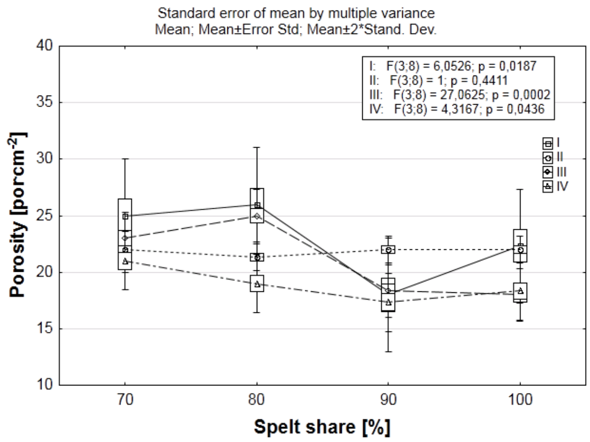

Fig. 8 - Influence of spelt content on porosity changes of extrudates

Together with spelt content the porosity of extrudates slightly reduces its values (Fig. 8), so that the amount of air voids in cm^2 was the smallest for extrudates involving 100% spelt. The same samples obtained at 120°C had a porosity higher than the ones generated at the temperature of 140°C. In the higher screw speed range III and IV porosity strongly correlates with parameters such as Aw (-0.672) and Area (-0.74).

Less than that of corn extrudates porosity is not positive feature of such products. There may also be a link between extrudates obtain with a lower density and a larger expansion (in this case no significant correlation was found). The literature research shows that more fine pores are far more positively perceived by consumers. Studies of this type are, however, subjective experiments, because in the case of the analyzed samples this thesis cannot be unambiguously confirmed without performing sensory analysis, planned in other studies.

CONCLUSIONS

The results of research and literature analysis indicate that spelt is a perspective grain which despite the weaker baking properties compared to the typical varieties of wheat can be a very interesting and, at the same time, healthy raw material for the production of various food products. It was found that spelt is a very good material for baro-thermal extrusion process, and the quality parameters of the products obtained do not differ significantly from products with a high proportion of corn.

The use of raw materials such as spelt to produce the typical snacks or crispy bread can reduce the impact of spelt on its poor baking properties. Despite the clear differences in the quality parameters in products containing spelt, the results for the largest content of spelt are satisfactory, and it can be used as a basic component of the mixture, e. g. in combination with corn or other starchy raw materials.

REFERENCES

[1] Alvarez-Martinez L., Kondury K., P., Harper J. M., (1988), A general model for expansion of extruded products. *Journal of Food Science,* Vol. 53, pp.609-615;

[2] Abdel-Aal, El-Sayed M., Rabalski I., (2008), Effect of baking on nutritional properties of starch in organic spelt whole grain products. *Food Chemistry,* Vol. 111(1), pp.150-156;

[3] Anderson R. A., Conway H. F., Pfeifer V. F., Griffin E. L. (1969), Gelatinization of corn grits by roll and extrusion cooking. *Cereal Science Today, Vol.* 14(1), pp.4-12;

[4] Bonafaccia G., Galli V., Francisci R., Mair V., Skranbanja V., Kreft I., (2000). Characteristics of spelt wheat products and nutritional value of spelt wheat based bread. *Food Chemistry,* Vol. 68, pp.437–441;

[5] Borkowska B., Robaszewska A., (2014), Roasted and Unroasted Buckwheat Groats (Kasza gryczana prażona i nieprażona), *Food Industry,* Vol. 68, pp.36-38;

[6] Choszcz D. J., Konopka S., Zalewska K., (2010), Characteristics of physical properties of selected varieties of spelt, *Agricultural Engineering*. Vol. 4 (122), pp.23-28;

[7] Ekielski A., Majewski Z., Żelaziński T., (2007), Effect of extrusion conditions on physical properties of buckwheat –maize blend extrudate. *Polish Journal of Food and Nutrition Sciences.* Vol. 57, Issue 2(A), pp.57-61;

[8] Ekielski A., (2011), Effect of selected parameters of double-screw extruder operation on fractal dimensions of the extrudate. *Annals of Warsaw University of Life Sciences-SGGW. Agriculture,* Vol. 57, pp.41-47;

[9] Escarnot E., Agneessens R., Wathele B., Paquot M., (2010), Quantitative and qualitative study of spelt and wheat fibers in varying milling fractions. *Food Chemistry.* Vol. 3 (122), pp. 857-863;

[10] Frączek J., Reguła T., (2010), Method of evaluation of susceptibility of spelt grains to mechanical damages during the threshing process, *Agricultural Engineering,* Vol.4 (122), pp.51-58;

[11] Kim J.H., Tanhehco E.J., Ng, P.K.W., (2006), Effect of extrusion conditions on resistant starch formation from pastry wheat flour, *Food Chemistry,* Vol. 99, pp.718–723;

[12] Marconi E., Carcea M., Graziano M., Cubadda R. (1999), Kernel properties and pasta-making quality of five European spelt wheat (Triticum spelta L.) cultivars, *Cereal Chemistry,* Vol. 76, pp.25–29;

[13] Marconi E., Carcea M., Schiavone M., Cubadda R., (2002), Spelt (Triticum spelta L) Pasta quality: combined effect of flour properties and drying conditions, *Cereal Chemistry,* Vol. 79, pp.634–639;

[14] Pierogiovanni A.R., Laghetti G., Perrino P., (1996), Characteristics of meal from hulled wheats (*Triticum dicoccon Schrank and T. spelta L.*): an evaluation of selected accessions, *Cereal Chemistry,* Vol. 76, pp.732–735;

[15] Radomski G., Bać A., Mierzejewska S., (2007), A comparative assessment of baking value of wheat flour and German wheat flour, *Agricultural Engineering,* Vol. 5, Issue 93, pp.369-374;

[16] Ruibal-Mendieta N.L., Delacroix D.L., Meurens, M., (2002), A comparative analysis of free, bound and total lipid content on spelt and winter wheat whole meal, *Journal of Cereal Science,* Vol. 35, pp.337–342;

[17] Sacchetti G., Pinnavaia G. G., Guidolin E., Dalla Rosa M., (2004), Effects of extrusion temperature and feed composition on the functional, physical and sensory properties of chestnut and rice flour-based snack-like products, *Food Research International,* Vol. 37, Issue 5, pp.527-534;

[18] Skrabanja V., Kovac B., Golob T., Elmståhl H. G. M. L., Björck I. M. E., Kreft I., (2001), Effect of spelt wheat flour and kernel on bread composition and nutritional characteristics, *Journal of Agricultural and Food Chemistry,* Vol. 49, pp.497–500, PubMed;

[19] Yuan-Yuan Wang, Krittika Norajit, Mi-Hwan Kim, Young-Ho Kim, and Gi-Hyung Ryu, (2013), Influence of Extrusion Condition and Hemp Addition on Wheat Dough and Bread Properties. *Food Sci. Biotechnol,* Vol. 22, Issue S, pp.89-97, Springer/Korea;

[20] Żelaziński T., Ekielski A., Zdanowska P., Florczak I, (2014a), The effect of ultrasound treatment on selected maize and buckwheat extrudates parameters, *INMATEH - Agricultural Engineering,* Vol. 43, Issue 2, pp.127-136, Bucharest/Romania;

[21] Żelaziński T. ,Ekielski A., Florczak I., (2014b), The vision system usage as data source for statistical process control in the food extrusion, *INMATEH - Agricultural Engineering,* Vol.44, Issue 3, pp.111-120, Bucharest/Romania.

CFD STUDY OF A SWEEP-TWIST HORIZONTAL AXIS WIND TURBINE BLADE
/
BOYUNA-EĞİMLİ BİR YATAY EKSENLİ RÜZGÂR TÜRBİNİ KANADININ HAD ÇALIŞMASI

Ph.D. Stud. Eng. Kaya M. N.*[1], Asst. Prof. Ph.D. Eng. Köse F.[2]
[1]Karamanoglu Mehmetbey University, Engineering Faculty, Mechanical Engineering Department, Karaman / Turkey
[2]Selcuk University, Engineering Faculty, Mechanical Engineering Department, Konya / Turkey
Tel: +90 3382262000-5067; E-mail: mnumankaya@kmu.edu.tr

Keywords: *wind, turbine, blade, performance, sweep, twist*

ABSTRACT
Wind energy is being used to generate electricity in many countries all over the world and still the contribution of wind energy to electricity supply increases every day. Researchers work on innovative solutions to increase the efficiency and decrease the cost of wind turbine components, especially those of blades. Various blade designs for different operation conditions are presented in the literature and sweep-twist blades are new type of blades introduced recently. This paper focuses on the numerical investigation of a sweep-twist wind turbine blade using ANSYS-Fluent. NREL Phase VI wind turbine blade is used as the baseline blade and the sweep-twist blade is designed by adding an offset that is 5% of the blade span to the tip. Power output and thrust forces are calculated using the simulation results for both original and sweep blades. In addition, results are compared to the experimental data of original NREL Phase VI blade.

ÖZET
Rüzgâr enerjisi elektrik üretmek amacıyla dünyada birçok ülkede kullanılmaktadır ve rüzgâr enerjisinin elektrik üretimine katkısında günden güne yükselmektedir. Araştırmacılar rüzgâr türbini bileşenlerinin – özellikle kanatların - verimlerinin arttırılması ve maliyetlerinin azaltılması için yenilikçi çözümler üzerinde durmaktadırlar. Literatürde çeşitli çalışma koşulları için değişik tasarımlar mevcut olup, eğimli kanatlar bunlardan biridir. Bu çalışmada ANSYS-Fluent programı ile eğimli bir rüzgâr türbini kanadının numerik analizi üstünde durulmuştur. NREL Faz VI rüzgâr türbini kanadı baz alınmış ve eğimli kanadı ise uç kısmına kanat boyunun %5'si kadar eğim verilerek tasarlanmıştır. Güç çıkışları ve itme kuvvetleri simülasyon sonuçlarına göre hesaplanmıştır. Buna ek olarak, sonuçlar NREL Faz VI rüzgâr türbininin deneysel sonuçları ile karşılaştırılmıştır.

INTRODUCTION
Each passing day the need for the use of clean energy sources raises since power production from fossil fuels damage our planet continuously. Within this scope, many developed and developing countries have set some goals to generate some part of energy consumption from renewable energy sources. For instance, the ministry of energy of Turkey has decelerated in the strategic plan for 2015-2019 an increase in installed renewable energy capacity by nearly twice compared to the value of 2013 *(GWEC, 2016; Kaya and Köse, 2016; Köse and Kaya, 2013; MENS, 2014).* Hence, wind energy – recognized as an efficient renewable energy source – has taken the role of being one of the leading alternative sources. In past few decades, huge improvements have taken place in wind power technology especially on the design of blades which influences the efficiency directly. Within this scope, many experts who are interested in aerodynamics contributed to the literature with some studies about various blade designs. Sweep-twist wind turbine blades were firstly introduced by Sandia National Laboratories of U.S. Energy Department. After completing the research, they presented a final report (2010) where they introduced analysis results of Sweep Twist Adaptive Rotor (STAR) blades. In the report, they stated that the STAR technology provided significantly greater energy capture – about 10-12% compared to baseline Z48 turbines - without higher operating loads on the turbine. The results are also presented by *Ashwill et al. (2010)*. *Sing and Ahmed (2013)* performed a study about design and performance testing of a small wind turbine rotor for low wind speed applications. A new airfoil was designed and the performance of a 2-bladed rotor for low Re application fitted to an Air-X marine 400 W wind turbine was tested at a wind speed range of 3-6 m/s. Authors stated that the new 2-bladed rotor produced more electrical power at the same freestream velocity in comparison with the baseline

3-bladed rotor. *Wang and Zhan (2013)* investigated the performance of a micro-wind turbine using CFD and concluded that the performance of the wind rotor with semi-circular blades is comparable to that of the semi-cylindrical wind rotor, and is slightly lower than that of the helically twisted wind rotor. *Bai et al. (2013)* designed a 10 kW horizontal axis wind turbine blade and performed aerodynamic investigation using numerical simulation of it. It has been reported that CFD is a good method compared to the improved BEM theory method on the aerodynamic investigation of HAWT blades. *Koc et al. (2015)* studied the hydrodynamic performance of a twin-blade hydrofoil numerically and experimentally in three dimensions for tip speed ratios ranging between 1.5 and 5.5. Authors reported that the optimum tip speed ratio of 3.5 for twin blade turbine is too low comparing the optimum tip speed ratio of 5.0 for the slat hydrofoil or standard hydrofoil turbine applications and added that the wind and hydrokinetic turbines with the twin blade hydrofoil can operate in lower wind and current speeds. A detailed review of aerodynamic developments on small horizontal axis wind turbine blades is presented by *Kartikeyan (2015)*. In the present study, numerical investigation of the aerodynamics around a sweep-twist wind turbine blade using ANSYS-Fluent is performed. NREL Phase VI wind turbine blade is used as a baseline blade and the sweep-twist blade is designed by adding an offset to the tip as that is 5% of the blade diameter. Results are compared with the original NREL Phase VI wind turbine.

MATERIAL AND METHOD

NREL Phase VI and Sweep-Twist Blade

NREL Phase VI wind turbine blade is selected as a baseline blade. It has S809 airfoil sections from root to tip and a pitch angle of 3 degrees. The description of the NREL Phase VI blade is given in Table 1 *(Hand et al., 2001)*. In this study, some sections including the ones which have radial distance between 0.660 and 1.257 and the one with 3.185 radial distance are excluded since the sections are very close to the previous section.

Table1

Description of NREL Phase VI (Hand et al., 2001)

Number of blades	2
Rotor diameter	10.06 m
Cone angle	0 degrees
RPM	71.6
Blade tip pitch angle	3 degrees (down)
Blade profile	S809
Blade chord length	0.358 m – 0.728 m (linearly tapered)
Twist angle	Non-linear twist along the span

The 3-D drawings of the blades are given in Fig. 1. To draw the sweep-twist blade, all the same properties as NREL Phase VI blade are used except a root axis tip offset which is 5% of the blade diameter (0.25 m). Offsets of each sectionfrom the beginning of the sweep – located at the 2.562 m radial distance- until the tip of the blade are calculated interpolation method. Dimensions of the original and sweep-twisted blades are given in Fig. 2.

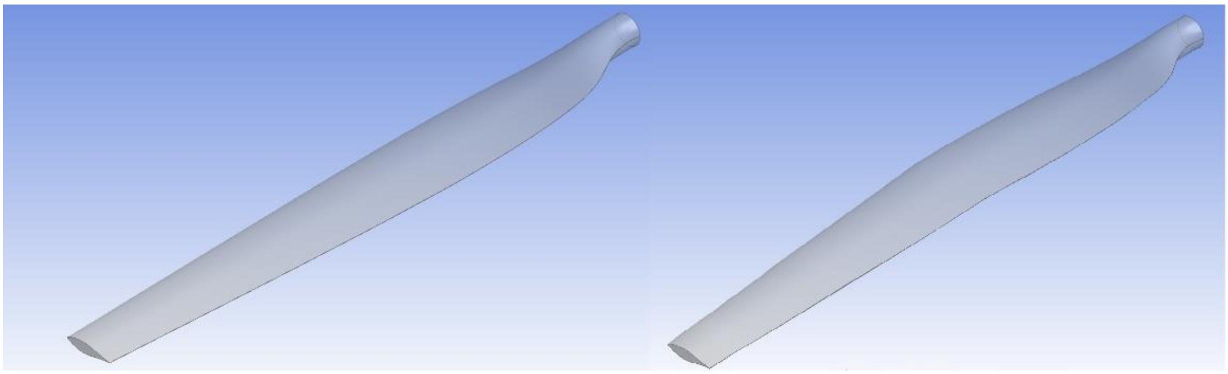

Fig. 1 – 3D drawings of the NREL PHASE VI (left) and sweep-twisted blade (right)

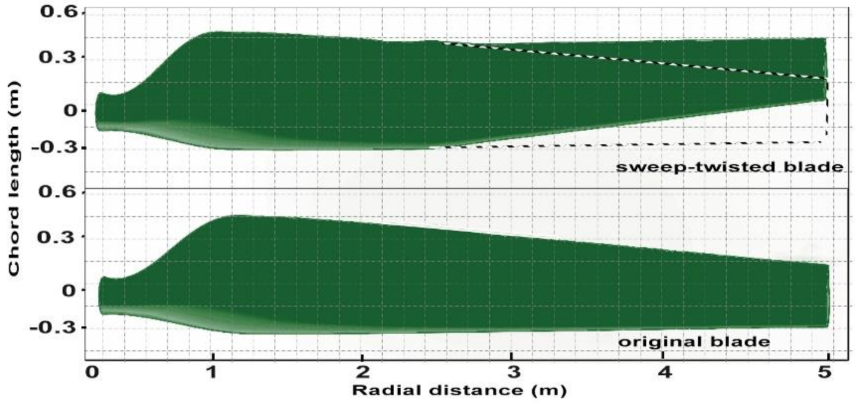

Fig. 2 – Dimensions of the original and sweep-twisted blade

Numerical simulation

In this study, 3-D air flow around the wind turbine blade is simulated using ANSYS Fluent 16. The dimensions of the flow field are 12 R in the stream-wise direction extruded from a circle having 3 R dimension where R is the radius of the blade. The domain of flow field including boundary conditions is given in Fig. 3.

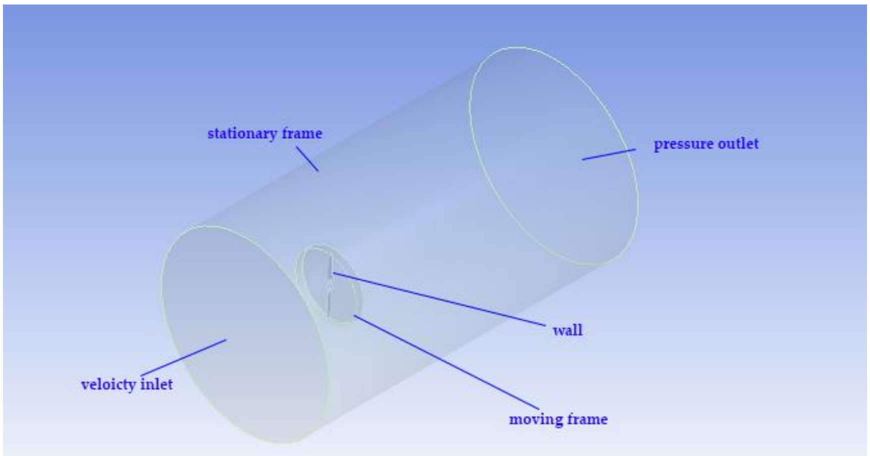

Fig. 3 - Domain of the flow field and boundary conditions

Meshing of the fluid domain is performed using ANSYS meshing. The thickness of the first cell to the wall was kept at 2 x 10^{-5} m to obtain proper y+ value for the used turbulence models. In order to increase the mesh quality, sharp trailing edge of the blades is rounded. Mesh construction and a sliced section of the mesh around the blade and rotor hub can be seen in Fig. 4. Mesh independence study is performed for various models containing different number of elements and a model containing 9.8 million elements is used.

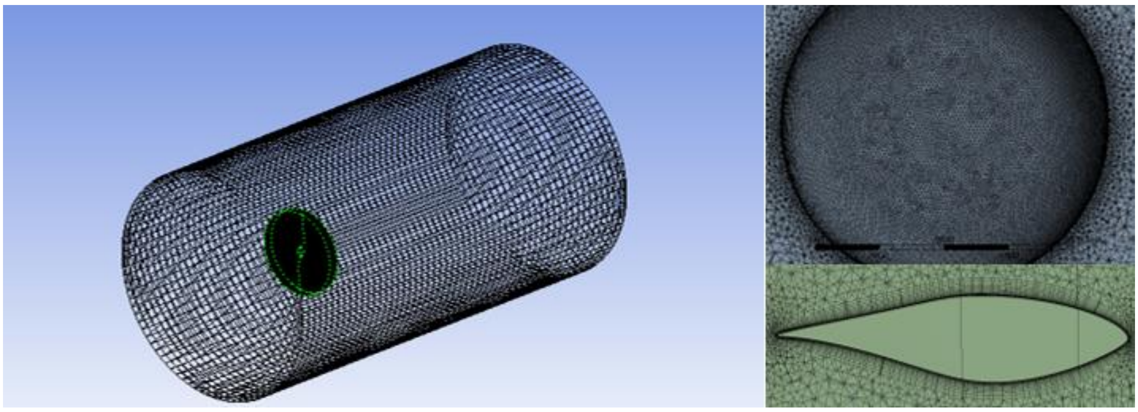

Fig. 4 - Mesh construction and a sliced section of the mesh around the blade and rotor hub

k- ε Turbulence Model

One of the turbulence models used for tests is k –ε Realizable turbulence model. The k- ε model is a two-equation turbulence model consists of turbulence kinetic energy and turbulence dissipation rate equations given below *(Kody et al., 2014).*

$$\rho \frac{D_y}{D_x} = \frac{\partial}{\partial x}[(\mu + \frac{\mu_t}{\mu_k})] + P_k - \rho\varepsilon + L_k \tag{1}$$

$$\rho \frac{D\varepsilon}{D_t} = \frac{\partial}{\partial x_j}[(\mu + \frac{\mu_t}{\sigma_k})\frac{\partial \varepsilon}{\partial x_j}] + c_{\varepsilon 1} f_1 P_k \frac{\varepsilon}{k} - c_{\varepsilon 2} f_2 \rho P_k \frac{\varepsilon^2}{k} + L_e \tag{2}$$

Where:

P_k is turbulent production and viscosity are defined by the Eq. 3 and Eq. 4, respectively.

$$P_k = \tau_{ij} \frac{\partial u_i}{\partial x_j} \tag{3}$$

$$\mu_t = \rho f_u c_\mu \frac{k^2}{\varepsilon} \tag{4}$$

k- ω SST turbulence model

This turbulence model combines both *k-ε* and *k–ω* models. The original *k-ε* turbulence model has the problem of over predicting the shear stress that might delay or prevent the separation where inverse pressure gradients are possessed, and the original k – ω model is very sensitive to free stream values that are specified outside the shear layer *(Kody et. al., 2014)*. The original *k–ω* model is defined by the Equations 5 and 6 *(Kody et. al., 2014; Wilcox, 2008)*.

$$\frac{\partial(\rho k)}{\partial_t} + \frac{\partial(\rho u_j \omega)}{\partial x_j} = P - \beta^* \rho \omega k + \frac{\partial}{\partial x_j}\left[\left(\mu + \sigma_k \frac{\rho k}{\omega}\right)\frac{\partial k}{\partial x_j}\right] \tag{5}$$

$$\frac{\partial \rho \omega}{\partial t} + \frac{\partial(\rho u_j \omega)}{\partial x_j} = \frac{\gamma\omega}{k} P - \beta\rho\omega^2 + \frac{\partial}{\partial x_j}\left[\left(\mu + \sigma_\omega \frac{\rho k}{\omega}\right)\frac{\partial \omega}{\partial x_j}\right] + \frac{\rho\sigma_d}{\omega}\frac{\partial k}{\partial x_j}\frac{\partial \omega}{\partial x_j} \tag{6}$$

Validation of the solver

The solver is validated against experimental data of NREL Phase VI. The mechanical power of numerical and experimental tests is presented in Fig.5. The mechanical power is simply calculated by multiplying rotation speed, Ω (rad/s) by torque, T (Nm) obtained from FLUENT as given in Eq.7.

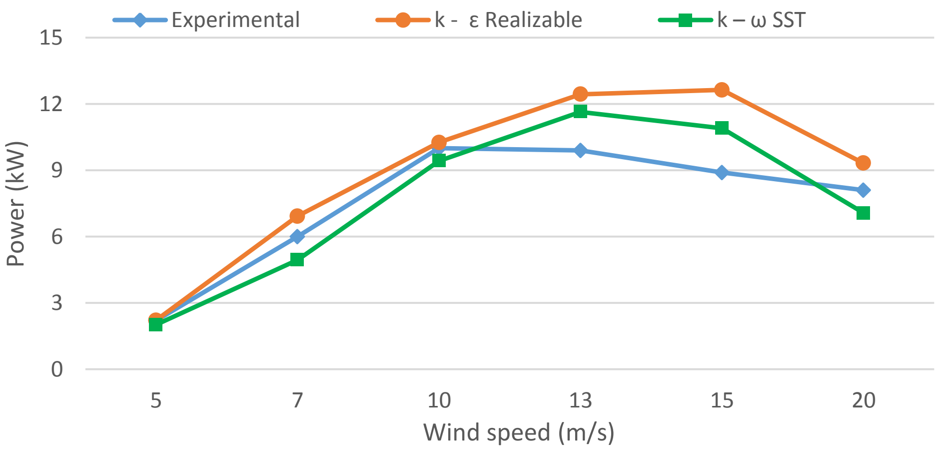

Fig. 5 – Comparison of measured and CFD predicted power

As seen from the Fig. 5, experimental and numerical power outputs are in general agreement. However, after 10 m/s CFD predictions cannot predict the stall very accurately. Thrust force measurements and CFD predictions are in very good agreement as it can be seen from the Fig.6. Also, pressure distributions for 5 m/s case at 47% and 80% span are according to experimental data as shown in Fig.7.

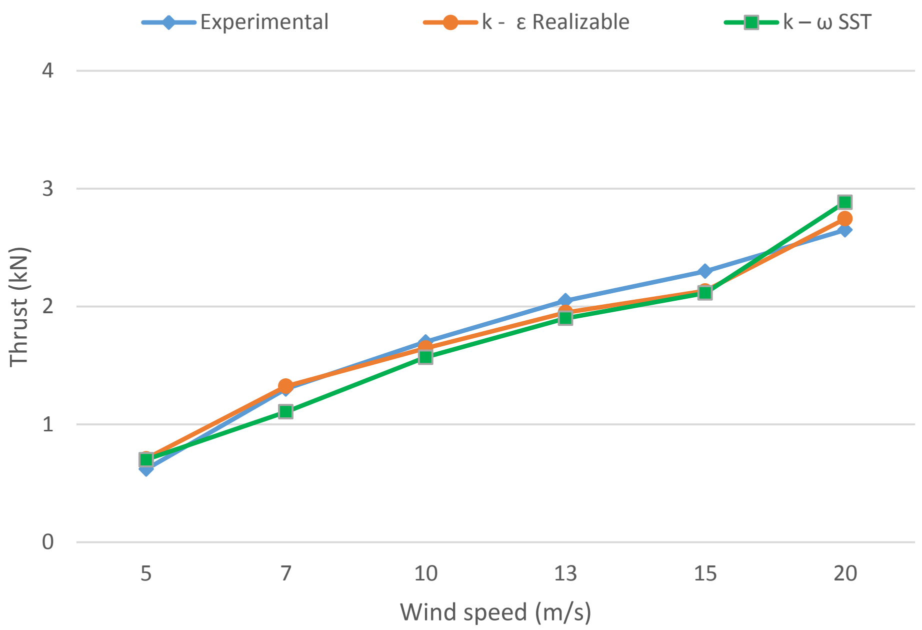

Fig. 6 – Comparison of measured and CFD predicted thrust force

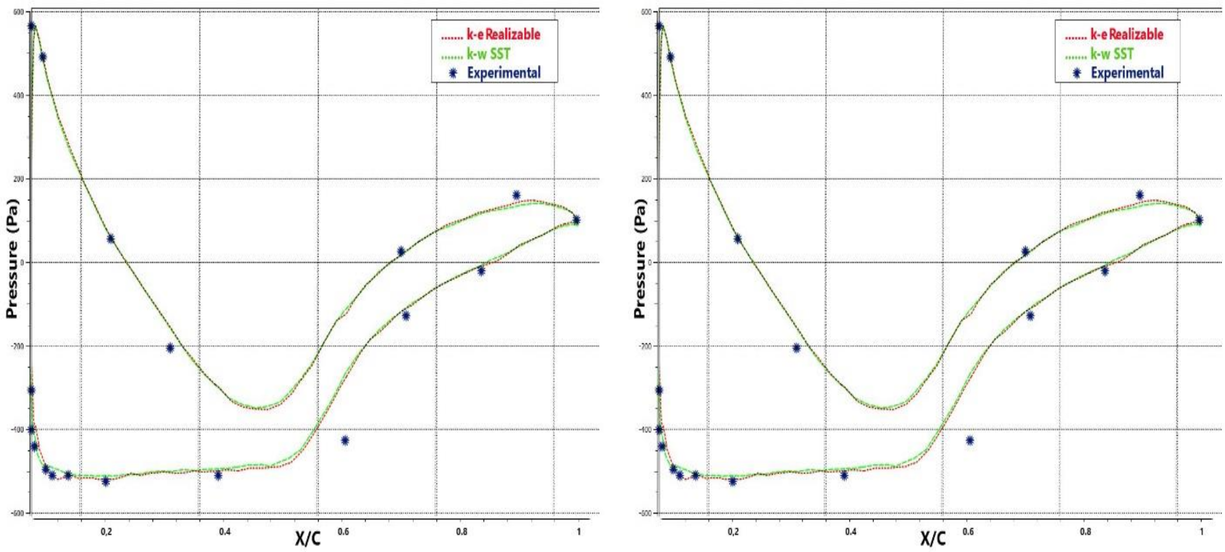

Fig. 7 – Pressure distribution for 5 m/s case at 47% (left) and 80% (right) span

RESULTS

This study compared the original NREL Phase VI blade with a sweep-twisted model of it. Power results are compared in Fig.8 for the sweep-twist and original blade. It is observed that wind turbine blades sweep-twisted to the leading edge side of the blade generate lower power than the original blade. In addition, it is obtained that the *k–ω* SST turbulence model predicts lower power output than the *k-ε* realizable. In Fig. 9, the thrust force for sweep-twist and original blade are compared and results show that the sweep-twisted blade has lower thrust force (more than 10%) at each wind speed except 20 and 25 m/s. The pressure distributions for 5 m/s case at 47% and 80% span are compared in Fig.10. It is clear that the pressure distribution on the original blade is able to generate more power than the sweep-twist blade.

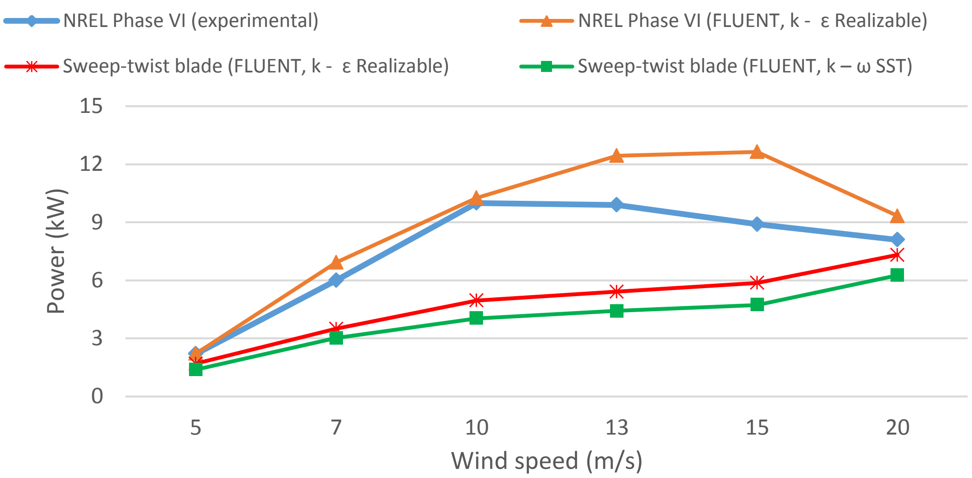

Fig. 8 – Comparison of power outputs for the original and sweep-twist blade

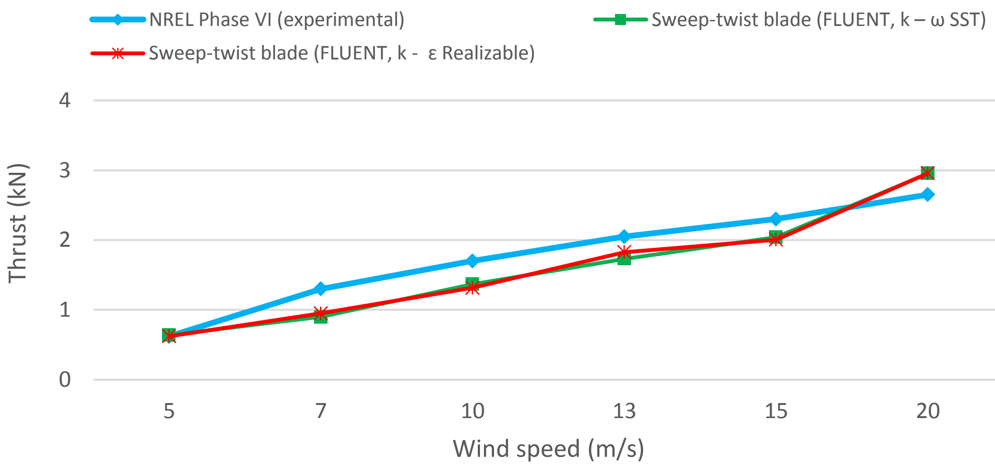

Fig 9 – Comparison of thrust forces for the original and sweep-twist blade

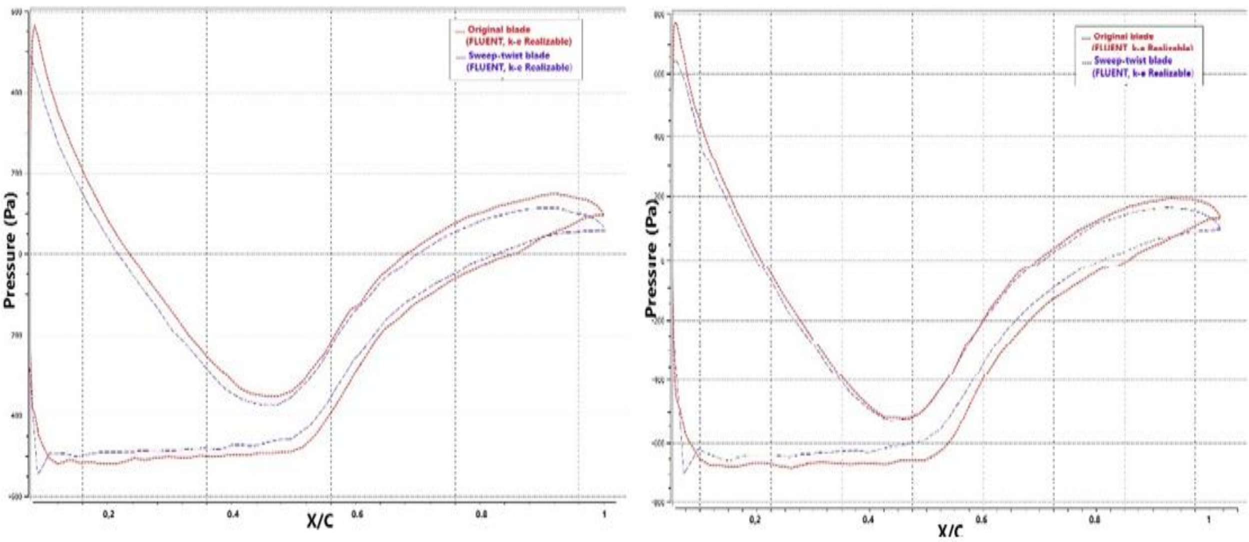

Fig. 10 – Comparison of pressure distribution for 5 m/s case at 47% (up) and 80% (down) span

CONCLUSION

In this paper, mechanical power outputs and thrust forces of original NREL VI and a sweep-twist wind turbine blade are compared. Both *k–ω* SST and *k-ε* realizable turbulence models predicted the thrust force very close to experimental measurements. In addition, CFD predictions of mechanical power output are found to be overall in agreement with experimental data, however, after the wind speed of 10 m/s when the stall occurs, CFD predictions were not very successful. Generally, the *k–ω* SST turbulence model predicted lower power output than *k-ε* Realizable for both original NREL Phase VI and sweep-twisted blade. Results of comparison of original and sweep-twist blades show that sweep-twisting the blade against the direction of rotation causes to decrease in both power output and thrust force. So, the load on the wind turbine tower will be lower if sweep-twist wind turbine blades that are twisted in the leading edge direction and that have same rotor diameters are used. This means that sweep-twist wind turbines blades with larger rotor diameters may be used on same towers that carry original wind turbine rotors. The direction of sweep-twisting is crucial because twisting in opposite direction may show adverse effects.

ACKNOWLEDGMENT

The authors would like to thank to Scientific Research Project Coordination Unit of Karamanoglu Mehmetbey University for the support.

REFERENCES

[1] Ashwill T., Sandia National Laboratories, (2010), *Sweep-Twist Adaptive Rotor Blade: Final Project Report*;

[2] Ashwill T.D., G Kanaby, K. Jackson, M. Zutech. (2010), Development of the Swept Twist Adaptive Rotor (STAR) Blade, *48th AIAA Aerospace Sciences Meeting*, Orlando, FL;

[3] Bai C. J., HsiaoF.B.,LiM.H., HuangG.Y., ChenY.J., (2013), Design of 10 kW Horizontal-Axis Wind Turbine (HAWT) Blade and Aerodynamic Investigation Using Numerical Simulation, *Procedia Engineering*, Vol. 67, pp. 279-287;

[4] Elfarra M. A., (2011), *Horizontal Axis Wind Turbine Rotor Blade: Winglet and Twist Aerodynamic Design and Optimization Using CFD*, PhD Thesis, Ankara, Turkey;

[5] GWEC - Global Wind Energy Council, (2016), *Global Wind Report: Annual Market (2015)*, Brussels, Belgium;

[6] Hand M., Simms, D., Fingersh L., Jager D., Cotrell J., Schreck S., Larwood S, (2001), *Unsteady Aerodynamics Experiment Phase VI: Wind Tunnel Test Configurations and Available Data Campaigns*, NREL/TP 500-29955;

[7] Karthikeyan N., Kalidasa Murugavel K., Arun Kumar S., Rajakumar S., (2015), Review of aerodynamic developments on small horizontal axis wind turbine blade, *Renewable and Sustainable Energy Reviews*, Vol. 42, pp. 801-822;

[8] Kaya M N. and Kose F., (2016), Wind Power Plants for Low Rated Wind Speed Regions: Feasibility Analysis and Simulation of a System, *E3S Web of Conferences,* Vol. 10, EDP Sciences;

[9] Koç E., YavuzT., Kılkış B., Erol Ö., Balas C., Aydemir T., (2015), Numerical and experimental analysis of the twin-blade hydrofoil for hydro and wind turbine applications, *Ocean Engineering* 97:12-20;

[10] Kody S., Alpman E., Yılmaz B., (2014), *Computational Studies of Horizontal Axis WindTurbines Using Advanced Turbulence Models*, Marmara Üniversitesi Fen BilimleriDergisi, Vol. 26(2), pp. 36-46;

[11] Kose F., Kaya M.N., (2013), Analysis on meeting the electric energy demand of an active plant with a wind-hydro hybrid power station in Konya, Turkey, Konya water treatment plant, *Renewable energy*, Vol. 55, pp. 196-201;

[12] Schmidt R. C., Kerstein A. R., McDermott R, (2010), A multi-scale model for 3D turbulent flow based on one-dimensional turbulence modelling, *Computer Methods in Applied Mechanics and Engineering*, Vol. 199, pp. 865-880;

[13] Singh R.K. and Ahmed M.R., (2013), Blade design and performance testing of a small wind turbine rotor for low wind speed applications, *Renewable Energy*, Vol. 50, pp. 812-819;

[14] Wang Y. F., Zhan M. S., (2013), 3-Dimensional CFD simulation and analysisonperformance of a micro-wind turbine resembling lotus in shape, *Energy and Buildings*, Vol. 65, pp.66–74;
[15] Wilcox, D. C., (2008), Formulation of the k-omega Turbulence Model Revisited, *AIAA Journal*, Vol. 46, No. 11, pp. 2823-2838;
[16] MENS - Ministry and Natural Sources of Turkey, (2014), Strategic plan 2015-2019, http://www.enerji.gov.tr/File/?path=ROOT%2f1%2fDocuments%2fStratejik+Plan%2fETKB+2015-2019+Stratejik+Plani.pdf.

AGRICULTURAL RESIDUES GASIFICATION, DEPENDENCY OF MAIN OPERATIONAL PARAMETERS OF THE PROCESS ON FEEDSTOCK CHARACTERISTICS
/
ГАЗИФІКАЦІЯ СІЛЬСЬКОГОСПОДАРСЬКИХ ВІДХОДІВ, ЗАЛЕЖНІСТЬ ОСНОВНИХ ЕКСПЛУАТАЦІЙНИХ ПАРАМЕТРІВ ПРОЦЕСУ ВІД ХАРАКТЕРИСТИК СИРОВИНИ

Assoc.prof. Ph.D.Eng. Zolotovs'ka O.V. [1], Prof.Ph.D. Kharytonov M. [1], Ph.D. Stud. Onyshchenko O.[1],
[1] State Agrarian and Economic University, Center of Ecological Agriculture, Dnipro / Ukraine
Tel: 0973456227; E-mail: envteam@ukr.net

Keywords: *agricultural residues, pyrolysis unit, heat generation*

ABSTRACT

Pilot-scale trial data on combined energy cycle – adjustment for boiler system for pyrolysis gas use had demonstrated technical feasibility of implementation of combined energy cycles for facilities where secondary agricultural residues are available in sufficient quantities.

The results of the energetic analysis of technologies of gas production from solid biomass through the pyrolysis are considered. Examples of the introduction of the technology of direct gasification of secondary agricultural residues and wood (buckwheat husk, rice husk, sunflower husk, sawdust) are shown. It was determined that optimal technological conditions for low-temperature pyrolysis processes depend on character of the feedstock and moister content in the feedstock.

Temperature and pressure pulsing were found to be most important parameters that influence gas quality and yield during pyrolysis process and optimized through developing of mathematical equations describing the process.

РЕЗЮМЕ

Результати експериментального випробування комбінованого енергетичного циклу – коригування бойлерної системи для отримання піролізного газу показали технічну доцільність впровадження комбінованих енергетичних циклів на об'єктах, де вторинні відходи сільського господарства є в достатній кількості.

Зроблений енергетичний аналіз даних технологій виробництва газу з біомаси шляхом піролізу. Наведені приклади впровадження технології прямої газифікації вторинних відходів сільського господарства і деревини (лушпиння гречки, рисового лушпиння, лушпиння соняшника, тирси). Було встановлено, що оптимальні технологічні умови для низькотемпературного піролізу процеси залежать від характеру сировини і вмісту вологи у вихідній сировині.

Зміни у температурі та тиску виявилися найбільш важливими параметрами, які впливають на якість і вихід газу та оптимізовані за допомогою математичних рівнянь, що описують процесс піролізу.

INTRODUCTION

Ukraine is among the countries which have stocks of all kinds of fuel and energy resources (oil, natural gas, coal, peat, uranium, etc.), but the coverage, production and the use are not equally distributed and they do not create the necessary energy safety level, especially in light of existing political situation. The agri-food complex is one of the most important sectors of Ukrainian economy *(Velychko O., 2015*). Agricultural waste and woody biomass are key components of renewable energy potential in Ukraine. Energy crops currently represent a "virtual" part of the potential, except of several experimental plantations (*Bielski S., 2015)*. There are two major sources of the feedstock in agricultural forestry sector, which are primary, and secondary agricultural residues. Primary agricultural residues are those materials which remain in fields as by-products after the primary product of crops has been harvested. These include different materials like cereal grain straws, of wheat, barley, rice etc., corn stover (stalk and leaves) etc.

Secondary agricultural residues are specific type of residues and include quite wide variety of biomass by-products of processing of agricultural products for food or feed production *(Czernik and Bridgwater, 2004)*. Bagasse, sunflower husks, rice husks, nut shells, cocoa bean shells, kidney bean shells and other biomass of such kind is generated and collected at the enterprises which process agricultural crops for food/feed production. Food processing by-products represent a huge amount of waste resources that could be valorized for recovery of compounds for fuels and energy via thermos-chemical, biological and microbial methods. The biomass pyrolysis is attractive because solid biomass and wastes can be readily converted into liquid products. Although the primary agricultural residues represent the largest share of the technical potential (83 %), distribution of secondary agricultural residues are more equal and there are more options to process them using infrastructure of the facilities where agricultural feedstock is processed *(Geletukha et al, 2010)*. Ukraine has quite a big potential of agricultural residues which mainly consists of straw from cereals and production residues from sunflower and maize from grain. At present, less than 1 % of the primary agricultural residues potential is used for energy purposes (combustion in boilers, production of pellets and briquettes), mainly because of undeveloped infrastructure and logistics system for the feedstock supply. The situation with secondary agricultural residues is much better though their technical potential is lower than for primary. Over 77 % of sunflower husks biomass, for example, is directly burned in boiler systems, another 20 % is used for pellets production. Almost all sunflower processing facilities have biomass boilers for utilization of sunflower husks.

Agricultural residues from the waste streams of commercial processes have typically been considered to have very little inherent value, mainly constituting a disposal problem in the past. Most of the waste generated by sunflower and crop processing for bioenergy facilities are also confronted with the costs associated with collection and transportation in addition to the supply uncertainties in particular case.

Although direct burning of secondary agricultural residue was widely introduced into de practice during last 10 years, when wood or other solid biomass are directly combusted and coupled to a steam turbine, it is not possible to achieve high rate of efficiency. Only combined energy cogeneration cycles allow versatile and high effective use of biomass residues but in this case using of biomass in combustion/boiler system requires primary production of power from biomass *(Wang et al, 2014)*.

As far as solid biomass cannot be fed into a gas turbine or diesel engine – a liquid or gaseous fuel is required to operate an advanced cycle, which means direct liquefaction or gasification of biomass is required.

An economic analysis was conducted for biomass gasification and pyrolysis and electricity generated to meet local market demand, including the higher-value peaking power. Biomass-based gasification eliminates the need for waste disposal and reduces electricity consumption from the grid, making it a valid investment (*Lau et al, 2002)*.

Although pyrolysis technologies are more developed and available at the present day, they are preferable to others. Pyrolysis is one of thermos-chemical processes, which convert the solid biomass in to liquid (bio-oil), gas, and char. Pyrolysis has been practiced for centuries for production of charcoal. More recently, studies into the mechanisms of pyrolysis have suggested ways of substantially changing the proportions of the gas, liquid and solid products by changing the rate of heating, temperature and residence time *(Tilmann D., 2000; Wang et al, 2002)*. This requires relatively slow reaction at very low temperatures to maximize solid yield (*Suri and Horio, 2010*). The diverse range of biochar applications depends on its physicochemical properties, which are governed by the pyrolysis conditions (heating temperature and duration) and the original feedstock *(Jindo et al, 2014; Lei and Zhang, 2013).*Thus, detailed information on the complete production process is a key factor in defining the most suitable application of biochars.

Biomass pyrolysis converts essentially 80–95% of the feed material into gases and bio-oil. The pyrolysis process is to maximize the production of gaseous fraction (*Williams and Besler, 2006)*.

There are few fundamental experimental and theoretical studies, dealing with the biomass combustion and emission characteristics and physical and chemical properties of various biomass feed stocks (*Gaskin et al, 2008; Lei and Zhang, 2013; Mimmo et al, 2014)*. There are several studies made on development of reliable kinetic and thermos-transport models for investigation of biomass thermal conversion process *(Brewer et al, 2009; Mc Beath et al, 2013)*. Although some certain adjustment to every type of feedstock and to every type of combined energy cycle is required.

In light of existing situation in the alternative energy sector of Ukraine, it is important to obtain a better understanding of this technology and their potential for implementation and existing markets.

MATERIAL AND METHOD

The aim of the present study is to perform a technical and economic assessment of the pyrolysis operation as a secondary agricultural residues utilization process. The study included pilot test at the facility that might be suitable for implementation of biomass utilization combined cycle for evaluation of operating costs and revenue potential for a generic gasification process, and a cost sensitivity study. To perform general evaluation of the technological process of oxidative pyrolysis, laboratory pyrolysis unit was constructed. The general scheme of the pyrolysis unit is shown in figure 1.

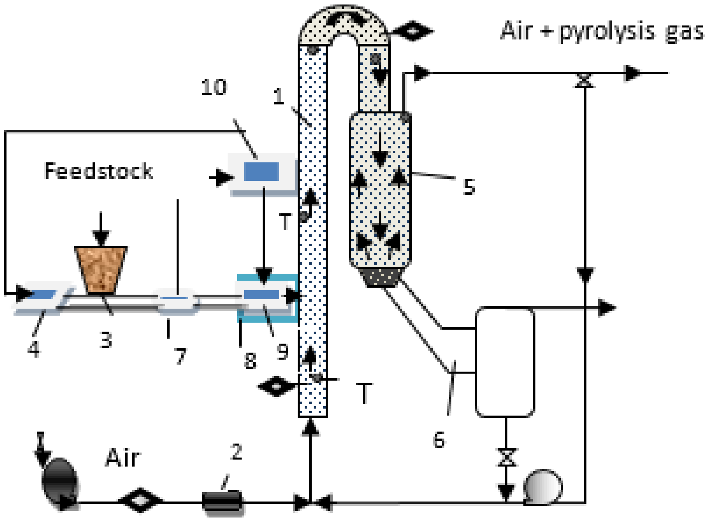

Fig. 1 - The general scheme of the pyrolysis unit

C1–C6 – plan sifter compartments; Break 1–5 – break rolls; MG1, MG2 – semolina machines; M1A, M1B, M2–M6 – reduction rolls; F, F1, F2 – flour

The unit consists of elbow shaped chamber (2) with internal diameter of 100 mm with total length of 5700 mm, which allows conducting the pyrolysis on fluidized bed. In the lower part of the chamber, the air primary heated up in radiator is blown (1). Before entering the chamber, air goes through the numerous ceramic rings to average out air velocity profiles along the tube section. The feedstock is loaded into the camera by the screw dispenser. The design of the dispenser is allows to control feed volume and impermeable inlet joint. In the pyrolysis chamber inlet the automatic moister control sensor (7) was installed. Thus in the feedstock before entering the chamber and passing though the moister the moister is automatically measured. The data from sensor is automatically transformed to converter (10) which controls the feed (4).

In the pyrolysis camera satellite-lifting motion of particles is supported when satellite motion of particles velocity is 1.5 – 2 times lower than the air movement. As particles have almost similar size and mass, the layer of particles can be considered as uniform substance with average thermos-physical parameters. Drying, heating and party pyrolysis occur during the movement of the particles suspended in air. The cyclone is installed on the camera outlet where the separation the gaseous and solid phases is taking place. Solid particles fall into cyclone bunker where further devolatilization is taking place up to full decomposition. The air mixture of gaseous products of pyrolysis is sucked out through the smokestack and 10 % of the mixture is returned back each time for the gas enrichment which increases its calorific value.

To avoid the condensation of resins, which gaseous products of pyrolysis contain, the cyclone, pyrolysis chamber, bunker and connecting pipes were insulated. The experimental study on evaluation of the process of biomass thermal conversion was performed in the following stages. First stage consists in heating up the system and determining initial moister content in the feedstock. Second stage – the setting of the parameters of the process (biomass and air feed rate), which define the overall process parameters. Third stage consists in achieving stability of the process (up to 15 minutes) and determination of its general efficiency indicators - the ration of certain pyrolysis products in the mixture, temperature along the pyrolysis camera. Fourth stage consists in finishing the process and evaluating the mass balance. Comprehensive experimental study was conducted to analyze new configuration for combined cycle heating system based on pyrolysis gas generation process for most common types of secondary agricultural residues.

RESULTS

At the beginning stage, biomass heating up process results in moister evacuation (strongly marked endothermic process), where moister content, accordingly, is one of the main process indicators. It was shown the condition of the plant material which is used as a feedstock for fuel production process. This process affects certain parameters, such as heating up time, particles movement velocity, bulk yield of the volatile products, gas permeability of the waste layer and its hydraulic resistance, biomass and air feed rate, initial temperature of air heating, actual biomass feed rate. Energy potential indexes of four types of secondary agricultural residues are shown in the table 1.

Table 1

Energy potential indexes of most common types of secondary agricultural residues

Type of biomass	Moister content, %	Energy capacity MJ/kg	KW hours/ kg
Sawdust	20	14.1	3.9
	6	18.2	
Buckwheat husk	12	13.8	3.8
	2	17.9	
Rice husk	12	14.3	3.9
	2	18.5	
Sunflower husk	17	14.2	3.9
	4	18.3	

Initial moister content of processed biomass is very variable. Feedstock with higher moister content requires more energy per batch, which is supported by increasing of temperature during the process of organic matter conversion. In order to adjust moister control sensor, the moister content was measured for biomass samples (sawdust) with moister content 1–40 %. Results of the measurements and optimal diapasons of drying for each type of biomass are depicted on plots “a”, “b”, “c” and ”d” in the figure 2.

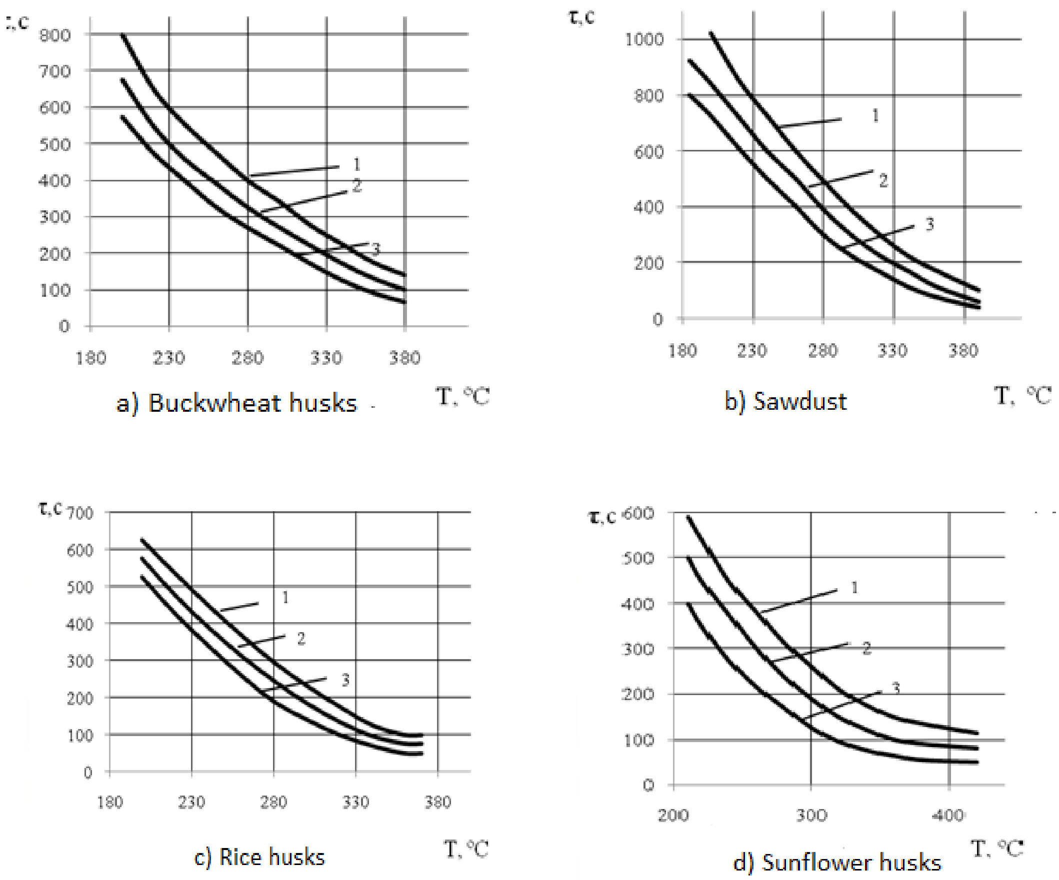

Fig. 2 - Dependence between heating temperature and moister content for different types of processed biomass

1 – particle with 40 % moister content; 2 – particle with 20 % moister content; 3 – particle with zero moister content.

After few runs of the pyrolysis unit analysis of the obtained data it has shown that it was necessary to decrease of the feedstock moister content, because overall energy gain of the process depends on the energy capacity of the feedstock entering the pyrolysis chamber. Whereas biomass-drying stage is included into pyrolysis unit scheme, the adjustment of the drying and pyrolysis regimes is required. Such adjustment, as experimental study demonstrated, could be performed by incorporation of online moister control automatic sensor. To support required temperature in the camber, it is crucial to provide certain feedstock and air proportion which can be defined theoretically. Accordingly, there is certain dependency of decomposition process parameters for the feedstock with certain moister content on the temperature regime and amount of air in mixture. The regulation of gas air mixture proportions also can be achieved by regulation of pressure pulsing. To evaluate the rate of impact of thermal treatment regimes on the quality and content of obtained gas mixture, a mathematical model was developed. As main indicator of obtained gas quality the volumetric output of gaseous products from the feedstock was taken as those having impact on the indicators of Y group, such parameters as amount of air (X_1), air temperature (X_2), moister content in the feedstock (X_3) and air pressure drop (X_4). General data obtained during experimentation with pyrolysis unit regimes are given in the table 2.

Table 2

Main process factors variation levels

№	Factor	Symbol	Variation levels					Δ
			-1.411	-1	0	1	1.414	
1	**Air content in pyrolysis gas, %**	X_1	50	57.5	65	72.5	80	7.5
2	**Air temperature, ° C**	X_2	140	200	260	320	380	60
3	**Particles moister content, %**	X_3	6	10	20	30	36	10
4	**Pressure drop in the chamber, MPa**	X_4	0.06	0.1	0.2	0.3	0.36	0.1

For developing the process model, orthogonal central composition plan of the second order was used. After elimination of the factors and interactions, which coefficients had lesser module meanings of set thresholds of significance for general level of significance $\alpha = 0.5$, following dependencies were obtained:

Hydrogen:
$$Y_1 = 4.124 - 0.3322X_1 + 0.1X_2 - 0.3157X_3 - 0.1415X_4 - 1.0483X_1^2 - 0.7983X_2^2 - \\ - 0.2985X_3^2 - 0.7983X_4^2 - 0.5563X_1X_2 - 0.98125X_1X_3 - 0.09377X_1X_4 - 0.1071X_2X_3; \quad (1)$$

Methane:
$$Y_2 = 3.4584 - 0.1319X_1 + 0.0634X_2 - 0.2561X_3 - 0.5382X_4 - 0.764X_1^2 - 0.514X_2^2 - \\ - 0.639X_3^2 - 0.514X_4^2 + 0.1251X_1X_2 - 0.606X_1X_3 - 0.0987X_2X_3; \quad (2)$$

Carbon oxide:
$$Y_3 = 4.132 - 0.1574X_1 + 0.0713X_2 - 0.2484X_3 - 0.55969X_4 - 0.8307X_1^2 - 0.581X_2^2 - 0.556X_3^2 - \\ - 0.556X_4^2 - 0.1068X_1X_2 - 0.759X_1X_3 - 0.185X_1X_4 - 0.085X_2X_4; \quad (3)$$

Carbon dioxide:
$$Y_4 = 3.6176 + 0.3238X_1 - 1.1171X_2 + 0.2484X_3 + 0.5341X_4 + 0.9044X_1^2 + 0.6544X_2^2 + \\ 0.7794X_3^2 + 0.7669X_4^2 - 0.0844X_1X_2 - 0.0794X_1X_3 - 0.4144X_1X_4 - 0.906X_2X_3 + 0.122X_3X_4 + \\ + 0.356X_3X_4; \quad (4)$$

Nitrogen:
$$Y_5 = 0.1997 + 0.0184X_1 - 0.087X_2 + 0.0075X_3 - 0.4082X_4 + 0.56X_3^2 + 0.0441X_4^2 + \\ + 0.016X_1X_3 - 0.018X_1X_4 - 0.017X_3X_4; \quad (5)$$

Carbohydrates:
$$Y_6 = 3.2532 + 0.075X_1 + 0.462X_2 - 0.2996X_3 - 0.331X_4 - 0.6834X_1^2 - \\ 0.581X_2^2 - 0.284X_1X_2 - 0.044X_1X_3 + 0.094X_1X_4 - 0.1025X_2X_3 - 0.0775X_3X_4; \quad (6)$$

Hydrogen sulfide:
$$Y_7 = 0.4488 + 0.0186X_1 - 0.0071X_2 - 0.0708X_4 + 0.0983X_2^2 + 0.129X_4^2 - \\ - 0.075X_1X_4 - 0.057X_2X_4 - 0.0365X_3X_4 \quad (7)$$

It was proved that proposed models are adequate with confidence level meaning of 0.95 (fig.3).

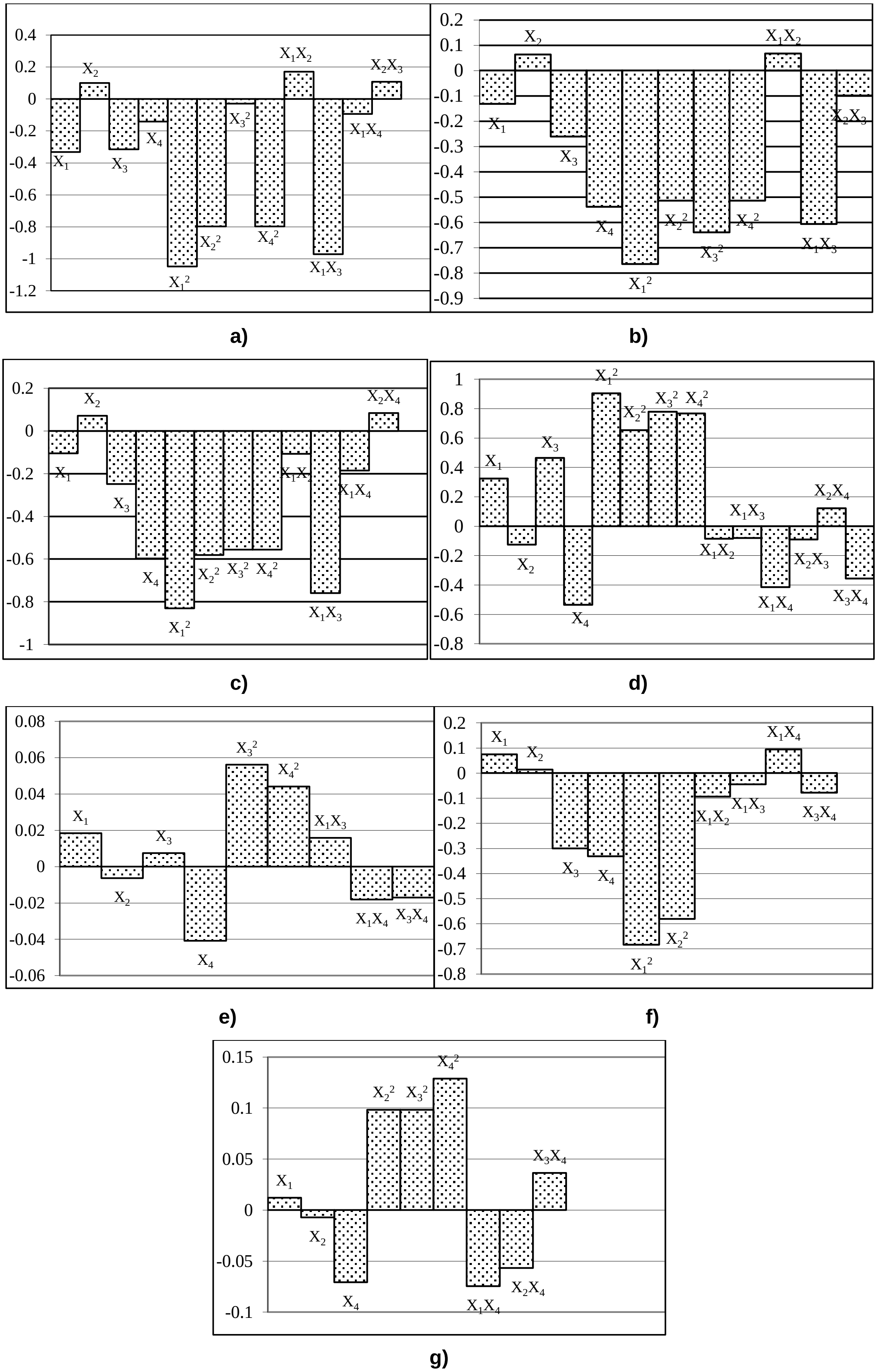

Fig. 3 - Diagrams representing levels of significance of model factors

a)hydrogen; b) methan; c) carbon oxide; d) carbon dioxide; e) nitrogen; f) heavy carbohydrates; g) hydrogen sulfide

It can be used for adjustment of the pyrolysis process and output prognosis for pilot large scale processes. When the temperature of pyrogas/air mixture is increased, range of conditions when ignition can occur are wider, thus pressure and temperature interaction effects are more complicated. Pressure increase (X_4) for hydrogen (Y_1) narrows down the range where ignition can occur, although for methane and other components of gas mixture (Y_3, Y_5, Y_6, Y_7) the range becomes wider. Thus, an obtained mathematical model proves result obtained in practice i.e. by regulating pressure pulsing, gas composition and temperature at which ignition occurs can be controlled.

Biomass decomposition process with generation of volatile substances, such as hydrogen (Y_1), methane (Y_2) and partly heavy carbohydrates (Y_6) plays the key role in pyrolysis process. As far other factors (X_1, X_3, X_4) besides temperature have influence on yield of volatile substances, it is obvious that all stated factors (X_1, X_2, X_3, X_4) should be considered to control mass transfer which is reflected inbuilt regression equations. Regression dependencies for all given factors appeared to be adequate physical processes, thus can be sued for pyrolysis process control and optimization. The content of gases with highest heating value in the pyrolysis gas was determined as main response function for optimization of the energy yield of the process. The amount of hydrogen Y_1 in the pyrolysis gas was optimized according to obtained optimization model, while numeric limitations were accepted after summarizing of average meanings with variance intervals.

Considering accepted assumptions the function optimization equations were following:

Hydrogen: $$L_1 = Y_1 + \lambda_1(Y_3 + X_5 + 20.8) + \lambda_2(Y_4 + X_6 - 19.2) + \lambda_3(Y_5 + X_7 + 15.54); \quad (8)$$

Methane: $$L_2 = Y_2 + \lambda_1(Y_3 + X_5 + 20.8) + \lambda_2(Y_4 + X_6 - 19.2) + \lambda_3(Y_5 + X_7 + 15.54); \quad (9)$$

Heavy carbohydrates:

$$L_3 = Y_6 + \lambda_1(Y_3 + X_5 + 20.8) + \lambda_2(Y_4 + X_6 - 19.2) + \lambda_3(Y_5 + X_7 + 15.54). \quad (10)$$

To determine optimal X_κ meanings, three systems of equations were resolved. After resolution of given equation system, the stationary point was found where meanings were: (X_1=10.44%, X_2=396ºC, X_3=3.35%, X_4=0.153). As it can be observed in given equations, it is hard to define Y_1 from Y_2, Y_3, Y_4, Y_5, Y_6, Y_7 thus regression was used to evaluate Y_1 in the same conditions. Multi collinearity was checked in Farrar - Glauber method for all three equation systems *(Farrar and Glauber, 1967)*. Proposed approach and found mathematical solutions allow controlling mass transfer during pyrolysis process by variation of meaning for (X_1, X_2, X_3, X_4) which can be done for process of any scale. Obtained results gave all sufficient data for process optimization and further up scaling. During the pilot testing of the pyrolysis unit, different types of feedstock (rice and buckwheat husks, sunflower husks and sawdust) with similar physical and chemical properties were used, which gave similar composition of pyrolysis products with not big differences. The pilot scale study was dedicated to establishing of dependencies of the process parameters on the composition of pyrolysis products and finding of the optimal process intensity to obtain certain gaseous products composition. Pilot unit for thermal conversion of biomass into fuel gas was designed to conduct large scale testing and incorporated into boiler house of municipal enterprise. The proposed technology was based on two stage process. The first stage feedstock undergoes thermal decomposition which results in gas production. This gas is burned on the second stage as depicted on the general process flow scheme (fig.4).

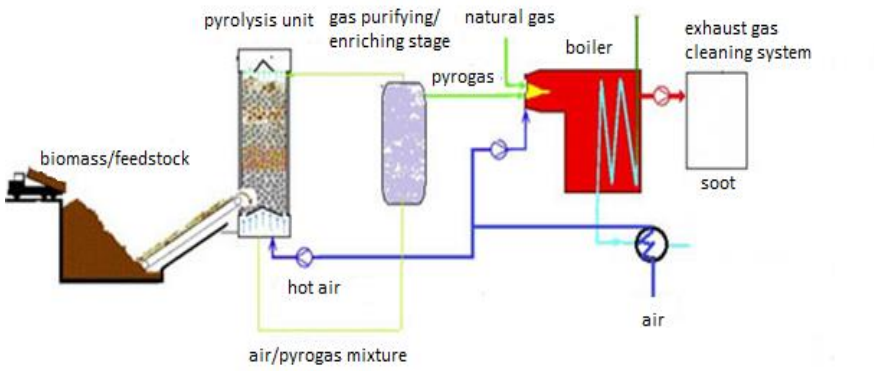

Fig. 4 - General process flow diagram

Pyrolysis gas that was obtained in the process used as fuel for water boiling system.

CONCLUSIONS

Agricultural residue/wastes are promising for producing bioenergy, despite the existing considerations, such as spatial distribution, production costs, and an unstable supply. Availability of the feedstock and regional concentration are good preconditions for local bioenergy generation. However, there is a lack of technologies able to support optimal production limits. Considering both positive and negative impacts of various bioenergy technologies and feedstock on social economics and ecological challenges, utilization of existing feedstock sources may be the most effective method to develop sustainable, renewable alternative fuel. Experimental methods used and results obtained in this study would be practical to address the challenges in biomass gasification process optimization and adaptation for large-scale implementation.

ACKNOWLEDGEMENT

The work has been funded by the Ukrainian Ministry of Education and Science.

REFERENCES

[1] Bielski S., (2015), The agricultural production of biomass for energy purposes in Poland. *Agriculture & Forestry*, Vol.61, Issue 1, pp.153-160;

[2] Brewer C. E., Schmidt-Rohr K., Satrio J. A. and Brown R. C., (2009), Characterization of biochar from fast pyrolysis and gasification systems, *Environ. Prog. Sustain. Energy*, 28, pp.386–396;

[3] Czernik S., Bridgwater A.V., (2004), Overview of application of biomass fast pyrolysis oil. *Energy & Fuels,* vol.18, p.590;

[4] Farrar D.E., Glauber R.R., (1967), Multi-disciplinarity in regression analysis: The problems revisited, *The review of Economics and statistics*, Vol.49, No.1, pp.92-107;

[5] Gaskin J.W., Steiner C., Harris K. C., Das C. and Bibens B., (2008), Effect of low-temperature pyrolysis conditions on biochar for agricultural use, *Transactions of the ASABE*, vol.51, pp.2061–2069;

[6] Geletukha G., Zhelyezna T., Lakyda D., Vasylyshyn R., Zibtsev S., Lakyda I., Böttcher, H., (2010). Potential of biomass for energy in Ukraine, Kyiv, p.27, http:// www.eu-bee.info

[7] Jindo K., Mizumoto H., Sawada Y., Sanchez-Monedero M. A., Sonoki T., (2014), Physical and chemical characterization of biochars derived from different agricultural residues, *Biogeosciences,* no.11, pp.6613–6621;

[8] Lau F.S., Zabransky R., Bowen D.A., (2002), Techno-Economic Analysis of Hydrogen Production by Gasification of Biomass Gas, *Hydrogen Program Review Proceeding,* p.12;

[9] Lei O., Zhang R., (2013), Effects of biochars derived from different feedstock and pyrolysis temperatures on soil physical and hydraulic properties, *J. Soil*, Sedim, no.13, pp.1561–1572;

[10] McBeath A.V., Smernik R.J., Krull E.S., Lehmann J., (2013), The influence of feedstock and production temperature on biochar carbon chemistry: A solid-state 13C NMR study, *Biomass Bionenergy*, no.60, pp.121–129;

[11] Mimmo T., Panzacchi P., Baratieri M., Davies C.A., Tonon G., (2014), Effect of pyrolysis temperature on miscanthus (Miscanthus x giganteus) biochar physical, chemical and functional properties, *Biomass Bionenergy*., no.62, pp.149–157;

[12] Suri A., Horio M., (2010), Solid biomass combustion, in: Handbook of Combustion, vol.4, Solid Fuels, edited by: Lackner M., Winter F., Agarwal, A. K., WILEY-VCH Verlag GmbH & Co. KGaA, Weinheim, chapter 3, pp.85–140;

[13] Tilmann D., (2000), The combustion of solid fuels. Academic Press, Boston, p.199;

[14] Velychko O., (2015), Logistical system Fortschrittzahlen in the management of the supply chain of a multi-functional grain cooperative. *Economics and Sociology,* Vol.8, no.1, pp.127-146 Szczecin/ Poland

[15] Wang X., Kersten S.R., Prins W., Van Swaaij W.P.M., (2002), Biomass-syngas from fast pyrolysis vapors of liquids. *Proceedings of the 12th Eurpean Conference on Biomass for Energy, Industry and Climate Protection*, Amsterdam, The Northlands, p.781;

[16] Williams P.T., Besler S. (1996). The influence of temperature and heating rate on the slow pyrolysis of biomass. *Renewable Energy*; 3:233-250.

WRITING NORMS

Article Types

Three types of manuscripts may be submitted:

1. **Regular articles:** These should describe new and carefully confirmed findings, and experimental procedures should be given in sufficient detail for others to verify the work. The length of a full paper should be the minimum required to describe and interpret the work clearly (max.10 pages, even number);
2. **Short Communications:** A Short Communication is suitable for recording the results of complete small investigations or giving details of new models or hypotheses, innovative methods, techniques or apparatus. The style of main sections has not necessarily to be in accordance with that of full-length papers (max. 6 pages, even number);
3. **Reviews:** Submissions of reviews and perspectives covering topics of current interest are welcome and encouraged (max.10 pages, even number).

Manuscripts should be written in English (American or British usage is accepted, but not a mixture of these) and submitted **electronically** at the following e-mail addresses: ***inmatehjournal@gmail.com***
Please be sure to include your full affiliation and e-mail address (see Sample manuscript)
The authors are responsible for the accuracy of the whole paper and references.
There are allowed 2 papers by each first author.
The text layout should be in single-column format. To avoid unnecessary errors it is strongly advised to use the "spell-check" and "grammar check" functions of your word processor.

Review Process

All manuscripts are reviewed by 2 members of the Scientifically Review Office. Decisions will be made as rapidly as possible and the journal strives to return reviewers' comments to authors in approx.3 weeks.
The editorial board will re-review manuscripts that are accepted pending revision.

NOTE:

Submission of a manuscript implies: that the work described has not been published before (excepting as an abstract or as part of a published lecture or thesis) that it is not under consideration for publication elsewhere.

1. REGULAR ARTICLES

- Manuscripts should be concise, in ***1.15 line spacing***, and should have 2 cm all over margins. The font should be ***Arial 10 pt.*** Ensure that each new paragraph is clearly indicated, using **TAB at 1 cm**.
- Title will be ***Arial 12 pt***. and explicit figures will be ***Arial 9 pt***.
- Text will be written in English.
- Chapters' titles are written by ***Arial 10 pt, Bold, Uppercase*** (e.g. **INTRODUCTION, MATERIAL AND METHODS**), between chapters is left a space for 10 pt. At the beginning of each paragraph, TAB of 1 cm.
- The paper body will be written in ***Arial 10 pt., Justify alignment***.

TITLE ***Arial 12 pt., Uppercase, Bold, Center*** *(in English language)* and ***Bold Italic*** *(in native language)*.
Should be a brief phrase describing the contents of the paper. Avoid long titles; a running title of no more than 100 characters is encouraged (without spaces).

AUTHORS ***ARIAL 9, Bold, Centre alignment***
Under the paper's title, after a space (enter) 9 pt., write ***authors' names*** and ***affiliations (Arial 8 pt.-Regular)***
When the paper has more than one author, their name will be followed by a mark (Arabic numeral) as superscript if their affiliation is different.
Corresponding author's name (next row), ***(Arial 8 pt.)***. Should be added also: phone, fax and e-mail information, for the paper corresponding author (***font: 8 pt., Italic***).

KEYWORDS ***(In English)*** about 4 to 7 words that will provide indexing references should be listed (title: ***Arial 10pt, bold italic,*** text ***Arial 10 pt., italic***).

A list of non-standard *Abbreviations* should be added. In general, non-standard abbreviations should be used only when the full term is very long and used often. Each abbreviation should be spelled out and introduced in parentheses the first time it is used in the text. Standard abbreviations (such as ATP and DNA) need not to be defined.

ABSTRACT ***(in English and Native language, Arial 10 pt.)***, the title *bold*; the text of abstract: *italic*) should be informative and completely self-explanatory, briefly present the topic, state the scope of the experiments, indicate significant data, and point out major findings and conclusions. The Abstract should be max.250 words. Complete sentences, active verbs, and the third person should be used, and the abstract should be written in the past tense. Standard nomenclature should be used and abbreviations should be avoided. No literature should be cited.

INTRODUCTION (***Arial 10 pt.)*** should provide a clear statement of the problem, the relevant literature on the subject, and the proposed approach or solution. It should be understandable to colleagues from a broad range of scientific subjects. We should refer to the current stage of researches performed in the field of the paper to be published, by quoting up-to-date specialty studies, preferably published after 2006, excepting certain referential specialty books/studies, especially papers issued in magazines/journals/conferences/ISI quoted symposia or in other international data bases, which are well known and available.

MATERIALS AND METHODS (***Arial 10 pt.)*** should be complete enough to allow experiments to be reproduced. However, only truly new procedures should be described in detail; previously published procedures should be cited, and important modifications of published procedures should be mentioned briefly. Methods in general use need not be described in detail.

RESULTS (***Arial 10 pt.)*** should be clarity presented. The results should be written in the past tense when describing findings in the authors' experiments. Results should be explained, but largely, without referring to the literature. Discussion, speculation and detailed interpretation of data should not be included in the Results, but should be put into the Conclusions section.

CONCLUSIONS (***Arial 10 pt.)*** The main conclusions drawn from results should be presented in a short Conclusions section. Do not include citations in this section.

Formulae, symbols and abbreviations: Formulae will be typeset in Italics (preferable with the Equation Editor of Microsoft Office 2003) and should be written or marked as such in the manuscript, unless they require a different styling. They should be referred to in the text as Equation (4) or e.g. (4). The formulae should be numbered on the right side, between brackets ***(Arial 10 pt.)***:

$$P = F \cdot v \tag{1}$$

Terms of the equation and the unit measure should be explained, e.g.

P is the power, [W];
F – force, [N];
v – speed, [m/s]

SI units must be used throughout.

Tables should be self-explanatory without reference to the text. The details of the methods used in the experiments should preferably be described in the legend instead of in the text. The same data should not be presented both in table and graph form or repeated in the text.

Table's title will be typed***Arial 9 pt, Bold, Centered***

In the table, each row will be written Arial 9 pt, single-spaced throughout, including headings and footnotes.

The table should be numbered on the right side, between brackets ***(Arial 10 pt)***:

Figure (Arial 9 pt., Bold, Center)should be typed in numerical order (Arabic numerals). Graphics should be high resolution (e.g.JPEG).Figure number is followed by what represent the figure or graph e.g.:

Fig.1 – Test stand

Legend: Arial 8 pt, Italic, Center, e.g.

1 - plansifter compartments; 2- break rolls; 3 – semolina machines; 4 – reduction rolls; 5 – flour

ACKNOWLEDGMENTS (***Arial 10 pt.)*** of people, grants, funds etc should be brief (*if necessarily*).

REFERENCES (***Arial 10 pt.)***

(In alphabetical order, in English and in the original publication language).
Minimum 10 references, last 10 years, minimum 3 references from the last 2 years

It can be used"*References*" tool from the *Word Editor*.

References should be cited in the text in brackets as in the following examples:

(Babiciu P., Scripnic V., 2000)

All references must be provided in English with a specification of original language in round brackets.

Authors are fully responsible for the accuracy of the references.

References should be alphabetically, with complete details, as follows:

Examples:

Books: Names and initials of authors, year (between brackets), title of the book (Italic), volume number, publisher, place, pages number or chapter, ISSN/ISBN:

[1] Vlădut V., (2009), *Study of threshing process in axial flow apparatus (Studiul procesului de treier la aparatele cu flux axial),* vol.1, ISSN/ISBN …………, "Terra Nostra" Publishing House, Iaşi/Romania;

Journal Article: Names and initials of authors, year (between brackets), full title of the paper, full name of the journal (Italic), volume number, publisher, place, ISSN, page numbers:

[1] Lizhi Wu, Yan Di., (2005), Demonstrational study on the land consolidation and rehabilitation (LCR) project of saline-alkali soil in arid areas: a case study of Lubotan LCR project in Pucheng County, Shaanxi Province（干旱区盐碱化土地整理工程实证研究-以陕西蒲城县卤泊滩土地整理项目为例）, *Transactions of the Chinese Society of Agricultural Engineering*,vol.21, no.1, pp.179-182, Madison/Wisconsin;

[2] Leonov I.P., (1973), Basic machine theory for tobacco stringing. Post-harvest care of tobacco and rustic tobacco (Основы теории машин для закрепления табака на шнуры. Послеуборочная обработка табака и махорки), *Collection of scientific articles (сборник научно-исследовательских работ)*, pp.37-45;

Conference or Symposium: Names and initials of authors, year (between brackets), full title of the paper (Regular), full name of the conference/symposium (Italic), volume number, publisher, place, ISSN, page numbers

[1] Bungescu S., Stahli W., Biriş S., Vlăduţ V.,Imbrea F., Petroman C., (2009), Cosmos program used for the strength calculus of the nozzles from the sprayers (Program Cosmos folosit pentru calculul de rezistenţ ă la zgomot al aparatelor de distribuţ ie), *Proceedings of the 35 International Symposium on Agricultural Engineering "Actual Tasks on Agricultural Engineering",* pp.177-184, Opatija / Croatia;

Dissertation / Thesis: Names and initials of authors, year (between brackets), full name of the thesis (Italic), specification (PhD Thesis, MSc Thesis), institution, place;

[1] Popa L., (2004), *Research on the influence of structural and functional parameters of the braking system on the braking performance of agricultural trailers (Cercetări privind influenţa caracteristicilor constructive şi funcţionale ale sistemelor de frânare asupra performanţelor de frânare ale remorcilor agricole)*, PhD dissertation, Transylvania University of Braşov, Braşov / Romania.

Patents: Names and initials of authors, year (between brackets), patent title (Italic), patent number, country:

[1] Grant P., (1989), *Device for Elementary Analyses*. Patent, No.123456, USA.

Legal regulations and laws, organizations: Abbreviated name, year (between brackets), full name of the referred text, document title/type (Italic), author, place:

[1] *** EC Directive, (2000), Directive 2000/76/EC of the European Parliament and of the Council of 4 December 2000, on the incineration of waste, Annex V, *Official Journal of the European Communities*, L332/91, 28.12.2000, Brussels.

Web references: The full URL should be given in text as a citation, if no other data are known. If the authors, year, and title of the documents are known and the reference is taken from a website, the URL address has to be mentioned after these data:

The title of the book, journal and conference must be written in Italic, the title of the article, chapter of the book, must be written Regular.

Citation in text

Please ensure that every reference cited in the text is also present in the reference list (and vice versa). Do not cite references in the abstract and conclusions. Unpublished results, personal communications as well as URL addresses are not recommended in the references list.

Making personal quotations (one, at most) should not be allowed, unless the paper proposed to be published is a sequel of the cited paper. Articles in preparation or articles submitted for publication, unpublished, personal communications etc. should not be included in the references list.

Citations style

Text: All citations in the text may be made directly (or parenthetically) and should refer to:

- ***single author***: the author's name (without initials, unless there is ambiguity) and the year of publication:
  "as previously demonstrated *(Brown, 2010)*".
- ***two authors***: both authors' names and the year of publication: *(Adam and Brown, 2008; Smith and Hansel, 2006; Stern and Lars, 2009)*
- ***three or more authors***: first author's name followed by "et al." and the year of publication: "As has recently been shown *(Werner et al., 2005; Kramer et al., 2000)* have recently shown ...."

Citations of groups of references should be listed first alphabetically, then chronologically.

Units, Abbreviations, Acronyms

- Units should be metric, generally SI, and expressed in standard abbreviated form.
- Acronyms may be acceptable, but must be defined at first usage.

Edited by: INMA Bucharest
6 Ion Ionescu de la Brad Blvd., sect. 1, Bucharest, ROMANIA
Tel: +4021.269.32.60; Fax: +4021.269.32.73
http://www.inmateh.eu
e-mail: ***inmatehjournal@gmail.com***